UNIVERSITAT DE VALÈNCIA

FACULTAT DE MEDICINA I ODONTOLOGIA

DEPARTAMENT DE FARMACOLOGIA

ANTIRETROVIRAL THERAPY AND ITS ROLE IN THE PROGRESSION OF ACUTE AND CHRONIC LIVER INJURY

Doctoral Thesis

ALBERTO MARTÍ RODRIGO

Directors:

Dra. Ana Blas García

Dr. Juan Vicente Esplugues Mota

Valencia, 2018

UNIVERSITAT DE VALÈNCIA

FACULTAT DE MEDICINA I ODONTOLOGIA

DEPARTAMENT DE FARMACOLOGIA

Dra. ANA BLAS GARCÍA, Investigadora CIBERehd del Departamento de Farmacología de la Universidad de Valencia y

Dr. JUAN VICENTE ESPLUGUES MOTA, Catedrático de Universidad en el Departamento de Farmacología de la Universidad de Valencia

CERTIFICAN:

Que el trabajo titulado "Antiretroviral therapy and its role in the progression of acute and chronic liver injury", presentado **D. Alberto Martí Rodrigo,** ha sido realizado bajo nuestra dirección y asesoramiento en el Departamento de Farmacología de la Facultad de Medicina y Odontología de la Universidad de Valencia.

Concluido el trabajo experimenal y bibliográfico, autorizamos la presentación y la defensa de esta Tesis Doctoral.

Para que así conste a los efectos oportunos, se expide la presente certificación en Valencia, a 3 de diciembre de 2018.

Fdo. Dra. Ana Blas García

Fdo. Dr. Juan Vicente Esplugues Mota

This doctoral thesis has been supported by the Instituto de Salud Carlos III, Ministerio de Economía y Competitividad (PI11/00327 and PI14/00312) and the Conselleria d'Educació, Generalitat Valenciana (PROMETEOII/2014/0359). I have been recipient of a FPU predoctoral grant (FPU13/00151) from the Spanish Ministry of Education and a mobility Short-Term Scholarship from the European Molecular Biology Organization (EMBO 7033).

Caminante, son tus huellas
el camino y nada más;
Caminante, no hay camino,
se hace camino al andar.
Al andar se hace el camino,
y al volver la vista atrás
se ve la senda que nunca
se ha de volver a pisar.

Caminante no hay camino
sino estelas en la mar.

(*Cantares.* A. Machado, 1917)

ABBREVIATIONS AND ACRONYMS

3TC	Lamivudine
ABC	Abacavir
AIDS	Acquired Immunodeficiency Syndrome
ALT	Alanine Transaminase
APS	Ammonium Persulfate
ARV	Antiretroviral
AST	Aspartate Transaminase
ATP	Adenosine Triphosphate
AZT	Zidovudine
BCA	Bicinchoninic Acid
BSA	Bovine Serum Albumin
cART	Combined ARV therapy
cDNA	Complementary DNA
CYP	Cytochrome P450
D4T	Stavudine
DAB	3,3'-Diaminobenzidine Tetrahydrochloride
DAMP	Damage-Associated Molecular Pattern Molecules
DEM	Diethyl Maletate
ddI	Didanosine
DILI	Drug Induced Liver Injury
DMSO	Dimethyl Sulfoxide
DNA	Deoxyribonucleic Acid
dsDNA	Double Strand DNA
ECACC	European Collection of Authenticated Cell Cultures
ECM	Extracellular Matrix
EDTA	Ethylenediaminetetraacetic Acid
EFV	Efavirenz
ER	Endoplasmic Reticulum
ETC	Electron Transport Chain
ETR	Etravirine
FBS	Fetal Bovine Serum
FDA	Food and Drug Administration
FTC	Emtricitabine
FU	Fusion Inhibitors
gp	Glycoprotein
GAPDH	Glyceraldehyde 3-Phosphate Dehydrogenase
GO	Gene Ontology

GSH	Glutathione
HAART	Highly Active Antiretroviral Therapy
HBSS	Hank's Balanced Salt Solution
HBV	Hepatitis B Virus
HCC	Hepatocellular Carcinoma
HCV	Hepatitis C Virus
HFD	High Fat Diet
HIV	Human Immunodeficiency Virus
HRP	Horseradish Peroxidase
HSC	Hepatic Stellate Cells
HTAB	Dexadecyltrimethylammonium Bromide
IFN	Interferon
IHC	Immunohistochemistry
II	Integrase Inhibitors
IL	Interleukin
JAK	Janus Kinase
KC	Kupffer Cells
KEGG	Encyclopedia of Genes and Genomes Pathways
LSEC	Liver Sinusoidal Endothelial Cells
MBB	Monobromobimane
MEM	Minimum Essential Medium
MMP	Metalloproteinase
MPO	Myeloperoxidase
mtDNA	Mitochondrial DNA
MTT	3-(4,5-dimethylthiazol-2-yl)-2,5-Diphenyl Tetrazolium Bromide
NAFLD	Non-Alcoholic Fatty Liver Disease
NAPQI	N-Acetyl-Para-Benzoquinoneimine
NASH	Non-Alcoholic Steatohepatitis
ND	Normal Diet
NEAA	Non-Essential Amino Acids Solution
NF-κB	Nuclear Factor κB
NNRTI	Non-Nucleoside-Analogue Reverse Transcriptase Inhibitor
NO	Nitric Oxide
NPV	Neviparine
NRTI	Nucleoside-Analogue Reverse Transcriptase Inhibitor
OxPhos	Oxidative Phosphorylation
PAGE	Polyacrylamide Gel Electrophoresis

PAMP	Pathogen-Associated Molecular Patterns Molecules
PBS	Phosphate-Buffered Saline
PCR	Polymerase Chain Reaction
PDGF	Platelet-Derived Growth Factor
PI	Protease Inhibitors
PIAS	Protein Inhibitor of Activated STAT
pol-γ	DNA Polymerase Gamma
PPAR	Peroxisome Proliferator-Activated Receptor
qRT-PCR	Quantitative-Real Time-Polymerase Chain Reaction
RIT	Ritonavir
RNA	Ribonucleic Acid
ROS	Reactive Oxygen Species
RPV	Rilpivirine
RT	Room Temperature
RT-PCR	Real Time-Polymerase Chain Reaction
SD	Standard Deviation
SDS	Sodium Dodecyl Sulfate
SEM	Standard Error of Mean
ssRNA	Single Strand RNA
STAT	Signal Transducer and Activator of Transcription
SOCS	Suppressor of Cytokine Signaling
TAF	Tenofovir Alafenamide
TBS-T	Tris-Buffered Saline-Tween
TDF	Tenofovir Disoproxil Fumarate
TEMED	N,N,N′,N′-Tetramethylethylenediamine
TGFβ	Transforming Growing Factor Beta
TIMP	Tissue Inhibitor of Metalloproteinases
TMB	3,3′,5,5′-Tetramethylbenzidine
TNFα	Tumor Necrosis Factor Alpha
TUNEL	Transferase dUTP Nick End Labeling
TYK	Tyrosine Kinase
Veh	Vehicle
WB	Western Blotting
αSMA	Alpha-Smooth Muscle Actin
$\Delta\Psi m$	Mitochondrial Membrane Potential

LIST OF FIGURES

LIST OF TABLES

RESUMEN

Durante las últimas décadas, la utilización de terapias antirretrovirales combinadas para combatir la infección por el virus de la inmunodeficiencia humana (VIH) ha convertido esta enfermedad en una patología crónica. Por ello, en la actualidad, la morbimortalidad asociada a los pacientes infectados por VIH está fundamentalmente relacionada con el envejecimiento, ciertamente acelerado en comparación con la población general, y con el efecto tóxico crónico tanto de la propia infección vírica como de la terapia antiviral. Así pues, el principal criterio clínico para la elección de unos fármacos antirretrovirales u otros es su seguridad en terapias administradas de por vida.

En la presente tesis doctoral se estudió la implicación de ciertos fármacos anti-VIH en la evolución de la enfermedad hepática aguda y crónica, así como los mecanismos celulares y moleculares responsables. En primer lugar, se estudiaron, a través de modelos *in vitro*, los mecanismos moleculares subyacentes a la toxicidad mitocondrial que presentan diversos fármacos de la familia de inhibidores de transcriptasa inversa análogos de nucleósidos (ITIAN), especialmente Abacavir (ABC) y Didanosina (ddI), en hepatocitos. De esta manera, describimos por primera vez como estos fármacos, a dosis clínicas, son capaces de reducir la actividad de los complejos I y III de la cadena de transporte de electrones mitocondrial y el consumo de oxígeno celular sin llegar a alterar significativamente su viabilidad. Sin embargo, cuando ABC y ddI se administraron en combinación con dosis clínicas de paracetamol, otro conocido fármaco hepatotóxico cuyo mecanismo también implica afectación mitocondrial, se observó una clara disminución de la viabilidad celular de los hepatocitos, con un significativo aumento de los niveles de especies reactivas de oxígeno y disminución de los niveles endógenos de glutatión. Cabe destacar que la combinación de estos ITIAN con otros fármacos cuya hepatotoxicidad no implica tan directamente a la mitocondria no produjo estos efectos citotóxicos.

El objetivo principal de la segunda parte de esta tesis fue estudiar la implicación de la terapia anti-VIH en la iniciación y progresión de la enfermedad hepática crónica. Para ello, en primer lugar, se llevaron a cabo un modelo nutricional de enfermedad de hígado graso no alcohólico (EHGNA) y diversas variantes del modelo clásico de fibrosis hepática inducida por tetracloruro de carbono en ratón. Durante la duración de los distintos modelos, distintos grupos experimentales fueron tratados diariamente, por vía oral, con dosis clínicas de distintos fármacos

antirretrovirales. Paralelamente a los modelos *in vivo*, se llevaron a cabo cultivos *in vitro* de hepatocitos y células estrelladas hepáticas, que fueron tratadas con nuestros fármacos a dosis clínicamente relevantes.

Como resumen de los datos obtenidos, podemos afirmar que, de entre los fármacos testados, Efavirenz (EFV) y Rilpivirina (RPV), pertenecientes a la familia de los inhibidores de la transcriptasa inversa no análogos de nucleósidos, ejercieron un inesperado e intenso efecto antiadipogénico, antiinflamatorio y antifibrogénico en nuestros modelos de EHGNA. Si bien el efecto antiadipogénico no queda completamente caracterizado en este estudio, sí que observamos una clara regulación de PPARγ y LXRβ en respuesta tanto a EFV como a RPV, que se traduce en una profunda reducción de la infiltración grasa en hígado. Además, el efecto antiinflamatorio de ambos fármacos parece estar claramente mediado por una inactivación de NF- κB y del inflamasoma NLRP3 así como a una disminución de la infiltración hepática de neutrófilos y macrófagos, ambas células directamente implicadas en la respuesta inmune innata.

El efecto ejercido por RPV se reprodujo también en diversos modelos de fibrosis hepática inducida por CCl_4, en los cuales fue capaz de disminuir la progresión del daño crónico y, además, contrarrestar dicha progresión cuando se administró en animales con fibrosis ya establecida. Podemos afirmar en este punto que el efecto hepatoprotector de RPV es independiente del tipo de daño producido en el hígado y se basa, fundamentalmente, en su capacidad para inducir selectivamente apoptosis en células estrelladas hepáticas a través de la activación directa del factor de transcripción STAT1. Además, RPV induce una respuesta regenerativa en hepatocitos, mediada por la activación de STAT3 inducida por el secretoma de las células estrelladas apoptóticas en respuesta a RPV, pero no por otros estímulos proapoptóticos independientes de STAT1. Cabe destacar que el efecto de RPV *in vitro* desapareció al silenciar STAT1 y que, además, este efecto se reprodujo en células estrelladas hepáticas primarias humanas.

Considerando la enorme incidencia de enfermedad hepática crónica en la sociedad actual y la ausencia de fármacos capaces de combatirla, defendemos, a través de este estudio, la posible utilización terapéutica de RPV como fármaco hepatoprotector y antifibrótico. Puesto que su seguridad a largo plazo viene dada

por su uso clínico como antirretroviral, su posicionamiento clínico requeriría únicamente de estudios confirmatorios en pacientes con enfermedad hepática crónica. De confirmarse este efecto terapéutico, supondría no solo un gran avance clínico, sino un nuevo enfoque en el desarrollo de estrategias antifibróticas cuya aplicabilidad iría más allá de la fibrosis hepática, pudiendo extenderse su estudio a trastornos fibróticos en otros órganos como riñón, pulmón, corazón o páncreas, entre otros.

ABSTRACT

In the last decades, the use of combined antiretroviral therapies (cART) has become human immunodeficiency virus (HIV) infection in a chronic disease. Thus, current clinical criteria to select the best antiviral combinations mainly rely on the safety of each drug in for life-therapeutic regimens.

In this doctoral thesis, the involvement of several antiretrovirals in the progression of both acute and chronic liver damage was studied. First of all, we assessed the mitochondrial disturbances which lead to the clinical toxicity of the nucleoside-analogue reverse transcriptase inhibitors Abacavir (ABC) and Didanosine (ddI) in hepatocytes. We described how these molecules, at clinical doses, undermined the mitochondrial function by inhibiting complexes I and III of the electron transport chain without affecting cellular viability. However, these drugs became cytotoxic in hepatocytes when they were combined with clinical doses of acetaminophen, whose hepatotoxicity also involves the mitochondria.

The second part of this study was aimed to describe the implication of the anti-HIV therapy in the onset and progression of chronic liver disease. After testing several drugs in a mouse model of non-alcoholic fatty liver disease (NAFLD), we focused on Efavirenz (EFV) and Rilpivirine (RPV), both non-nucleoside analogue reverse transcriptase inhibitors (NNRTI), because they exerted an unexpected and surprising anti-adipogenic, anti-inflammatory and anti-fibrogenic effect in the liver. To further analyse this effect, we performed both mouse models of CCl_4-induced liver fibrosis and *in vitro* studies with hepatocytes and hepatic stellate cells (HSC). In this case, we were able to reproduce the RPV-induced hepatoprotective effects observed in the rest of animal models, confirming that this drug exerts a striking anti-inflammatory and anti-fibrotic role in the liver. Additionally, we described that this effect is directly mediated by a selective induction of apoptosis in HSC, which depends on the activation of the transcription factor STAT1 in these cells. At the same time, the secretome of RPV-induced apoptotic HSC activates an intense regenerative response in the liver mediated by STAT3 activation in hepatocytes.

Considering that there is no cure for either NALFD or liver fibrosis, the relevance and the clinical applicability of this study is evident. We defend the utilization of RPV in all those HIV-infected patients with special susceptibility to liver disease. Furthermore, we also propose RPV as a potential anti-fibrotic drug, whose effectivity should be tested in patients with chronic liver disease in the next future.

Finally, we encourage the scientific community to deeply explore the role of JAK-STAT1 and 3 in the different cell subsets within the liver, as well as in other organs, as key targets to therapeutically manage different fibrotic disorders.

Chapter I: INTRODUCTION

I.A. HUMAN IMMUNODEFICIENCY VIRUS (HIV) AND ANTIRETROVIRAL THERAPY

I.A.1. HIV life cycle and infection

HIV is a retrovirus which includes two subtypes, HIV-1 and HIV-2. HIV-1 is more pathogenic and more prevalent than HIV-2, and is the main responsible for the pandemic known as acquired immunodeficiency syndrome (AIDS) [1,2]. HIV has infected over 78 million people since 1981 and is one of the main causes of morbidity and mortality worldwide. The highest burden of HIV is carried by Sub-Saharan Africa with more than 70.8% of the global infected population, especially Southern Africa [3,4]. According to the last official statistics, in 2017 there were 36.9 million people living with HIV, of which approximately 1.9 million were newly infected and 0.9 million died of the infection [5].

Activated CD4+ T lymphocytes are the main target of HIV, and its entry into cells is mediated by the binding of the viral *Env* glycoprotein to cell surface proteins CD4 and the chemokine co-receptors CXCR4 and CCR5. Other cells with these receptors are also infected, such as resting CD4+ T cells, macrophages, monocytes and dendritic cells [3]. Moreover, HIV infection can happen independently of the CD4 receptor, as occurs in astrocytes [6] and renal tubular epithelial cells [7]. Like all retroviruses, the genome of HIV is composed of two copies of single strand- (ss)RNA which is transcribed to double strand- (ds)DNA by the viral reverse transcriptase and is then integrated into the genome of the host cell by the viral integrase to allow viral replication. Viral protease activates newly formed virions by cleaving polyproteins from their surface into active infectious proteins (Figure I.1) [8,9].

HIV infection typically occurs by sexual transmission following exposure to cell-associate or cell-free infectious virus in semen or mucosal surfaces [3,10]. It is estimated that 50-90% of patients experience an acute HIV syndrome after two or four weeks following infection, a period during which HIV replicates aggressively, reaching the highest plasma levels of viral RNA (1-10 million copies/mL) [10,11]. The acute HIV syndrome is characterized by flu-like symptoms associated with high viral load, fever and lymphadenopathy [12]. Once the immune system develops a HIV-specific response, the viremia declines markedly for several months reaching the viral set point and most patients exhibit a period of

clinical latency that can last for years [10]. During this period, patients suffer a progressive depletion of the CD4+ T cells with a deterioration of the immune system, which leads to the development of an immunodeficiency status, or AIDS, where the individuals are more susceptible to opportunistic infections [2].

The different steps of the viral life cycle within the host cells (entry, reverse transcription, genome integration and proteolytic maturation) can be inhibited by several molecules commercially available which constitute the current pharmacological treatment of HIV infection. Nowadays, the availability and efficacy of these antiretroviral (ARV) drugs frequently avoid the development of AIDS in HIV-infected patients because of their high efficiency attenuating viral replication.

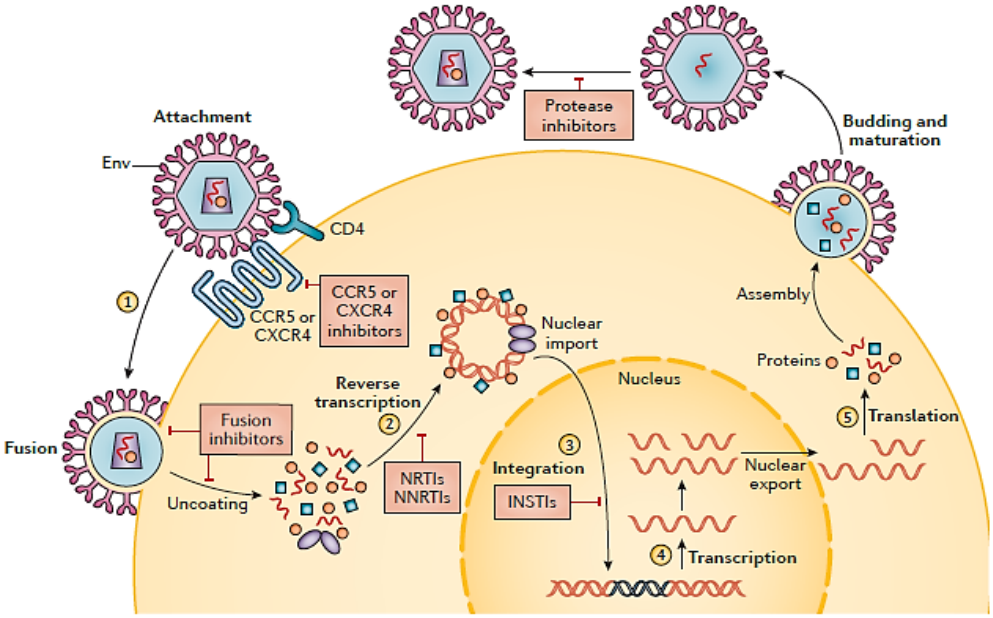

Figure I.1 Overview of HIV life cycle indicating the steps inhibited by ARV drugs [13].

I.A.2. ARV drugs

The first advance in anti-HIV therapy was made in 1987, when the US Food and Drug Administration (FDA) approved zidovudine (AZT) to treat HIV infection. AZT was originally developed for cancer treatment, but it was observed that its use decreased opportunistic infections and mortality in patients with AIDS. However, this monotherapy quickly developed viral resistance and the ineffectiveness of long-term therapy forced the development of newer anti-HIV compounds [14,15]. Anti-HIV drugs were mainly classified by the viral enzyme they targeted and by the endogenous biomolecule they mimicked. Thus, the first anti-HIV agents were

nucleoside analogue reverse transcriptase inhibitors (NRTI), non-nucleoside analogue reverse transcriptase inhibitors (NNRTI) and protease inhibitors (PI). Although they were individually active and produced a rapid decay in viremia, the success was limited, once again, due to the appearance of viral resistances and toxic effects [16,17]. The modern era of ARV therapy began in 1997 with the introduction of the combined ARV therapy (cART), or highly active ARV therapy (HAART), consisting in the combination of three different antivirals. cART effectively suppressed the HIV replication cycle, reduced HIV viral load and increased circulating levels of CD4+ T lymphocytes, resulting in a restoration of immune system [3]. The success of cART comes from the combination of different molecules directed against, at least, two different stages of the viral cycle, decreasing the probability of selecting virus clones and thus preventing the evolution of drug resistance. Although cART cannot completely eliminate the virus, this therapeutic regimen has transformed AIDS from a progressive and fatal disease to a chronic manageable infection, markedly reducing their associated morbidity and mortality [16,18].

The range of available drugs has continued to expand and, currently, 26 antiviral drugs are approved for use in adults by European and US agencies. They are classified in six families, each targeting a specific stage in the HIV replication cycle (Figure I.1): NRTI, NNRTI, PI, integrase inhibitors (II), fusion inhibitors (FI) and CCR5 co-receptor antagonist [16,18].

Due to their special relevance for this thesis, only NRTI and NNRTI will be further explained in the following sections.

a) Nucleoside reverse transcriptase inhibitors

NRTI were the first agents approved by FDA for the treatment of HIV infection (Table I.1) [19]. These drugs are analogues of the natural nucleoside substrates and are integrated preferentially into viral DNA [2]. NRTI are pro-drugs and hence, they need to be incorporated into the host cell and phosphorylated by cellular kinases in order to gain an antiviral effect [20]. NRTI inhibit HIV replication by substituting endogenous nucleotides during the reverse transcription of viral RNA, leading to the termination of the elongation of the new viral DNA chain [18,21,22]. Unluckily, they also act as substrates for DNA polymerase gamma (pol-γ) of host cells, and their interference with mitochondrial DNA (mtDNA) synthesis

leads to a reduction in the mtDNA content, thus inducing mitochondrial toxicity [22–24].

b) Non-nucleoside reverse transcriptase inhibitors

These drugs (Table I.1) are non-competitive inhibitors of HIV-1 reverse transcriptase by binding close to its active site and inducing the formation of a hydrophobic pocket, which causes a conformational change of the enzyme and reduces its activity [25]. NNRTI exhibit a substantial interindividual variability in their pharmacokinetics; therefore, their plasma levels can differ greatly among different patients. As these drugs are bio-transformed through cytochrome P450 (CYP) system and exert variable effects on specific isoenzymes, they can trigger variable effects on other drugs whose metabolism occurs through the same pathway [26,27].

NRTI	**Approval date**
Tenofovir alafenamide (TAF)	November 5, 2015
Emtricitabine (FTC)	July 2, 2003
Tenofovir disoproxil fumarate (TDF)	October 26, 2001
Abacavir (ABC)	December 17, 1998
Lamivudine (3TC)	November 17, 1995
Stavudine (d4T)	June 24, 1994
Didanosine (ddI)	October 9, 1991
Zidovudine (AZT)	March 19, 1987
NNRTI	**Approval date**
Rilpivirine (RPV)	May 20, 2011
Etravirine (ETR)	January 18, 2008
Efavirenz (EFV)	September 17, 1998
Neviparine (NPV)	June 21, 1996

Table I.1 NRTI and NNRTI drugs approved by FDA, 2018 [28].

I.A.3. Guidelines of ARV therapy

According to the current guidelines, first-line cART in adults consists of two NRTI combined with a third agent that can be a NNRTI, an II or a PI [29,30]. This combined therapy is largely considered the standard treatment for HIV-infected patients, both anti-HIV drug-naïve and drug-experienced individuals [31,32]. It was designed to decrease the probability of developing drug resistance, to reduce specific drug side effects by diminishing their individual dosages and to obtain a synergic effect between different drugs that exert their pharmacological action at different molecular targets [33].

Due to the fact that cART only suppresses HIV replication and does not eradicate it, HIV patients must be exposed to ARV compounds for decades, obtaining extended virologic suppression, improved clinical results and longer life expectancy. Moreover, due to this demographic aging shift, these patients are concomitantly treated for several age-related non-AIDS disorders, such as cardiovascular diseases, liver diseases, neurocognitive diseases or cancer [34–36]. Hence, treatment guidelines should recommend regimens based not only on their antiviral potency but also on their chronic toxicity. Although knowledge about ARV drugs toxicities is increasing, there is still not enough evidence to firmly establish which ARV drug class or combinations are safer in each patient [13,36].

I.A.4. Side effects of ARV therapy

ARV resistance, adherence and toxicity are the main problems of cART, which must be overcome in order to optimize their clinical efficacy. cART-related toxicity and adverse effects have been described with all ARV drugs, and have been considered the most common reason for discontinuing cART. The majority of cART-induced adverse effects arise from the therapeutic doses of ARV drugs and drug-drug interactions [37,38]. Overall, gastrointestinal disturbances, hypersensitivity and skin reactions, neuropsychiatric disorders and liver toxicity tend to appear early after initiation of treatment. Other side effects, such as lipid and glucose metabolism abnormalities, kidney alterations, bone metabolic disorders and mitochondrial toxicity, generally develop after chronic exposure to these drugs. (Tables I.2 and I.3) [39–41].

Different factors may influence the appearance of side effects, including gender, underlying diseases, concomitant medications and drug interactions, diet and genetic factors. Regarding the latter, the administration of standard doses of most anti-HIV drugs results in significant individual variations in their plasma concentrations and in their subsequent related toxicity due to differences in their metabolism [42,43].

Drug class	Adverse effects	Comments
NRTI	Nephrotoxicity	TDF
	Hypersensitivity reactions	Seen with ABC in human leukocyte antigen B*57:01-positive individuals
	Lactic acidosis	Rare. Common with AZT
	Lipoatrophy	AZT
	Loss of bone mineral density	Prolonged TDF use
	Bone marrow suppression, macrocytic anemia	AZT
	Fanconi syndrome	Rare condition associated with TDF
	Myopathy	AZT
	Increased risk of cardiovascular events	ABC, ddI
	Diarrhea, pancreatitis, neuropathy	ddI
	Non-cirrhotic portal hypertension, hepatic steatosis	Can occur months to years after starting ddI and d4T
	Hyperpigmentation	FTC

Table I.2 Common NRTI-associated adverse effects [28,44].

Drug class	Adverse effects	Comments
NNRTI	Several drug interactions	Mostly noted with EFV
	Rash	All NNRTI
	Neuropsychiatric side effects	Mostly associated with EFV. RPV has also been related to psychiatric effects
	Hepatic effects	NVP > other NNRTI
	Dyslipidemia	Mostly associated with EFV
	Stevens-Johnson syndrome	NVP > other NNRTI
	Teratogenicity	EFV
	Cardiovascular diseases	RPV: QT interval prolongation

Table I.3 Common NNRTI-associated adverse effects [28,44].

Mounting evidence shows that newer ARV display safer profiles than first-generation molecules, but drug-related adverse effects and drug interactions are still a big problem in the therapeutic managing of HIV infection. On the other hand, it is important to emphasize that the vast majority of HIV-infected people live in areas where the older ARV agents with worse side effects are still often prescribed as major treatments due to the lack of infrastructures and economic resources [41].

I.A.5. Drug-induced liver injury (DILI)

a) HIV infection, cART and liver disease

Introduction of effective cART has made HIV infection a chronic illness. Substantial reductions in the number of AIDS-related deaths have been accompanied by an increase in liver-related morbidity and mortality. In this regard, liver diseases rank in the three most-common causes of death in HIV-infected people [34,45,46]. ARV drug-associated toxicity arises as a key factor contributing to this morbidity and mortality since they are currently used in lifelong regimens, and their long-term security acquires an especial relevance and determines their use [47,48].

b) ARV therapy-associated hepatotoxicity

Hepatotoxicity, or DILI, is one of the most common disadvantages of cART, responsible for morbidity, mortality and treatment discontinuation in HIV-infected patients [49–51]. Elevated liver enzyme levels have been employed as a marker of liver toxicity in different clinical trials and cohort studies. AIDS Clinical Trials Group defined severe liver toxicity as presence of an increase in plasma aspartate transaminase (AST), alanine transaminase (ALT) and alkaline phosphatase levels greater than five- and two-fold above the upper normal limit, respectively [52,53]. Following this criterion, many studies have shown that the incidence of increased liver transaminases levels is around 2-18% after one or more months on cART, or even up to 30% in some reports [54,55]. It is difficult to ascertain the liver toxicity associated with each ARV because its combined administration, the co-exposure to other liver toxins or the presence of pre-existing hepatic conditions [56,57]. Nevertheless, extensive use of these compounds

has contributed to elucidate that AZT, ddI and d4T, as well as NVP and EFV are the most potentially hepatotoxic drugs among NRTI and NNRTI, respectively [51,58]. Besides the toxicity associated with a specific ARV drug or class, other risk factors have been associated with cART-induced liver injury in HIV-infected patients. One of the main non-drug related factors is chronic hepatitis produced either by hepatitis C (HCV) or hepatitis B (HBV) viruses, considering that co-infected patients experience up to 6 times greater increases in plasma levels of liver enzymes compared to HIV mono-infected patients. Other situations like severe alcohol consumption, drug abuse, drug interactions, age, gender or ethnicity also contribute to cART-induced liver damage [51,59]. The severity of this hepatic injury ranges from transient liver enzyme elevations to severe clinical syndromes, such as hepatitis, non-alcoholic fatty liver disease (NAFLD) or steatohepatitis (NASH), non-cirrhotic portal hypertension or even acute liver failure, which can eventually lead to death [41,50].

Importantly, it is assumed that newer ARV drugs are safer for the liver. However, due to the aging of HIV-infected patients, cART-associated liver toxicity will probably continue to be a major challenge in the future [60,61].

c) Acetaminophen-induced liver injury

Acetaminophen (APAP), or paracetamol, is a widely used analgesic and anti-pyretic drug used for the relief of fever and different minor aches and pains. It is extremely safe when administered at therapeutic doses but, due to its wide availability, deliberate or accidental overdoses are not uncommon. APAP, unlike other common analgesics such as aspirin and ibuprofen, has no anti-inflammatory properties or effects on platelet function, and it is not a member of the drug family known as non-steroidal anti-inflammatory drugs [62,63].

The therapeutic dose of APAP in adults is between 325 and 1000 mg, administered every 4 to 6 hours, with a maximum recommended daily dose of 3250 mg. Peak concentrations of APAP are achieved within the first 90 min after oral ingestion, and the therapeutic serum concentrations range from 10 to 20 mg/mL. Its protein binding is minimal at therapeutic doses and the serum half-life is around 2 hours. Approximately 85% to 90% of APAP at clinical doses undergoes phase II conjugation to sulfated and glucuronidated metabolites, which are then excreted in the urine; 2% of ingested APAP is excreted in the urine

unchanged and up to 10% undergoes phase I oxidation via the hepatic CYP2E1 to a toxic and highly reactive intermediate, N-acetyl-para-benzoquinoneimine (NAPQI). The small amount of NAPQI produced from normal doses of APAP is rapidly conjugated with hepatic glutathione (GSH), forming non-toxic mercaptate and cysteine compounds that are then excreted in the urine. At toxic doses of APAP, sulfation and glucuronidation pathways become rapidly saturated and more APAP is metabolized through CYP2E1 to NAPQI. Thus, this amount of NAPQI saturates and depletes GSH stores, binds to hepatocytes and causes cellular damage in an irreversible step that leads to oxidative injury and hepatocellular necrosis. Other mechanisms that are likely to play an important role in the early-phase of APAP-induced hepatotoxicity include mitochondrial damage, nuclear DNA fragmentation and lipid peroxidation [64–66]. Consequently, APAP is frequently used as a well-established model of DILI, both in *in vivo* and *in vitro* models, due to the induction of mitochondrial damage and reactive oxygen species (ROS) production [67].

I.A.6 ARV drugs especially relevant for this thesis

a) ABC

ABC (Figure I.2.A) is a NRTI that was approved and marketed all over the world by *GlaxoSmithKline* in 1998 as a single drug entity with the name of Ziagen®. It has been extensively used for more than 20 years for the treatment of HIV-1 infection, and it is still currently included as a first-line treatment option in combination with other ARV [68].

The recommended dose of Ziagen® for adults is 600 mg daily and can be taken either as a single daily dose or divided into 300 mg twice a day. As this compound has been widely employed in long-term treatments its toxicological profile has been well-established, being its most common side effects loss of appetite, headache, nausea, diarrhea, rash, fever and lethargy. Life-threatening hypersensitivity reactions can also occur in patients taking ABC within the first weeks of treatment, thus leading to treatment discontinuation [69,70].

ABC is primarily metabolised by the liver and its use is not recommended in patients with moderate or severe hepatic impairment unless judged necessary by clinicians, in which case close monitoring is required [71,72]. Clinical studies have

shown that there are no clinically significant interactions between ABC and others ARV drugs, which simplifies its therapeutic management [73].

All NRTI have been proven to cause a variable degree of mitochondrial damage *in vitro* and *in vivo*, especially the oldest compounds. These effects are particularly important in the context of liver toxicity, since mitochondrial activity is crucial for hepatocyte metabolism and hepatic function [73,74].

b) ddI

This NNRTI (Figure I.2.B) was approved and marketed in 1991 by *Bristol-Myers Squibb Pharmaceuticals* under the name of Videx®. Its recommended posologies are 250 mg per day for patient weighting less than 60 kg in a single dose and 400 mg for patients weighting more than 60 kg, divided in 200 mg twice a day. The toxicological profile of this compound is worse than those of newer NRTI, like ABC, and thus, its use is restricted to those patients in which other ARV drugs cannot be used [75,76]. Regarding its pharmacokinetics, ddI follows the same metabolism and elimination pathways that endogenous purines. Its half-life is really short, around 1.4 hours, and it is eliminated by renal clearance in an active tubular secretion process.

Besides the general gastrointestinal and hypersensitivity side effects related to all NRTI, ddI treatment has also been associated with acute pancreatitis, peripheral neuropathies and lipodystrophic processes leading to important subcutaneous fat accumulation [77,78]. Liver toxicity has rarely been observed in patients on ddI, but few cases of adverse events leading to liver transplantation have been described. Consequently, ddI administration should be closely monitored in all cases, and discontinued if hepatic enzymes rise to more than 5 times the upper limit of normality [74]. In addition, it is described that patients with pre-existing liver dysfunction have an increased frequency of liver function abnormalities during ddI treatment. Therefore, it is crucial to clarify the mechanisms leading to this ddI-induced liver damage in order to improve their clinical management [77,79].

c) EFV

EFV (Figure I.2.C) is a NNRTI developed by *Bristol-Myers Squibb Pharmaceuticals* in 1995 and marketed, after its approval by FDA, in 1998 as

Sustiva® in its single drug formulation. This compound has been widely employed during the last 20 years but, due to the availability of new ARV drugs with a safer toxicological profile (e.g. II), it is currently part of alternative cART regimens in developed countries. However, EFV is still one of the most commonly used anti-HIV drugs in developing countries because of its high efficacy and low cost [80–83]. Due to its long half-life (45-52h), the recommended dose of EFV in adults is 600 mg in one-daily dose. It usually results in plasma levels from 5.6 ± 3.2 µM to 12.9 ± 3.7 µM. Nevertheless, EFV plasma levels vary substantially as a result of interindividual variability in its pharmacokinetics, with levels as high as 30-50 µM in up to 40% of EFV-treated patients [84,85].

EFV is commonly considered an effective and safe drug [81,86]. Nevertheless, there is concern about the adverse effects induced by EFV-containing cART, including rash, neuropsychiatric disorders, lipid and metabolic disturbances and liver toxicity [87–90]. EFV-induced DILI has been reported in 1-8% of treated patients and it is correlated with significant morbidity and mortality [91–93].

The molecular mechanisms underlying this EFV-induced DILI remain unclear. Mitochondrial toxicity has been involved in the liver toxicity related to cART, but it has been usually attributed to NRTI and their ability to inhibit pol-γ [94,95]. However, the mechanism behind EFV-induced liver toxicity is different: *in vitro* experiments previously performed by our group have shown that acute treatment with EFV provokes deleterious effects in hepatocytes, inducing mitochondrial dysfunction through direct inhibition of complex I of the electron transport chain (ETC), and thus decreasing ATP production and mitochondrial membrane potential ($\Delta\Psi_m$), which finally leads to a rapid intracellular increase of lipid droplets. Furthermore, bioenergetic stress, elevated ROS, endoplasmic reticulum (ER) stress and cell survival-promoting autophagy were also reported in EFV-treated cells, suggesting mitochondria as a common key player in all these acute toxic effects [96–102].

In addition, several clinical studies have reported that hepatic alterations induced by EFV appear shortly after initiation of the treatment and rapidly disappear in several days or weeks [103,104]. In summary, long-term therapies containing EFV are largely considered safe to the liver [103,105].

d) RPV

RPV (Figure I.2.D) is the newest second-generation NNRTI, which was approved and marketed by *Janssen-Cilag International NV* in 2011 with the name of Endurant®. The recommended daily dose of RPV is 25 mg and it is primarily metabolised by CYP3A. For this reason, medicinal products that interact with these enzymes may thus modify the clearance of RPV [106].

The safety profile of RPV includes many frequently reported adverse reactions like headache, insomnia, rash and abdominal pain. Few cases of increased liver enzymes were also reported. However, it is important to consider that all those adverse reactions were observed in the first months following the treatment initiation and resulted in early small alterations that were rapidly normalized, thus not being considered clinically relevant [106].

Regarding RPV pharmacokinetics, after oral administration it has fast absorption, good bioavailability and approximately 99.7% is bound to plasma proteins. Moreover, RPV is primarily metabolised and eliminated by the liver by CYP3A4 and its plasmatic half-life is approximately 45 hours. It has also been described a considerable hepatic bioaccumulation of RPV, and thus, it can reach higher concentrations within the liver than in plasma. Even though it is not in the first line of HIV treatment, is one of the most used NNRTI worldwide because it is safer and presents an easy dosing regimen that improves adherence and clinical efficacy [107–109].

RPV has only been clinically used since 2011 and its long-term effects are still under study. However, in the last years, several ongoing clinical studies have reported that chronic RPV treatment is mainly safe for the liver [110,111]. These retrospective studies have demonstrated that the frequency of liver toxicity in both HIV-patients and HIV/HCV-coinfected patients receiving RPV-containing regimens is extremely low and does not lead to drug discontinuation [47]. Furthermore, many different prospective and retrospective studies have shown that RPV could be even beneficial since it is able to improve the lipid profiles of dyslipemic HIV patients after switching from non-RPV-containing therapies [112,113]. Finally, it has also been demonstrated that treatment with RPV is still effective even in patients whose liver function is severely impaired, like in HCV-HIV co-infected cirrhotic patients [110].

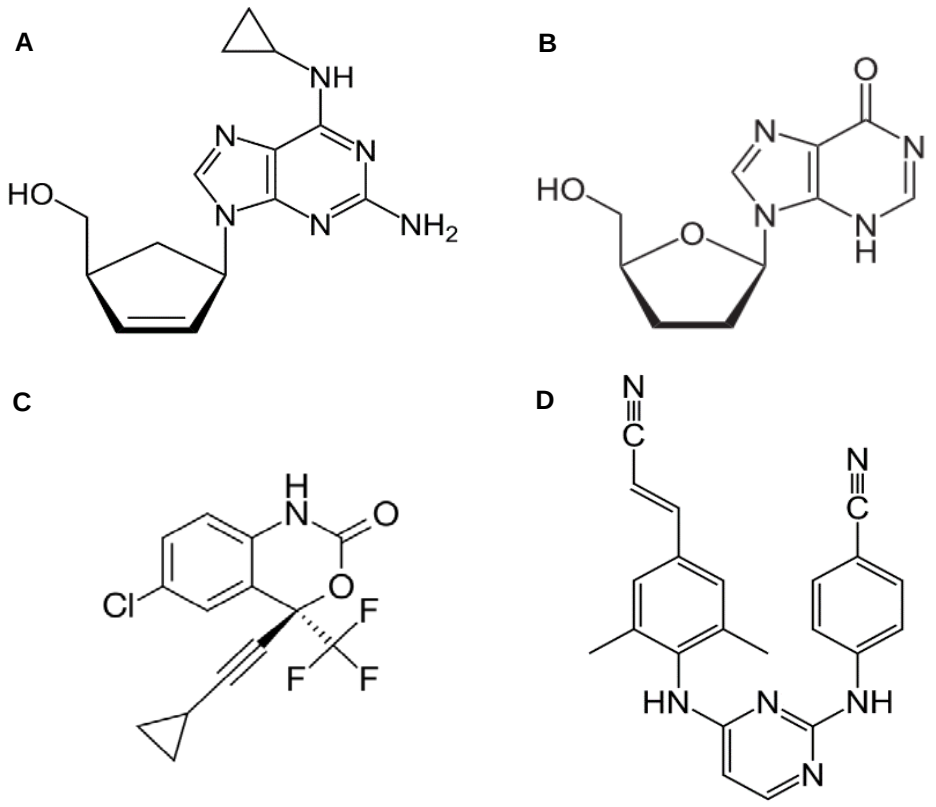

Figure I.2. Chemical structure of Abacavir (A), Didanosine (B), Efavirenz (C) and Rilpivirine (D).

I.B. LIVER PATHOPHYSIOLOGY

I.B.1. Liver physiology and functional structure

The liver is a central organ that carries out a wide range of crucial functions for the organism such as metabolism, glycogen storage, drug detoxification, production of serum proteins and bile secretion. To develop these purposes, the liver requires a high level of vascularization, slow blood flow and highly permeable fenestrated endothelia, which allows direct contact between liver cells and blood stream. Since all those liver functions are essential for homeostasis maintenance, severe liver diseases, such as hepatitis, fibrosis and cirrhosis, often result in high rates of morbidity and mortality [114–116].

Liver structure is organized forming many lobules, which constitute its functional units (Figure I.3.A). Each lobule is composed of a central vein from which hepatocyte cords radiate towards portal triads (portal vein, hepatic artery and biliary duct). Hepatocyte cords are single-cell sheets of hepatocytes separated by sinusoids that carry blood from the portal triads to the central vein. Each lobule (Figure I.3.B) contains a varied number of sinusoids, which are discontinuous

vessels built from specialized fenestrated liver sinusoidal endothelial cells (LSEC) of the liver. Hepatic stellate cells (HSC) are located in the space of Disse between the hepatocyte cords and sinusoids. Kupffer cells (KC), which are the specialized resident macrophages of the liver, are also found in sinusoids [115,117,118].

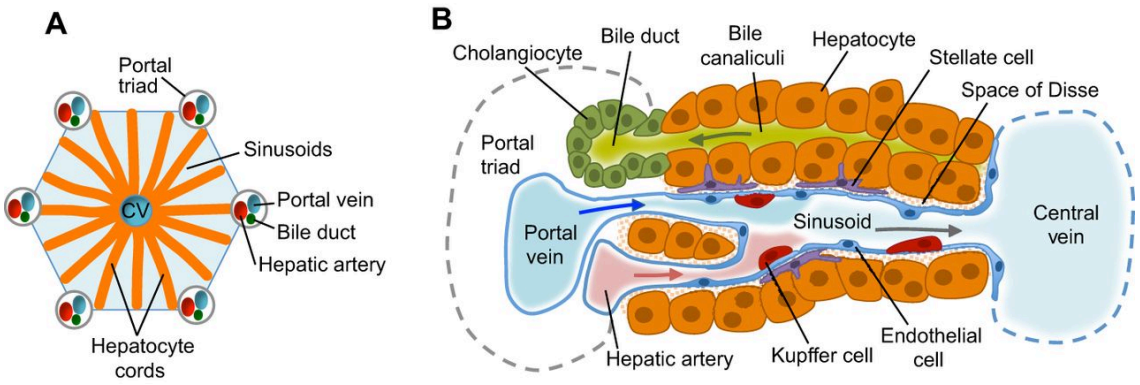

Figure I.3 Functional structure of the liver: hepatic lobule (A) and liver sinusoid (B) [119].

I.B.2. Key cellular players in liver health and disease

a) Hepatocytes: from homeostasis to liver injury

Most of the metabolic and synthetic functions of the healthy liver are carried out by hepatocytes, which account for approximately 60% of total liver cells and 80% of liver volume. Hepatocytes are highly polarized epithelial cells: their basolateral surfaces face fenestrated LSEC, facilitating the exchange of materials between hepatocytes and blood vessels [119,120].

Liver injury can result from multiple etiologies in different pathophysiological contexts but, in many cases, it occurs due to direct damage of hepatocytes, which is considered the main driver of liver inflammation. Once liver damage has occurred, injured and dying hepatocytes release a wide range of pro-inflammatory signals, generally known as damage-associated molecular pattern molecules (DAMP) [121,122]. These DAMP are a group of chemically heterogeneous molecules also known as alarmins due to their capability to alert the immune system. They include, among other molecules, ROS, phagocytosis mediators, pro-inflammatory and chemotactic molecules, immunostimulatory and immunosuppressive mediators, activators of repair pathways as well as proliferation-associated cytokines [123–125]. Through this DAMP-associated response, damaged hepatocytes interact with surrounding cells (including

neighbouring hepatocytes, HSC, KC, LSEC and infiltrating immune cells) and strongly activate the inflammatory response in the liver, leading to HSC activation, which is the first step to fibrosis progression (Figure I.4 and I.7) [116,126].

In hepatocytes, mitochondria are the main source of DAMP. This organelle is able to sense and react to multiple cellular stresses. It can be considered as a master regulator of danger signaling since it is able to control and activate both cell-intrinsic and systemic adaptive responses through distinct molecular pathways [127–129]. ROS generation by hepatic mitochondria usually comes as a normal by-product of the mitochondrial respiratory chain, mainly produced by ETC complex I and III. This ROS production is physiologically counteracted by a wide range of anti-oxidant systems, which include catalases, superoxide dismutases, thioredoxin and GSH. However, in response to multiple stimuli or organelle disorders (e.g. mitochondrial dysfunction), ROS production exceeds the buffer capacity of the endogenous anti-oxidant systems, resulting in oxidative stress. This effect leads to the activation of a cellular response in order to re-establish the redox homeostasis and this can be coupled to an inflammatory response, followed by cellular damage, progressive mitochondrial dysfunction and cell death by apoptosis or necrosis [130–132].

b) HSC: inductors of fibrogenic response

HSC are non-parenchymal cells within the perisinusoidal space of Disse, interposed between sinusoidal endothelium and hepatocytes. This privileged localization, besides their dendritic cytoplasmic processes, facilitates their direct contact with other HSC, hepatocytes, LSEC and KC [133,134]. HSC contribute to key homeostatic functions of the liver such as development and regeneration (e.g. quiescent HSC can produce hepatocyte and vascular endothelial-growth factors), retinoid metabolism (they are the main reservoir of vitamin A in the organism), extracellular matrix (ECM) homeostasis, lipid metabolism, immunoregulation and drug detoxification [135,136].

Besides these important functions, when the liver is injured, HSC coordinate a tightly regulated cellular network, which results in net deposition of fibril-forming collagen-rich ECM at the sites where liver has been damaged. To develop the scar, activated HSC undergo trans-differentiation of quiescent vitamin A-rich cells to myofibroblast-like cells, which are characterized by augmented proliferation

and migration, loss of lipid droplets, abundant secretion of ECM proteins, enhanced contractility and release of pro-fibrogenic (e.g. transforming growing factor (TGF) β) and pro-inflammatory factors (e.g. interleukin (IL) 6 and IL8) [137,138]. Activated HSC are characterized by an enhanced expression of alpha-smooth muscle actin (αSMA), desmin and vimentin, massive secretion of scar-forming type I and III collagens (among other ECM proteins), and expression of a wide range of matrix metalloproteinases (MMP, such as MMP2 and MMP9) and specific tissue inhibitors of metalloproteinases (TIMP, such as TIMP1), proteins that prevent matrix MMP-directed degradation of collagen, thus allowing the scar formation (Figures I.4 and I.7) [133,139,140].

HSC activation involves two well-established stages: initiation (or pre-inflammatory stage) and perpetuation. Initiation refers to early events initiated by paracrine signals from neighbouring cells that render the cells responsive to many extracellular signals. The signals involved in this HSC-activating process include ROS, lipopolysaccharide and other pathogen-associated molecular patterns (PAMP), lipid peroxides, nucleotides, inflammatory cytokines, apoptotic bodies and other cell death signals. Many viral agents have been also reported to directly activate HSC, including HCV, HBV and HIV [140,141]. Perpetuation is characterized by events that amplify the activated phenotype of HSC: sustained release of cytokines and growth factors, predominantly from macrophages, results in retinoid loss, scar formation through enhanced proliferation, contractility, fibrogenesis, matrix degradation and pro-inflammatory signaling (Figure I.4) [140–142].

Apart from their crucial role in fibrogenic responses, HSC functions are much more diverse. For example, they also play a crucial role in the inflammatory and immune responses since they are highly responsive to DAMP, resulting in the activation of pro-inflammatory pathways, such as those regulated by nuclear factor κB (NF-κB), and subsequent production of pro-inflammatory cytokines and chemokines. These enhanced inflammatory responses can induce hepatocyte cell death, and thereby enhance and perpetuate fibrogenic stimuli [143,144].

It is important to note that HSC produce lower cytokine levels when compared to immune cells, thus contributing minimally to overall liver inflammation. In this regard, HSC probably behave as recipients of inflammatory signals to regulate their activation and subsequently ensure their survival [145]. During liver injury,

activated HSC can also modulate the hepatic immune response by acting as antigen presenting cells and expressing several chemokines (e.g. CCL2, CXCL10, CCL5) and integrins (e.g. VCAM1, ICAM1), thereby altering the adaptive immunity and modifying immune cell chemotaxis, respectively [144,146].

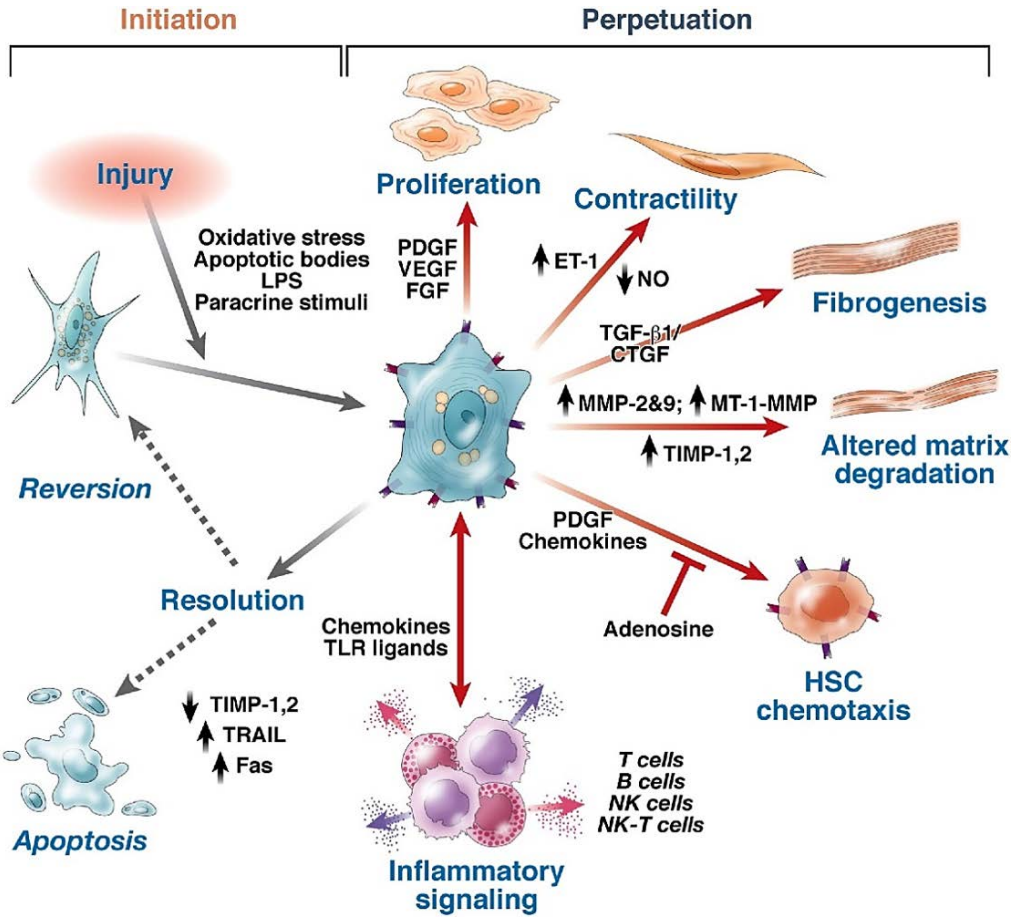

Figure I.4 Pathways of HSC activation, including initiation and perpetuation phases as well as paracrine crosstalk among different liver cell subtypes [134].

c) Macrophages: coordinating liver-associated immune response

The liver shelters roughly 80% of all macrophages in the body, and they are divided in two main types depending on their origin: resident liver macrophages or KC, which are positioned in liver sinusoids, and inflammatory macrophages derived from infiltrating blood monocytes [147,148]. Liver macrophages are key players in hepatic inflammation and also hold remarkable functional diversity, being implicated in hepatic homeostasis, progression and regression of acute and chronic inflammation and fibrosis [116]. Their pleiotropic actions and diverse roles in liver diseases are due to their high plasticity, as a response to

environmental signals arising from parenchymal and immune cells. Macrophages have been traditionally categorized either into ‘pro-inflammatory’ M1 or ‘immunoregulatory’ M2, but now it is known that the complex biology of macrophages subsets is not reflected by this simple dichotomous nomenclature [147,149].

Beyond these classifications, it is well known that upon liver injury macrophages can develop multiple actions depending on their microenvironment, which is finely regulated by multiple processes, including transcription factors, epigenetic mechanisms, signaling pathways and post-transcriptional regulators [150]. Pro-inflammatory actions of macrophages are induced by, among others, pro-inflammatory cytokines, lipoproteins or necrotic cells, and are controlled by different transcription factors like NF-κB or signal transducer and activator of transcription (STAT) 1. These actions usually lead to high production of nitric oxide (NO) and ROS, and the secretion of pro-inflammatory cytokines and chemokines, promoting Th1 response and strong tumoricidal and microbicidal activity [151,152]. Conversely, a predominance of STAT6, STAT3 and peroxisome proliferator-activated receptor (PPAR) γ activation promotes immunoregulatory, wound-healing and pro-resolutive responses by macrophages, mostly conducted by efficient phagocytosis and secretion of many immunomodulatory mediators [150,153,154].

During liver damage, hepatocyte injury triggers release of DAMP and subsequently activates innate immune and tissue-destructive responses via the production of NF-κB-dependent pro-inflammatory cytokines and ROS. This results in a dramatic expansion of hepatic macrophage population with their subsequent polarization towards the M1 phenotype and release of additional inflammatory mediators enhancing the inflammatory response, which may increase hepatocyte cell death (Figure I.5) [147,155]. Importantly, at the later stages of inflammation or once the liver insult has been eliminated, macrophages may undergo a functional switch towards pro-resolving or anti-inflammatory M2-like phenotype in order to repair damaged tissue [148,149].

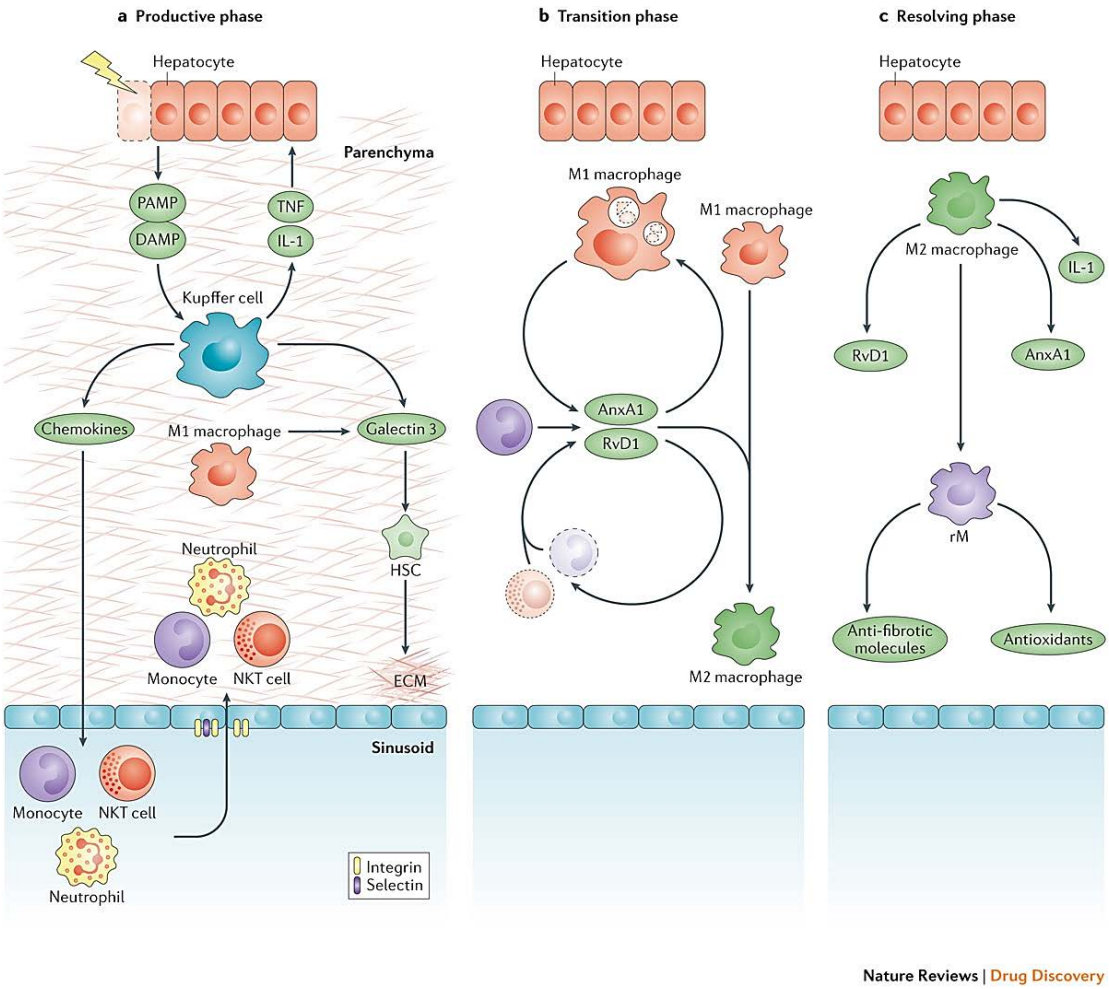

Figure I.5. Interplay between macrophages, hepatocytes and immune cells during liver inflammation and resolution. a) When liver injury occurs, DAMP and PAMP are firstly recognized by KC which undergo M1 phenotype, produce pro-inflammatory chemokines and increase hepatocyte apoptosis. Endothelial cells increase the immune cell recruitment by expressing different adhesion molecules. In addition, HSC undergo activated. b) Afterwards, macrophages switch to pro-resolving M2 phenotype and trigger leukocyte apoptosis and phagocytosis of damaged cells. c) In the last phases of resolution, M2 macrophages increase their phagocytic activity and produce big amounts of anti-inflammatory, anti-fibrotic and pro-resolving molecules which attenuate immune cell recruitment and inflammation and restore tissue homeostasis [106].

I.B.3. Liver immunology

From an immunological point of view, liver homeostasis is regulated through an intense intercellular interplay between parenchymal and non-parenchymal cells. Hepatocytes and cholangiocytes, as well as LSEC, KC and HSC act as primary sensors for pathogens and PAMP from enterohepatic microcirculation. Moreover, LSEC and KC are capable of antigen presentation, as well as of cytokine and chemokine production. Thus, it is easy to understand the importance of the liver to initiate and shape immune responses [116,156,157].

The role of different immune cell types in the initiation, progression and resolution of liver injury depends on their capacity to induce changes in the HSC phenotype (Figure I.6) [134,135]. As it has previously been explained, hepatocytes and liver macrophages directly interact with HSC via paracrine secretion of DAMP and modulatory cytokines [147,155,158]. Also LSEC play an important role in liver homeostasis since they maintain HSC in a quiescent state through paracrine signaling, and they lose this ability during capillarization, allowing HSC to proliferate [159–161].

A particular case of direct cell-cell interaction is produced by NK cells, which are able to kill or inactivate HSC through their cytotoxic potential as well as to secrete big amounts of cytokines that mainly coordinate the immunological restoration after liver injury [162,163]. Moreover, B lymphocytes indirectly promote fibrosis in an antibody-independent manner [164], while T lymphocytes are responsible for initiating and maintaining the adaptive immunity with no directly interaction with HSC [165].

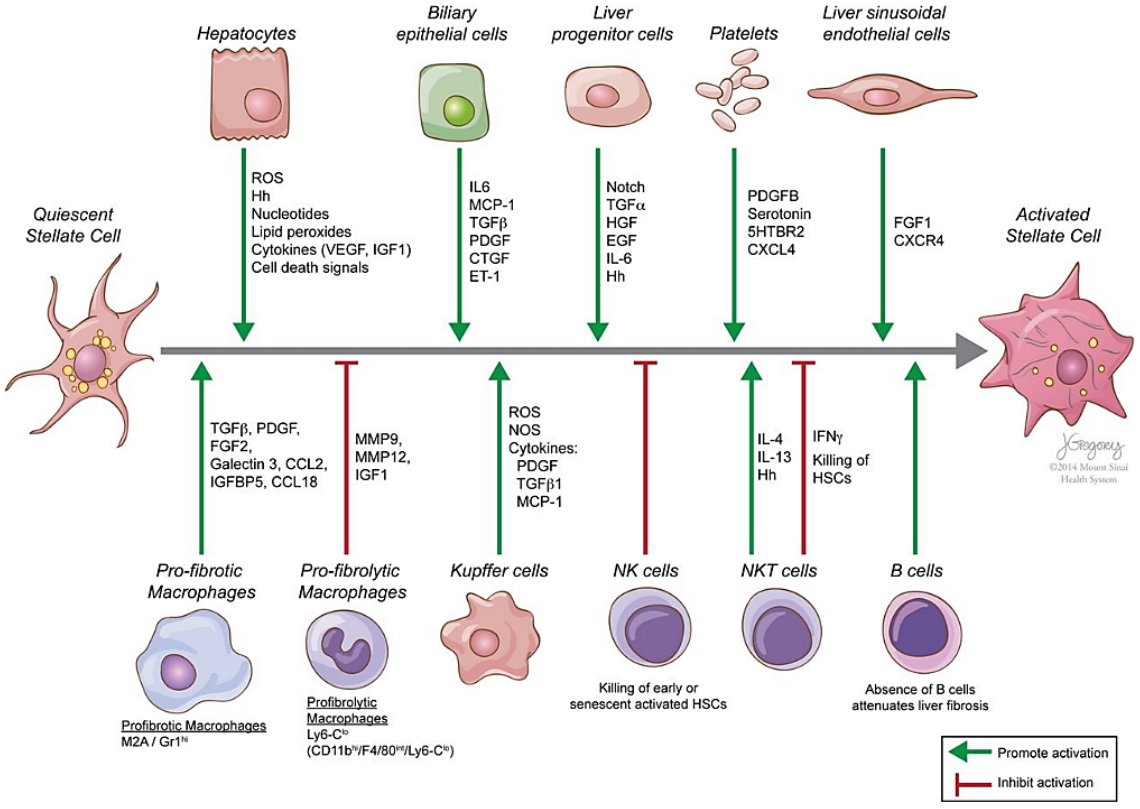

Figure I.6. Immune cell interactions that promote or inhibit the activation of HSC [166].

I.B.4. Inflammasomes in liver disease

Inflammasomes are cytosolic multiprotein complexes that assemble after sensing intracellular danger signals (DAMP and PAMP), and they serve as scaffolds to recruit and activate the pro-inflammatory caspase-1 [167]. Particularly, NLRP3 inflammasome is the most fully characterized member of the inflammasome family in liver diseases [168–170], and it is considered as a general sensor of tissue damage and infection [171].

Inflammasome activation is a 'two-hit' process, which represents a key regulatory checkpoint to avoid unnecessary immune responses capable of damaging the host [172,173]. The first hit, known as 'priming', requires a non-activating stimulus to trigger the transcription of the components of the inflammasome through the activation of NF-κB signaling, including its main downstream effector pro-IL1β; [174,175]. Priming stimuli involve any ligand able to activate NF-κB, such as tumor necrosis factor (TNF) α. Once primed, a second hit or 'activation' of NLRP3 occurs in response to either the same and/or additional stimuli, usually a DAMP derived from damaged cells, that promote the activation and the assembly of the NLRP3 inflammasome components [176–178]. Once pro-caspase-1 has been enzymatically activated by cleavage, it is capable of provoking a pro-inflammatory form of cell death known as pyroptosis, which is characterized by cytoplasmic swelling, hyper-permeabilization and subsequent rupture of the plasma membrane, and release of the cellular content [179,180]. On its hand, mature IL1β is one of the most potent pro-inflammatory cytokines and has been described as a major driver of the pathogenesis of many autoimmune, inflammatory and infectious diseases. Its multiple functions include recruitment of innate immune cells and modulation of adaptive immune cells, triggering, altogether, transcription of pro-inflammatory genes and enhancing the inflammatory response to injury [168,181].

NLRP3 inflammasome has emerged as a crucial player in the onset and progression of several liver diseases [169,182,183]. In response to acute or chronic liver injury, dying hepatocytes release DAMP that induce the activation of the NLRP3 inflammasome and consequently promote liver inflammation. Furthermore, *in vitro* studies have shown that IL1β directly promotes HSC activation [184,185]. Consequently, many different studies have demonstrated that

NLRP3 inflammasome activation is an essential early process that drives to chronic injury progression and fibrosis development in the context of many liver disorders, especially DILI, NAFLD and NASH [169,170,182,186]. This association between NLRP3 inflammasome and liver injury has also been explored in human studies, showing that NLRP3 inflammasome components and IL1β levels in liver tissue are enhanced in both HCV-infected and NASH patients [187,188].

I.B.5. Chronic liver disease

a) General features: when liver injury becomes chronic

After acute liver injury the immune system rapidly activates repair mechanisms by inducing a controlled and self-limiting fibrotic and wound-healing response. Through this response, ECM generated by active HSC protect hepatocytes against several toxic stimuli and renders the liver more resistant to subsequent acute injuries. In this context, the liver can restore its complete mass and original architecture in a relatively short interval, even when a large fraction of the organ has been destroyed. However, fibrotic response becomes problematic and clinically relevant when dysregulated and excessive scarring occurs in response to persistent injury. Liver tissue undergoes an impaired regenerative response characterised by altered inflammatory infiltrate and chronic wound-healing response, including necrosis and/or apoptosis of parenchymal cells and their massive replacement by ECM, distortion of the liver vascular architecture and angiogenesis leading to organ dysfunction [117,189,190].

Once injury becomes chronic, perpetuation of wound-healing and inflammatory response is mediated by several positive feedback loops that involve autocrine and paracrine effects of cytokines and growth factors, cell-cell and cell-matrix interactions. In this context, a wide range of pro-inflammatory and pro-fibrogenic mediators (IL6, TNF, IL1β, TGFβ…), as well as ROS and DAMP, derived from recruited immune cells and damaged hepatocytes, rapidly activate HSC and attract resident KC. Both KC and HSC act as phagocytes of parenchymal-derived debris, and as enhancers of immune cells recruitment by paracrinely contributing to pro-inflammatory and pro-fibrogenic signaling. At the same time, all these signals act in an autocrine manner increasing HSC activation (mainly by TGFβ) and proliferation (mainly by platelet-derived growth factor (PDGF)) in a harmful loop [189].

At the same time, the microenvironment in the damaged area leads to the inhibition of all the cellular mechanisms aimed to tissue repair. For instance, the macrophage capacity to degrade newly synthetized scar matrix through the secretion of MMP is inhibited by the concurrent production of TIMP by active myofibroblasts and inflammatory-recruited macrophages, which results in increased ECM deposition and scar accumulation [118,155,191]. Main cellular interactions upon liver injury are summarized in the Figure I.7.

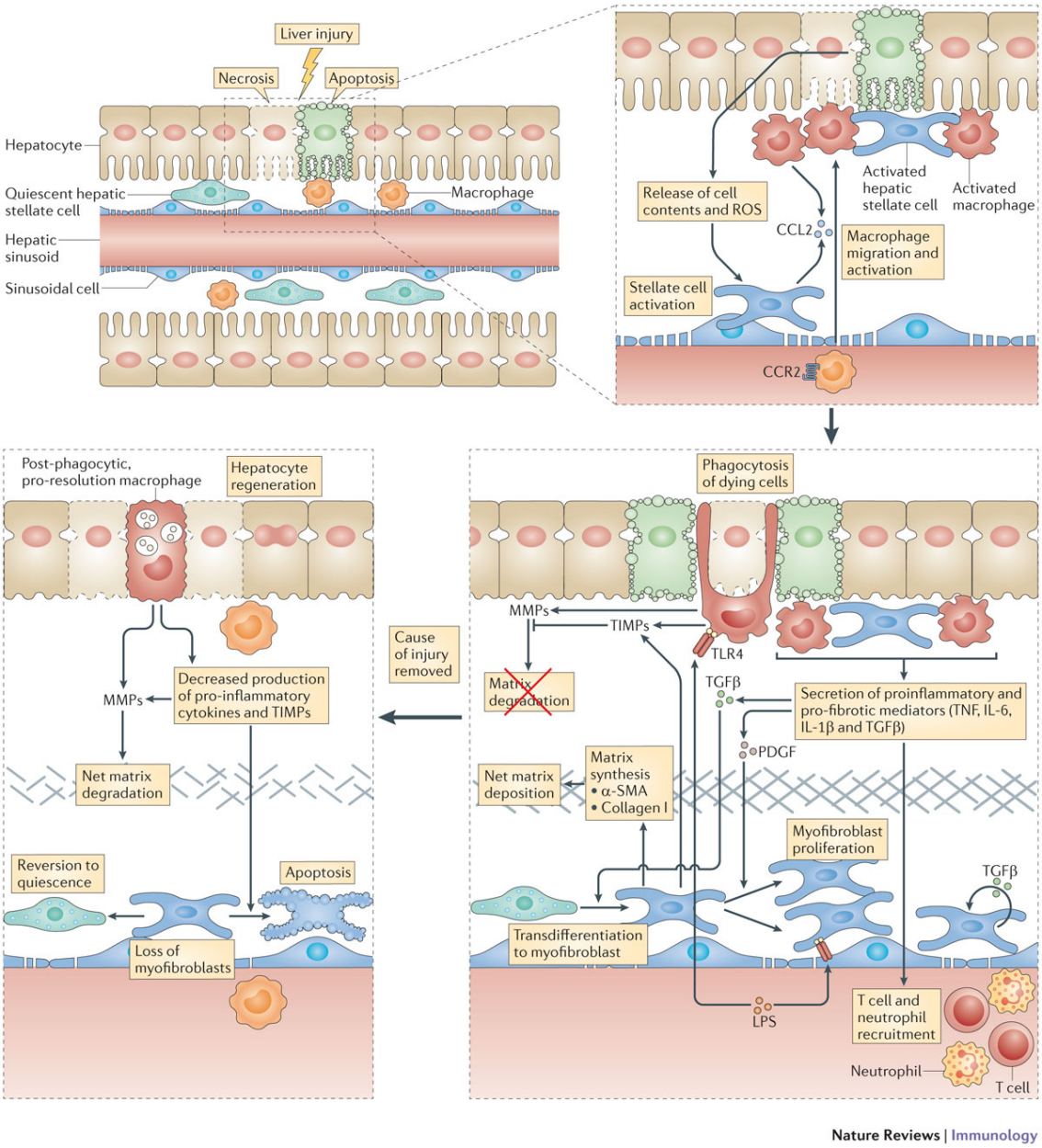

Figure I.7. Cascade of signals following liver injury (kindly provided by Dr. J. Fallowfield) [138].

b) NAFLD

NAFLD is the most common chronic liver disease worldwide and is considered the hepatic manifestation of the metabolic syndrome. It affects up to 30% of the entire adult population, being more than 75% of them individuals that are obese and diabetic. Consequently, its prevalence is rapidly increasing in association with unhealthy lifestyle habits and metabolic diseases. NAFLD is nowadays the major cause of liver-related morbidity and mortality and, along with alcoholic-related liver disease, the first pathology among those adults awaiting liver transplantation [192,193]. In severe cases, NAFLD can eventually progress to hepatocarcinoma (HCC) and, in spite of being infrequent, the risk of associated mortality in such situations is significant [194,195].

The natural history of NAFLD mirrors the natural history of the metabolic syndrome and encompasses a histological spectrum ranging from simple steatosis (where an excess of fat accumulation can be observed in hepatocytes), with no clinical significance, to NASH, where besides fat accumulation, parenchymal inflammation and lipotoxicity drive to hepatocyte death. Depending on the duration and severity of this inflammation, NASH can undergo different degrees of fibrosis, sometimes leading to clinically relevant fibrosis and cirrhosis (Figure I.8) [138,196]. It is currently estimated that 30-40% of people with NAFLD progress to NASH. From this pathological state, approximately 40-50% progress towards more severe states of liver fibrosis and cirrhosis, with only 3-5% developing HCC [193,197]. Although NAFLD itself does not increase the risk of HCC, it is well-accepted that NASH is a clear risk factor for this type of cancer, even in all those patients who do not develop fibrosis or cirrhosis [198–200].

The underlying mechanisms for the development and progression of NAFLD are complex and multifactorial. According to the currently accepted ‘multiple-hit hypothesis’ [201,202], insulin resistance and gut flora are key factors that determine NAFLD progression. During insulin resistance, adipose tissue becomes dysfunctional and produces an altered pattern of adipokines and cytokines, which leads to inflammation and increased lipid accumulation in the liver through increased lipogenesis and impaired lipolysis. This altered interplay between adipose tissue and liver triggers lipotoxicity in hepatocytes and subsequent mitochondrial dysfunction and oxidative and ER stress [198,203].

The contribution of the gut-liver axis in this process is also very important, since altered gut flora leads to further production of fatty acids in the bowel, increased small bowel permeability and increased fatty acid and PAMP absorption to the portal circulation, effects that, in summary, contribute to increase fat storage and inflammatory activation in the liver [204]. Genetic predisposition and epigenetic modifications have been also described as important features to determine the interindividual susceptibility to NAFLD development, affecting different parameters such as hepatocyte fat content, inflammatory microenvironment, HSC activation and/or evolution to more severe phases of the disease [201,205].

Although initially it was assumed that steatosis always precedes inflammation in the progression of this disease, it is now recognized that NASH can be the original liver lesion, and the timing and combination of genetic, external and intracellular events rather than the simple addition of hepatic insults result in different pathways which lead to steatosis and/or NASH [202,204].

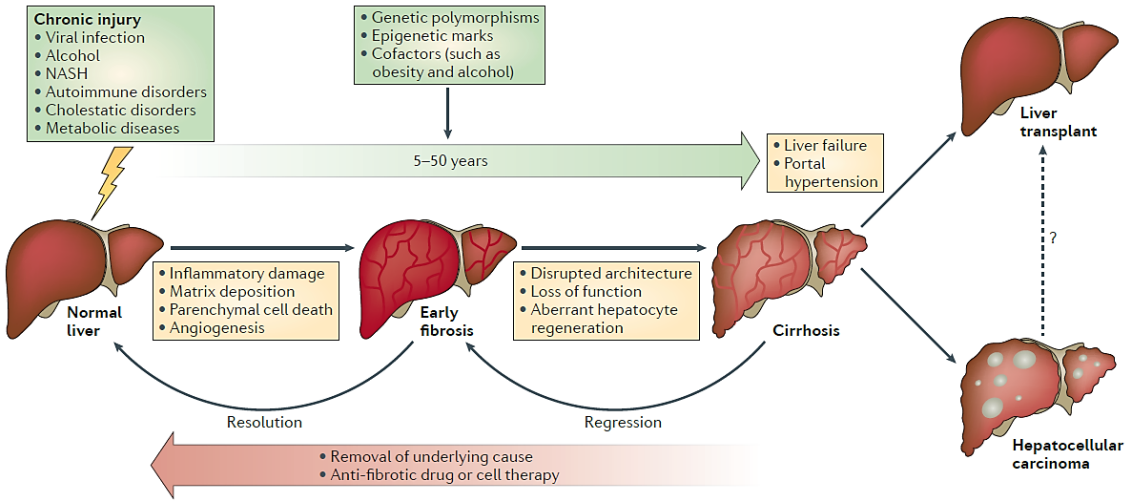

Figure I.8. Natural history of chronic liver disease [138].

c) Liver fibrosis and cirrhosis

The two key features that lead to chronic liver disease progression are fibrogenesis and aberrant angiogenesis. Sustained wound-healing response results in a severe distortion of both liver parenchyma and vascular architecture. Most of the key features which lead to fibrogenesis progression have been already explained in the corresponding chapter of HSC biology (I.B.2 b). On its hand, the angiogenic process leads to shunting of the portal and arterial blood supply directly into the hepatic outflow (central veins), compromising exchange

between hepatic sinusoids and the adjacent liver parenchyma. In cirrhosis, the space of Disse is filled with scar tissue and LSEC lose their characteristic fenestrations and develop basal membrane in a process known as sinusoidal capillarization (Figure I.9). Histologically, cirrhosis is characterised by vascularised fibrotic septa that link portal tracts with each other and with central veins, resulting in hepatocyte islands surrounded by fibrotic septa that are devoid of a central vein [206,207]. The major clinical consequences of cirrhosis are liver dysfunction, portal hypertension, ascites and HCC development. Portal hypertension results from the combination of structural disturbances associated with advanced liver disease, and of functional abnormalities leading to endothelial dysfunction and increased hepatic vascular tone [208,209].

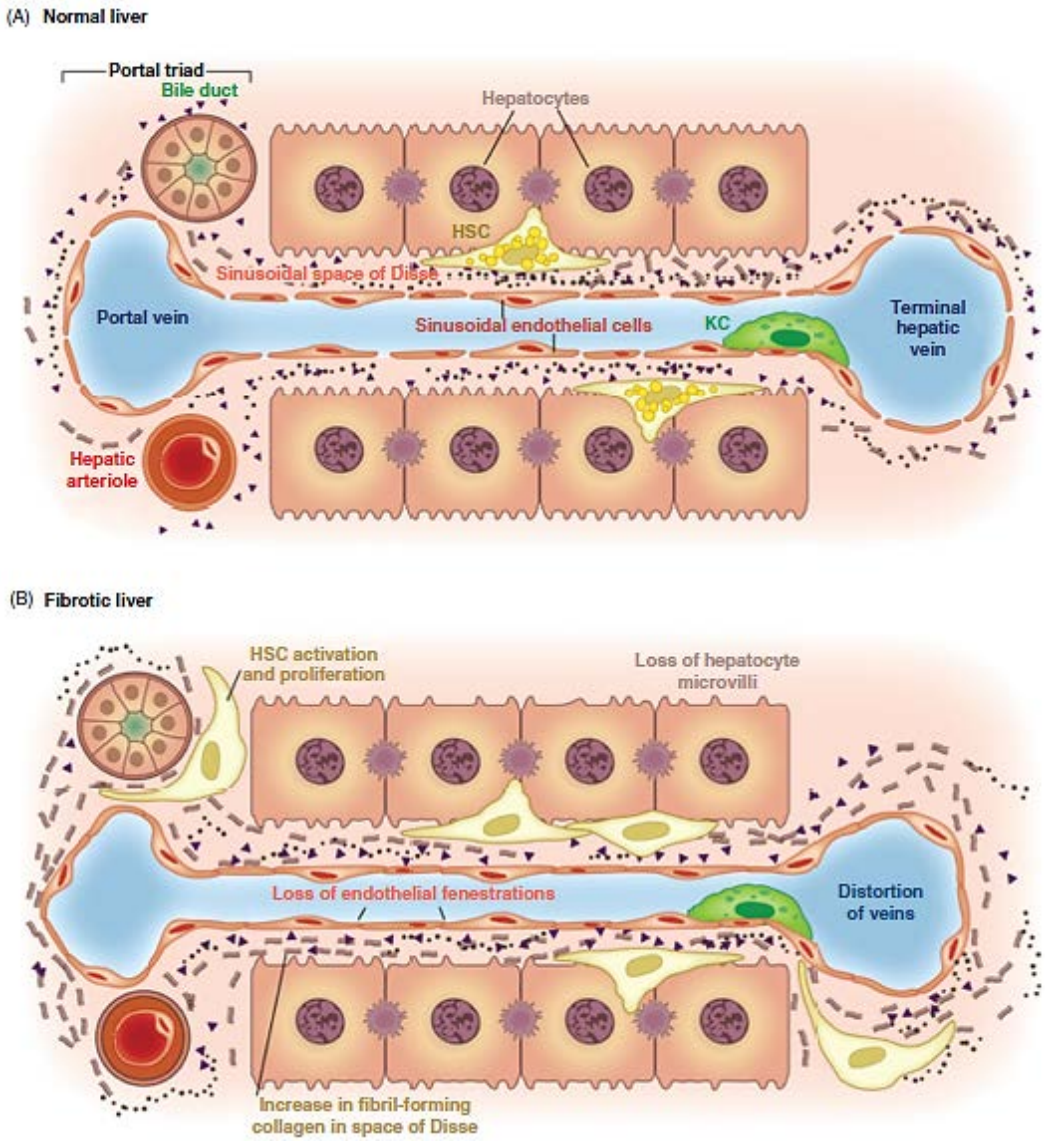

Figure I.9 Matrix and cellular alterations in hepatic fibrosis [133].

I.B.6. Liver regeneration

Despite the classical conception of liver fibrosis as a passive and irreversible process due to hepatocyte collapse, the idea of fibrosis regression was proposed in the 1970s, and it was definitely demonstrated in the 1990s, being completely assumed nowadays by basic researchers and physicians [210,211]. It is considered that, at a certain stage of advanced disease, fibrosis may become irreversible, likely due to significant collagen cross-linking and development of an insoluble and hypocellular matrix, which may correspond with the appearance of clinical manifestations of advanced cirrhosis. However, even this conception is still in debate as explained afterwards in this chapter.

a) Liver regeneration in health and disease

Following an acute injury or resection, the remaining healthy liver rapidly undergoes a strong compensatory response known as 'hepatostat' aimed to regain its original volume and structure, as well as its optimal metabolic and homeostatic status [190,212].

In a healthy liver, this compensatory system triggers a fantastic regeneration response. However, when this organ is chronically damaged by different insults (viral infections, alcohol, DILI, NAFLD, etc.), liver architecture becomes aberrant and hepatic regenerative capacity results severely altered. In brief, at a cellular level, hepatocytes are increasingly senescent and unable to divide efficiently, and HSC are activated; thus, both excessive cellular debris and settled scar tissue hamper an efficient regeneration. At the same time, most of the liver macrophages and immune cells are activated in a pro-inflammatory and pro-fibrogenic way, which also hinders a proper regenerative response [117,213] (Figure I.10).

Finally, it is important to note that even in the context of liver cirrhosis the natural history can be modified and patient outcome improved. Specifically, treatment and/or elimination of the hepatic insult favours certain liver regeneration and remodelling, as it has been recently demonstrated in patients with HCV-induced liver cirrhosis who had been successfully treated for the infection with direct-acting antiviral drugs. These patients presented a significant decrease in collagen content and cirrhosis regression, which led to the reduction of the clinical incidence of hard end-points like HCC and death [214,215].

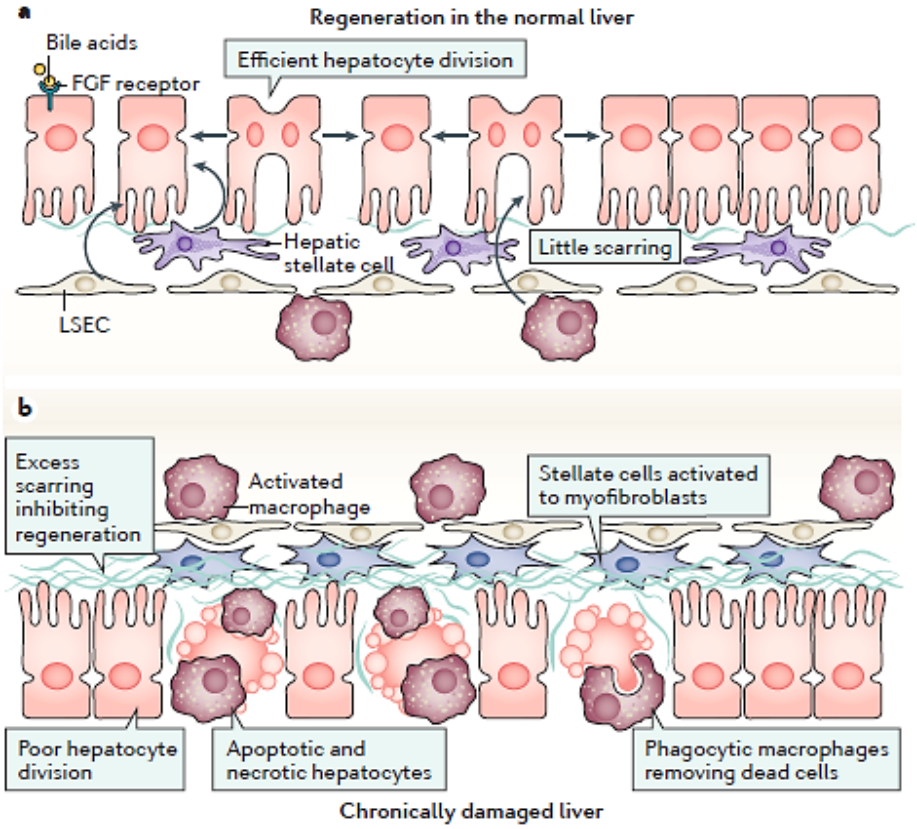

Figure I.10 Cellular interplay in normal and abnormal liver regeneration [117].

b) Liver regeneration by targeting HSC

Since HSC are an important contributor to ECM synthesis and fibrosis progression, they also play a crucial role in its regression. There are three main mechanisms for fibrosis regression by direct targeting HSC inactivation: apoptosis, senescence and cell cycle arrest with reversion to their quiescent stage [216,217].

Apoptosis of HSC during liver fibrosis decreases their number and subsequently contributes to the partial degradation of ECM through TIMP1 expression decrease [218,219]. Of interest, NF-κB plays an important role protecting HSC from apoptosis during fibrosis progression and, thus, its inhibition can directly favour recovery and regeneration [220]. Finally, as explained elsewhere in this chapter and observed in Figure I.6, many other liver cells contribute to HSC activation and deactivation. In this line, all hepatocytes, NK cells and KC are able to induce apoptosis of HSC by different mechanisms and paracrine mediators, all of which aimed to increase anti-proliferative and pro-apoptotic pathways as well as to decrease pro-survival signaling pathways [221,222].

Regarding senescence induction, recent studies have established that under specific circumstances, HSC reach their replicative limit, adopt a more inflammatory and less fibrogenic phenotype and undergo senescent in a p53-dependent manner [223,224]. Interestingly, those inactivated cells have an enhanced capacity to reactivate, compared to those that have never been activated. Quantitatively, reversion of activated HSC to quiescence is likely to be a significant pathway in fibrosis regression that involves approximately 50% of the stellate cell population, and it may in part be regulated by changes in PPARγ activity [133].

Finally, despite the fact that signals that induce myofibroblast reversion remain largely unknown, it is well assumed that under certain conditions, activated HSC can exhibit cell cycle arrest with reversion to a quiescent phenotype, similarly to all those inactivated by senescence [225,226]. In addition to this, a fourth option for HSC deactivation and fibrosis amelioration has been recently described: recent studies have demonstrated that hepatic myofibroblasts have an intrinsic capacity to reprogramme into hepatocyte-like cells by simultaneous expression of several transcription factors (FOXA1, FOXA2, FOXA3, GATA4, HNF1A and HNF4A), faithfully reproducing the function and proliferation of primary hepatocytes and thus reducing liver fibrosis [227,228].

I.B. 7. Animal modelling of liver disease

In the last years different experimental approaches have been developed in rodents and used by researchers all over the world in chronic liver disease modelling, from NAFLD and NASH to liver fibrosis, cirrhosis and hepatocellular carcinoma. In this context, two key features should be considered in these *in vivo* models. First, they should reproduce the pathological pattern of liver injury that defines human liver disease. Second, they must be able to reproduce systemic metabolic and immune responses that humans develop during liver disease progression. This characteristic is especially relevant in all those models which aim to induce NAFLD and NASH, as they always develop in a metabolic syndrome context.

However, it is important to highlight that none of the currently available mice models has been able to fully reproduce all symptoms and features of human disease. The main reasons for this are the obvious interspecific differences

(between rodents and humans, mainly associated with metabolism). Also, the inherent complexity of the multiple etiologies involved in liver disease progression, together with the long time required for its development, plays a key role [229,230].

From a physiological point of view, chronic liver disease in animals can be reproduced by a wide variety of factors that lead to changes in hepatic fat disposition, hepatocyte injury, HSC transdifferentiation and inflammatory activation. Major approaches to liver disease induction have been done employing genetic, nutritional, chemically-induced and surgical models.

a) Genetic models

In this type of models, animals with spontaneous or targeted alterations of certain genes involved in the progression of the disease are used. Some examples of genetic models with spontaneous development of NAFLD, among others, are *Ob/ob* and *Ob/rb* mice, which are deficient in leptin signaling; *AOX*, *MAT1A* or *NRF1* null mice, that present impaired β-oxidation pathways, or *KK-Ay/a* and *MRC4* mice, which have no hypothalamic control in the appetite suppression (5,6). Generally, these models display pathogenic features of human NAFLD (obesity, steatosis, and insulin resistance). However, they do not generally have a distinctive phase of steatosis before the development of steatohepatitis and do not progress to fibrosis. Therefore, the use of these mice in NASH studies is limited by the lack of widespread availability and high costs for long-term maintenance [232,233].

b) Nutritional models

Within this category, we can distinguish between all those models based on a nutritional deficiency, such as the ‘methionine and choline deficient diet’ (MCD) or ‘choline-deficient L-amino acid-defined diet’, and all those based on overnutrition, usually with high fat diet (HFD) but also with high lipogenic and aterogenic nutrients like glucose or fructose (commonly known as Western diet). Models based on the lack of essential nutrients result in impaired β-oxidation and altered production and secretion of lipoproteins from the liver, which leads to steatosis progression. They have long been used, especially that based on MCD diet, and are able to elicit a severe NASH phenotype in a relatively short time

frame. However, the mechanisms they use do not correspond with human NAFLD progression and they fail to induce the metabolic co-morbidities that are typically observed in patients [232,234].

On the other hand, overnutrition models are able to generate considerable levels of steatosis, inflammation and fibrosis, which mimic quite well the pathophysiology and phenotype observed in human NAFLD, but they need longer experimental procedures. Typically, the severity of NAFLD induced by these models depends on the rodent species, the composition of the diet and the duration of the procedure. In addition, as none genetic or nutritional models fully reflect the real picture of human NAFLD/NASH, certain mouse models use combined transgenic mice plus nutritional modifications to better reproduce the pathogenesis of the disease [232,234].

c) Surgical and chemically-induced models

Chemically-induced liver injury is also a good strategy to quickly induce several diseases. Examples of this approach are streptozotocin-induced NAFLD in the context of type 1 diabetes, carbon tetrachloride (CCl_4)-induced liver fibrosis or diethylnitrosamine (DEN)-induced HCC. As happens with genetic models, these models are not able to exactly reproduce all features of human diseases, so their use is generally limited to certain stages of liver pathology [232,234].

The most commonly used procedure to quickly induce liver fibrosis in rodents is chronic CCl_4 injection. It is a well-established model that induces oxidative stress in the liver, leading to the accumulation of toxic lipids and protein peroxidation products, accompanied by a strong necrotic response. In mice, peritoneal injection of CCl_4 twice or three times per week induces extensive liver damage with ballooned, necrotic hepatocytes, as well as a mild mononuclear cell infiltration in the affected areas. In addition, transaminase and triglyceride levels are substantially higher compared to those of control animals. Most importantly, CCl_4 induces a dose-dependent fibrosis that regresses after discontinuing compound administration. Single administration of CCl_4 induces fibrosis, but no obesity nor insulin resistance. In addition, despite this is not a model of NAFLD itself, as CCl_4 is dissolved in different types of oil prior administration (generally corn oil), these injections are also able to induce mild macro- and microsteatosis. Furthermore, it is also frequently combined with dietary models to efficiently

induce NAFLD. In this experimental setting, CCl_4 potentiates the effects of HFD towards the development of NASH and fibrosis. In all cases, the intensity of liver damage directly correlates with the duration of the treatment and the doses employed [235].

Finally, there are also many surgical approaches employed in animal modelling of liver diseases. The most common one is based in bile-duct ligation (BDL), which induces an obstructive cholestasis that progresses to liver inflammation, immune recruitment, hepatocyte necrosis and fibrosis progression [234].

d) Importance of the species, strain and sex

Election of species, strains and sex of experimentation animals may directly affect the development of liver diseases. It has been reported that C57BL/6 strain in mice and Wistar and Sprague Dawley strains in rats are generally preferred to generate these pathologies because of their higher sensitivity to liver damage in response to several insults, as well as because of their intrinsic capacity to develop liver disease with similar characteristics to human disorders [236,237]. Moreover, both male rats and mice are slightly more sensitive to the induced liver injury than females. Specifically in mice, male C57BL/6 animals display higher liver inflammation, even though steatosis progression and liver enzymes do not present significant differences between both sexes [238]. Despite these observations, many chronic studies use female animals as their behavior facilitates their housing in groups during extended periods of time.

I.C. JAK-STAT signaling pathway

I.C.1 Overview: biological function, structure and regulation

The cytokine-activated Janus kinase (JAK)-STAT signaling pathway is one of a handful of pleiotropic cascades used to transduce a multitude of signals for development and homeostasis in animals. Its activation is involved in cell proliferation, differentiation, cell migration, apoptosis and many other cellular processes that regulate hematopoiesis, immune development, lactation or adipogenesis [239,240]. Furthermore, JAK-STAT signaling has a central role in the control of mammalian immune responses, and thus its dysregulation is largely associated with various auto-immune disorders and pathologies where the

immunity contribution becomes decisive, like inflammatory and wound-healing disorders and cancer [241,242].

Cytokines have essential roles in the control of immune responses and their biological functions mainly depend on their intrinsic capacity to activate or repress gene expression. JAK-STAT pathway has been described as a common signaling pathway used by many cytokines and, given its intrinsic pleiotropic nature, the same JAK-STAT pathway can be activated in different cell types in response to the same or different cytokines triggering diverse cellular responses, often with opposite biological functions [243,244].

As displayed in Figure I.11, intracellular activation occurs when ligand binding induces the multimerization of receptor subunits: the binding of a cytokine to its cell-surface receptor results in receptor dimerization and the subsequent activation of JAK tyrosine kinases, which are constitutively associated with the receptor. Specific tyrosine residues on the receptor are then phosphorylated by activated JAK and serve as docking sites for a family of latent STAT cytoplasmic transcription factors. These STAT are phosphorylated by JAK, dimerize, and subsequently leave the receptor and translocate to the nucleus, where they activate gene transcription. Therefore, the JAK-STAT cascade provides a fast and direct mechanism to translate an extracellular signal into a transcriptional response [245,246].

The mammalian JAK family has four members: JAK1, JAK2, JAK3 and tyrosine kinase 2 (TYK2). In addition, there are seven mammalian STAT: STAT1, STAT2, STAT3, STAT4, STAT5A, STAT5B and STAT6, which are highly homologous in several regions, especially in all those involved in their activation and dimerization [247,248].

Recent studies have shown that JAK-STAT signaling pathways can be regulated through distinct mechanisms. Key regulators include suppressor of cytokine signaling (SOCS) proteins and the protein inhibitor of activated STAT (PIAS) family, as well as various protein tyrosine phosphatases. The modulation of JAK and STAT by various protein modifications and the crosstalk between different JAK-STAT pathways and other cellular signaling cascades provide additional levels of regulation that might be crucial in the orchestration of different biological processes in which this pathway is essential [249].

SOCS proteins are the most extensively studied regulators of JAK-STAT signaling. These proteins are generally expressed at low levels in unstimulated cells and become rapidly induced by cytokines, thereby inhibiting JAK-STAT signaling and forming a classic negative-feedback loop [250]. SOCS proteins complete a simple negative feedback loop in the JAK-STAT circuit: activated STAT stimulate transcription of the SOCS genes and the resulting SOCS proteins bind phosphorylated JAK and their receptors to turn off the pathway. SOCS can affect their negative regulation by three means: first, by binding phosphotyrosine residues on the receptors, SOCS physically block the recruitment of signal transducers, such as STAT. Second, SOCS proteins can bind directly to JAK or to receptors to specifically inhibit JAK kinase activity. And third, SOCS facilitates the ubiquitination of JAK and their receptors, targeting them for proteasomal degradation [251,252].

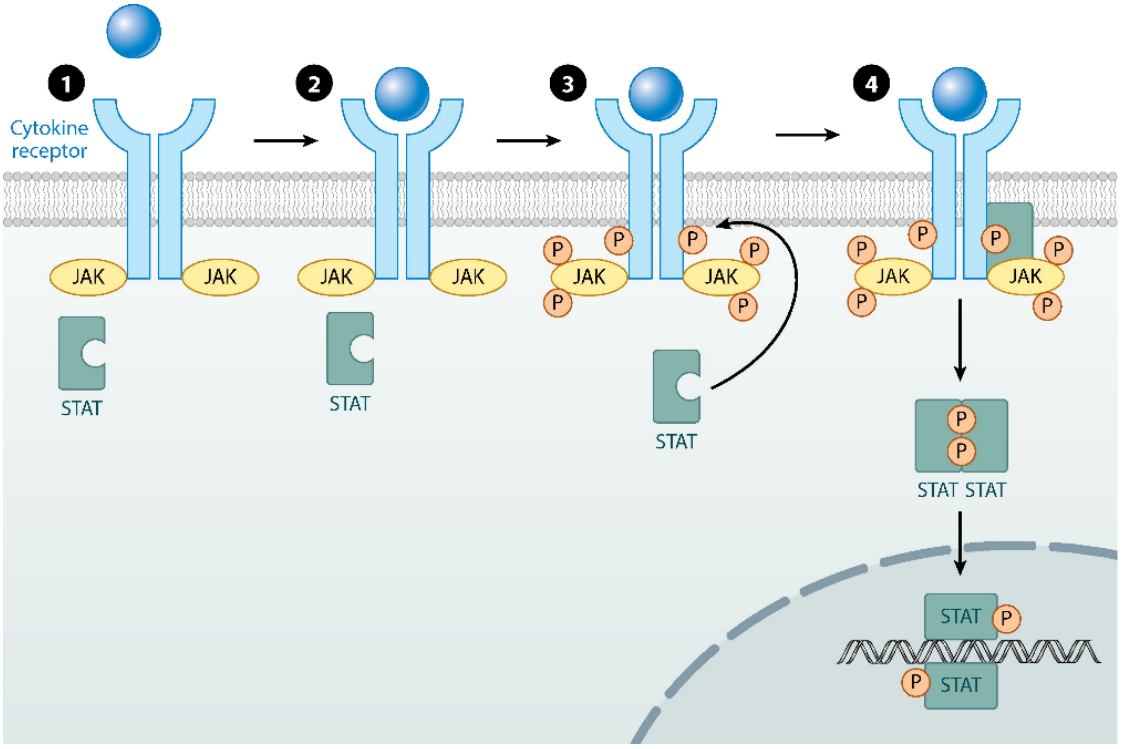

Figure I.11 Intracellular activation of JAK-STAT pathway after cytokine stimulation [240].

I.C.2 JAK-STAT in the liver

a) JAK-STAT in liver metabolism and homeostasis

Recently, the JAK-STAT pathway has been implicated in the pathogenesis of several metabolic diseases in humans. The development of tissue-specific JAK-STAT knockout (KO) mice has been fundamental in elucidating the role of this pathway in various metabolic organs. Cumulative evidence demonstrates that the role of any given JAK-STAT protein in metabolism is highly context-dependent and cell type-specific. This signaling pathway has crucial functions in metabolically active tissues including adipose, liver, skeletal muscle, and pancreatic β cells, as well as in immune cells [239,253]. Specific disruption of JAK-STAT signaling in these tissues leads to metabolic derangements or, in some cases, protection from obesity and its associated perturbations [254,255].

Regarding lipid metabolism, multiple JAK-STAT pathways have been directly implicated in energy homeostasis by integrating both anabolic and catabolic responses. Studies have consistently demonstrated that STAT3 signaling integrates multiple signals in the regulation of hepatic glucose and lipid metabolism, since hepatocyte-specific deficiency of STAT3 leads to insulin resistance and increased expression of gluconeogenic genes, at least partly through disruption of IL6 signaling [256,257]. Also STAT5 has a pivotal role in hepatic lipid metabolism maintenance since its action prevents lipid accumulation and steatosis progression by induction of several fatty acid transporters and lipolytic enzymes [258,259]. Finally, STAT6 is also important in hepatic metabolism because it promotes glucose and fatty acid oxidation by specific inhibition of PPARα activity in hepatocytes [260]. Together, all these data demonstrate that JAK-STAT signaling is crucial for a variety of metabolic functions of the liver and its disruption results in dysregulation of hepatic homeostasis, which may lead to hepatic steatosis and subsequent NAFLD progression [253].

b) At a glance, JAK-STAT in liver disease

As previously described, cytokine trafficking and signaling in the liver are crucial for its normal function, and JAK-STAT pathway orchestrates the signaling transduction cascade of many of the core cytokines involved in hepatic pathophysiology among different hepatic cells.

In order to completely understand the function of JAK-STAT signaling in liver pathophysiology, it is essential to clarify which effect is induced by each STAT in each cell subtype. The biological effects induced by all the different STAT in hepatocytes and non-parenchymal cells in the liver are displayed in Table I.4 and Table I.5, respectively.

STAT2. Activation of both STAT1 and STAT2 plays a key role not only in host defense against HCV infection but also in interferon (IFN) α treatment-induced HCV clearance. After HCV infection, the infected hepatocytes produce IFNβ, which activates STAT1 and STAT2 in uninfected neighbouring hepatocytes and subsequently upregulates expression of various antiviral proteins that prevent further infection [261].

STAT4. In general, STAT4 is important in generating inflammation during protective immune responses and immune-mediated diseases. Its IL12-mediated activation leads to liver injury and inhibits liver tumor growth by activating NK and NKT cells to produce IFNγ. Despite these observations, the role of STAT4 in the pathogenesis of liver diseases is still controversial [262,263].

STAT5. Many studies suggest that STAT5 activation plays an important role in promoting tumorigenesis via upregulation of anti-apoptotic, cell-proliferative, invasion and metastasis-related genes. However, it has also been controversially reported that STAT5 activation mediates hepatoprotective effects preventing the development of HCC [264,265]. Nevertheless, it is generally assumed that STAT5 acts as a tumor suppressor in liver tumorigenesis via its anti-steatogenic and hepatoprotective effects. However, it is not clear whether STAT5, similar to STAT3, can also promote HCC cell proliferation once cells have become neoplastic [266,267].

STAT6. Both IL4 and IL13 strongly induce STAT6 activation in the liver and are likely to play complex roles in controlling liver injury and inflammation. IL4 seems to induce pro-inflammatory/pathogenic effects via activation of STAT6. However, a hepatoprotective function of this cytokine has also been described in DILI, mostly mediated by the upregulation of hepatic GSH synthesis [262,263,268]. In addition, both IL4 and IL13 have been reported to exert protective actions against ischemia/reperfusion liver injury, apparently through STAT6 activation and the subsequent inhibition of inflammation and protection against hepatocyte and endothelial cell damage [269,270].

STAT	Major activators	Major functions
STAT1	IFN (α, β, γ, λ)	Promotes anti-viral responses Promotes anti-tumor responses Induces hepatocyte apoptosis Inhibits hepatocyte proliferation Promotes liver inflammation
STAT2	IFN (α, β, λ)	Promotes anti-viral response
STAT3	IL6, IL22, IL6 family	Promotes hepatocyte survival Promotes hepatocyte proliferation Ameliorates steatosis Induces innate immune response Promotes liver tumor, cell survival and growth
STAT4	Unknown	Unknown
STAT5	Growth hormone	Upregulates liver metabolism Promotes hepatocyte survival Promotes hepatocyte proliferation Ameliorates steatosis
STAT6	IL4, IL13	Promotes liver injury and inflammation Protects against ischemia/reperfusion and DILI

Table I.4 Major activators and functions of STAT proteins in hepatocytes [261].

STAT	Cell types	Major activators	Major functions
STAT1	in HSC	IFN (α, β, γ)	Inhibits fibrosis
	in KC	IFNγ	Promotes inflammation
	in NK cells	IFN (α, β, γ)	Promotes anti-viral, anti-tumor and anti-fibrotic responses
STAT2	in non-parenchymal cells	Unknown	Unknown
STAT3	in HSC	IL10	Promotes fibrogenesis
	in KC	IL6, leptin	Inhibits inflammation
	in endothelial cells	Unknown	Inhibits inflammation
STAT4	in NK and NKT cells	IL12, IFNα/β	Promotes inflammation
STAT5	in HSC	Leptin	Promotes fibrogenesis
STAT6	in HSC	IL4, IL13	Promotes fibrogenesis

Table I.5 Major activators and functions of STAT proteins in non-parenchymal cells [261].

As observed above, the most important STAT involved in chronic liver disease are both STAT1 and STAT3, as they are able to induce different responses in liver parenchymal, non-parenchymal and immune cells [269,270].

c) Opposing roles of STAT1 and STAT3 in liver injury and repair

STAT1 and STAT3 can be ubiquitously activated in many different liver cell subtypes and their activation generally plays opposing roles in many aspects of liver pathophysiology [271,272]. Interestingly, hepatic STAT1 and STAT3 not only functionally antagonize each other, but they also mutually inhibit each other's activation through the induction of SOCS1 and SOCS3, respectively, that inhibit both STAT1 and STAT3 activation [273,274]. Attending to this SOCS-mediated mutual inhibition, STAT3 activation rapidly induces STAT1 inhibition and vice-versa; for this reason, the simultaneous activation of both transcription factors in the same cell is certainly impossible (Figure I.12).

The involvement of STAT1 and STAT3 signaling pathways in induction of damage or in liver regeneration directly depends on the cytokine microenvironment, which determines the type and the amount of cells that overexpress STAT1 or STAT3 at a certain point of time [261,272,275].

Although it is a reductionist explanation, to clearly understand this hepatic regulation we can assure that, in general, STAT3 activation in any cell induces pro-survival and pro-proliferative pathways and increases the resistance of these cells to the damage [276–279]. Conversely, STAT1 activation triggers anti-proliferative pathways and induces cell cycle arrest, senescence and/or apoptosis [280–282].

Consequently, STAT1 activation in hepatocytes is a pro-apoptotic signal that leads to cell death and increased liver damage, whereas STAT3 activation is a pro-survival and proliferative signal that protects against hepatocyte death [283–285]. In contrast, STAT1 activation in HSC inhibits their proliferation and induces cell cycle arrest and apoptosis, thus limiting the fibrogenic response [281,286]. On its hand, STAT3 activation in these same cells has a pro-fibrotic effect since it increases their activation and proliferation and enhances the ECM deposition in the scarring tissue [277,279].

Similar effects are observed during liver regeneration. Upon an acute liver injury, hepatostat sensing in the liver rapidly induces quiescent hepatocytes to enter the cell cycle and replicate under the control of a broad spectrum of cytokines, growth factors, and hormones. Among these factors, IL6 represents the major cytokine that activates STAT3 in hepatocytes, whose activity is crucial

for their proliferation. STAT1 activation, mainly driven by IFNγ, plays a deleterious effect in this context, since it induces cell cycle arrest and apoptosis in hepatocytes and thus impairs parenchymal regeneration [287,288].

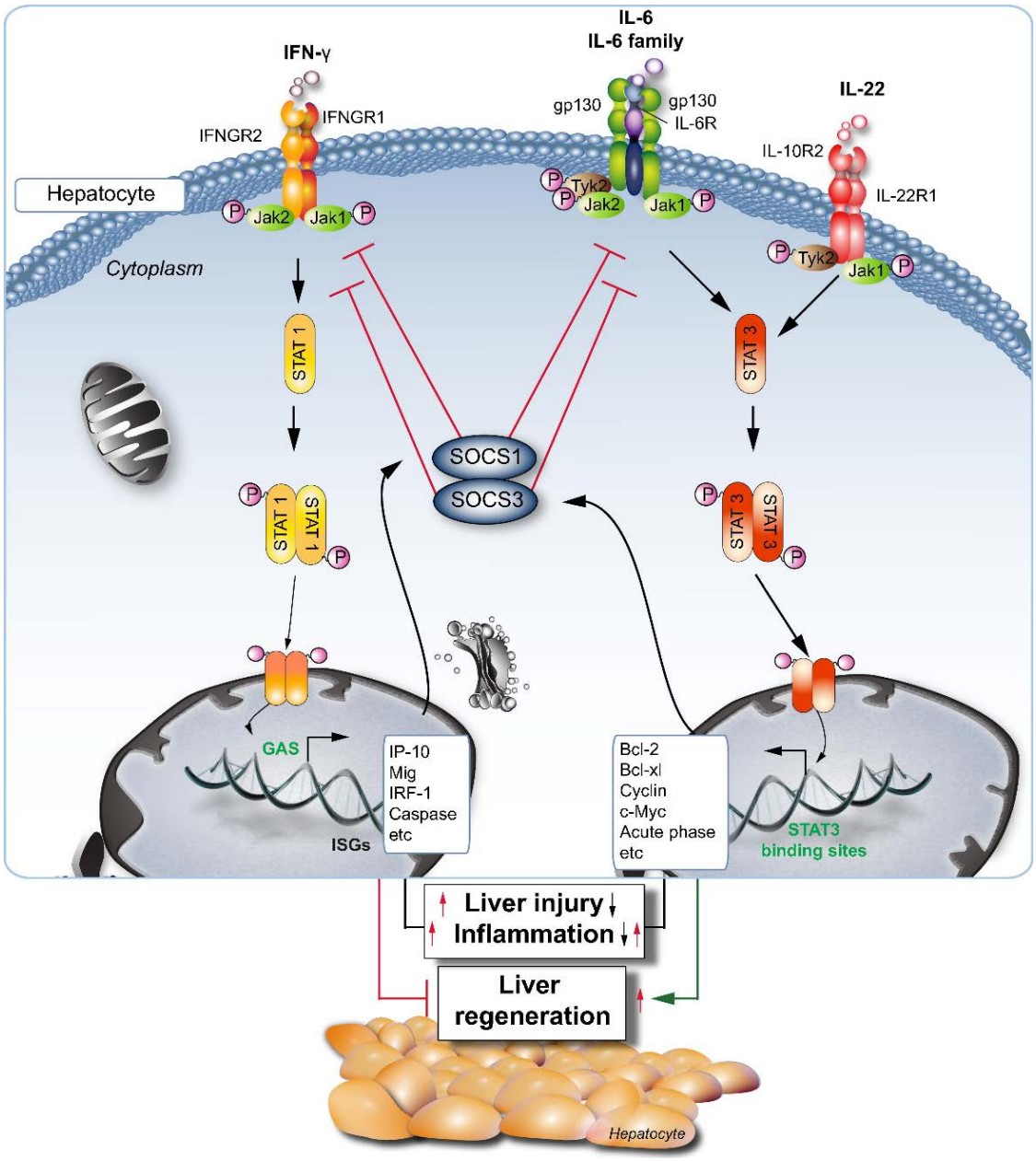

Figure I.12 Hepatocyte STAT1 and STAT3 balance in liver injury and regeneration [289].

Chapter II: AIMS

The general aim of this study was to explore the role of the most widely used antiretroviral drugs in the onset and/or progression of acute and chronic liver diseases, and to characterize the cellular and molecular mechanisms involved, using both *in vitro* and *in vivo* models.

The specific aims were:

- To systematically analyse the acute mitochondrial effects of nucleoside-analogue reverse transcriptase inhibitors and their impact in the function of hepatic cells.
- To explore potential synergisms between these antiretrovirals and other drugs whose hepatotoxicity is attributed to mitochondrial dysfunction.
- To characterize the chronic effects of non-nucleoside reverse transcriptase inhibitors on hepatic alterations associated with steatosis, inflammation and fibrogenesis using a nutritional animal model of non-alcoholic fatty liver disease.
- To analyze the potential of these drugs to modulate the onset, progression and resolution of liver damage in animal models of fibrosis induced by CCl_4.
- To determine the hepatic cell subsets and the molecular mechanisms mainly involved in the RPV-related effects observed *in vivo,* with the aim of identifying potential therapeutic targets, specially focusing on the role of JAK-STAT signaling pathway.

Chapter III: MATERIALS AND METHODS

III.A. DRUGS AND REAGENTS

III.A.1. ARV drugs

The ARV drugs employed in this thesis for *in vitro* experiments were purchased from Sequoia Research Products (Pangbourne, UK) and were dissolved in their respective vehicles (see Table III.1). No significant impact was found on any of the analysed parameters with the concentrations employed of the vehicles. Antiviral drugs used *in vivo* experiments were obtained from the Service of Pharmacy of the Hospital Clínico Universitario of Valencia (Spain). ARV pills were pulverized using a glass mortar, dissolved in pure DMSO and introduced in an ultrasound bath for 5 min until homogenous dissolutions were obtained, ready to be orally administered in animals.

DRUG	BRAND NAME	VEHICLE
3TC	Epivir®	Distilled water (*in vitro*)
ABC	Ziagen®	Distilled water (*in vitro*)
ddI	Videx®	Distilled water (*in vitro*)
AZT	Retrovir®	Distilled water (*in vitro*)
FTC	Emtriva®	Distilled water (*in vitro*)
TDF	Viread®	Distilled water (*in vitro*)
EFV	Sustiva™	Methanol (*in vitro*) / DMSO (*in vivo*)
RPV	Endurant®	DMSO (both *in vitro* and *in vivo*)

Table III.1 ARV drugs employed in this thesis. Active principles, brand names and vehicles.

III.A.2. General chemical reagents

All general chemical reagents were of analytical grade and were acquired from Sigma-Aldrich (Stenheim, Germany), Panreac Química S.L.U. (Barcelona, Spain), Merck Milipore (Darmstadt, Germany) and Roche Life Science (Penzberg, Germany).

III.A.3. Cell culture reagents

Media and supplements for cell culture were obtained from Gibco™ (Thermo Fisher Scientific, Waltham, MA, USA), Sigma-Aldrich and Lonza (Basel, Switzerland) (see Table III.2).

REAGENT	COMPANY
Dimethyl sulfoxide (DMSO)	Sigma-Aldrich
Dulbecco′s Modified Eagle′s Medium (DMEM) with high glucose concentration (4.5 g/L)	Gibco
Fetal bovine serum (FBS)	Lonza
Hank's balanced salt solution (HBSS)	Sigma-Aldrich
Hydrocortisone hemisuccinate	Sigma-Aldrich
Insulin from bovine pancreas	Sigma-Aldrich
L-glutamine	Gibco
Minimum essential medium (MEM)	Gibco
Non-essential amino acids solution (NEAA)	Gibco
Penicillin/streptomycin	Gibco
Phosphate-buffered saline (PBS, pH 7.4)	Gibco
Sodium pyruvate	Gibco
Trypsin-Ethylenediaminetetraacetic acid (EDTA) 0.25%	Gibco
William's medium E	Sigma-Aldrich

Table III.2 Reagents used in cell culture and their supplier companies.

III.B. EXPERIMENTAL MODELS AND TECHNIQUES

III.B.1. *In vitro* approaches

a) Human cell lines

The human hepatoblastoma cell line Hep3B (86062703, European Collection of Authenticated Cell Cultures (ECACC), Salisbury, UK) was used as a human hepatocyte model because they display a good CYP activity capable of metabolizing ARV drugs in a similar way to human primary hepatocytes [290,291]. These cells were cultured in MEM supplemented with 10% heat-inactivated FBS (iFBS), 1 mM NEAA, 2 mM L-glutamine and 1 mM sodium pyruvate. In some experiments also the human hepatocellular carcinoma cell line HepG2 (85011430, ECACC, Salisbury, UK) was used in order to confirm if the effect observed in response to some drugs was cell type-specific and not related to the particular cell line employed. The medium used for culturing these cells was

DMEM with high glucose concentration, supplemented with 10% iFBS, 1 mM NEAA, 2 mM L-glutamine and 1 mM sodium pyruvate.

LX-2 cells, a human immortalized HSC line, were routinely cultured in DMEM with high glucose concentration supplemented with 10% iFBS. These cells were kindly provided by Dr. Scott L. Friedman (Icahn School of Medicine at Mount Sinai, New York, USA).

HepaRG™ cells (HPRGC10, Gibco) are bipotent progenitors isolated from a human hepatoma. They differentiate into hepatocyte-like and biliary epithelial-like cells. Cells were initially maintained at a density of 2.7 x 10^4 cells/cm^2 in William's medium E supplemented with 10% iFBS, 5 µg/mL insulin from bovine pancreas, 2 mM L-glutamine, and 50 µM hydrocortisone hemisuccinate. After 2 weeks, undifferentiated HepaRG™ were cultured in presence of 2% DMSO in the medium for a further 2-week period to induce cell differentiation [292,293]. Thereafter, hepatocyte-like cells were selectively harvested from differentiated HepaRG through mild tripsinization (0.125% trypsin-EDTA) and reseeded at a density of 8x10^4 cells/cm^2 in medium containing 2% DMSO. For treatment, cells were maintained in DMSO-free medium with the drug concentration under assay.

All cell culture media were supplemented with 50 U/mL penicillin and 50 µg/mL streptomycin. Cell cultures were maintained in a cell culture incubator (MCO-19AICUV-PE, Panasonic Healthcare Co. Ltd., Gunma, Japan) at 37º C, with a humidified atmosphere of 5% CO_2 and 95% air (AirLiquide Medical, Valencia, Spain). All cell lines were subcultured when they reached 90-95% confluence, using 0.25% Trypsin-EDTA. Sub-confluent cell cultures of passage number lower than 30 were used for all the experiments.

b) Human liver tissue

Human liver tissue was obtained from biopsies from patients (two women and four men) who had undergone surgical resection of liver tumours (Hospital Universitario Doctor Peset, Valencia, Spain) and had provided informed consent. Experiments were approved by the institutional ethics committee (CEIC Hospital Universitario Doctor Peset; reference number of approved report: 62/11).

c) Human primary HSC isolation

All experiments with primary human HSC were done in collaboration with the Liver Vascular Biology Research Group from the Institut D'Investigacions Biomèdiques August Pi i Sunyer (IDIBAPS) and Hospital Clínic (Barcelona, Spain), headed by Dr. Jordi Gracia Sancho, and with the special support of Dr. Anabel Fernández Iglesias.

Human HSC were isolated from remnant tissue, approximately weighing 20 g, obtained from human partial hepatectomy to excise tumor metastasis from colon carcinoma and from the discarded tissue after liver transplantation. Healthy samples obtained from peritumoral tissue were confirmed as "normal" by anatomical pathologists from the Hospital Clínic. This experimental protocol was approved by the Ethics Committee of this hospital (HCB/2015/0624) and, in all cases, patients agreed to an informed consent.

Human liver tissue was perfused through major vessels for 10 min at a flow rate of 20 mL/min at 37° C with HBSS without Ca^{+2} and Mg^{+2} and containing 12 mM HEPES ((4-(2-hydroxyethyl)-1-piperazineethanesulfonic acid; Sigma-Aldrich) pH 7.4, 0.6 mM ethylene glycol-bis (2-aminoethylether)-N,N,N′,N′-tetraacetic acid; Sigma-Aldrich) and 0.23 mM bovine serum albumin (BSA; Applichem). Then, sample was perfused for 30 min at a flow rate of 5-20 mL/min at 37° C with 0.015% collagenase A (Roche), prepared in HBSS containing 12 mM HEPES pH 7.4 and 4 mM $CaCl_2$. The resultant digested liver was excised and *in vitro* digestion was performed at 37° C with 0.01% collagenase A, in HBSS containing 12 mM HEPES pH 7.4 and 4 mM $CaCl_2$ for 10 min. Disaggregated tissue was fractionated by density gradient centrifugation using Histodenz (Sigma-Aldrich). Cells were grown in Iscove's modified DMEM supplemented with 10% FBS, 1% L-glutamine, 1% penicillin/streptomycin, and 1% amphotericin B [294–296]. Experiments were performed 3-5 days after isolation.

d) *In vitro* treatments

Unless stated otherwise, cells were treated for 1 to 72 h with clinically relevant concentrations of APAP and ARV drugs, chosen considering the interindividual pharmacokinetics variability reported in several clinical studies. Treatments were performed using sub-confluent cell cultures in medium supplemented with 10% iFBS. Several concentrations of each drug were tested in order to analyse the

concentration-dependence of the studied effect. Additionally, a negative control (untreated cells) and a vehicle control were used in every experiment. Also, several positive controls were used depending on the biological process that was studied in each experiment. Additionally, some experiments in Hep3B cells were carried out with conditioned medium from treated LX-2 cells.

III.B.2. *In vivo* approaches

a) Animal studies

Ten-week-old female C57BL/6J mice were supplied by Janvier Labs (Le Genest Saint Isle, France). Animals (20 ± 3 g of body weight) were given ad libitum access to water and chow diet (Envigo, Huntingdon, UK), they were kept at 21 ± 1º C under a standard light/dark regimen (12 h/12 h). Mice were always randomly divided into the different experimentation groups (ten mice per group).

All animal procedures were performed in accordance with the guidelines for the care and use of laboratory animals of the University of Valencia (Valencia, Spain), and were approved by the local ethics committee (authorization codes A1406879617392 and A1415981032459).

b) ARV drug administration

Animal dosage were calculated using the normalized interspecies allometric scaling factor, based on interespecific body surface area calculations, stablished by FDA to reach a dose for mice equivalent to the daily maximum therapeutic dose of EFV (600 mg) and RPV (25 mg) [297,298]. Therefore, animals were orally treated *(p.o.)* on a daily basis with 2.47 mg of EFV or 0.1 mg of RPV dissolved in 10 µL of DMSO.

All mice were sacrificed at the end of the protocol using isoflurane-inhaled anaesthesia. Blood samples were collected from the cave vein. Livers were weighed and fixed in 10% formalin for histological analysis or snap-frozen in liquid nitrogen followed by storage at -80° C.

c) Mice models of chronic liver disease

1. Nutritional model of NAFLD

After carefully reviewing numerous studies about NAFLD modelling, we finally decided to establish an overnutrition model of NAFLD in female C57BL/6 mice

for 12 weeks, in order to study the implication of several anti-HIV drugs in the development and progression of chronic liver disease (Figure III.1).

Specifically, we used a highly lipogenic and aterogenic diet ('high fat diet', HFD) specially prepared by Ssniff Spezialdiäten GmbH (Soest, Germany), composed by 59% of fat, 26% of carbohydrates, 15% of proteins and 2% of cholesterol (Ssniff® *EFR/M D12330 mod.*/Surwit*). In order to analyse the progression of NAFLD, and the actions of representative drugs from different ARV families in this process, animals were divided in different experimental groups:

- **Normal diet (ND) control group:** mice fed with normal diet.
- **HFD control group:** mice fed with HFD.
- **Vehicle ND group:** mice fed with ND and daily administered with 10 µL of pure DMSO.
- **Vehicle HFD group:** mice fed with HFD and daily administered with 10 µL of pure DMSO.
- **Drug-treated ND group:** mice fed with ND and daily administered with the ARV drug dissolved in 10 µL of DMSO.
- **Drug-treated HFD group:** mice fed with HFD and daily administered with the ARV drug dissolved in 10 µL of DMSO.

Mice were monitored daily and weighed once a week. Importantly, no differences between Control and Vehicle groups were found in all the studied parameters.

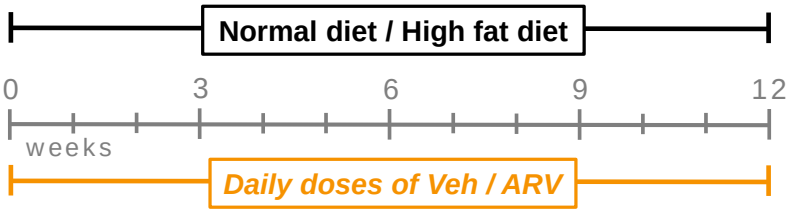

Figure III.1: Nutritional model of NALFD.

2. Liver fibrosis models

We used different variations of the CCl_4-induced liver injury model in mice to study the capacity of the compounds under study to modulate the pathophysiological mechanisms involved in liver fibrosis progression, regression and liver regeneration.

2.1 Effect of ARV drugs in the progression of liver fibrosis

In this model, 0.5 mg/Kg CCl_4 dissolved in 50 µL of corn oil were intraperitoneally injected (*i.p.*) in mice in alternate days for 4 weeks. ARV administration was done exactly as in the nutritional model. Thus, drugs were administered (*p.o.*) on a daily basis during the whole duration of the experiment (see Figure III.2).

Three different experimental groups were defined for the study of each compound:

- **Control group (Veh):** daily oral DMSO administration and corn oil injections in alternate days for 4 weeks.
- **Liver fibrosis group:** daily oral DMSO administration and CCl_4 injections in alternate days for 4 weeks.
- **Drug-treated fibrosis group:** daily oral ARV administration and CCl_4 injections in alternate days for 4 weeks.

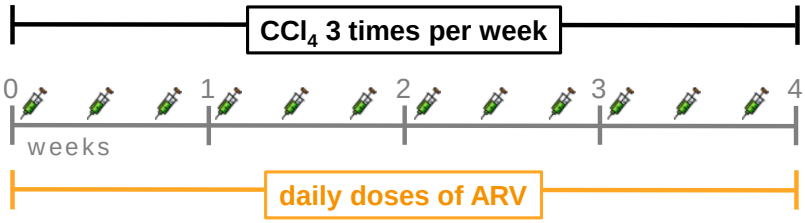

Figure III.2 Mice model to study the effect of ARV drugs in the progression of liver fibrosis.

2.2 Effect of ARV drugs in the regression of liver fibrosis

CCl_4 injections were administered in the same way than in the previous protocol (section 2.1), but the duration of the procedure was increased until six weeks. Alike, ARV administration was done orally and in a daily basis, but only during the last two weeks of the procedure (see Figure III.3). Therefore, three experimental groups were defined:

- **Control group (Veh):** corn oil injections in alternate days for 6 weeks and daily oral DMSO administration only during the last 2 weeks.
- **Liver fibrosis group:** CCl_4 injections in alternate days for 6 weeks and daily oral DMSO administration only during the last 2 weeks.
- **Drug-treated fibrosis group:** CCl_4 injections in alternate days for 6 weeks and daily oral ARV administration only during the last 2 weeks.

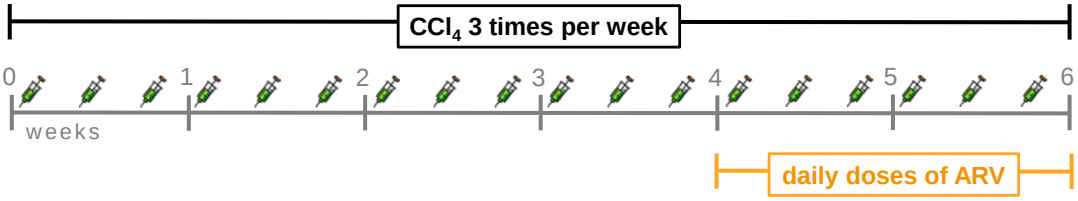

Figure III.3: Mice model to study the effect of ARV drugs in the regression of liver fibrosis.

2.3 Effect of ARV drugs in the spontaneous regeneration of the liver

In this procedure, CCl_4 injections were administered following the same protocol but only for four weeks. Afterwards, control and vehicle groups were allowed to regenerate by themselves for two weeks, whereas treated groups were daily administered with ARV drugs for this same period of time (see Figure III.4). Thus, three experimental groups were defined:

- **Control group (Veh):** corn oil injections in alternate days for 4 weeks and then only daily oral DMSO administration for two more weeks.
- **Liver fibrosis group:** CCl_4 injections in alternate days for 4 weeks and then only daily oral DMSO administration for two more weeks.
- **Drug-treated fibrosis group:** CCl_4 injections in alternate days for 4 weeks and then only daily oral ARV administration for two more weeks.

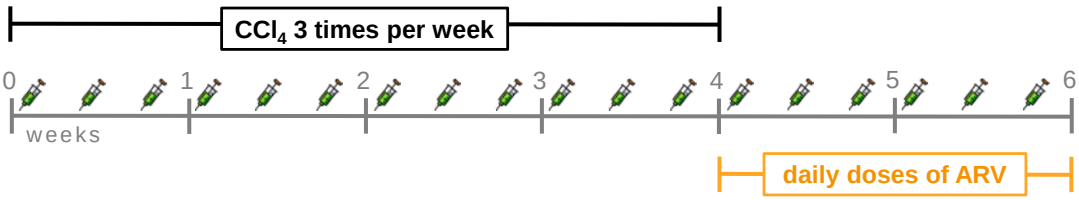

Figure III.4 Mice model to study the effect of ARV drugs in spontaneous liver regeneration.

III.B.3. Transfection of mammalian cell lines: transient gene silencing

Endo-ribonuclease prepared small interfering (si)RNA (esiRNA) are a heterogeneous mixture of siRNAs that all target the same mRNA sequence. As higher specificity and lesser off-target effects have been demonstrated when compared with classic siRNA, esiRNA were used in our experiments targeting both STAT1 and Luciferase (Sigma-Aldrich). esiRNA targeting Luciferase was used as transfection control (SiC), since it is not expressed in our cells [299,300].

LX-2 cells were transiently transfected using Lipofectamine™ 2000 (Invitrogen, Thermo Fisher Scientific), according to the manufacturer's instructions. Cells

were seeded the day before the transfection in 6-well plates and maintained at 37º C in a CO_2 incubator overnight. For the transfection, 100 pmol of STAT1 esiRNA (Sigma-Aldrich) and 10 µL of Lipofectamine™ 2000 were diluted gently in 250 µL of serum-free Opti-MEM® (Invitrogen, Thermo Fisher Scientific) in two separate tubes.

Diluted esiRNA and diluted Lipofectamine™ 2000 were combined (total volume of 500 µL), mixed gently and incubated for 20 min at room temperature (RT). The transfection mixture was added to LX-2 cells (80-90% confluence) in 6-well plates containing 1.5 mL of supplemented MEM without antibiotics and mixed gently before incubation for 6 h at 37º C in a cell culture incubator. After 6 h, the medium was replaced by fresh supplemented MEM. The following day, transfected cells were treated according to the different experimental conditions.

III.B.4. Cell viability assay

Cell viability and proliferation was detected using a MTT based-colorimetric assay (Cell Proliferation Kit I MTT, Roche Life Sciences). This assay is based on the reduction of the yellow tetrazolium salt MTT [3-(4,5-dimethylthiazol-2-yl)-2,5-diphenyl tetrazolium bromide] to purple formazan [301], which takes place only by active mitochondrial reductases, such as NADH and NADPH (Figure III.5), and hence, MTT reduction is related to the number of viable and metabolically active cells. The purple formazan crystals are solubilized, usually with an organic solvent or a sodium dodecyl sulfate (SDS) solution, and the absorbance of the resulting colored solution is finally quantified spectrophotometrically at 570 nm.

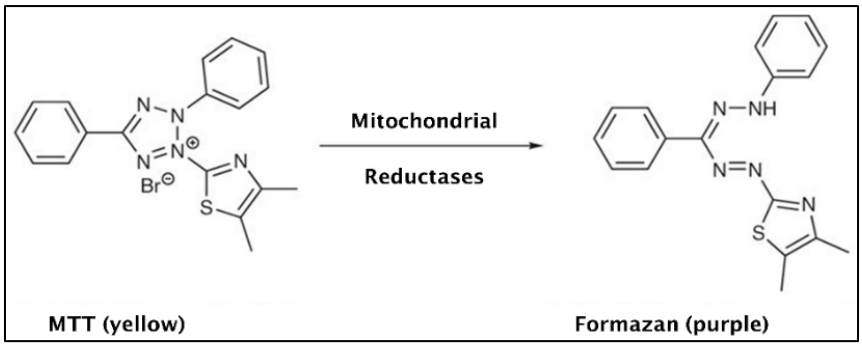

Figure III.5: Metabolization of MTT to a formazan salt by viable cells.

To perform the MTT assay, cells were seeded in 96-well cell culture plates. MTT reagent was added (20 µL/well) to the cells for the last 4 h of treatment. Medium

was then discarded and 100 µL/well DMSO were added to each well, and the plate was incubated at 37º C for 5 min, in darkness. Following incubation, absorbance was measured at 570 nm and 690 nm employing a Multiskan™ Ascent 354 microplate spectrophotometer (Thermo Scientific). To achieve accurate results, the absorbance measured at 690 nm (background absorbance) was subtracted from the 570 nm absorbance value.

III.B.5. Mitochondrial respiration measurement

Cellular O_2 consumption was measured in Hep3B cells, employing a Clark-type electrode (Oxytherm System, Hansatech Instruments, Norfolk, UK). The Clark electrode consists of a silver anode, a platinum cathode, and an electrolyte (3 M KCl), where both anode and cathode are immersed. In addition, a thin teflon membrane is placed onto both electrodes, which is permeable to O_2 and allows this molecule to reach the platinum cathode, where it is electrolytically reduced (Figure III.6). The reduction of O_2 generates a current of electrons between both electrodes, producing a potential difference, which is simultaneously recorded by the software connected to the electrode. The Oxytherm System is connected to an integral thermoelectric temperature control that provides measurements at constant temperature [302].

$$O_2 + 2e^- + 2H_2O \longrightarrow H_2O_2 + 2OH^-$$

Figure III.6: Clark-type electrode's chemical reaction: oxidation of atmospheric O_2.

The electrode was calibrated in air-saturated respiration buffer (HBSS) before performing each measurement: the atmospheric O_2 concentration was considered as maximal (200 µM), and the electrode zero setting was achieved by adding excess of sodium dithionite (Panreac Química) to the respiration chamber. The measurement of the O_2 consumption was performed in intact cells, which were detached by trypsinization and counted using a hemocytometer (Neubauer Improved, Laboroptik Ltd.) immediately prior to the measurement. For each experiment, 3 million cells were resuspended in 1 mL respiration buffer (HBSS) and taken into the respiration chamber, where the cellular suspension was constantly stirred and maintained at 37º C. The mitochondrial origin of O_2 consumption was confirmed by addition of 1 mM potassium cyanide (KCN), which is an OxPhos specific inhibitor, acting on mitochondrial cytochrome *c* oxidase.

Data obtained with the Clark-type electrode were acquired and analysed with the program O_2 View (Hansatech Instruments).

III.B.6. Fluorescence microscope: static cytometry

Static cytometry software connected to a fluorescence microscope is a useful tool for analysing automatically a broad range of cellular parameters in living adherent cells. Unlike in flow cytometry, cells remain adherent, avoiding appearance of artefacts such as those generated by trypsin-induced cell damage or aggregate formation.

These experiments were performed using an Olympus IX81 fluorescence inverted microscope (Olympus, Hamburg, Germany) connected to the static cytometry software ScanR® v.2.03.2 (Olympus). In addition, the Cell^R software v.2.8 was employed to take images manually. All treatments were performed in duplicate in 48- or 24-well plates, and 15-25 live-cell images per well were recorded and analysed. For the last 30 min of treatments, cells were incubated with specific fluorescent probes at 37º C in darkness, and subsequently washed with HBSS; cells were maintained in this buffer during the process of life cell imaging. For all experiments, nuclei were stained with the fluorescent dye Hoechst 33342 (2.5 µM), with the purpose of focusing the cells and performing cell count. All fluorescent probes were purchased from Molecular Probes™ (Thermo Fisher Scientific), except for Hoechst® 33342, which was supplied by Sigma-Aldrich.

a) Cell survival/proliferation analysis

Cells were treated and allowed to proliferate exponentially for 24-72 h and then counted according to Hoechst® 33342 fluorescence, which emits blue fluorescence when bound to dsDNA [303]. 25 images per well were analysed and detection filters used were 348/496 nm (excitation/emission).

b) Mitochondrial superoxide production

To assess mitochondrial superoxide production, cells were incubated with 5 µM MitoSOX™, which permeates selectively mitochondria (due to its positive charge) and is immediately oxidized by superoxide, but not by other ROS, producing a red fluorescence. Rotenone was used as positive control. Detection filters used were 510/590 nm (excitation/emission).

c) Mitochondrial membrane potential

Tetramethylrhodamine methyl ester (TMRM 5 µM) was employed to assess $\Delta\Psi_m$, given it is only sequestered within active mitochondria. As a positive control, an uncoupler of OxPhos, carbonyl cyanide m-chlorophenyl hydrazine (CCCP, 10 µM) was employed. Detection filters used were 510/590 nm (excitation/emission).

III.B.7. Spectrophotometric analysis of the activity of the ETC complexes

The mammalian mitochondrial ETC includes proton-pumping enzymes known as complex I (NADH–ubiquinone oxidoreductase, CI), complex II (succinate-quinone oxidoreductase), complex III (cytochrome bc1, CIII) and complex IV (cytochrome *c* oxidase, CIV), whose electron transfer activity is mediated by the mobile membrane-embedded carriers ubiquinone and soluble cytochrome *c*. The free energy and electrons released at each step along the chain creates an energetic potential in the mitochondrial membrane which is finally used by the ATP synthase (complex V, CV) to generate ATP (Figure III.7).

The global activity of the ETC can be directly measured by the respiration analysis explained in the chapter III.B.5. However, the specific determination of the enzymatic activity of each mitochondrial complex provides additional and accurate information about the mitotoxic mechanisms exerted by the different drugs under study [304,305].

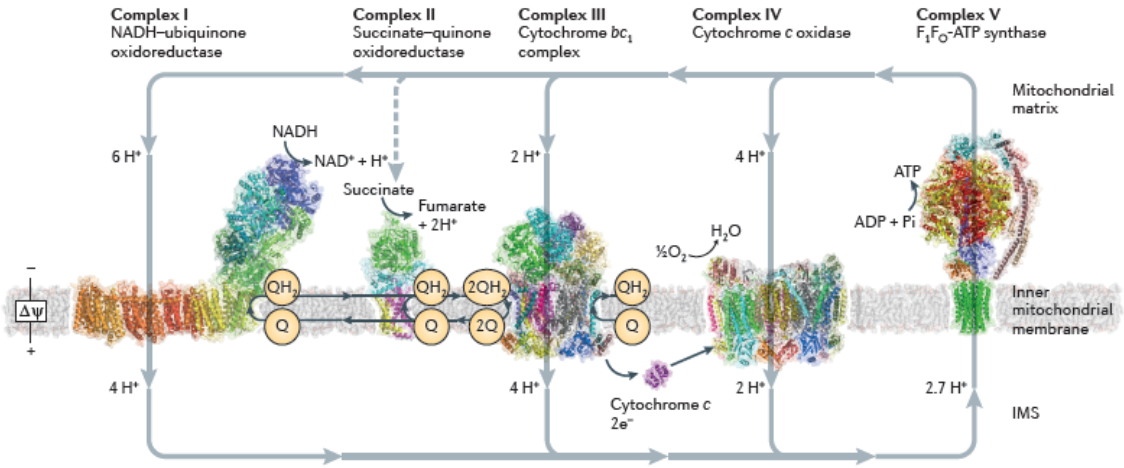

Figure III.7: The electron transport chain [304].

a) Protein extraction

Cell pellets from Hep3B cells were resuspended in 0.5 mL MOPS-Sucrose buffer (20 mM and 0.25 mM, respectively), kept 5 min in ice and centrifuged at 5000 g

for 3 min. After that, supernatant was discarded and the pellets were resuspended in MOPS-Sucrose-EDTA buffer (20 mM, 0.25 mM and 1 mM respectively), maintained again in ice for 5 min and centrifuged at 1000 g for 3 min. Finally, the obtained pellets were resuspended in potassium phosphate (KP) buffer pH 7.4 and kept at -20° C until enzymatic determination.

b) Protein quantification

The Bradford assay is based on the binding of Coomassie Brilliant Blue G-250 dye to proteins. Under acidic conditions, the dye is predominantly in the doubly protonated red cationic form, but when the dye binds to protein, it is converted to a stable unprotonated blue form that can be detected at 595 nm using a spectrophotometer [306,307].

A standard protein curve was prepared by serial dilutions of BSA in the same KP buffer as the samples to minimize the background absorbance. 10 µL of diluted sample (1:15) or standard were used per well in a 96-well plate and immediately after 200 µL of diluted working solution of Bradford reagent (BioRad; 1:5) was added to each well. Both samples and standard curve points were assayed in duplicate. Next, the plate was incubated (protected from light) at 37º C for 10 min with gentle rocking. Finally, absorbance was measured at 595 nm employing a Multiskan™ Ascent 354 microplate spectrophotometer (Thermo Labsystems, Thermo Fisher Scientific).

c) Determination of CI enzymatic activity

CI is essential for oxidative phosphorylation in mammalian mitochondria. It couples electron transfer from NADH to ubiquinone with proton translocation across the energy-transducing inner membrane, providing electrons for respiration and driving ATP synthesis [305].

The enzymatic activity of this macroprotein complex was evaluated by triplicate in 96-well plates. Briefly, KP buffer 100 mM (pH 7) containing 0.2 mM NADH, 1 mM NaN_3 and 0.1% BSA-EDTA was added to 15 µg of sample dissolved in the same KP buffer. After 8 min of incubation at 30° C, oxidized ubiquinone (CoQ1) was added at a final concentration of 0.1 mM as a proton recipient from NADH. The mixture was incubated for 2 min and the absorbance progression was measured every 30 sec for 3 min at 340 nm. In order to determine the intrinsic CI

activity non-susceptible to drug-inhibition, the specific inhibitor rotenone was added at 5 µM in each well. It was incubated for 2 more min and the absorbance was measured as previously described. This intrinsic activity was subtracted from the total activity recorded to obtain the final drug-sensitive complex I activity [304,305].

d) Determination of CII enzymatic activity

CII is a component of both the Krebs cycle and the respiratory chain. CII oxidizes the Krebs cycle intermediate succinate, generating fumarate by passing electrons from succinate to FAD. Unlike respiratory CI or CIII, CII does not pump protons across the inner membrane, but is capable of reducing ubiquinone to ubiquinol, which can then be re-oxidized by CIII and thus participate in the proton pumping of oxidative phosphorylation [308,309].

CII enzymatic activity was measured by the reduction of the chemical compound 2,6-dichlorophenol-indophenol (DCPIP), which was reduced by the electrons from succinate oxidation. When oxidized, DCPIP is blue with a maximal absorption at 600 nm and, when reduced, DCPIP is colorless [308]. Briefly, 20 µg of sample dissolved in KP buffer (100 mM, pH 7) containing 0.1 mM DCPIP and 0.3 mM KCN were incubated 2 min at 30° C. Next, succinate was added at a final concentration of 30 mM. The mixture was then incubated for 30 sec and the absorbance progression was measured every 30 sec for 3 min at 600 nm. Finally, once DCPIP was completely reduced due to the high concentration of succinate, oxidized ubiquinone was added at 50 µM to assess its reduction by the DCPIP. Once again, this process was measured every 30 sec for 3 min.

As KCN is a specific inhibitor of CIV, it was added in this protocol to increase the specificity of the determination.

e) Determination of CIII enzymatic activity

Mitochondrial CIII is a proton-pumping enzyme that catalyzes the reduction of ferricytochrome *c* by the reduced coenzyme Q through transferring electrons in the respiratory chain. This activity also contributes to generate proton motive force that in turn drives CV to generate ATP [279,310].

CIII specific activity was measured analysing the reduction of cytochrome *c* at 550 nm. Briefly, a mixture of 40 µL of 0.25 mM cytochrome *c*, 80 µL of ddH_2O

and 50 µg of samples dissolved in KP buffer (100 mM, pH 7) were transferred into a 96-well plate. The reaction was started by the addition of 40 µL of the freshly prepared reaction mixture containing 250 mM Tris (2-Amino-2-(hydroxymethyl)-1,3-propanediol)-HCl pH 7.4, 20 mM NaN_3 and 0.25 mM decylubiquinol. The increase of absorbance at 550 nm was recorded spectrophotometrically every 30 sec for 3 min at 30° C. The antimycin A-insensitive CIII activity (non-enzymatic reaction) or antimycin A-treated residual activity were determined simultaneously adding 0.01 mM antimycin A to the reaction mixture. CIII specific activity was calculated as total activity minus antimycin A-treated residual activity [311].

f) Determination of CIV enzymatic activity

CIV uses reduced cytochrome *c* from CIII to reduce molecular oxygen to water, which is the ultimate electron acceptor and the last step in the oxidative phosphorylation prior to ATP synthesis by CV. CIV acts also as a proton-pumping enzyme and contributes to the proton motive force generation in the mitochondrial intermembrane space [304,305,312,313].

CIV activity was measured analysing the decrease in absorbance at 550 nm due to the oxidation of reduced cytochrome *c*. Previously to this determination, 0.8 M cytochrome *c* diluted in buffer KP 100 mM (pH 7) was completely reduced by the addition of solid sodium borohydride (BH_4Na). For the enzymatic determination, 20 µg of protein extracts were incubated for 2 min at 37° C with KP buffer containing cytochrome *c* at a final concentration of 80 mM. After that, absorbance was measured every 30 sec for 3 min at 550 nm.

III.B.8. Fluorimetric determinations

a) Determination of ROS production

ROS production in Hep3B cells was determined by using the esterified form of dichlorofluorescin, dichlorofluorescin diacetate (DCFH-DA). This molecule crosses cell membranes and then undergoes deacetylation by intracellular esterases, resulting in dichlorofluorescin (DCFH). This new compound is susceptible to intracellular ROS-mediated oxidation and generates the fluorescent compound dichlorofluorescein (DCF).

Drug-induced ROS production was studied by addition of 2.5 µM DCFH-DA before treatment with ARV for 1 h. Hydrogen peroxide (100 µM) and rotenone (a

specific inhibitor of the CI of the ETC; 100 µM) were used as positive controls. Fluorescence was detected every 5 min for 1 h using a Fluoroskan Ascent FL reader (Thermo Labsystems).

b) Determination of intracellular ATP concentration

The intracellular ATP concentration in Hep3B cells was determined using the ATP Bioluminescence Assay Kit HSII (Roche). This determination is based on the oxidation of luciferin to oxyluciferin by the luciferase enzyme, as showed in Figure III.8. ATP can be measured in the samples as it is directly proportional to the light emitted by the chemiluminescent reaction.

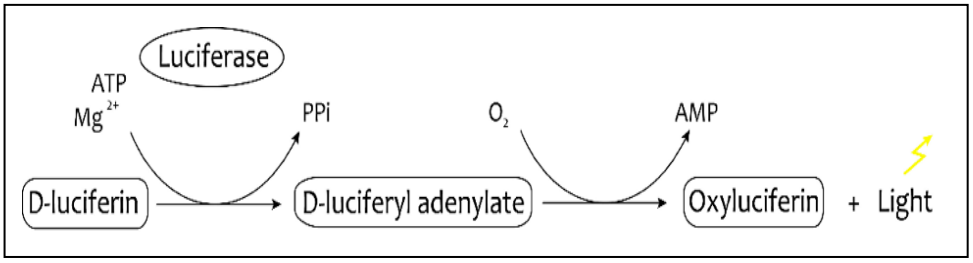

Figure III.8: Oxidation of luciferin to oxyluciferin by luciferase [314].

According to the manufacturer's instructions, cell pellets from Hep3B cells were resuspended in the dilution buffer provided by the kit. ATP standard curve was prepared from 10^{-11} to 10^{-2} M. All ATP dilutions and samples were distributed by triplicates in a black 96-well plate. After 5 min of incubation with the cell lysis reagent at RT, 30 µL of luciferase reagent were added and a Fluoroskan Ascent FL reader (Thermo Labsystems) was used to determine the luminescence.

ATP concentrations from samples, calculated by interpolation of the obtained luminescence in the standard curve, were normalized with the protein concentration in each sample (determined by BCA Protein Assay as described in the B.10.2 section of this chapter). Final values were expressed as nmol of ATP/mg of protein.

III.B.9. Flow cytometry analysis

Flow cytometry is a useful technology to study the effect of different molecules in living cells at the single-cell level. This approach has several advantages over other techniques such as microscopy, image analysis or those based on plate readers, like the possibility to analyse at the same time several variables in thousands of living cells in few seconds and with high sensitivity, and the lack of

influence of the medium where cells are suspended. Furthermore, the fluorescence values obtained are much more precise than those derived from plate readers and can be independently analysed in different fluorescence channels [315].

a) Measurement of reduced GSH

ROS are produced in eukaryotic cells as a result of the normal metabolism. Several cellular sources, including mitochondria, produce significant amounts of ROS that contribute to intracellular oxidative stress.

Dismutation of $O_2^{\bullet -}$ generates H_2O_2, which is usually removed by catalase and peroxidases, through the action of reducing molecules such as GSH and $NADH_2$. GSH is synthesized in the cytosol and then transported into different organelles, including mitochondria and the nucleus. It has a major role in protecting the cell against oxidants and electrophiles, and its intracellular concentration can be very high (up to 10 mM). GSH can be detected by flow cytometry by monobromobimane (MBB), a molecule that, if excited with a 405 nm violet laser or an ultraviolet (UV) lamp, becomes fluorescent only after its conjugation with thiols. MBB binds non-enzymatically with GSH, and reacts much more rapidly with this molecule than with sulfhydryl proteins [315].

For these experiments, HepaRG cells were used. After detaching them by trypsinization, they were stained with 50 mM MBB for 10 min at 37° C, and washed with PBS. Reduced GSH was then detected using MBB and, simultaneously, propidium iodide was employed to assess cellular viability. Fluorescence was detected by a BD FACSVerse flow cytometer (BD Biosciences), and data were analysed with BD FACSuite software (BD Biosciences). Given the high concentrations of GSH present in hepatocytes, cells were divided in two populations, those with high and those with low levels of GSH, to detect more easily differences in MBB fluorescence once cellular debris and dead cells had been discarded. Diethyl maleate (DEM) was used as a positive control of GSH depletion.

b) Measurement of apoptosis induction

Cells undergoing apoptosis show characteristic morphological and biochemical features, which include chromatin condensation, cell and nuclear shrinkage,

formation of membrane-bound cell fragments, known as apoptotic bodies, and rapid phagocytosis by neighbouring cells or macrophages without associated inflammation. In apoptotic cells, membrane phospholipid phosphatidylserine (PS) is translocated from the inner to the outer leaflet of the plasma membrane, thereby exposing PS to the external cellular environment. Annexin V is a Ca^{2+}-dependent phospholipid-binding protein that has high affinity for cells with exposed PS. When Annexin V is conjugated to fluorochromes, it retains its high affinity for PS and thus serves as a sensitive probe for flow cytometric analysis of apoptotic cells. Since externalization of PS occurs in the earlier stages of apoptosis, FITC Annexin V staining can identify apoptosis at an earlier stage than assays based on nuclear changes such as DNA fragmentation [316–318].

Therefore, the Annexin V-FITC Apoptosis Detection Kit (Abcam) was used. After 72 h of treatment, LX-2 cells were detached by trypsinization from 6-well plates, washed with PBS, resuspended in binding buffer (provided by the kit), and stained with both Annexin V and propidium iodide according to the manufacturer's instructions. Fluorescence was detected by a BD FACSVerse flow cytometer, and data were analysed with BD FACSuite software (BD Biosciences).

III.B.10. Protein expression analysis

III.B.10.1. Protein extracts

a) *In vitro* sample collection and preparation

After removing cell culture medium, cells were washed once with warm PBS and detached by adding trypsin-EDTA (at 37º C for 1 min). The resulting cellular suspension was centrifuged at 800 g for 3 min at RT, supernatant was then discarded and cell pellet was resuspended in 1 mL ice-cold PBS. This suspension was centrifuged again at 500 g for 5 min at 4º C. Finally, supernatants were discarded and cell pellets were obtained.

b) Whole-cell protein extraction

Cells pellets were resuspended in 40-90 µL of complete lysis buffer, whose composition was 20 mM HEPES pH 7.4, 400 mM NaCl, 20% (v/v) glycerol, 0.1 mM EDTA, 10 µM Na_2MoO_4 and 10 mM NaF. Immediately prior to their use, 1 mM DTT, 5 mM broad-spectrum serine and cysteine protease inhibitors (Complete Mini™ and Pefabloc®, both from Roche Life Science) and 0.05%

detergent solution (NP-40 Surfact-Amps™, Thermo Fisher Scientific) were added. Samples were then vortexed twice at maximum speed for 10 sec, incubated on ice for 15 min, vortexed again at maximum speed for 30 sec and subsequently centrifuged at 16000 g for 15 min at 4º C. Pellets were discarded, and supernatants (whole-cell protein extracts) were collected in new ice-chilled tubes and stored at -20º C until use.

c) Total protein extracts from liver tissue

Liver samples (20-35 mg) were homogenized in 900 µL extraction buffer (0.66 M Tris-HCl pH 7.5, 1 mM EGTA, 1 mM Na_3VO_4, 1 mM NaF and the protease inhibitor Complete Mini™) using a MACS™ Dissociator (MACS Miltenyi Biotec, Bergisch Gladbach, Germany). After adding 10 µL of 10% NP-40 Surfact-Amps™, the homogenized samples were sonicated for 5 min at 15º C, and then centrifuged at 16000 g for 40 min at 4º C. The resulting supernatants (total protein extracts) were collected and stored at -20º C.

III.B.10.2 Protein quantification: bicinchoninic acid (BCA) assay

The BCA assay was used to quantify protein content in the extracts. This method combines the reduction of Cu^{2+} ions from Cu_2SO_4 to Cu^{+} by proteins in an alkaline medium (the well-known Biuret reaction) with the highly sensitive colorimetric detection of Cu^{+}, based in the chelation of two molecules of BCA with one Cu^{+} ion. The purple-colored reaction product of this assay exhibits a strong absorbance at 562 nm, which is approximately linear with increasing protein concentrations over a broad working range (0.02-2 mg/mL) [319].

This assay was performed following the manufacturer's instructions (Pierce™ BCA Protein Assay Kit, Thermo Fisher Scientific). A standard protein curve was prepared by serial dilutions of BSA (0.03125-1 mg/mL) in the same extraction buffer as the samples to minimize the background absorbance. 20 µL of diluted samples (1:20 and 1:30 for *in vitro* and *in vivo* protein samples, respectively) or standard dilutions were used per well in a 96-well plate placed on ice, and immediately after 200 µL of working mixture reagent were added to each well. This working mixture was always prepared fresh before use, mixing 50 parts of Pierce™ BCA reagent A with 1 part of reagent B. Both the samples and standard curve points were assayed in duplicate. Next, the plate was incubated (protected

from light) at 37º C for 30 min with gentle rocking. Finally, absorbance was measured at 570 nm employing a Multiskan™ Ascent 354 microplate spectrophotometer (Thermo Labsystems, Thermo Fisher Scientific).

III.B.10.3 Western Blotting (WB)

a) SDS-polyacrylamide gel electrophoresis (PAGE)

SDS-PAGE was performed using the Mini-PROTEAN® Tetra Cell System (Bio-Rad Laboratories, Hercules, CA, USA). Polyacrylamide gels were made using a mixture of acrylamide/bis-acrylamide solution (37.5:1) (Ultrapure ProtoGel® supplied by National Diagnostics, Hessle, UK). Resolving gels were prepared with different percentage of polyacrylamide (6-15%) in 0.375 M Tris-HCl pH 8.8 and 0.1% SDS, whereas stacking gels were always prepared with 3.75% polyacrylamide in 0.125 M Tris-HCl pH 6.8 and 0.1% SDS. The polymerization reaction was catalysed by 0.1% ammonium persulfate (APS) (SERVA, Heidelberg, Germany) and N,N,N′,N′-tetramethylethylenediamine (TEMED, Sigma-Aldrich).

Extracts with equal total protein amounts were loaded; previously prepared by adding Laemmli sample buffer (0.5 mM Tris-HCl pH6.8, 25% glycerol v/v, 10% SDS, 0.5% β-mercaptoethanol and 0.5% bromophenol blue) and boiled at 100º C for 5 min in order to achieve protein denaturation. To determine the molecular weight of the polypeptides, a molecular weight marker (EZ-Run™ Pre-Stained Rec Protein Ladder, Thermo Fisher Scientific) was also loaded. Electrophoresis was performed in a buffer tank with running buffer (25 mM Tris pH 8.3, 0.1% SDS and 192 mM glycine) at a constant voltage of 120 V.

b) Protein transfer to nitrocellulose membrane

SDS-PAGE-resolved proteins were transferred from the resolving polyacrylamide gel to a 0.45 µm nitrocellulose blotting membrane (GE Healthcare Life Science), using a Mini Trans-Blot® Cell (Bio-Rad Laboratories). The transfer was performed at 4º C for 1 h (proteins with molecular weight up to 100 KDa) or 1.5 h (proteins over 100 KDa) at a constant amperage of 0.4 A, in transfer buffer (25 mM Tris pH 8.3, 192 mM glycine and 20% methanol).

c) Ponceau and antibodies staining

In order to verify the transfer efficiency and quality, the nitrocellulose membrane was soaked in a 0.1% Ponceau/5% acetic acid solution (Sigma-Aldrich) for 1 min, which stains proteins. Ponceau staining was removed with Tris-buffered saline-Tween (TBS-T, 20 mM Tris-HCl pH 7.2, 150 mM NaCl and 0.1% Tween-20 v/v) before incubating the membrane in fresh blocking solution (5% fat-free milk powder or BSA, diluted in TBS-T) with continuous gentle shaking, for 1 h, at RT. Once the membrane was blocked, it was incubated with the primary antibody, prepared in blocking solution supplemented with 0.02% NaN_3 (Sigma-Aldrich) for 3 h, at RT or overnight at 4º C with continuous gentle shaking. Subsequently, the membrane was washed four times in TBS-T for 10 min, at RT and with vigorous shaking, incubated with a secondary antibody in fresh blocking solution at RT for 1 h, and washed again.
All primary and secondary antibodies used are listed in Table III.3

d) Chemiluminescence detection

Immunolabeling was detected by enhanced chemiluminescence, employing Luminata™ Crescendo Western HRP substrate (Merck Millipore, Billerica, MA, USA), Amersham™ ECL™ Start Western Blotting Detection Reagent (GE Healthcare Life Science) or SuperSignal™ West Femto Maximum Sensitivity Substrate (Thermo Fisher Scientific), following manufacturer's instructions. This detection method is based in an oxidation reaction of luminol catalyzed by the enzyme horseradish peroxidase (HRP), conjugated to the secondary antibody, in the presence of hydrogen peroxide, and giving rise to 3-aminophthalate that emits light at 425 nm [320].

Immunolabeling was visualized with a digital luminescent image analyser, Fujifilm LAS-3000 Imager (Fujifilm, Tokio, Japan). Densitometric analyses were performed using Multi Gauge V3.0 software (Fujifilm, Tokio, Japan). The protein expression was normalized versus that of the β-actin or GAPDH (employed as loading controls).

e) Stripping for reprobing

Stripping, a method that removes antibodies from a nitrocellulose membrane, enables reutilization of the membrane and its incubation with other antibodies. The stripping process was performed in two different ways:

1. Incubation with a stripping solution (62.5 mM Tris-HCl pH 6.7, 100 mM β-mercaptoethanol and 2% SDS), at 56º C for 30 min with vigorous shaking. After that, the membrane was washed with TBS-T three times for 10 min, at RT.
2. Incubation with 0.5 M glycine pH 2.5 for 10 min at RT with vigorous shaking. Subsequently, the membrane was washed twice with TBS-T for 10 min, at RT.

Regardless of the protocol used, the membrane was blocked with the blocking solution again before incubating it with the antibodies, following the protocol described above (III.B.10.3 b).

PRIMARY ANTIBODIES				
PROTEIN	**SOURCE/CLASS**	**MW (KDa)**	**DILUTION**	**COMPANY**
Plin2	Rabbit polyclonal	48	1:2000	Abcam (ab52356)
PPARγ	Mouse monoclonal	56	1:1000	Invitrogen (419300)
LXRβ	Rabbit polyclonal	63	1:1000	Santa Cruz (sc1000)
p65	Mouse monoclonal	65	1:500	Invitrogen (339900)
p-p65	Rabbit monoclonal	65	1:1000	Cell Signaling (3033)
Caspase-1	Rabbit polyclonal	20/45	1:1000	Cell Signaling (2225)
Vimentin	Mouse monoclonal	57	1:1000	Abcam (ab8978)
Desmin	Mouse monoclonal	53	1:1000	Santa Cruz (sc23879)
Col1A1	Rabbit polyclonal	130	1:1000	Cell Signaling (84336)
STAT3	Rabbit monoclonal	88	1:1000	Abcam (ab68153)
p-STAT3	Rabbit monoclonal	88	1:1000	Abcam (ab76315)
p-STAT1	Mouse monoclonal	87	1:1000	Abcam (ab29045)
GAPDH	Rabbit monoclonal	38	1:10000	Sigma-Aldrich (G9545)
SECONDARY ANTIBODIES				
ANTIBODY		**LABELING**	**DILUTION**	**COMPANY**
Goat Anti-Mouse IgG Antibody		HRP	1:2000	Thermo Fisher (31430)
Goat Anti-Rabbit IgG Antibody		HRP	1:5000	Vector (PI-1000)

Table III.3 List of primary and secondary antibodies employed in WB experiments.

III.B.11. Gene expression analysis

III.B.11.1. RNA isolation

a) RNA extraction from cell cultures

RNA isolation and purification from cell cultures was performed using the RNeasy® Mini Kit supplied by Qiagen (Hilden, Germany), according to manufacturer's instructions. Briefly, cell pellet was resuspended in 350 µL lysis buffer and was homogenized by passage through a 25-gauge needle. Next, 350 µL of 70% ethanol were added and the solution was transferred to a column which retains RNA. After washing three times, RNA was eluted in 30 µL RNase-free water. The purity and concentration of the RNA were determined spectrophotometrically, using a NanoDrop™ ND-1000 spectrophotometer (Thermo Scientific).

b) RNA extraction from liver tissues

RNA extraction from liver tissues was performed using TriPure Isolation Reagent (Roche Life Science). Liver samples (30-40 mg) were homogenized by MACS™ Dissociator (MACS Miltenyi Biotec) in 750 µL TriPure and samples were then centrifuged at 16000 g for 15 min at 4º C. Afterwards, 150 µL chloroform were added to the supernatant, in order to separate the different phases (aqueous, interphase and organic), and subsequently the samples were vigorously vortexed, incubated on ice for 15 min and centrifuged at 16000 g for 15 min, at 4º C. The colorless aqueous upper phase, which contains RNA, was transferred to new tubes and RNA was precipitated by incubation with 500 µL isopropanol for 1 h or overnight at -20º C. Precipitated RNA was pelleted by centrifugation at 16000 g for 20 min at 4º C, washed with 1 mL 70% ethanol and pelleted again at 16000 g for 15 min at 4º C. Finally, RNA pellet was air-dried at RT and was resuspended in 50 µL RNase-free water.

The purity and concentration of the RNA was determined using a NanoDrop™ ND-1000 spectrophotometer (Thermo Scientific).

III.B.11.2 Complementary DNA (cDNA) synthesis by reverse transcription

cDNA was synthetized by reverse transcription, employing the PrimeScript™ RT Reagent Kit (Perfect Real Time) (TaKaRa Bio Inc., Otsu, Japan). In accordance with the manufacturer's protocol, the reaction was performed using 2 µg RNA and

1X PrimeScript Buffer, 1 µL PrimeScript RT Enzyme Mix I, 50 pmol Random 6-mers and 25 pmol Oligo dT Primer (20 µL final volume). The reaction was carried out in a GeneAmp® PCR System 2400 (PerkinElmer Inc, Waltham, MA, USA) under the following conditions: 37º C for 15 min, 85º C for 5 sec and 4º C for infinity.

III.B.11.3 Quantitative RT-PCR (qRT-PCR)

qRT-PCR was performed with SYBR® Premix Ex Taq™ (Tli RNaseH Plus) (TaKaRa Bio Inc.), containing TaKaRa Ex Taq HS, dNTP mixture, Mg^{2+}, Tli RNase H and SYBR Green I (DNA intercalator that emits fluorescence only when bound to dsDNA, and thus, detection of its fluorescent signal allows quantification of the amplification products). The reaction was performed mixing 1 µL cDNA, 5 µL SYBR® Premix Ex Taq™, 2 µM primers (forward and reverse) and RNase-free water (10 µL final volume). qRT-PCR were carried out in a Lightcycler® 96 Real-Time PCR System (Roche Life Science), following this protocol: 95º C for 30 sec; 95º C for 5 sec, 60º C for 20 sec (50 cycles); 95º C for 1 sec; 65º C for 15 sec; 95º C for 1 sec and 40º C for 30 sec. All experiments were performed in duplicate, together with a negative control (RNase-free water instead of cDNA).

The primer pairs for mice (Table III.4) and human (Table III.5) genes used were synthetized by IDT® (Integrated DNA Technologies, Coralville, IA, USA) or Metabion (Planegg, Germany). Before their use in qRT-PCR, primers were tested by performing melting curve analysis and standard electrophoresis on 2% agarose gel containing Goldview™ DNA Safe Stain (UVAT Bio C.B., Valencia, Spain) and using buffer TAE 1x (20 mM Tris pH 7.8, 0.5 mM EDTA and 10 mM sodium acetate).

qRT-PCR data were analysed using the comparative C_T method (21,22) obtaining the relative gene expression of the gene of interest. This method of presenting quantitative gene expression consists in this equation: Fold Change = $2^{-\Delta(\Delta CT)}$, where ΔC_T = C_T (target gene) - C_T (housekeeping gene), and $\Delta(\Delta C_T)$ = ΔC_T (treated) - ΔC_T (control). *ACTB*/*Actb* (β-actin) was used as a housekeeping gene.

MURINE PCR PRIMER PAIRS		
GENE	**FORWARD PRIMER (5'→3')**	**REVERSE PRIMER (5'→3')**
Acta2	GTCCCAGACATCAGGGAGTAA	TCGGATACTTCAGCGTCAGGA
Actb	GCCAACCGTGAAAAGATGACC	GAGGCATACAGGGACAGCAC
Adgre1	TGACTCACCTTGTGGTCCTAA	CTTCCCAGAATCCAGTCTTTCC
Arg1	GTGGGGAAAGCCAATGAAGAG	TCAGGAGAAAGGACACAGGTTG
Casp1	ACAAGGCACGGGACCTATG	TCCCAGTCAGTCCTGGAAATG
Cd86	GCACGGACTTGAACAACCAG	CCTTTGTAAATGGGCACGGC
Col1a1	GCTCCTCTTAGGGGCCACT	CCACGTCTCACCATTGGGG
Ifng	TCTGGAGGAACTGGCAAAAGG	TTGAATGCTTGGCGCTGGA
Il10	TGGACAACATACTGCTAACCGA	CTGGGGCATCACTTCTACCA
Il10r2	AAGCATACCTTCCGTTCTGGG	AGTTTGGGGTCATCGTGTGG
Il1b	GAAATGCCACCTTTTGACAGTG	CTGGATGCTCTCATCAGGACA
Il22a1	GGACACATCCGGTCTCCTTC	GGTTGCGGGTCTCCATAGTC
Il6	TGGACAACATACTGCTAACCGA	CTGGGGCATCACTTCTACCA
Il6st	GAGTGAGGAGGCTAGTGGGA	GCGACATAGCGGTCATTGGT
Jak1	AGAAGACTGAGGTGAAGCAGG	ACAGGGCGAAGAGGTTGTG
Jak2	CTGTAGTGGCAGCAGCAGAA	GTCTAACACCGCCATCCCAA
Ly6C	CAACTCTTGGCGCTGCTTGG	GGGTGCAGGTTCGGGATTCA
Mmp2	CAAGTTCCCCGGCGATGTC	TTCTGGTCAAGGTCACCTGTC
Mrc1	TGTGGAGCAGATGGAAGGTC	TGTCGTAGTCAGTGGTGGTTC
Nlrp3	ATTACCCGCCCGAGAAAGG	CATGAGTGTGGCTAGATCCAAG
Nos2	CGCTTGGGTCTTGTTCACTC	GGTCATCTTGTATTGTTGGGCTG
S100a4	GCACTTCCTCTCTCTTGGTCTG	AACTTCATTGTCCCTGTTGCTG
Serpine 1	ACCGTTACCCTGATTTGCCC	CCACTCACAGATGGCGTTGA
Socs1	CTCGCTCCTTGGGGTCTGTT	GGGAGATCGCATTGTCGGCT
Socs3	CAAGGCCGGAGATTTCGCTTC	CGGGAAACTTGCTGTGGGTG
Stat1	CTGTCATCCCGCAGAGAGAAC	CTCAGGGTATGGAGCAGAGC
Stat3	TTTCATCAGCAAGGAGCGGG	GGGGTAGAGGTAGACAAGTGGA
Tgfb1	GCGGACTACTATGCTAAAGAGGG	TCAAAAGACAGCCACTCAGG
Timp1	CTTGGTTCCCTGGCGTACTC	ACCTGATCCGTCCACAAACAG
Tnf	CCCTCACACTCAGATCATCTTCT	GCTACGACGTGGGCTACA

Table III.4 List of murine primer pairs used in qRT-PCR.

HUMAN PCR PRIMER PAIRS		
GENE	**FORWARD PRIMER (5'→3')**	**REVERSE PRIMER (5'→3')**
ACTA2	CCAAGCAACCGGGAGAAAATGA	GCATAGAGAACAGCACCGCCTGG
ACTB	GGACTTCGAGCAAGAGATGG	CTGTACGCCAACACAGTGCT
COL1A1	AAGCTGGAAAACCTGGTCGT	AGCACCATCATTTCCACGAG
MMP2	CAAGTTCCCCGGCGATGTC	TTCTGGTCAAGGTCACCTGTC
PDGFB	CCATCAGCAGCAAGGACACCA	CCCGAGCAGGTCAGAACGAA
PPARG	GACAGGAGACAACAGACAA ATC	GGGGTGATGTGTTTGAACTTG
SERPINE1	CGCTGTCAAGAAGACCCACA	ACCTGCTGAAACACCCTCAC
TGFB1	CTTCAGCTCCACAAGAAGAACTG	CACGATCATGTTGGACAACTGCTC
TIMP1	AATTCCGACCTCGTCATCAGG	ATCCCCTAAGGCTTGGAACC
VIMENTIN	ATGAAGGAGGAAATGGCTCGTC	GGGTATCAACCAGAGGGAGTGAA

Table III.5 List of human primer pairs used in qRT-PCR.

III.B.11.4 Transcriptomic analysis

a) Affimetrix Expression analysis.

Total RNA from whole liver tissue was isolated as previously described by using TriPure Isolation Reagent (Roche Life Science). All the following steps for transcriptomic analysis were carried out by the Multigenic Analysis Unit at the Central Service for Experimental Research (Faculty of Medicine, University of Valencia).

Genequant Pro Classic spectrophotometer (GE Healthcare) was used to determine the concentration and purity of RNA samples. The integrity analysis was performed using the RNA-6000 Nano Lab-on-a-Chip kit and the Bioanalyser 2100 (Agilent Technologies). The array used in this transcriptomic analysis was the GeneChip Mouse Gene 2.0 ST Array (Affymetrix). Before this, all samples were normalized to 300 ng of RNA and were hybridized by using the Hybridization Oven 645, also from Affymetrix, for 16 h at 45° C. During this protocol, the Fluidics Station 450 (Affymetrix) was used in all required washing steps. Finally, all samples were scanned through the GeneChip Scanner 3000 7G (Affymetrix).

b) Data analyses

Bioinformatic analyses of the transcriptomic data were carried out by Dr. Francisco García García from the Biostatistics Unit at Centro de Investigación Príncipe Felipe (Valencia).

Data were standarized using Robust Multi-array Average method [321] and quantile normalization. Differential gene expression was analysed using the limma [322] and masigpro [323] packages from Bioconductor. Multiple testing adjustment of p-values was done according to Benjamini and Hochberg methodology [324]. Gene set analysis was carried out using the Gene Ontology (GO) terms and the Kyoto Encyclopedia of Genes and Genomes Pathways (KEGG), using a logistic regression model [325,326]. This method detects significantly up- or down-regulated blocks of functionally related genes in lists of genes ordered by differential expression. Given that many functional terms are simultaneously tested, the results of the test are corrected for multiple testing to obtain an adjusted p-value. Gene set analysis returns adjusted p-values based on False Discovery Rate method [324,327]. GO annotation for the genes in the microarray where taken from Ensembl 78 release (http://www.ensembl.org) and KEGG Pathways from the KEGG web page (http://www.genome.jp/kegg/). Paintomics was used to visualize gene expression data onto the significant KEGG pathway maps [328].

III.B.12. Myeloperoxidase (MPO) activity assay

MPO is a pro-inflammatory enzyme mostly stored in the azurophilic granules of neutrophilic granulocytes. It plays a crucial role in intracellular pathogen killing, but it can provoke inflammatory damage when extracellularly released. MPO catalyzes generation of HOCl from H_2O_2 and Cl^-. This reaction is employed as an indirect estimation of neutrophil infiltration and intensity of the inflammatory response in different tissues [329,330]. Thus, the extent of liver inflammation and neutrophil infiltration in our mice models was evaluated by measuring MPO activity.

Briefly, frozen liver samples were homogenized in 0.02 M Na_2HPO_4 buffer (pH 4.7) containing 0.1 M NaCl and 0.015 M Na_4EDTA (1 g tissue/19 mL buffer) using an UltraTurrax® T-45 Homogenizer (IKA®-Werke GmbH & Co. KG, Staufen, Germany). After a centrifugation at 300 g for 10 min at 4° C, the obtained pellet underwent hypotonic lysis of 0.2% NaCl solution (1 g tissue/15 mL buffer),

followed 30 sec later by addition of an equal volume of a solution containing 1.6% NaCl and 5% glucose (1 g tissue/150 mL). After further centrifugation, the pellet was then homogenized in 1 mL of 0.05 M Na_2HPO buffer (pH 5.4) containing 0.5% dexadecyltrimethylammonium bromide (HTAB), followed by three freeze-thaw cycles using liquid nitrogen and a water bath at 37º C. Samples were then centrifuged at 10000 g for 15 min, resuspended in the same buffer and sonicated at 15º C for 10 min. Finally, samples were kept on ice until their use [331,332].

MPO activity was assessed by a colorimetric assay. For this, 100 µL of the samples were added in a 96-well plate followed by 50 µL H_2O_2 and 50 µL 3,3′,5,5′-tetramethylbenzidine (TMB; Sigma Aldrich) per well, and the plate was incubated at 37º C for 15 min. TMB is oxidized by HOCl, thus generating a blue product. The reaction was stopped by addition of 50 µL 1 M H_2SO_4 (color of reaction solution changes to yellow) and the absorbance was measured at 450 nm in an Infinite® 200 PRO series spectrophotometer (Tecan, Männedorf, Switzerland). All activity assays were performed in duplicate. Fold-increase in MPO activity was determined by comparing the results obtained of the liver samples of treated mice with those treated with vehicle.

III.B.13. Plasmatic determinations

a) Plasma isolation

Mice blood samples were obtained from cave vein of isoflurane-anaesthetised mice using a 25-gauge needle, and coagulation was avoided with EDTA (0.5 M, pH 7.4). To obtain plasma, samples were centrifuged at 500 g for 5 min.

b) Biochemical determinations

Frozen plasma samples were sent to a specialized laboratory in veterinarian diagnosis (CEDIVET©, Valencia, Spain), where auto-analysers were employed to quantify the concentrations of different markers of lipid metabolism (cholesterol) and liver injury (bilirubin, AST and ALT).

III.B.14. Histological determinations

Fresh mouse liver samples were washed in saline solution and fixed using 10% neutral-buffered formalin solution (Histofix® Preservative, PanReac) for 48-72 h. Samples were then dehydrated, embedded in paraffin and subsequently cut in a microtome at 3-5 µm of thickness.

Prior to staining, samples were deparaffinized (at 65º C for 60 min), rehydrated and rinsed with distilled water for 10 min. After staining with the different procedures, tissue sections were dehydrated again and coverslips were placed onto the slides just after the addition of the mounting medium (DPX® Mountant for histology, Sigma-Aldrich).

All images obtained in histological experiments were acquired using a digital light microscope (Leica DMD108; Leica Microsystems, Barcelona, Spain) at different magnifications. Quantifications were performed using the Image J software V1.50i.

III.B.14.1. Haematoxylin & Eosin Staining

After hydration, slides were incubated with Haematoxylin solution (Gill No. 3; Sigma-Aldrich) for 2 min at RT. After sequentially washing with distilled water for 2 min, acid ethanol for 30 sec and diluted H_2CO_4 for 1 min, slides were incubated with 0.5% aqueous eosin Y solution (Sigma-Aldrich, previously activated with 1 µL/mL glacial acetic acid), for 4 min. Finally, slides were washed with distilled water, dehydrated and mounted as previously described (section III.B.12).

III.B.14.2. Sirius Red Staining

Sirius Red staining is a simple and sensitive method that identifies fibrillar collagen networks in tissue sections. Sirius Red is a strong, linear anionic dye comprising six sulfonate groups that can associate along cationic collagen fibers and enhance their natural birefringence under cross-polarized light [333,334]. This staining is useful to characterize collagen network alterations in tissues and allows the identification of different collagen subtypes according to their colors under polarized light [335,336]. As the aim of our experiments was to assess fibrosis progression among our different experimental groups, we did not distinguish between different collagen subtypes and all the sections were analysed under light microscopy, where collagen was stained in red and the background of the tissue in green.

After hydration, slides were incubated with 0.01% Fast Green (Fast Green FCF dye content ≥ 85%, Sigma-Aldrich) in a saturated aqueous solution of picric acid (1.3% in water, Sigma-Aldrich) at RT for 15 min. Next, they were washed with distilled water and incubated again with Sirius Red for 30 min. Sirius Red reagent

was composed by 0.1% Direct Red 80 (Sigma Aldrich) and 0.04% Fast Green in picric acid [336]. Finally, slides were washed with distilled water, dehydrated and mounted as previously described (section III.B.12).

III.B.14.3. Immunohistochemistry (IHC)

IHC is a method for detecting the location of proteins and other antigens in tissue sections using specific antibodies.

a) Heat-induced epitope retrieval

After deparaffinization and hydration, an antigen retrieval step is required to perform immunohistochemical staining, due to the formation of methylene bonds during fixation that can cross-link proteins and mask the antigens. The antigen retrieval step breaks the aforementioned bonds, exposing the antigenic sites, and therefore allowing antibodies to bind [337]. For this purpose, slides were immersed in buffer citrate unmasking solution (Dako Target Retrieval Solution 1x; 10 mM, pH 6; Agilent, Santa Clara, USA) and heated in a microwave until boiling started. Then, the process was followed by 15 min incubation at sub-boiling temperature. Finally, slides were allowed to cool down for 30 min and washed in distilled water 3 times for 5 min.

b) Endogenous peroxidase blocking

Liver contains endogenous peroxidases, which can react with the chromogenic substrate solution in IHC, leading to high and non-specific background staining (false positives). To block this reaction, slides were incubated with peroxidase blocking solution (3% H_2O_2 in distilled water) for 20 min at RT, and washed twice in distilled water and twice in TBS-T (5 min each).

c) Immunohistochemical staining

All the incubations were carried out in a humidified chamber. In order to block non-specific binding sites, samples were incubated with 5% normal serum diluted in TBS-T from the species in which the secondary antibody was generated for 1-3 h. Slides were then incubated with the primary antibody (see Table III.6) diluted in the same blocking solution, overnight at 4º C. The following day, slides were rinsed 3 times for 5 min in TBS-T and incubated with the secondary antibody (see Table III.6), also diluted in the same blocking solution. Finally, prior chromogenic detection, slides were washed with TBS-T 3 times for 5 min.

PRIMARY ANTIBODY			
PROTEIN	SOURCE/CLASS	DILUTION	COMPANY
Vimentin	Rabbit polyclonal	1:200	Abcam (ab8978)
F4/80	Rat monoclonal	1:150	BioRad (MCA497)
STAT3	Rabbit monoclonal	1:200	Cell Signaling (30835)
STAT1	Rabbit monoclonal	1:250	Cell Signaling (14994)
Ki67	Rabbit monoclonal	prediluted	Abcam (ab21700)

SECONDARY ANTIBODY			
ANTIBODY	LABELING	DILUTION	COMPANY
Mouse Anti-Rabbit IgG	Biotinylated	1:100	Vector (PI-1000)
Goat Anti-Rat IgG	HRP	1:100	Thermo Fisher (31470)
SignalStain® Detection Reagent	HRP	prediluted	Cell Signaling (8114)

Table III.6 List of primary and secondary antibodies used in IHC determinations.

d) Chromogenic detection

The chromogenic substrate 3,3'-diaminobenzidine tetrahydrochloride (DAB Enhanced Liquid Substrate System, Sigma-Aldrich) was employed to immunodetect target antigens. DAB is a precipitating substrate, which produces an intense brown stain by peroxidase action (enzyme present in secondary antibody and avidin-biotin complexes). DAB was prepared following the manufacturer's protocol, and was then added on the sample for 4-15 min (depending on the requirements of the primary antibody employed), continuously checking the appearance of the brown stain. Once tissue was properly stained, the reaction was stopped immersing slides in water for 2 min, and washing three times with PBS for 10 min. The specificity of the immunostaining was verified by the absence of staining in analogous tissue sections in which the primary or secondary antibodies were excluded.

e) Signal amplification

Two different methods were used to enhance the signal from the peroxidase reaction between biotinylated secondary antibodies and DAB. For Vimentin, F4/80 and Ki67 IHC determinations, the Vectastain® Universal Elite ABC Kit (Vector Laboratories, Burlingame, CA, USA) was used. The ABC Complex method is based on biotinylated secondary antibodies that act

as links between a tissue-bound primary antibody and an avidin-biotin-reporter enzyme complex. As avidin is tetravalent, it forms large complexes containing multiple copies of the biotinylated reporter enzyme, resulting in high signal intensity [338,339]. Following the manufacturer's instructions, slides were incubated in ABC solution for 45 min, and washed four times with TBS-T for 5 min.

Although biotin-based detection procedures are still widely used, they can lead to significant background staining in certain tissues and, consequently, several non-biotin-based detection methods are also employed. Specifically, we used a polymer-based method for IHC determination of STAT3 and STAT1. This technology uses a dextran backbone to which multiple enzyme molecules and secondary antibodies are attached. The dextran backbone-secondary antibody complex then binds to the primary antibody, thereby generating a greater reaction with the subsequent chromogen, compared with a secondary antibody directly conjugated with enzyme. Additionally, use of a one-step polymer method shortens the IHC procedure by avoiding the two-step biotinylated secondary antibody and ABC reagent that are required for standard avidin-biotin systems.

III.B.14.4. TUNEL determination of apoptotic cells

The main biochemical hallmark of apoptosis is degradation of DNA by endonucleases, which produce double-stranded oligonucleosomal DNA fragments. These DNA fragments are 180-200 bp in size and can be detected by the terminal deoxynucleotidyl transferase (TdT) dUTP nick end labeling (TUNEL) assay. This method is based on the template-independent identification of blunt ends of dsDNA breaks by TdT. The enzyme catalyzes the addition of labeled dUTPs to 3'-hydroxyl termini of DNA ends, which can be visualized using immunohistochemical techniques [340–343].

In order to study the possible implication of apoptosis in the effects observed in our in vivo models, In situ cell death detection kit (Roche) was used. According to the manufacturer's instructions [344], after hydration of tissue slides, the antigen unmasking procedure was performed by incubating them for 15 min with Proteinase K PCR Grade (Roche; 2.5 U/mg, pH 7.5) at 37° C.

For labeling steps, the TUNEL reaction mixture was prepared by diluting the enzyme solution, containing the terminal deoxynucleotidyl transferase enzyme, and the label solution, containing a nucleotide mixture, in a 1:10 proportion. Then,

tissue sections were incubated with this solution for 1 h in a humidified chamber at 37° C in the dark.

After three washes with PBS for 5 min, the slides were incubated with an anti-fluorescein antibody conjugated with a peroxidase enzyme, and were then analysed using a fluorescence microscope, using an excitation wavelength of 450-500 nm and a detection wavelength of 515-565 nm. Thus, we observed the positive brown stain after DAB development as previously described for the chromogenic detection of the IHC experiments [344].

III.B.15. Presentation of data and statistical analysis

All values are expressed as mean ± standard deviation (SD). The number of independent experiments (n) for each parameter is indicated in figure legends; all measurements were repeated 4-7 times. Unless stated otherwise, data are represented as percentage of control (untreated mice or cells considered 100%). Data were analysed using GraphPad Prism® V6.01 (GraphPad Prism® Software Inc., La Jolla, CA, USA).

In *in vivo* experiments, comparisons were done between two different groups and were independently analysed by Student *t*-test. Statistical significance between control and vehicle-treated mice was expressed as #$p < 0.05$, and significance between vehicle-treated and drug-treated groups was expressed as *$p < 0.05$.

In *in vitro* experiments, one-way ANOVA followed by a Bonferroni multiple comparison test was done between treatments and their respective vehicles. Statistical significance was expressed as *$p < 0.05$. In LX-2 cells and primary hHSC experiments, comparisons between vehicles (unstimulated versus TGFβ-stimulated cells) were performed using a Student *t*-test (#$p < 0.05$). Results using primary hHSC were derived from triplicates from three independent isolations.

Chapter IV: RESULTS

SECTION A. EXACERBATION BY NRTI OF ACUTE APAP-INDUCED HEPATOTOXICITY: KEY ROLE OF MITOCHONDRIA

IV.A.1. Effect of NRTI on mitochondrial function

Acute treatment with NRTI exerted different effects in respiration and mitochondrial function in Hep3B cells. Pyrimidine analogues ZDV, 3TC and FTC did not alter the rate of O_2 consumption at clinically relevant concentrations, though they did significantly reduced this parameter at higher concentrations, and more so in the case of AZT and 3TC than in that of FTC (Figure IV.A.1 A). The purine analogues ABC and ddI induced a significant and concentration-dependent reduction in O_2 consumption at concentrations similar to those present in patients (10 µM; Figure IV.A.1 B). Tenofovir, the only nucleotide analogue currently used in anti-HIV therapy (used in the chemical form of TDF) did not affect the respiration of hepatic cells at any of the concentrations tested (Figure IV.A.1 C). Analysis of ETC activity showed that 1 h treatment with ddI significantly reduced the activity of both CI and CIII. On its hand, ABC-treated cells manifested a slight, but statistically significant, concentration-dependent decrease in the activity of CIII, with no alteration in that of CI. As expected, both rotenone and antimycin A induced a significant reduction of CI and CIII activity, respectively (Figure IV.A.1 D). Neither of these compounds induced changes in CII or CIV (data not shown).

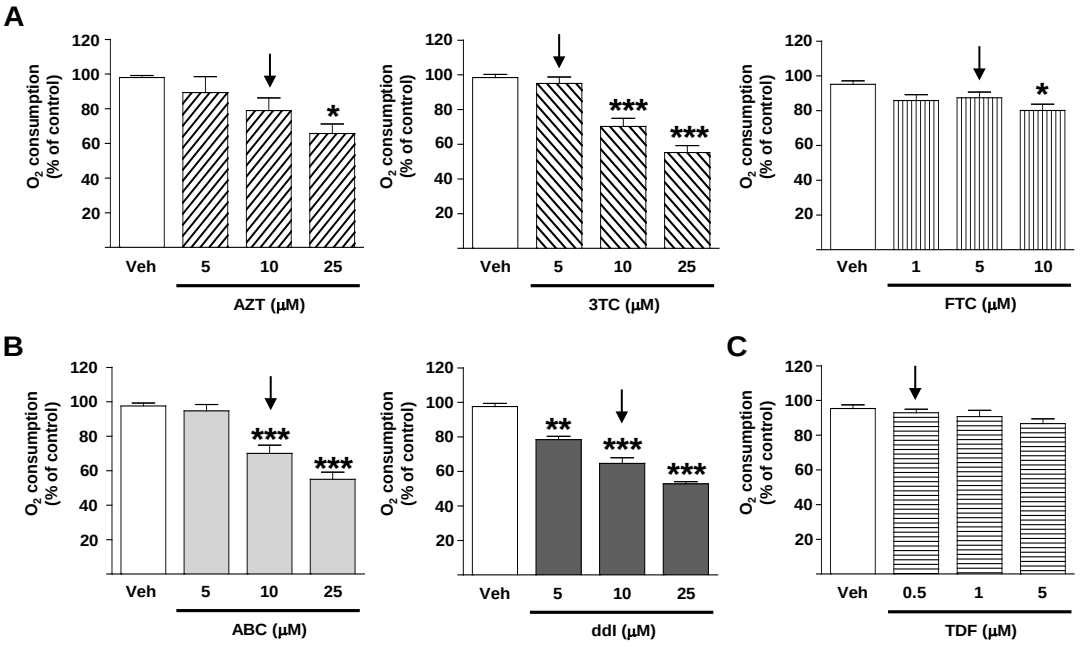

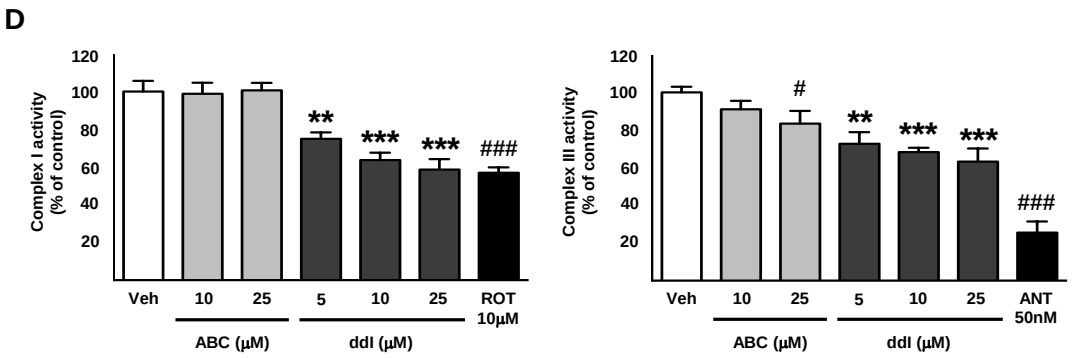

Figure IV.A.1. Differential mitochondrial O_2 consumption following acute administration of NRTI drugs. Acute effects of solvent (white bar) or various concentrations of the pyrimidine analogues ZDV, 3TC and FTC (A), the purine analogues ABC and ddI (B), and the nucleotide analogue TDF (C) on O_2 consumption in Hep3B cells. Clinically relevant concentrations of each drug are indicated by an arrow. Impact of purine analogues and positive controls rotenone and antimycin A (1h) on ETC CI and CIII activity (D). Data (mean ± SEM, n= 5–6) were calculated as percentage of control (untreated cells) and analysed by one-way ANOVA multiple comparison test followed by a Newman–Keuls test (*p<0.05, **p<0.01, ***p<0.001 versus the respective solvent). Positive controls were independently analysed by a Student's *t*-test (###P<0.001)

We performed additional analyses of mitochondrial function to evaluate the relevance of these inhibitory effects on cell respiration (Figure IV.A.2). We studied through fluorescence microscopy both the production of ROS (DCFH-DA fluorescence) and $\Delta\Psi_m$ (TMRM fluorescence).

There was a significant and concentration-dependent increase in the production of ROS following 1 h-incubation with ddI, shown by enhanced DCFH-DA signal (Figure IV.A.2 A). This effect was absent in hepatocytes incubated with ABC, although a trend towards a slight increase was observed as the concentration rose. Rotenone, used as a positive control (not displayed), clearly enhanced ROS levels [173.6 ± 20.2** %]. In addition, ddI produced a profound reduction of $\Delta\Psi_m$ at all the concentrations evaluated. ABC also influenced this parameter, but to a lesser extent, reaching statistical significance only at the highest concentration of 25 µM (Figure IV.A.2 B). Despite differences in the way they affected complex activity, mitochondrial ROS and $\Delta\Psi_m$, both purine analogues produced a similar and concentration-dependent decrease in intracellular ATP levels (Figure IV.A.2 C). Interestingly, when the period of incubation with ddI and ABC was extended to 24 h, levels of TMRM fluorescence did not differ significantly between vehicle- and drug-treated cells, while CCCP clearly reduced them (Figure IV.A.2 D). Nevertheless, inhibition of CI and CIII activity was maintained with ddI, while ABC significantly inhibited CI and enhanced its effect on CIII (Figure IV.A.2 E).

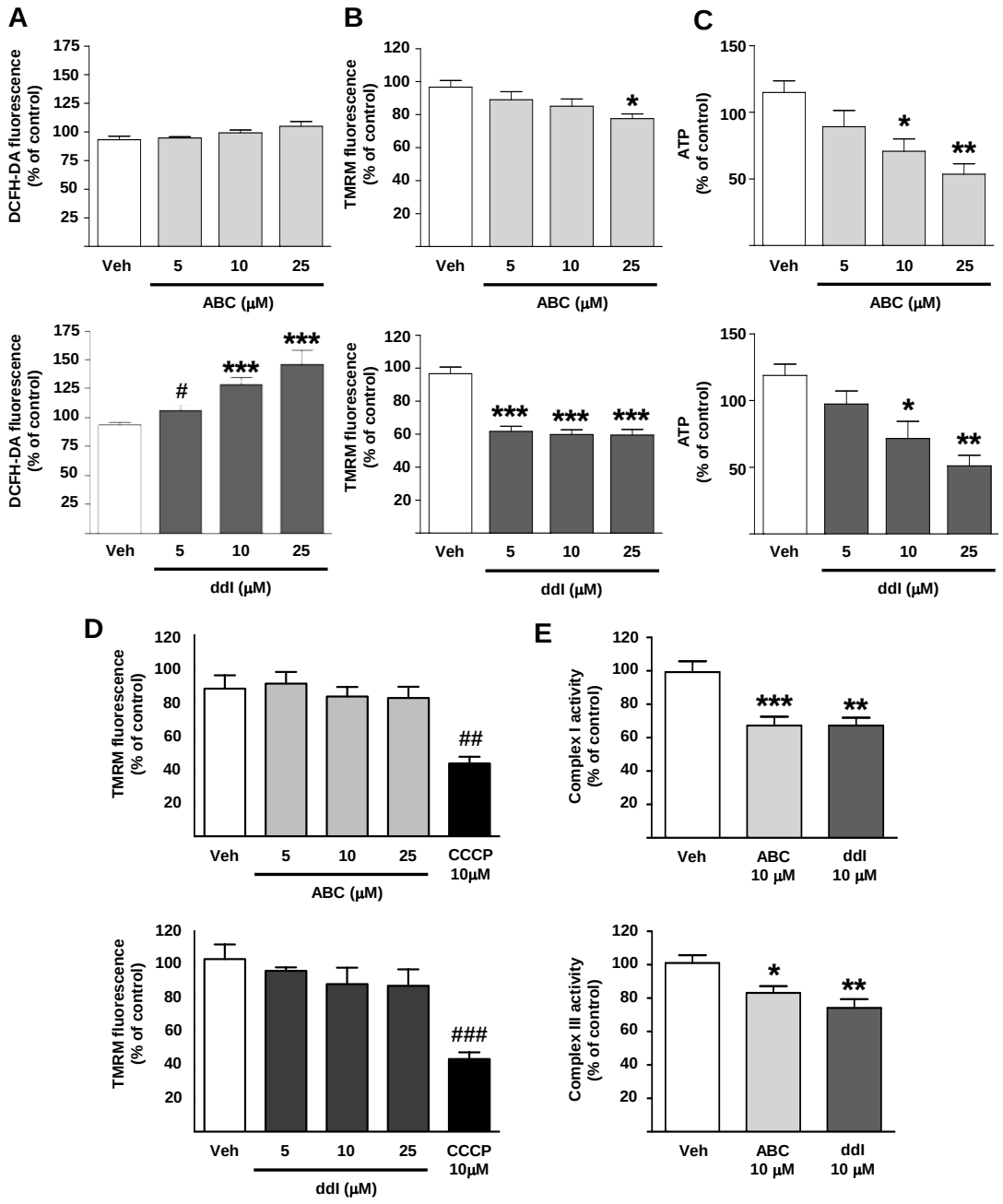

Figure IV.A.2. Analysis of mitochondrial function of Hep3B cells treated (1h) with increasing concentrations of purine analogues. Total ROS production was analysed after incubation with the fluorescent probe DCFH-DA (2.5 μM) (A). $\Delta\Psi_m$ was assessed by measuring TMRM fluorescence (B). Intracellular ATP levels previously normalized to protein concentration (C). $\Delta\Psi_m$ recovery and inhibition of CI and CIII activity after 24 h treatment with ABC or ddI (D). Data (mean ± SEM, n=5–6) were calculated as percentage of control (untreated cells) and analysed by one-way ANOVA multiple comparison test followed by a Newman-Keuls test (*p<0.05, **p<0.01, ***p<0.001) or Student's *t*-test (#p<0.05). The positive control CCCP was independently analysed by a Student's *t*-test (##p<0.01, ###p<0.001).

IV.A.2. APAP-induced mitochondrial and cellular toxicity

Incubation of Hep3B cells with APAP (from 1.25 to 10 mM for 24 h) induced a concentration-dependent decrease of $\Delta\Psi_m$ that reached statistical significance with 2.5 mM. However, only the concentration of 10 mM significantly increased mitochondrial superoxide production (Figure IV.A.3 A). Static cytometry experiments revealed a radical decrease in cell proliferation and/or survival at the four concentrations evaluated, as the number of cells was dramatically lower in all cases (Figure IV.A.3 B). The MTT assay revealed no significant changes in cellular viability after 24 h (data not shown); however, APAP undermined this parameter when incubation lasted 48 h (Figure IV.A.3 C). Finally, cell cycle was appraised by analysing total Hoechst fluorescence in Hep3B cells treated with the vehicle or APAP. A severe alteration of this parameter was observed in APAP-treated cells, with a substantial enhancement of the subG$_1$ peak and a decrease in the G$_2$M subpopulation, even at the lowest dose (1.25 mM) (Figure IV.A.3 D).

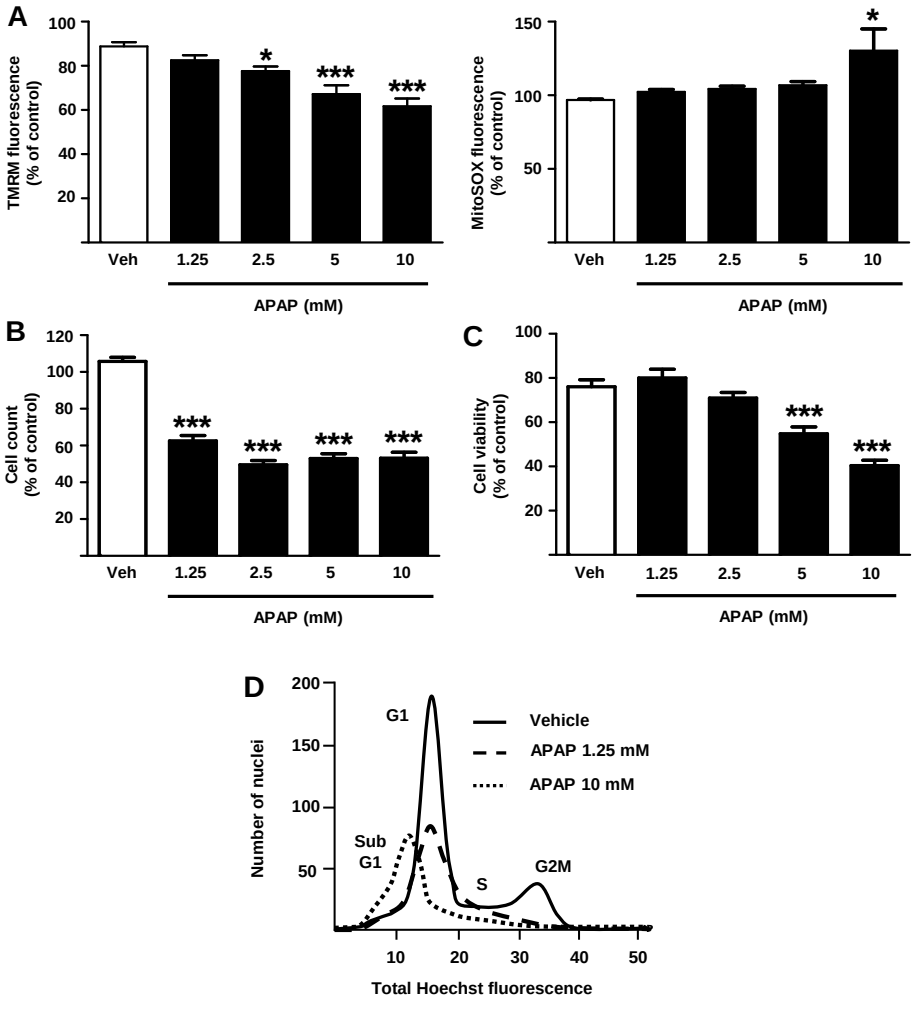

Figure IV.A.3. (Previous page) Effect of APAP on mitochondrial function and cellular viability in Hep3B cells. Quantitative analysis of mitochondrial membrane potential (TMRM fluorescence) and mitochondrial superoxide production (MitoSOX fluorescence) by fluorescence microscopy after 24 h treatment (A). Cell count after 24 h treatment (B). MTT assay of cells cultured for 48 h in the presence of the different compounds (C). Representative cytogram of cell cycle analysis by static cytometry (Hoechst fluorescence) in cells treated with vehicle or APAP (1.25 or 10 mM) for 24 h (D). Data (mean ± SEM, n=4–8) were calculated as percentage of control (untreated cells) and analysed by one-way ANOVA multiple comparison test followed by a Newman–Keuls test. *p<0.05, **p<0.01, ***p<0.001 versus solvent.

IV.A.3. Purine analogues increase susceptibility to APAP-induced toxicity in the liver

We chose the concentration of 1.25 mM APAP for co-administration experiments after observing how it induced a minor toxic effect by which it reduced cell proliferation but did not compromise cellular viability or mitochondrial function after 24 h. As shown in Figure IV.A.4, co-administration of APAP significantly enhanced the effects of the purine analogues on CI activity in cells incubated for 1 h (Figure IV.A.4 A), especially in the case of ABC, while no such enhancement was observed at 24 h (Figure IV.A.4 B). Regarding CIII activity, no cumulative actions were observed after 1 or 24 h treatment with APAP and ABC or ddI (Figure IV.A.4 A and B). APAP alone induced a significant decrease in CIII activity at 24 h (Figure IV.A.4 B).

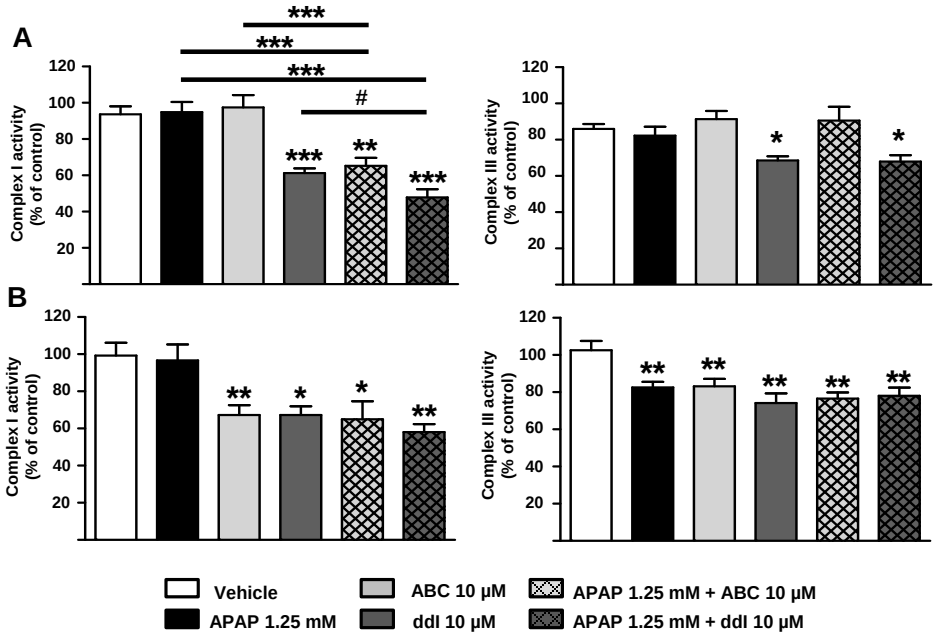

Figure IV.A.4. Mitochondrial function of Hep3B cells co-administered with NRTI and APAP. Analysis of CI and CIII activity in cells treated for 1 h (A) or 24 h (B). Data (mean ± SEM, n=4–8) were calculated as percentage of control (untreated cells) and analysed by one-way ANOVA multiple comparison test followed by a Newman-Keuls test (*p<0.05, **p<0.01, ***p<0.001 versus solvent) or Student's *t*-test (#p<0.05)

Further analysis showed that co-incubation with both APAP and 10 µM of either ABC or ddI significantly potentiated the effects of each drug on $\Delta\Psi_m$ (Figure IV.A.5 A). This synergism was evident with both NRTI drugs when mitochondrial ROS production was measured, but was statistically significant only in the case of ddI (Figure IV.A.5 A). The cumulative action of APAP and the purine analogues also influenced cell number and viability: APAP induced a significant reduction in cell proliferation, and its combination with either of the two purine analogues diminished cell number even further after 24 h of treatment (Figure IV.A.5 B). APAP alone did not modify the viability of Hep3B cells after 48 h, but this parameter was significantly reduced in cells co-treated with ABC or ddI (Figure IV.A.5 C).

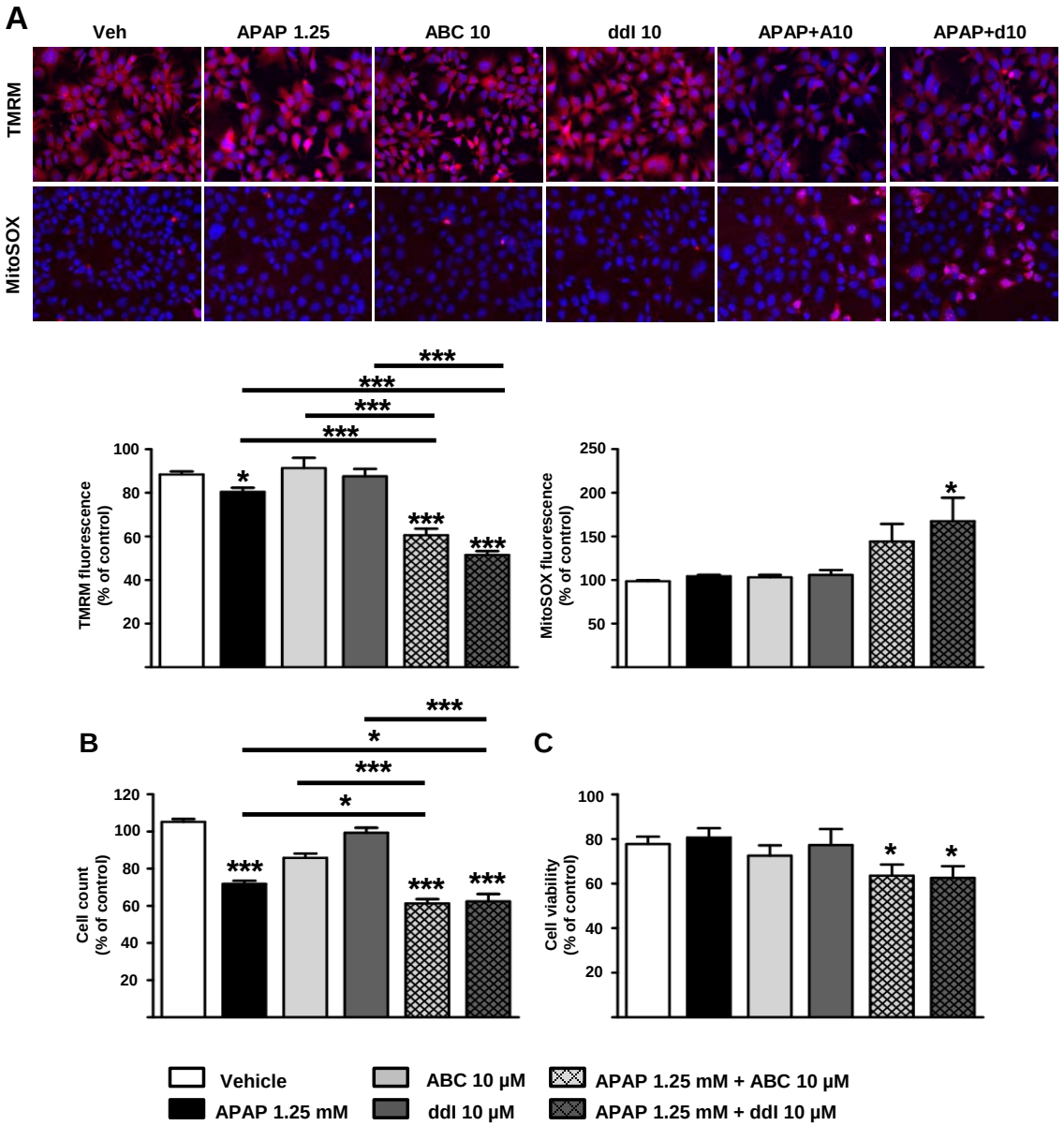

Figure IV.A.5. (Previous page) Mitochondrial function and cellular viability after NRTI and APAP co-administration. Fluorescence microscopy images (10x) and quantification of mitochondrial membrane potential (TMRM fluorescence, red; Hoechst 33342 fluorescence, blue) and mitochondrial superoxide production (MitoSOX fluorescence, red; Hoechst 33342 fluorescence, blue) assessed after 24 h treatment (A). Cell count after 24 h treatment (B). MTT assay after 48 h treatment (C). Data (mean ± SEM, n=4-8) were calculated as percentage of control (untreated cells) and analysed by one-way ANOVA multiple comparison test followed by a Newman–Keuls test (*p<0.05, **p<0.01, ***p<0.001 versus solvent) or Student's *t*-test (#p<0.05).

To analyse the specificity and reproducibility of the deleterious effects of the aforementioned drug combinations, ABC and ddI were also administered in combination with three other hepatotoxic agents at concentrations known not to induce liver damage: ethanol (at 50 mM) and antiretroviral drugs ritonavir (RIT) and NPV (both at 10 µM). In sharp contrast with APAP, none of these stimuli enhanced the effects of purine analogues on $\Delta\Psi_m$ or cell number (Figure I.A.6).

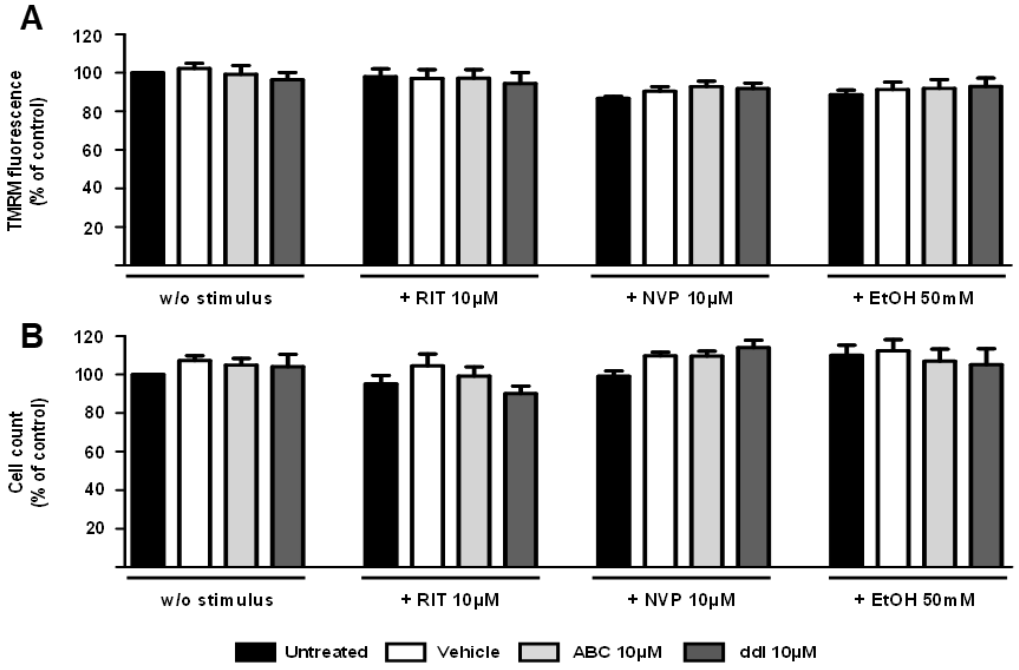

Figure IV.A.6. Mitochondrial membrane potential assessed by TMRM fluorescence in Hep3B cells treated with ABC or ddI (10 µM) and three different hepatotoxic stimuli: nevirapine (NVP, 10 µM), ritonavir (RTV, 10 µM) or ethanol (EtOH, 50 mM) (A). Cell count after 24 h treatment (B). Data (mean ± SEM, n=5-6) were calculated as percentage of control value (untreated cells) versus Veh and analysed by one-way ANOVA and Newman–Keuls post-test.

The consistency of these results was assessed in key experiments in human liver tissue and differentiated hepatocyte-like HepaRG cells. In these cells, APAP increased mitochondrial superoxide production to a greater extent than in Hep3B cells, producing statistically significant results even at 5 mM (Figure IV.A.7 A). It

also altered HepaRG cell number and viability in a concentration-dependent manner, both at 24 h (Figure IV.A.7 B and C) and 48 h (Figure IV.A.7 D).

Likewise, treatment of HepaRG cells with a combination of APAP and either ABC or ddI reproduced the pattern of potentiation previously observed in Hep3B cells. Thus, superoxide production was significantly enhanced with respect to single treatments (Figure IV.A.8 A), while it did not induce changes in cell number or viability following 24 h treatment (Figure IV.A.8 B and C). Nevertheless, co-administration produced a slight decrease in cellular viability after 48 h (Figure IV.A.8 D), similar to that observed in Hep3B cells (Figure IV.A.5 C).

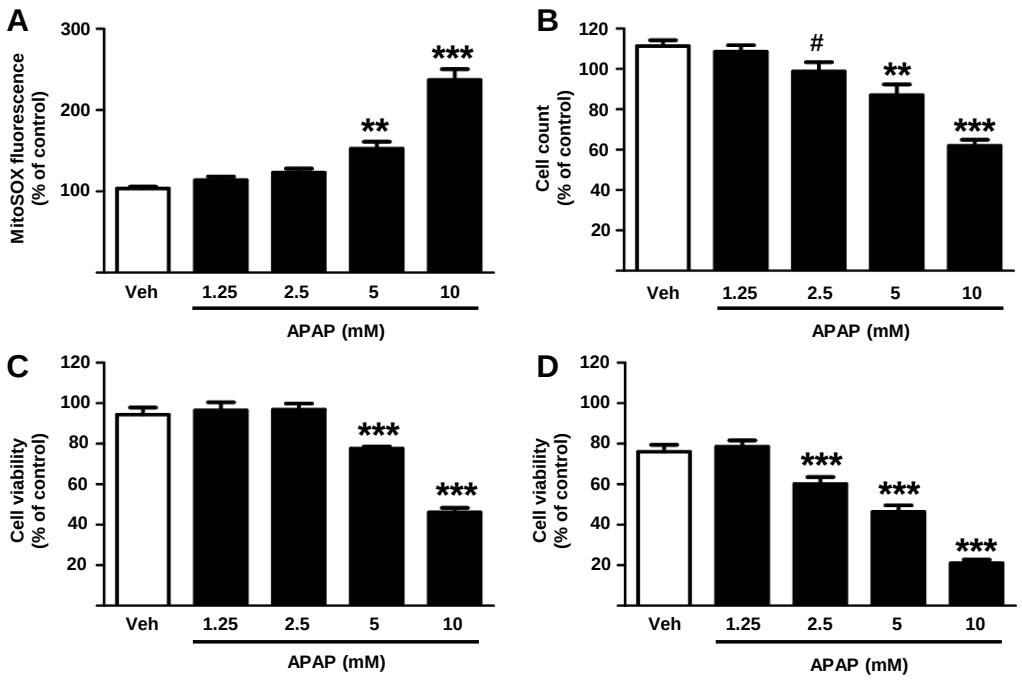

Figure IV.A.7. Effects of APAP treatment on HepaRG cells. Quantitative analysis of mitochondrial superoxide production by MitoSOX fluorescence after 24 h treatment (A), cell count after 24 h treatment (B) and MTT assay of cells after 24 or 48 h culture in the presence of different concentrations of APAP (C and D respectively). Data (mean ± SEM, n=4-8) were calculated as percentage of control value (untreated cells) and analysed by one-way ANOVA multiple comparison test followed by a Newman-Keuls test (*p<0.05, **p<0.01, ***p<0.001 versus solvent) or Student's *t*-test (#p<0.05).

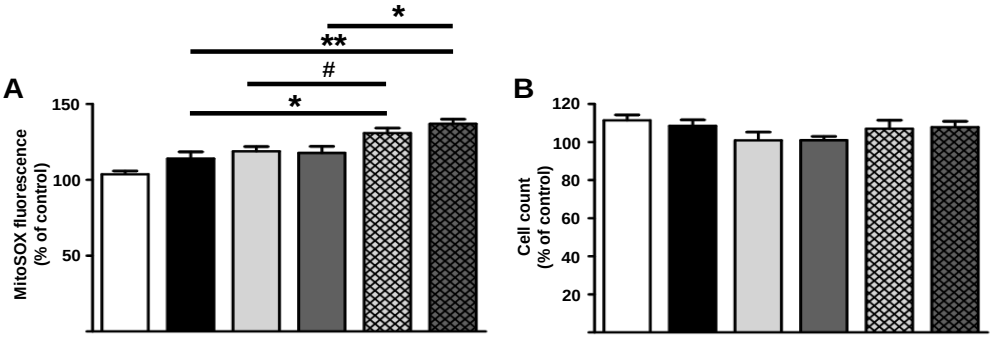

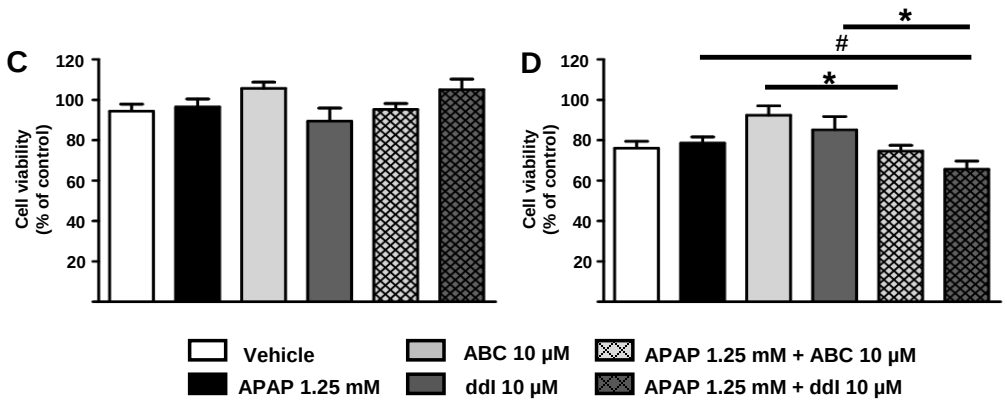

Figure IV.A.8. Effects of APAP and its combination with NRTI on HepaRG cells. Quantitative analysis of mitochondrial superoxide production by MitoSOX fluorescence after 24 h treatment (A), cell count after 24 h treatment (B) and MTT assay of cells after 24 or 48 h culture in the presence of the different compounds (C and D, respectively). Data (mean ± SEM, n=4-8) were calculated as percentage of control value (untreated cells) and analysed by one-way ANOVA multiple comparison test followed by a Newman-Keuls test (*p<0.05, **p<0.01, ***p<0.001 versus solvent) or Student's *t*-test (#p<0.05).

Finally, flow cytometry analysis of GSH levels in living HepaRG cells revealed that ABC and ddI produced a concentration-dependent reduction in the median of MBB fluorescence in the low-GSH population at 48 h (Figure IV.A.9 B), but not at 24 h (data not shown). The DEM-induced decrease was similar to that observed in cells treated with 25 µM NRTI (Figure IV.A.9 B). Co-administration with 10 µM of either ABC or ddI enhanced APAP-induced depletion of GSH levels (Figure IV.A.9 C), with a positive and significant correlation existing between the levels of this antioxidant and cellular viability (Figure IV.A.9 D). No changes were observed in the high-GSH population.

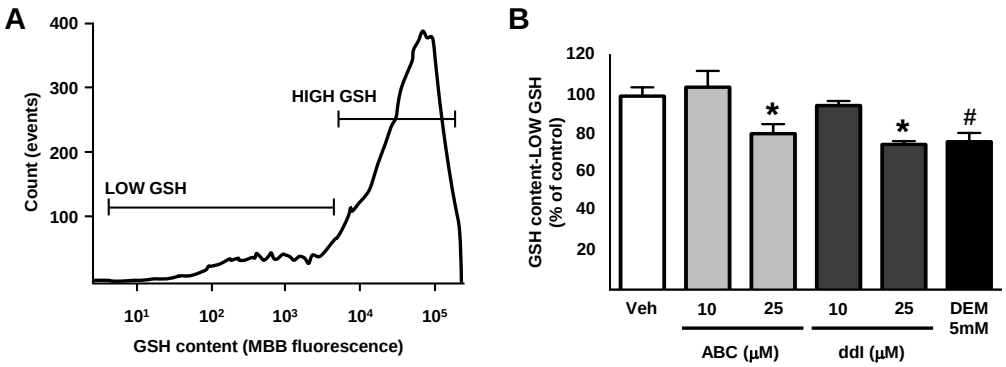

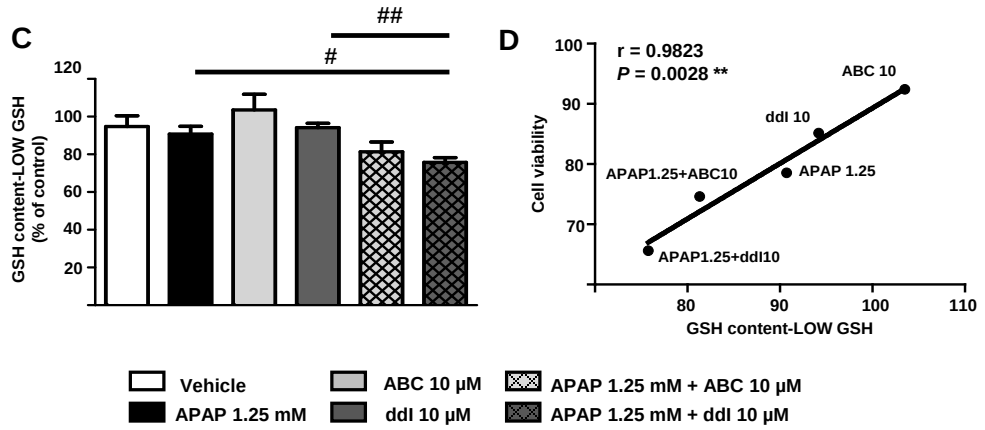

Figure IV.A.9. ABC and ddI decrease GSH levels in HepaRG cells. Representative curve of MBB fluorescence obtained by flow cytometry in living cells after 48 h treatment; two gates were set to differentiate cells with low and high GSH content (A). Quantification of intracellular GSH levels (MBB fluorescence) in the low GSH population (B and C). There was a positive and significant correlation between the levels of GSH in this population and cellular viability (D). Results (median ± SEM, n=3-5) are expressed as percentage of control (untreated cells). Statistical analysis was performed by one-way ANOVA multiple comparison test followed by a Newman–Keuls test (*p<0.05, versus solvent) or Student's *t*-test (#p<0.05, ##p<0.01). DEM was analysed separately by a Student's *t*-test (#p<0.05). Functional correlation was analysed using Spearman's correlation coefficient.

SECTION B. EFFECT OF NNRTI IN THE PROGRESSION OF CHRONIC LIVER DISEASE

IV.B.1. Mouse model of NAFLD

After testing several anti-HIV drugs of different pharmacological families in this chronic model of NAFLD induced by HFD (12 weeks), we decided to focus our work in the NNRTI EFV and RPV because they showed an interesting protective profile in the steatotic livers. Thus, we decided to characterize their effect in three key aspects associated with the progression of NAFLD: lipid deposition, inflammation and fibrogenesis.

a) Effect of NNRTI in hepatic fat deposition

As shown below, chronic feeding with HFD significantly induced steatosis in mice livers (Figure IV.B.1 A), increased body and liver weight (Figure IV.B.1 B and C, respectively), and augmented plasmatic levels of cholesterol and hepatic enzymes AST and ALT (Figure IV.B.1 D).

Unexpectedly, chronic treatment with both EFV and RPV significantly decreased HFD-induced lipid deposition in the liver; however, a little increase in fat deposition was also observed in response to EFV in ND groups (Figure IV.B.1 A). Regarding body and liver weight, RPV did not show any change but EFV significantly reduced these parameters in the HFD-fed group (Figure IV.B.1 B and D). Finally, EFV increased cholesterolaemia in HFD groups and, surprisingly, induced an increase in the ALT levels in ND groups, whereas it decreased this same parameter in HFD (Figure IV.B.1 C).

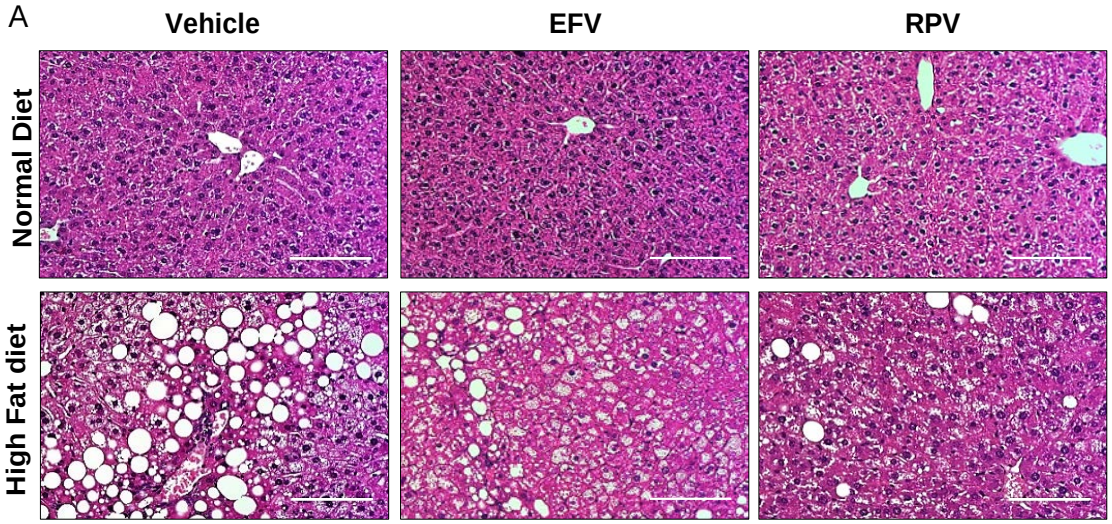

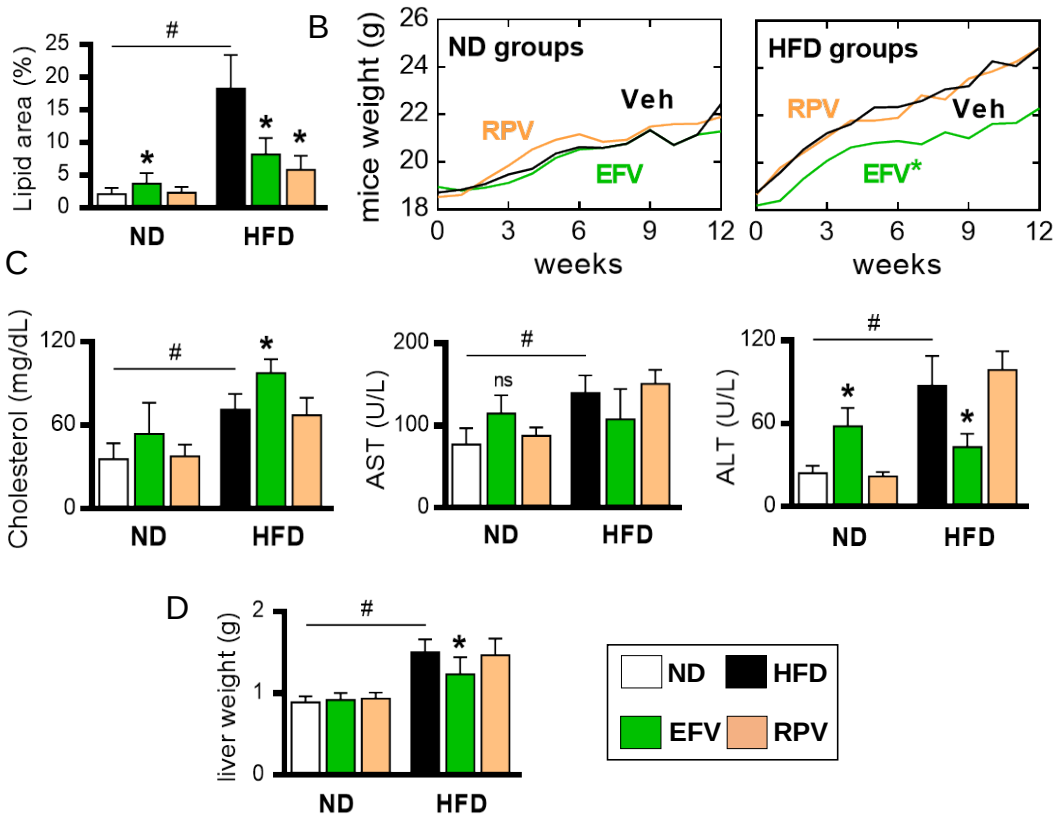

Figure IV.B.1. EFV and RPV decrease lipid deposition in the liver. Haematoxylin & Eosin staining of liver sections from mice treated with Vehicle, EFV and RPV, and fed with ND and HFD; quantification of lipid infiltration (n=5) (A). Mice weight evolution in all experimental groups (n=10) (B). Plasmatic determinations of cholesterol and hepatic enzymes AST and ALT (n=5) (C). Liver weight after 12 weeks of treatment (n=10) (D). Data are mean ± SD; #p<0.05 vs. ND group, *p<0.05 vs. HFD group; Student's *t*-test. Scale bar = 0.1 mm.

In order to understand the effect of EFV and RPV in the evolution of lipid deposition in HFD groups, we studied by WB the relative expression of key proteins involved in hepatic fat metabolism in whole-liver samples. We observed that HFD itself was able to significantly increase the protein expression of PLIN2 and PPARγ, which is in line with an increased adipogenic activity. Both EFV and RPV were able to decrease this tendency in all the HFD groups (Figure IV.B.2). Interestingly, both EFV and RPV also increased the expression of LXRβ (Figure IV.B.2). This receptor is present in many tissues and plays a pivotal role in different aspects of lipid pathophysiology, including cholesterol trafficking from blood to tissues and regulation of the lipogenesis/lipolysis balance [345]. High LXR activity in the liver has been associated with increased steatosis, especially through the action of the LXRα isoform, whose expression in enhanced in pathological conditions of lipid dysregulation. However, LXRβ activity is mainly involved in the maintenance of cellular and systemic levels of cholesterol and

triglycerides, working in a coordinated way with the sterol regulatory element-binding protein 2 (SREBP2) in the liver [346,347]. Thus, its hepatic overexpression in response to our treatments has a net homeostatic and beneficial effect aimed to decrease fat deposition, in accordance with H&E images shown in Figure IV.B.1.

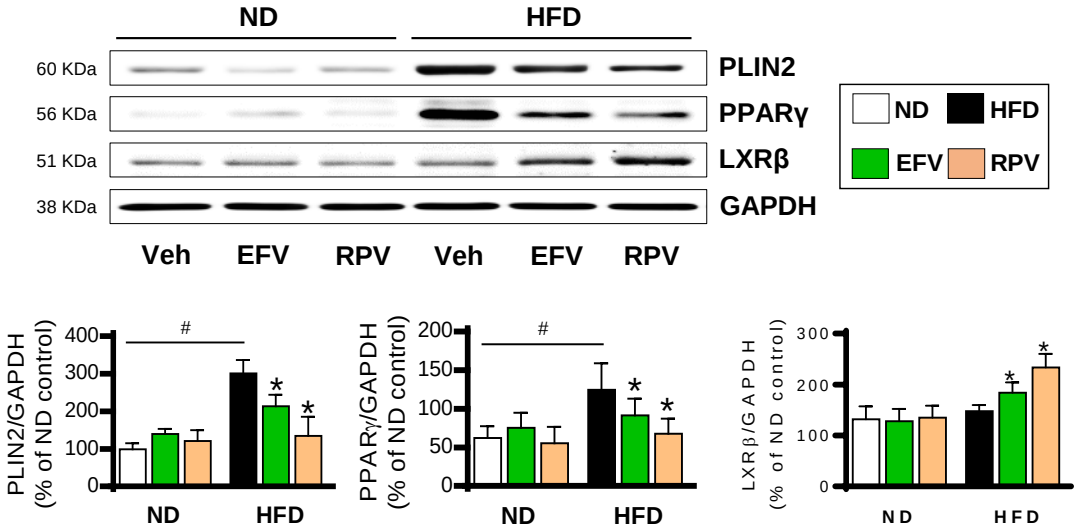

Figure IV.B.2. EFV and RPV regulate lipid metabolism in the liver. Protein expression of PLIN2, PPARγ and LXRβ. Representative Western Blot images and quantifications. Mice treated with vehicle, EFV and RPV and fed with ND or HFD (n=5). Data are mean ± SD; #p<0.05 vs. ND group, *p<0.05 vs. HFD group; Student's *t*-test.

b) Effect of NNRTI in hepatic inflammation

To assess the potential of these drugs to induce changes in the inflammatory pathways activated in HFD-fed animals, we analysed a broad spectrum of markers involved in hepatic inflammation. Both EFV and RPV were able to significantly decrease, in whole-liver samples, the activation of NF-κB and NLRP3 inflammasome induced by HFD (Figure IV.B.3 A), two key protein complexes whose activity is essential in the progression of hepatic inflammation. It is important to note that, in both cases, RPV-induced effect was stronger than that of EFV. In addition, RPV was more effective decreasing MPO activity (Figure IV.B.3 B). Regarding macrophage polarization, in spite of the limitations found using only RT-PCR to assess this complex process, it seemed that any of these two drugs induced a clear pattern of M1 or M2 polarization in liver samples. Importantly, RPV decreased *Adgre1* gene expression, which encodes for F4/80 protein, a marker of net macrophage content in mice. This reduction is in line with the anti-inflammatory profile showed by RPV (Figure IV.B.3 C).

Finally, we observed a general decrease in the gene expression of several classic pro-inflammatory cytokines following EFV and RPV treatment (Figure IV.B.3 D), especially in all those involved in the expression of NLRP3 inflammasome components (*Il1b*, *Nlrp3* and *Casp1*). Gene expression of *Tnfa*, one of the main protein targets of NF-κB activation [348,349], was similarly and significantly decreased by these NNRTI. Interestingly, only RPV induced a significant increase in the gene expression of several anti-inflammatory and hepatoprotective genes, as *Il10* and *Ifng*, and over-expressed *Il6*. The systemic function of this interleukin is clearly pro-inflammatory, but it also plays an important role in the activation of many hepatoprotective mechanisms, such as those described in the introduction of this thesis.

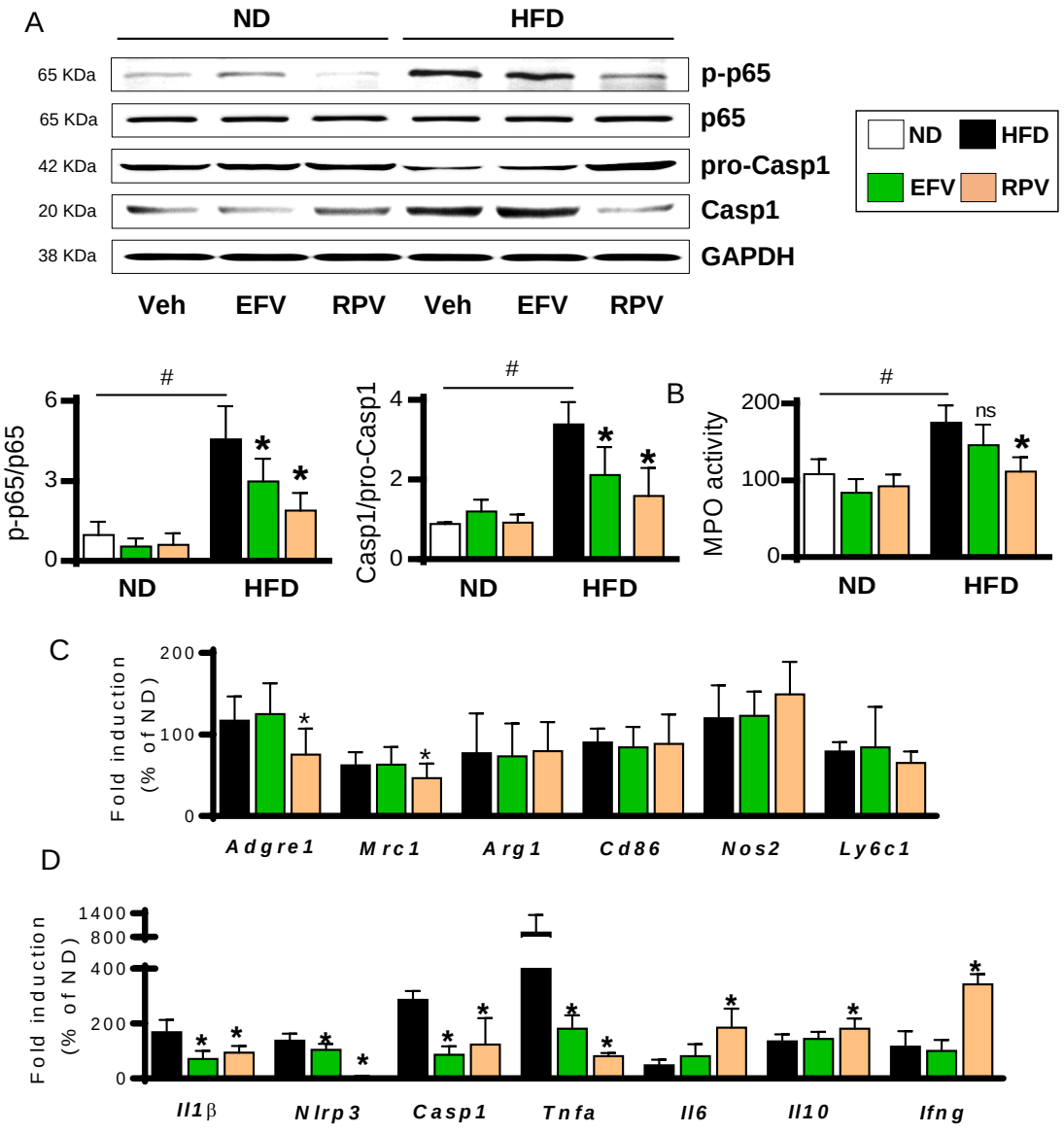

Figure IV.B.3. (Previous page) EFV and RPV exert an anti-inflammatory effect in the liver. Representative WB of whole-liver samples and quantifications of the activation of both NF-κB and NLRP3 inflammasome, assessed by phosphorylation of p65 protein (ratio between the phosphorylated form (p-p65) and the total form of the protein) and Casp1 cleavage (ratio between active Casp1, of 20 KDa, and the pro-Casp1 of 42 KDa), respectively (n=5) (A). Enzymatic determination of MPO activity (n=5) (B). Quantitative RT-PCR of markers of macrophage infiltration and polarization (C), as well as of classic pro- and anti-inflammatory genes (n=7) (D). In C and D panels, only HFD groups are displayed, since their gene expression is calculated assuming ND vehicle group as 100%. Gene expression data were normalized versus the expression of *Actb* gene. GAPDH is only displayed as a quality control of the experiment. Data are mean ± SD; #p<0.05 vs. ND group, *p<0.05 vs. HFD group; Student's *t*-test.

c) Effect of NNRTI in fibrogenesis progression

Determination of classical parameters of fibrogenesis in murine liver samples demonstrated, once again, that both EFV and RVP exerted a protective effect in this organ limiting fibrogenic progression in response to HFD feeding, as it can be observed in Sirius Red staining images (Figure IV.B.4). It is important to note that this technique also stains reticulin and, thus, ND groups and controls also showed low levels of red signal that are completely normal and physiologic (Figure IV.B.4 A).

Analysis of protein expression also revealed a clear anti-fibrogenic effect of EFV and RPV characterized by decreased Col1a1 expression and inhibited HSC activation, demonstrated by the reduction of both Vimentin and Desmin protein expression. Finally, also RT-PCR experiments displayed a general decrease in gene expression of many fibrogenic markers after chronic treatment with NNRTI. Once more, RPV had a stronger effect decreasing fibrogenic response than EFV, similarly to what happened in the study of hepatic inflammation (Figure IV.B.3).

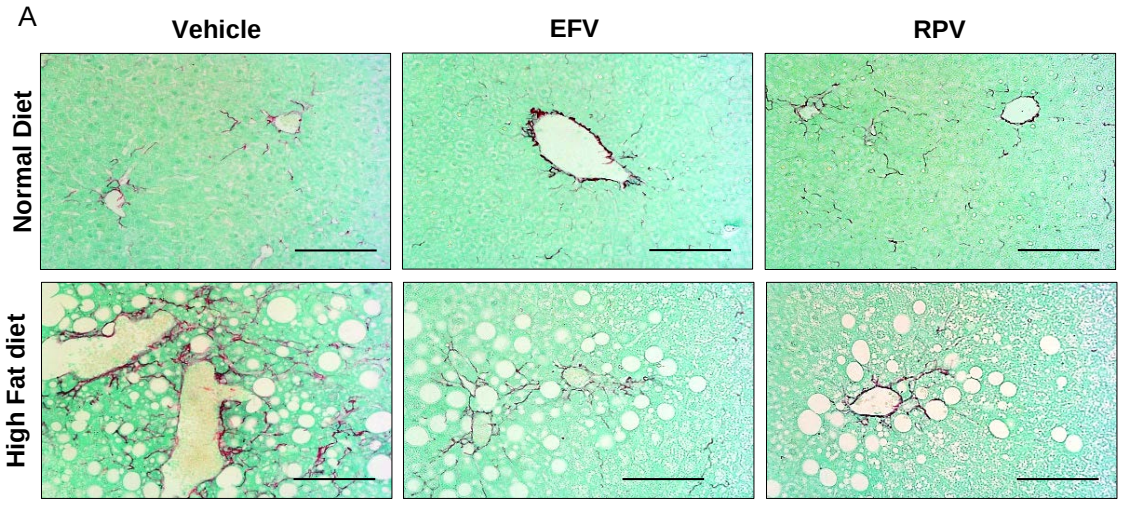

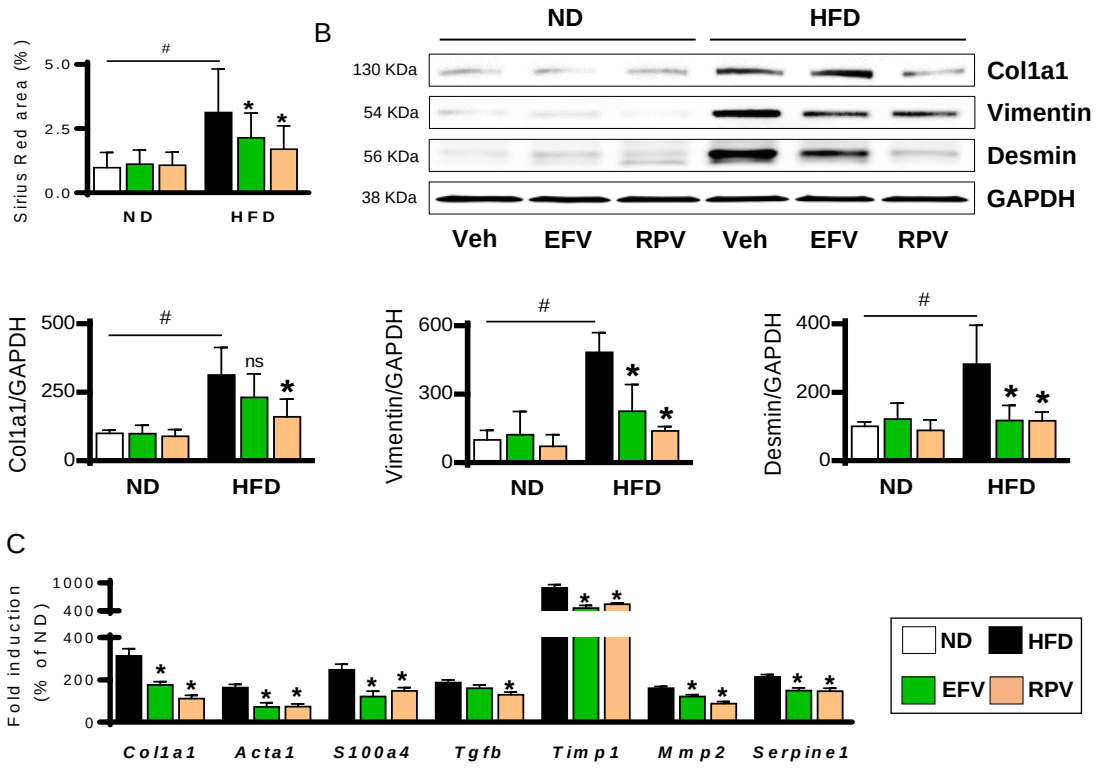

Figure IV.B.4. EFV and RPV exert an anti-fibrogenic effect in the liver. Sirius Red staining of liver sections from mice treated with Vehicle, EFV and RPV and fed with ND and HFD; representative images and quantification of collagen deposition (red signal) (n=5) (A). Representative WB (of whole-liver samples) and quantifications of Col1a1, Vimentin and Desmin (n=5) (B). Gene expression of several markers associated with ECM deposition (*Col1a1, Acta2, Timp1, Mmp2*) and HSC activation (*S110a4, Tgfb, Serpine1*) (n=7) (C). In panel C only HFD groups are displayed, since their gene expression is calculated assuming ND vehicle group as 100%. Gene expression data were normalized versus the expression of *Actb* gene, while protein expression was normalized versus GAPDH expression. Data are mean ± SD; #p<0.05 vs. ND group, *p<0.05 vs. HFD group; Student's *t*-test. Scale bar = 0.1 mm.

d) Modulation of JAK-STAT signaling by NNRTI

As shown in Figures IV.B.3 D and IV.B.5 A, RPV, but not EFV, induced a substantial over-expression of *Il6* in HFD mice groups. Traditionally, this cytokine has been considered pro-inflammatory and is able to activate the innate immune response during tissue injury. However, it has also been reported as the natural ligand of membrane receptors Gp130 and IL6-R, whose activation induces the intracellular phosphorylation of STAT3.

Considering the crucial role that both STAT1 and STAT3 have in the hepatic pathophysiology (see section I.C.2.c and Figure I.12), we decided to investigate the effect of these NNRTI in their regulation. First, we studied the relative gene expression of the main activator cytokines of these routes, namely IL6, IL22

(through its membrane receptors IL22R1 and IL10R2) and IFNγ (Figure IV.B.5 A). In addition, we also analysed the gene expression of main components of the JAK-STAT signaling pathways (both 3 and 1; Figure IV.B.5 B). In both cases (IV.B.5 A and B), we observed that no evident changes were observed in response to EFV, while RPV clearly enhanced the expression of the main activator cytokines (Figure IV.B.5 A), over-expressed STAT3 components and down-regulated those involved in STAT1-mediated pathways (Figure IV.B.5 B). Finally, we studied the activation of STAT3 by WB, assessing the ratio between phosphorylated STAT3 (pSTAT3) and the total STAT3 protein (STAT3) (Figure IV.B.5 C). These experiments showed that HFD clearly inhibited the activation of this protein in our murine whole-liver samples. EFV did not induce significant changes in HFD-fed animals, but RPV was able to revert this inactivation, restoring STAT3 activity to levels similar to those found in ND groups.

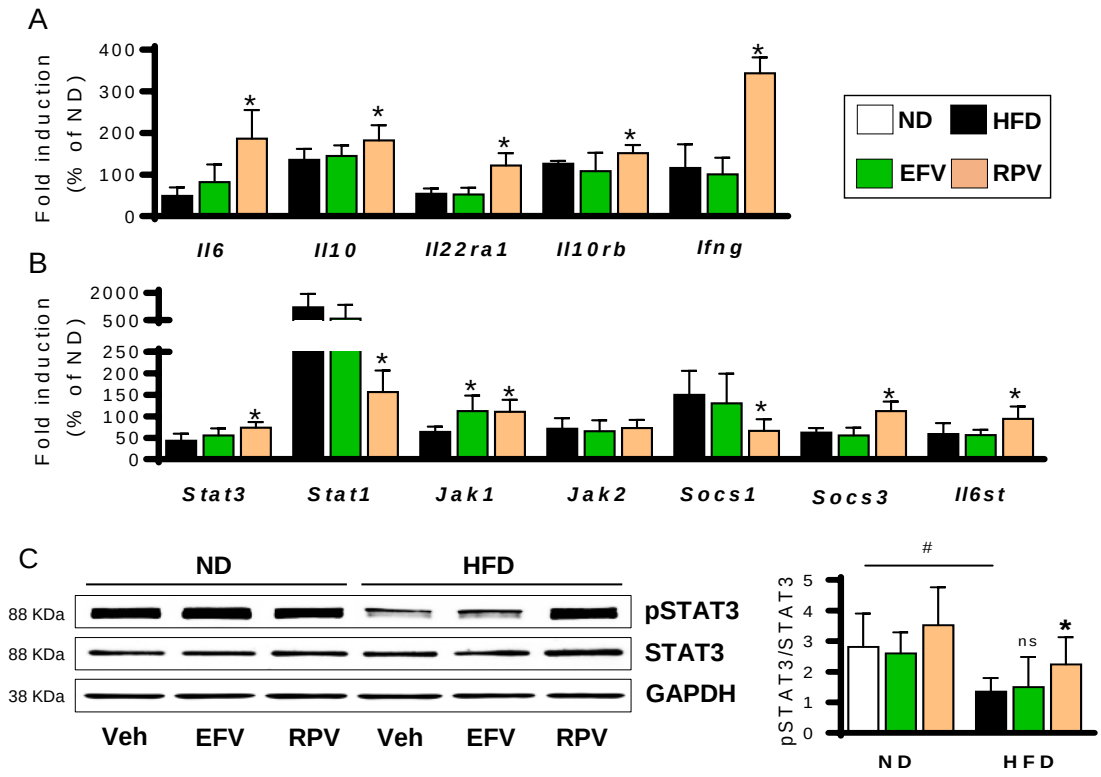

Figure IV.B.5. RPV, but not EFV, activates hepatic STAT3. Gene expression of cytokines involved in the hepatic JAK-STAT signaling regulation (A) and of constitutive members of both STAT1 and STAT3 pathways (n=7) (B). Only HFD groups are displayed in A and B panels, since their gene expression is calculated assuming ND vehicle group as 100%. Representative WB of whole-liver samples and quantifications of the activation of STAT3 by phosphorylation (n=5) (C). Gene expression data were normalized versus the expression of *Actb* gene, while protein expression was calculated by the ratio between the phosphorylated form of STAT3 (pSTAT3) and the total protein (STAT3); GAPDH is displayed as a quality control of the experiment. Data are mean ± SD; #p<0.05 vs. ND group, *p<0.05 vs. HFD group; Student's *t*-test.

Given all the previous results, we decided to further continue investigating only the effect of RPV in the progression of NAFLD since it showed a really surprising effect decreasing lipid infiltration, inflammation and fibrogenesis. We definitely chose RPV because its effects were more intense than those of EFV, and also because these intriguing results pointed to a RPV-induced regulation of STAT3/STAT1 balance as a potential underlying factor of these effects. In addition, as explained in the introduction (section A.6.d, Chapter I), chronic treatment with RPV has been recently associated with an improved lipid profile in dyslipemic HIV patients, even when they present an advanced stage of chronic liver disease [47,110,112,113,350], effects that could be somehow related to its actions in the liver.

Therefore, hereinafter, we will only show results obtained in the description of the effect of RPV in the progression of chronic liver injury. In addition, since no differences have been found in response to RPV in ND mice groups in previous data, following figures will display only three experimental groups: healthy (ND), steatotic (HFD) and HFD-fed and RPV-treated (HFD+RPV) mice groups.

e) Regulation of the STAT3/STAT1 balance

Previously, we have shown an increase in STAT3 activation in the liver of mice treated with RPV. However, WB experiments did not allow us to identify the liver cell type in which this factor is activated as we used whole-liver protein extracts. To study the different expression patterns in the main cell subpopulations of the liver we performed IHC experiments, using antibodies that targeted total STAT1 or STAT3. This protocol enabled us to assess activation of these transcription factors since they appeared as a diffused cytoplasmic signal when they were inactive and as a nuclear signal once they were activated.

STAT3 nuclear signal was mainly detected in hepatocytes (Figure IV.B.6 A). Moreover, this factor was largely expressed and activated in these cells under physiological conditions (ND), in spite of the general knowledge indicating that only a small amount of hepatocytes are actively proliferating in a certain time point in healthy livers [117,190,212]. However, this proliferative capacity mediated by STAT3 disappeared when HFD-induced chronic injury was present. Conversely, in these injured animals, treatment with RPV normalized this STAT3 activation in

hepatocytes. These results were certainly in line with those previously obtained by WB determinations (see Figure IV.B.5).

Regarding STAT1 expression (Figure IV.B.6 B), opposite to what happened with STAT3, its signal was mainly detected in non-parenchymal cells in healthy mice (ND), suggestive of an inactivated status of HSC and immune cells. Upon chronic liver injury (HFD), this staining disappeared, suggesting that all those cells were actively proliferating. Once again, RPV treatment partially rescued STAT1 expression in non-parenchymal cells, which could point to HSC inactivation.

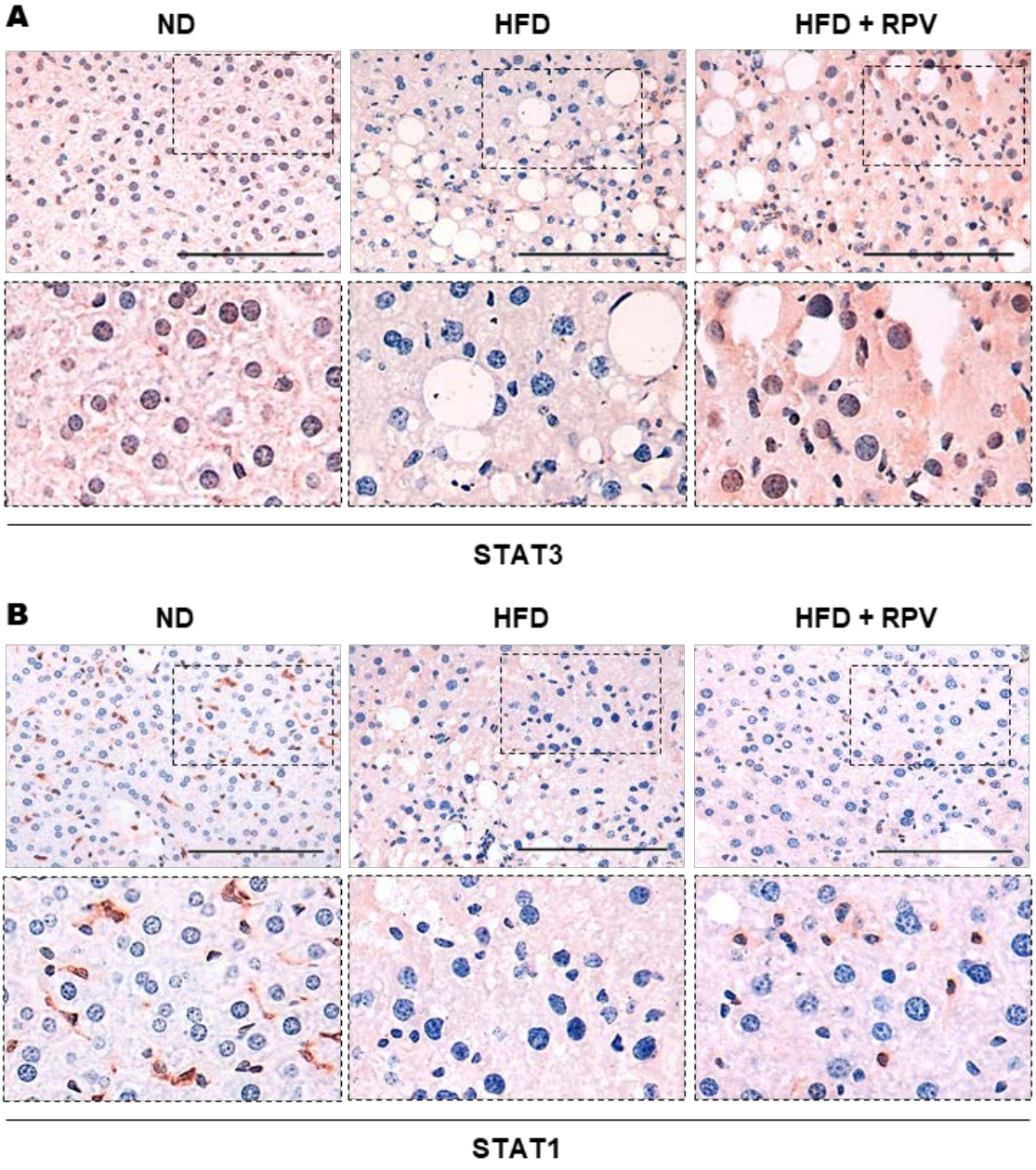

Figure IV.B.6. Hepatic regulation of STAT3 and STAT1 in response to HFD and RPV treatment. Representative images of STAT3 (A) and STAT1 (B) IHC determinations in mice liver tissue (n=4). Scale bar = 0.1 mm.

f) Transcriptomic analysis of HFD groups

We next carried out a transcriptomic analysis of both HFD and HFD+RPV liver samples. During this bioinformatic approach, a gene set enrichment analysis was performed in order to detect significantly up- or down-regulated blocks of functionally related genes, grouped as biological processes of functions.

Among the obtained results, two groups of biological processes especially drew our attention, namely cell proliferation (Figure IV.B.7 A) and cell cycle arrest and apoptosis (Figure IV.B.7 B), because they highlighted the coexistence of many different pathways involved in these a priori opposite cellular processes. All these signals were displayed in two treemaps; in this kind of representation, all biological processes are hierarchically showed in nested rectangles, whose size is proportional to their differential expression between experimental groups. Importantly, only those functions that were up-regulated in response to RPV are displayed.

As observed in the first treemap (Figure IV.B.7 A), proliferative and anti-proliferative processes are mixed. For instance, we simultaneously found a general increase in ‘mitotic spindle assembly’, ‘cell growth’ and ‘cell cycle transition’, but also an enhancement of ‘negative regulation of the cell cycle’, ‘negative regulation of cell growth’ and ‘negative regulation of cellular proliferation’, among many others. On its hand, the second treemap (Figure IV.B.7 B) clearly pointed to cell death activation by apoptosis.

All these apparently controversial results could be understood bearing in mind the type of samples we used for transcriptomic analysis. RNA extraction from whole-liver tissue was done for this experimental procedure, thus including all the different hepatic cell subsets. These contradictory signals thus pointed to a differential effect induced by RPV in different cell types, which could be in line with the different regulation of both STAT3 and STAT1 shown in Figure IV.B.6 (A and B, respectively).

A

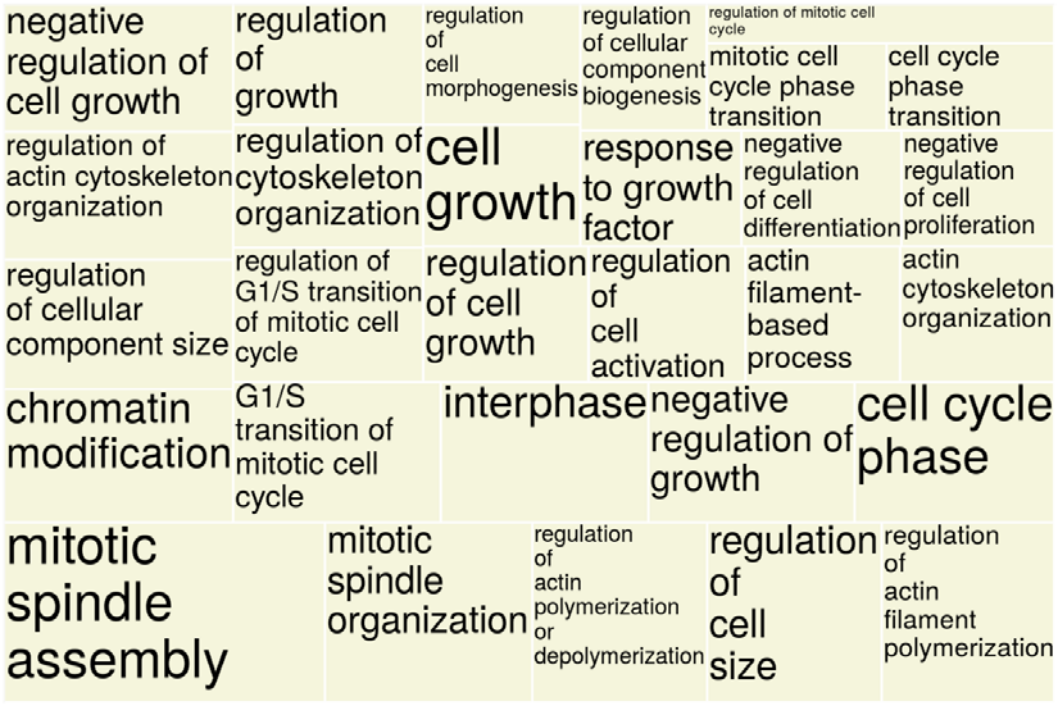

B

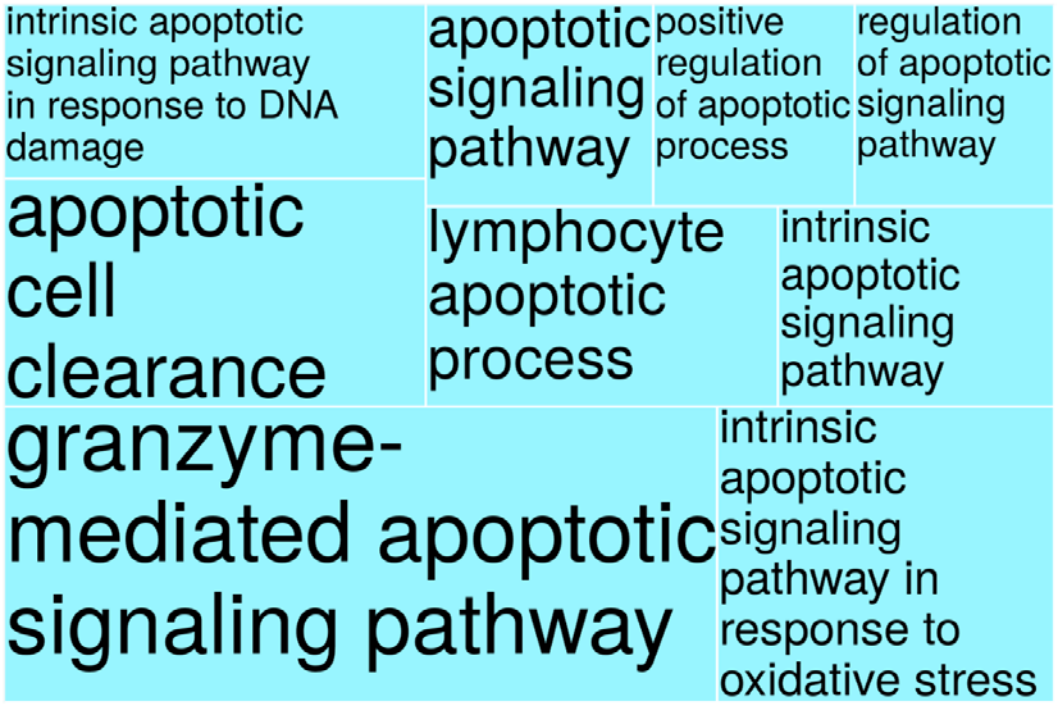

Figure IV.B.7. Treemaps showing the different biological responses upregulated in liver samples of RPV-treated HFD mice, associated with cell proliferation (A) and apoptotic processes (B). Data were obtained from bioinformatics gene set enrichment analysis performed after transcriptomic analysis of whole-liver tissue RNA from HFD and HFD+RPV mice groups (n=3). All displayed processes are significantly overexpressed in HFD+RPV animals.

g) Histological determination of cell proliferation and apoptosis induction

We next assessed the potential of RPV to modulate the proliferation of different liver cell subpopulations and to induce apoptotic-mediated cell death. With this aim, we performed IHC staining of Ki67, a protein widely used as a proliferation marker since it is present during all active phases of the cell cycle but is absent from quiescent or resting cells [351,352]. In these experiments, Ki67-positive cells clearly appeared as well-defined brown nuclei; large nuclei corresponded to hepatocytes whereas small nuclei belonged to non-parenchymal cells (Figure IV.B.8.A). In healthy livers (ND) only few hepatocytes and non-parenchymal cells were actively proliferating, but in HFD-fed animals Ki67 signal was almost completely lost in hepatocytes, while the number of positive non-parenchymal cells increased. Of note, in response to RPV treatment, the quantity of proliferating hepatocytes significantly augmented if compared with HFD groups; conversely, the number of positive non-parenchymal was clearly decreased.

TUNEL assay was employed to detect apoptosis in murine liver sections. In this technique, nuclei from apoptotic cells are stained in brown whereas those of healthy cells appear in blue. In our studies, healthy livers (ND) did not show apoptotic cells; however, apoptotic hepatocytes were clearly detected in response to HFD, while most non-parenchymal cells were still negative. Livers from mice fed with HFD and treated with RPV exerted a completely different staining pattern: the number of positive hepatocytes clearly decreased and that of positive non-parenchymal cells increased (Figure IV.B.8.A). Consequently, these data suggested that RPV is able to induce different cellular responses in different cell subtypes, inducing at the same time hepatocyte proliferation and apoptosis of non-parenchymal cells. This dual effect of the NNRTI was totally in line with its actions on STAT3 and STAT1 activation.

Interestingly, there was a clear difference between the amount of hepatocytes in which STAT3 was active (Figure IV.B.6 A) and the number of these cells that were actively proliferating. Technically, this may be due to the different specificity of the antibodies used in both determinations. Alternatively, it could also be a consequence of a biological delay between STAT3 activation and the ultimate triggering of proliferation. Despite this controversy, the effect induced by chronic treatment with RPV seemed clear and relevant.

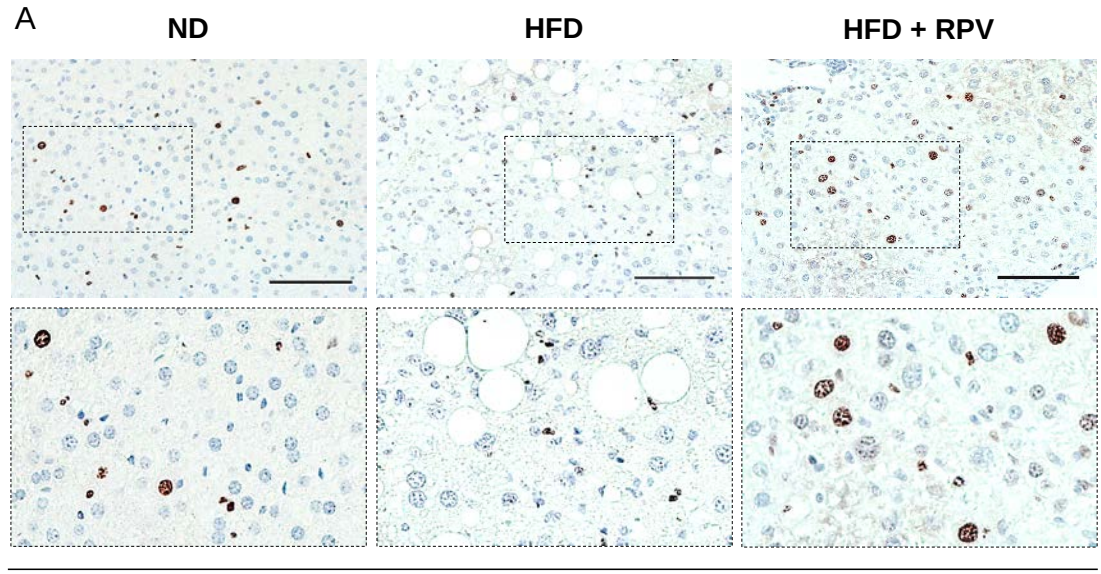
A
ND
HFD
HFD + RPV

Ki67

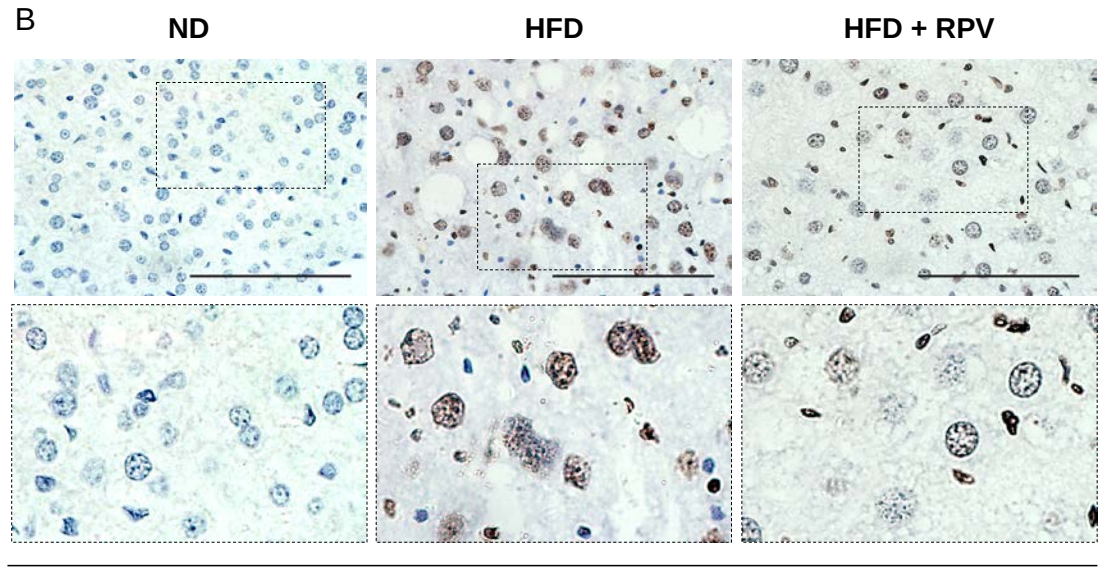
B
ND
HFD
HFD + RPV

TUNEL

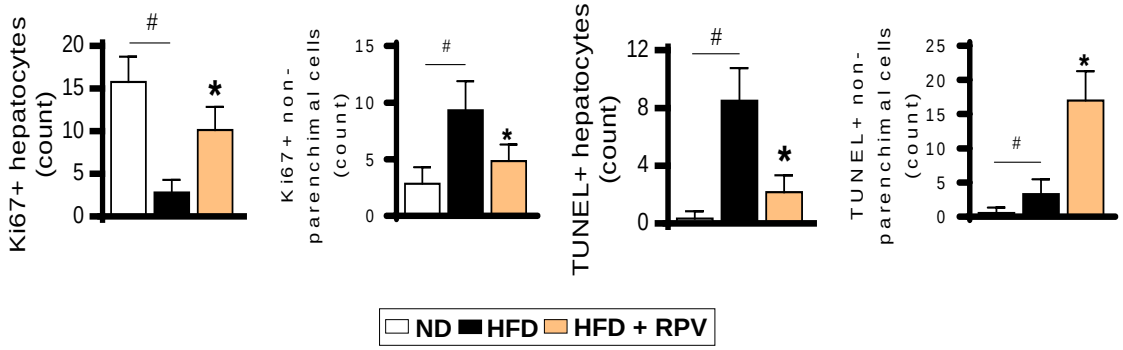
Ki67+ hepatocytes (count)
Ki67+ non-parenchimal cells (count)
TUNEL+ hepatocytes (count)
TUNEL+ non-parenchimal cells (count)
#
*
ND
HFD
HFD + RPV

Figure IV.B.8. (Previous page) RPV increases the proliferation of hepatocytes and induces apoptosis in non-parenchymal cells in our mouse model of NAFLD. Evaluation of cell proliferation and apoptosis in mice liver tissue. Representative pictures of Ki67 immunohistochemistry (A) and TUNEL staining (B) in mice liver tissue. Healthy (ND), steatotic (HFD) and HFD-fed + RPV-treated (HFD+RPV) groups are displayed in the different panels (n=5), showing cell counts of positive hepatocytes and non-parenchymal cells for both determinations. Data are mean ± SD; #p<0.05 vs. ND group, *p<0.05 vs. HFD group; Student's *t*-test. Scale bar = 0.1 mm.

IV.B.2. Mouse models of liver fibrosis

Once we had demonstrated the ability of RPV to clearly limit the progression of NAFLD in our experimental model, we decided to assess if the anti-inflammatory and anti-fibrotic effects of this drug were also present in other models of liver injury not related to fat accumulation. To ascertain this point, we established three more animal models by using CCl_4 injections to directly induce liver fibrosis in our wild-type animals (see Chapter III.B.2 c). By using this experimental approach, we aimed to determine the effect of RPV in the progression and regression of chemically induced liver fibrosis, as well as to assess its potential to modulate the spontaneous regeneration in the liver.

a) Effect of RPV in the progression of liver fibrosis

In this model, as previously described, both CCl_4 and RPV were administered simultaneously for 4 weeks (Figure IV.B.9 A), and inflammation and fibrosis progression were studied. As expected, CCl_4 itself induced a potent inflammatory response, observed by an intense increase in macrophages recruitment (assessed by F4/80 IHC), MPO activity, and NF-κB activation (Figures IV.B.9 and IV.B.10). Additionally, it triggered an important fibrotic response characterized by an enhanced collagen deposition, and augmented Vimentin and Desmin protein expression (Figures IV.B.9 and IV.B.10).

Histological analysis (Figure IV.B.9) demonstrated that RPV was able to decrease the CCl_4-mediated inflammatory and fibrotic responses in the liver. Sirius Red staining and Vimentin IHC showed that collagen deposition and HSC activation were intensely enhanced in CCl_4-treated groups and RPV significantly decreased them (Figure IV.B.9 B). In addition, RPV also diminished CCl_4-induced increase in both F4/80 expression and MPO enzyme activity, pointing to an intense anti-inflammatory effect involving regulation of different immune cell populations (Figure IV.B.9 B and C, respectively).

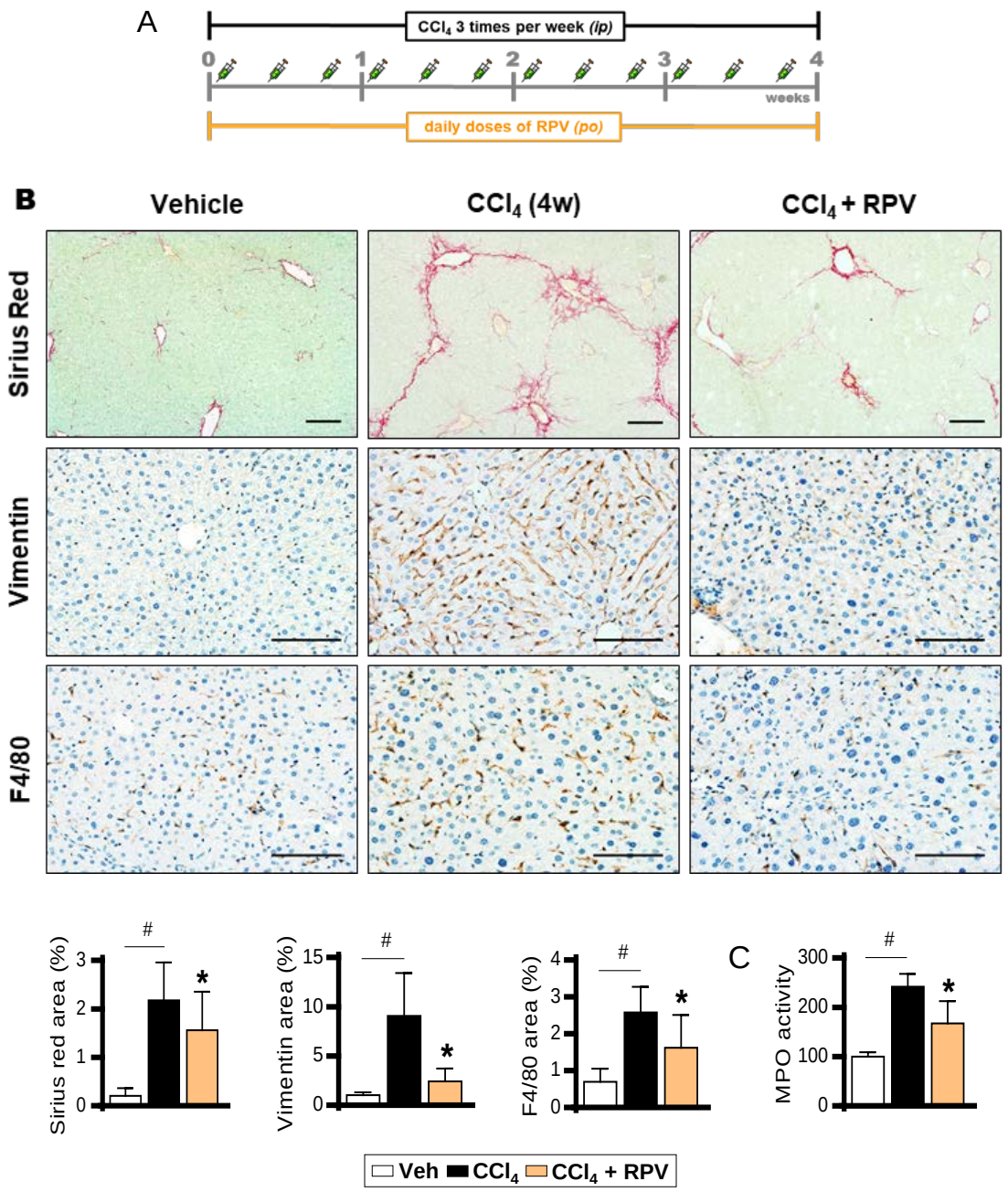

Figure IV.B.9. RPV decreases the progression of CCl_4-induced liver inflammation and fibrosis. Schematic representation of the fibrosis progression mouse model (A). Representative images and quantifications of Sirius Red staining and Vimentin and F4/80 IHC (n=5) in mice liver tissue (B). Enzymatic determination of MPO activity (n=5) (C). Data are mean ± SD; #p<0.05 vs. Veh group, *p<0.05 vs. CCl_4 group; Student's *t*-test. Scale bar = 0.1 mm.

In this line, we also studied the anti-inflammatory and anti-fibrotic effect of RPV by WB analysing the activation of NF-κB and the protein expression of Desmin. We observed the same protective role of RPV, significantly decreasing both parameters (Figure IV.B.10 A). In addition, RPV diminished the plasmatic levels

of several markers of liver injury that were increased in response to the CCl_4 insult, namely bilirubin and hepatic enzymes AST and ALT.

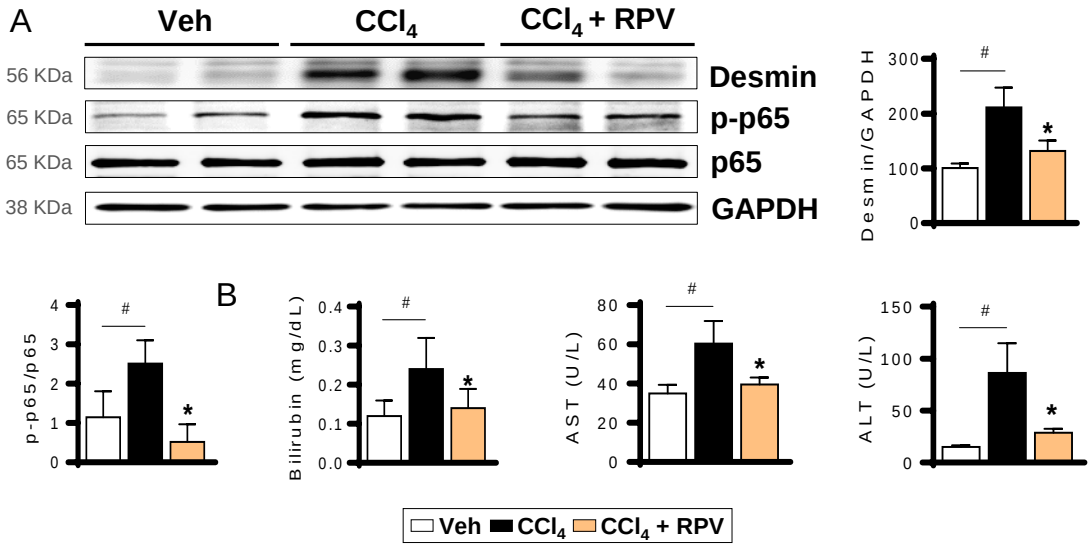

Figure IV.B.10. RPV decreases the progression of CCl_4-induced liver inflammation and fibrosis. Representative WB images from whole-liver samples and quantifications of Desmin protein expression and activation of NF-κB by phosphorylation of the p65 subunit (n=5) (B). Protein expression of Desmin was normalized versus GAPDH expression. NF-κB activation was calculated by the ratio between the phosphorylated form of p65 (p-p65) and the total form of the protein (p65). Determination of plasmatic levels of bilirubin, AST and ALT (B). Data are mean ± SD; #p<0.05 vs. Veh group, *p<0.05 vs. CCl_4 group; Student's *t*-test

Considering the previous studies carried out in the NAFLD model, we then analysed the capacity of RPV to modulate the balance between STAT3 and STAT1 signaling and, consequently, its potential to modulate both proliferation and apoptotic cell death in different cell subpopulations. Importantly, we observed that RPV was able to reproduce in this model all the regulatory and hepatoprotective actions described in the nutritional model of NAFLD.

We observed that CCl_4-induced injury clearly decreased nuclear translocation and activation of STAT3 in hepatocytes, both in liver sections (Figure IV.B.11 A) and in whole-liver extracts (Figure IV.B.11 B), while it decreased STAT1 activation in non-parenchymal cells (Figure IV.B.11 C), in a similar way than in the NAFLD model. One more time, RPV normalized both STAT3 (Figure IV.B.11 A and B) and STAT1 (Figure IV.B.11 C) expression in parenchymal and non-parenchymal cells, respectively.

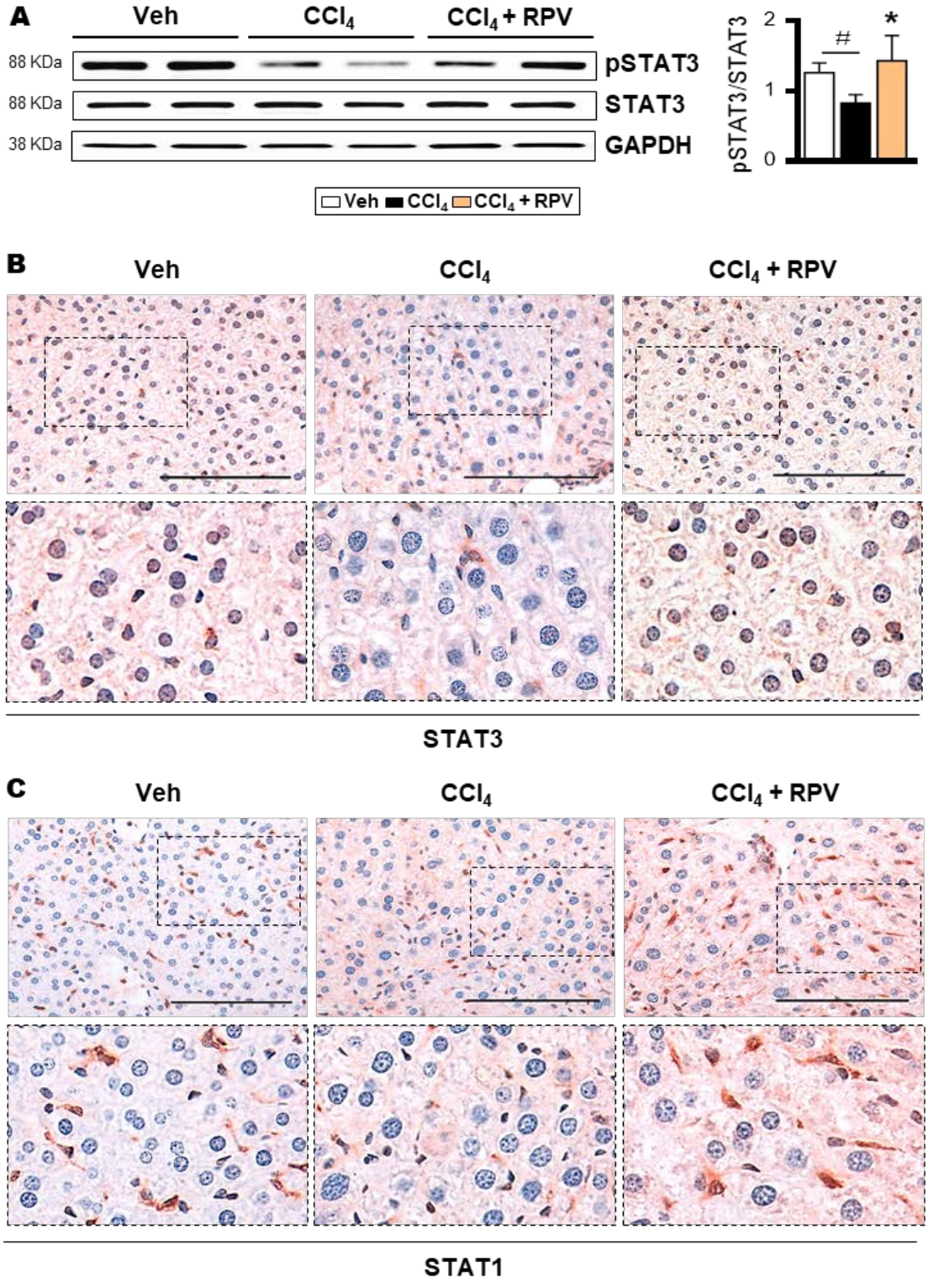

Figure IV.B.11. Hepatic regulation of STAT3 and STAT1 in response to CCl_4 and RPV treatment. Representative WB images of whole-liver samples and quantification of the activation of STAT3 by phosphorylation (n=5). Activation was calculated by the ratio between pSTAT3 and the total protein (STAT3); GAPDH is only displayed as a quality control of the experiment (A). Representative images of STAT3 IHC in mice liver tissue (B). Representative images of STAT1 (C) IHC determinations in mice liver tissue (n=5). Data are mean ± SD; #p<0.05 vs. Veh group, *p<0.05 vs. CCl_4 group; Student's *t*-test; Scale bar = 0.1 mm.

Further analysis of proliferation and apoptosis in these murine liver samples demonstrated that CCl_4 significantly induced hepatocyte apoptosis and non-parenchymal cells proliferation (Figure IV.B.12 A and B, respectively), which is compatible with a considerable injury induction. RPV reverted this tendency and clearly enhanced the number of Ki67-positive hepatocytes; this compound also induced apoptosis of non-parenchymal cells simultaneously decreasing the total number of dying hepatocytes (Figure IV.B.12 B).

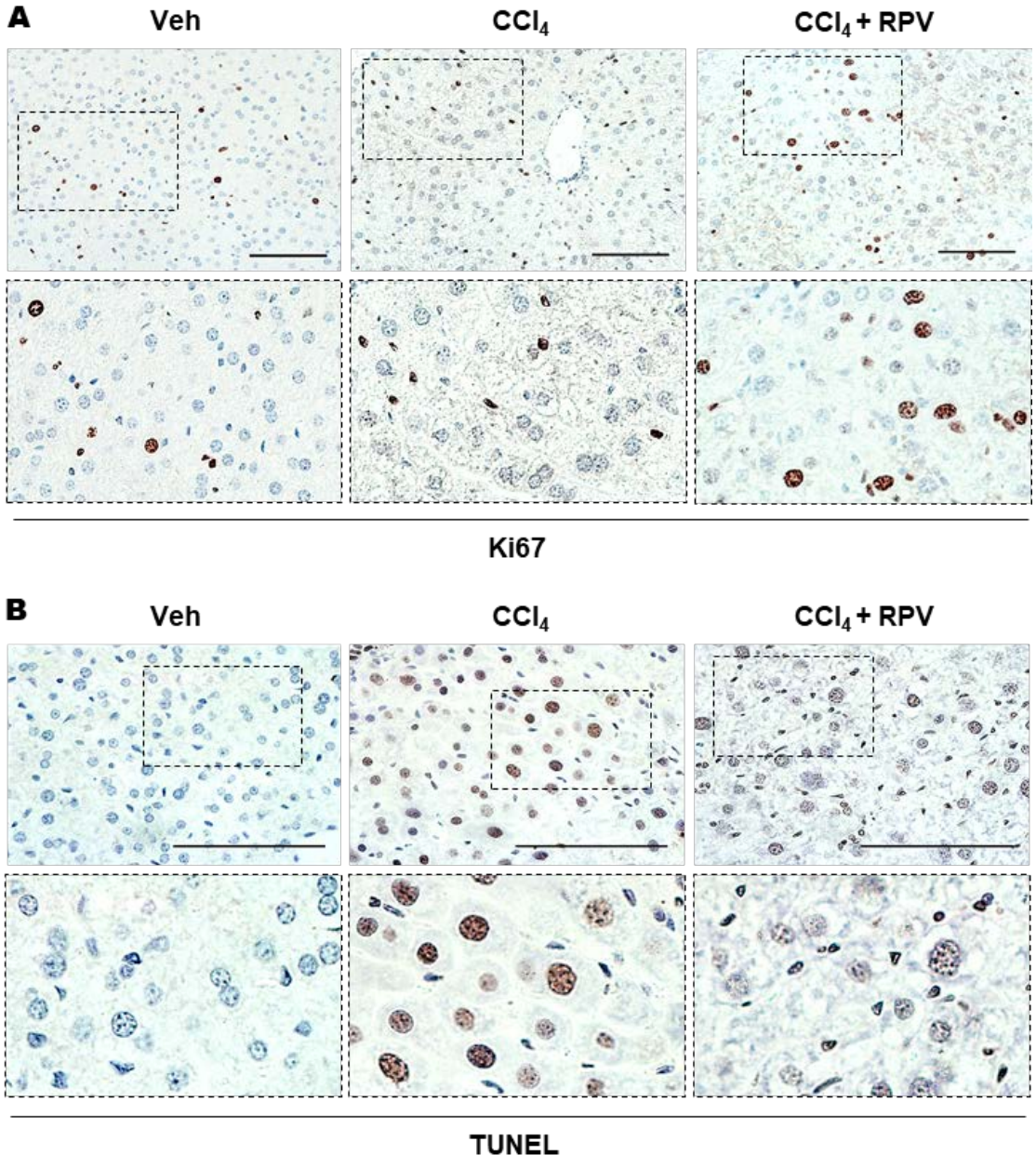

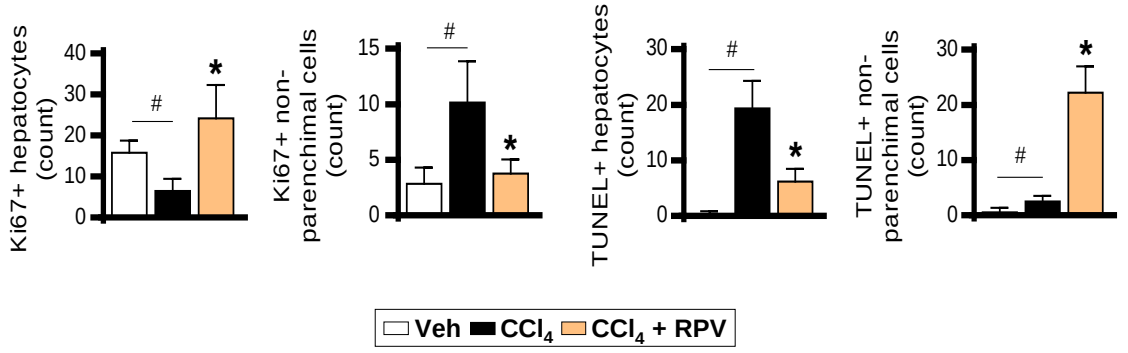

Figure IV.B.12. RPV increases the proliferation of hepatocytes and induces apoptosis in non-parenchymal cells in our mouse model of CCl_4-induced liver fibrosis. Representative images of Ki67 immunohistochemistry (A) and TUNEL staining (B) in mice liver tissue (n=5), and cell counts of positive hepatocytes and non-parenchymal cells for both determinations. Data are mean ± SD; #p<0.05 vs. Veh group, *p<0.05 vs. CCl_4 group; Student's *t*-test. Scale bar = 0.1 mm.

b) Contribution of RPV to the regression of liver fibrosis

Data obtained in our experiments suggested that RPV has a strong capacity to prevent chronic liver disease progression but, as it was always administered from the very beginning of the procedure in combination with the deleterious stimuli, we could not determine its potential to induce regression of liver injury and, specifically, of fibrosis. For this reason, our next step was to study the potential of this compound to ameliorate a liver pathological condition once it has been already produced. In order to investigate this, we modified the previous protocol, administering CCl_4 injections for 6 weeks and treating with RPV only during the last two weeks, once a substantial grade of liver fibrosis had already been established (Figure IV.B.13 A).

As expected, CCl_4 treatment for 6 weeks induced important collagen deposition, HSC activation and macrophage infiltration, determined by Sirius Red staining and Vimentin and F4/80 IHC, respectively (Figure IV.B.13 B). CCl_4 also increased the MPO enzyme activity (Figure IV.B.13 C) and the plasmatic concentration of many liver injury markers (Figure IV.B.14 A). Furthermore, it also enhanced Desmin protein expression and NF-κB activation (assessed by p65 phosphorylation). According to the literature, CCl_4-induced liver damage among different mouse models completely correlated with the duration of the CCl_4 injections [235,353,354]. Thus, the toxic effect of CCl_4 in our model (six weeks) was significantly greater than in our four-week model in all the parameters evaluated (Figure IV.B.9 A). Although the direct comparison between both models is not

displayed in this thesis, this enhancement of liver injury is evident when observing the extension of the alterations induced by both models in all these parameters (e.g. plasmatic levels of markers of liver injury, MPO determinations or WB quantifications).

Surprisingly, RPV also exerted a strong anti-inflammatory and anti-fibrotic effect in this model, since it decreased all the studied parameters of inflammation and fibrosis progression (as shown in Figures IV.B.13 and IV.B.14). These results confirmed the potential of this compound to be proposed as an antifibrotic drug and not only as a preventive option, being this a completely new and clinically relevant finding.

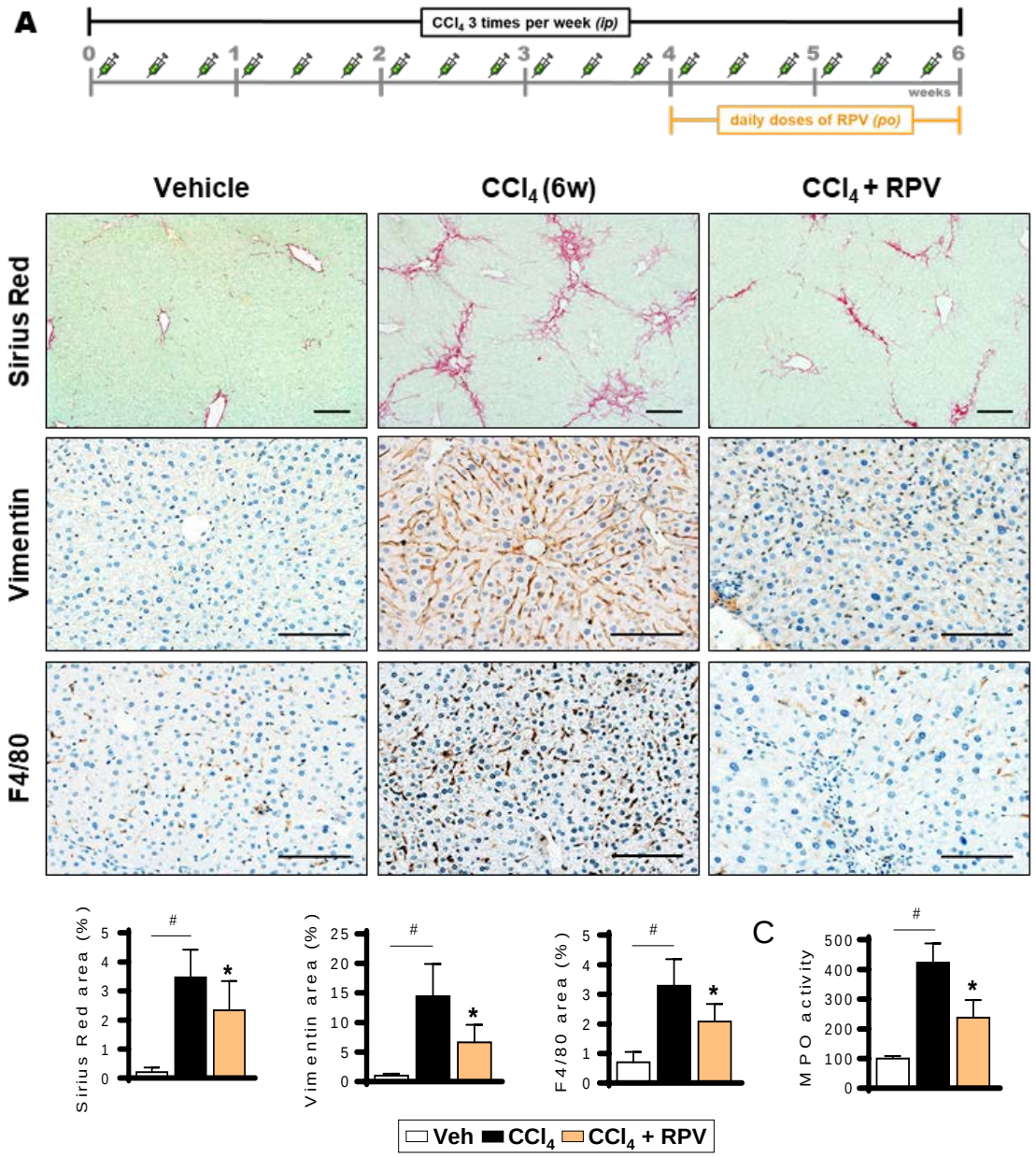

Figure IV.B.13. (Previous page) RPV induced anti-inflammatory and anti-fibrotic effects when administered in mice with liver fibrosis. Schematic representation of the mouse model employed (A). Representative images and quantifications of Sirius Red staining and Vimentin and F4/80 IHC (n=5) (B). Enzymatic determination of MPO activity (n=5) (C). Data are mean ± SD; #p<0.05 vs. Veh group, *p<0.05 vs. CCl_4 group; Student's *t*-test. Scale bar = 0.1 mm.

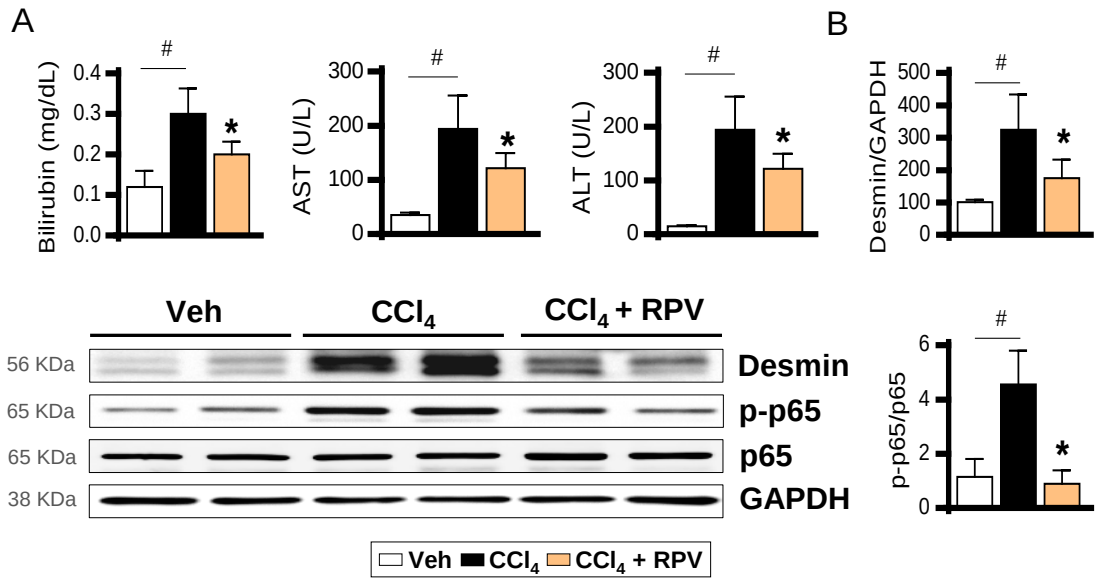

Figure IV.B.14. RPV has anti-inflammatory and anti-fibrotic capacity when is administered in mice with liver fibrosis. Determination of plasmatic levels of bilirubin and hepatic enzymes AST and ALT (A). Representative WB images from whole-liver samples and quantifications of Desmin protein and NF-κB activation by phosphorylation of the p65 subunit (n=5) (B). Protein expression of Desmin was normalized versus GAPDH expression. NF-κB activation was calculated by the ratio between the phosphorylated form of p65 (p-p65) and the total form of the protein (p65). Data are mean ± SD; #p<0.05 vs. Veh group, *p<0.05 vs. CCl_4 group; Student's *t*-test.

Despite this unexpected effect of RPV, we observed that this model provoked a severe damage in liver parenchyma, especially in CCl_4 groups but also in all those receiving RPV, detecting a high degree of hepatocyte ballooning (white and diffuse cytoplasm) and the loss of parenchymal architecture. Thus, the protective effect of RPV was evident and significant, but its administration was too short to completely normalize liver function.

To carry out this study, once again, we analysed RPV-induced STAT3 phosphorylation by WB (Figure IV.B.15 A), as well as the histological modulation of STAT3 and STAT1 by IHC (Figure IV.B.15 B and C, respectively). Additionally, we evaluated the proliferative potential of different liver cell populations by Ki67 IHC (Figure IV.B.16 A) and the induction of apoptosis by TUNEL (Figure IV.B.16 B).

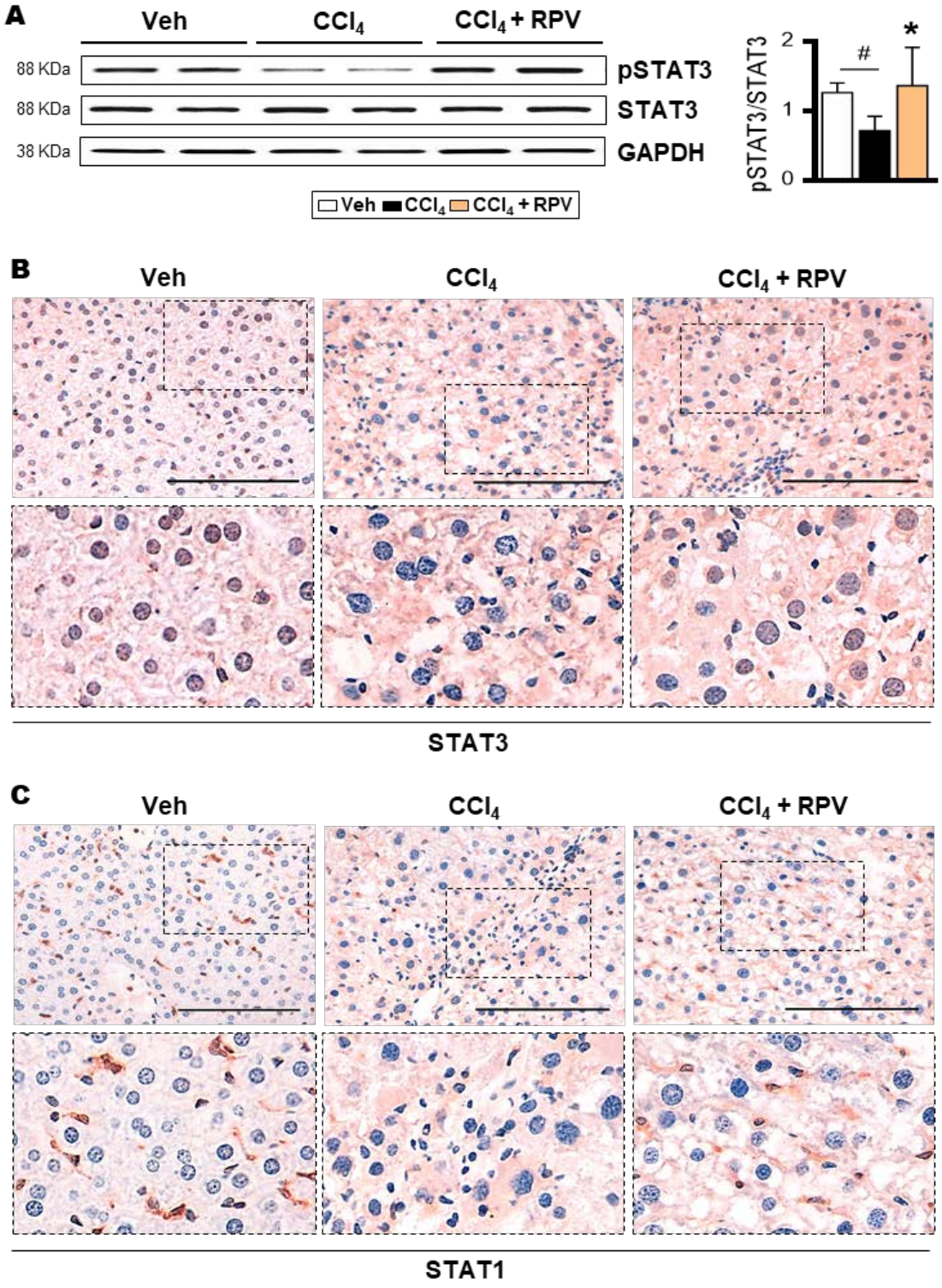

Figure IV.B.15. Hepatic regulation of STAT3 and STAT1 in response to RPV in a fibrotic liver. Representative WB images of whole-liver samples and quantification of STAT3 activation by phosphorylation (pSTAT3/STAT3) (n=5). GAPDH is only displayed as a quality control of the experiment (A). Representative images of STAT3 (B) and STAT1 (C) IHC in mice liver tissue (n=5). Data are mean ± SD; #p<0.05 vs. Veh group, *p<0.05 vs. CCl_4 group; Student's *t*-test; Scale bar = 0.1 mm.

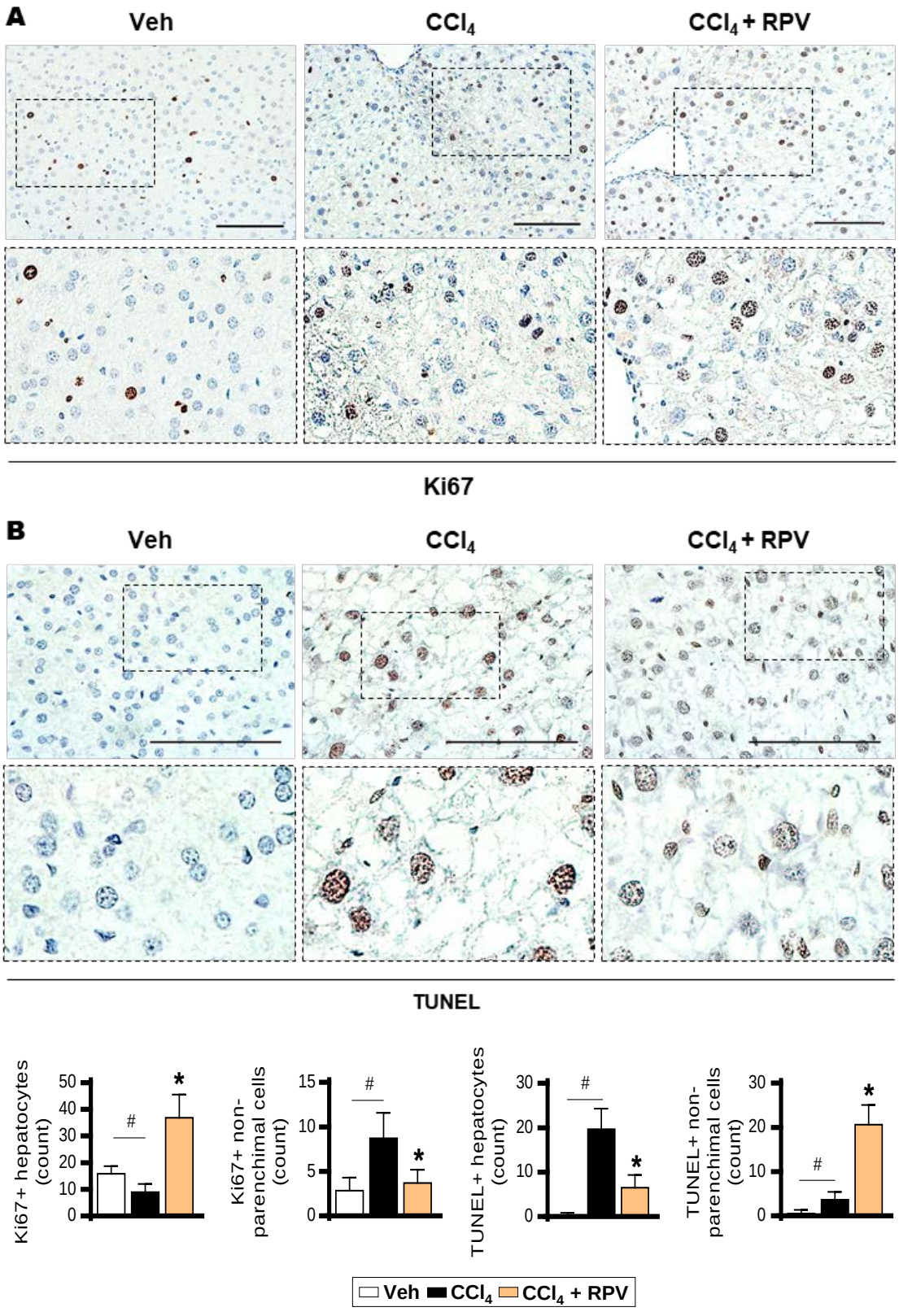

Figure IV.B.16. RPV increases the proliferation of hepatocytes and induces apoptosis in non-parenchymal cells when is administered in mice with liver fibrosis. Representative images of Ki67 IHC (A) and TUNEL staining (B) in mice liver tissue (n=5), and cell counts of positive hepatocytes and non-parenchymal cells for both determinations. Data are mean ± SD; #p<0.05 vs. Veh group, *p<0.05 vs. CCl_4 group; Student's *t*-test. Scale bar = 0.1 mm.

As observed in Figures IV.B.15 and IV.B.16, RPV had similar effects with regard to STAT3 and STAT1 modulation in hepatocytes and non-parenchymal cells (Figure IV.B.15), as well as in cell proliferation and apoptosis induction (Figure IV.B.16), when compared to those exerted in the previous experimental models of chronic liver disease.

c) Role of RPV in the spontaneous regeneration of the liver

Lastly, we established a similar murine model of CCl_4-induced liver fibrosis to determine the capacity of RPV to modulate the spontaneous regeneration that takes place in the liver after discontinuation of the toxic insult. To do so, we induced liver fibrosis by CCl_4 injections for 4 weeks and, after finishing this treatment, we daily administered vehicle or RPV for 2 weeks to assess whether this NNRTI could significantly modulate the liver recovery rate (Figure IV.B.17 A). As observed below, two weeks after stopping the CCl_4 injections, collagen deposition (Figure IV.B.17 A), MPO enzyme activity (Figure IV.B.17 B) and plasmatic levels of bilirubin, ALT and AST (Figure IV.B.17 C) spontaneously decreased if compared with mice groups that were just treated with CCl_4 for 4 weeks and were not allowed to recover. Interestingly, MPO activity and plasmatic markers decreased until similar levels to those shown by healthy mice. However, collagen content was still significantly higher in CCl_4 groups than in the controls. This makes sense since collagen degradation usually needs longer periods of time to finally reach physiological levels.

Data shown in Figure IV.B.17 demonstrate that RPV treatment did not accelerate hepatic recovery after interrupting CCl_4 injections. Specifically, it did not significantly decreased collagen content in treated groups if compared with the groups receiving only vehicle, and it neither decreased further plasmatic markers of liver injury (bilirubin, AST and ALT). Moreover, MPO enzyme activity was not influenced by antiretroviral treatment. These results could suggested that the effect of RPV directly targets activated HSC, since its effect disappeared when these cells physiologically become inactive after discontinuing the liver insult that keeps them active and proliferating.

Considering all these results, we could state that RPV had a protective effect in the liver, limiting its inflammation and preventing the progression of fibrosis through the induction of HSC apoptosis and hepatocyte proliferation. We then

postulated that these RPV-induced effects were directly related to the differential response observed in liver cell populations in the triggering of STAT-regulated pathways.

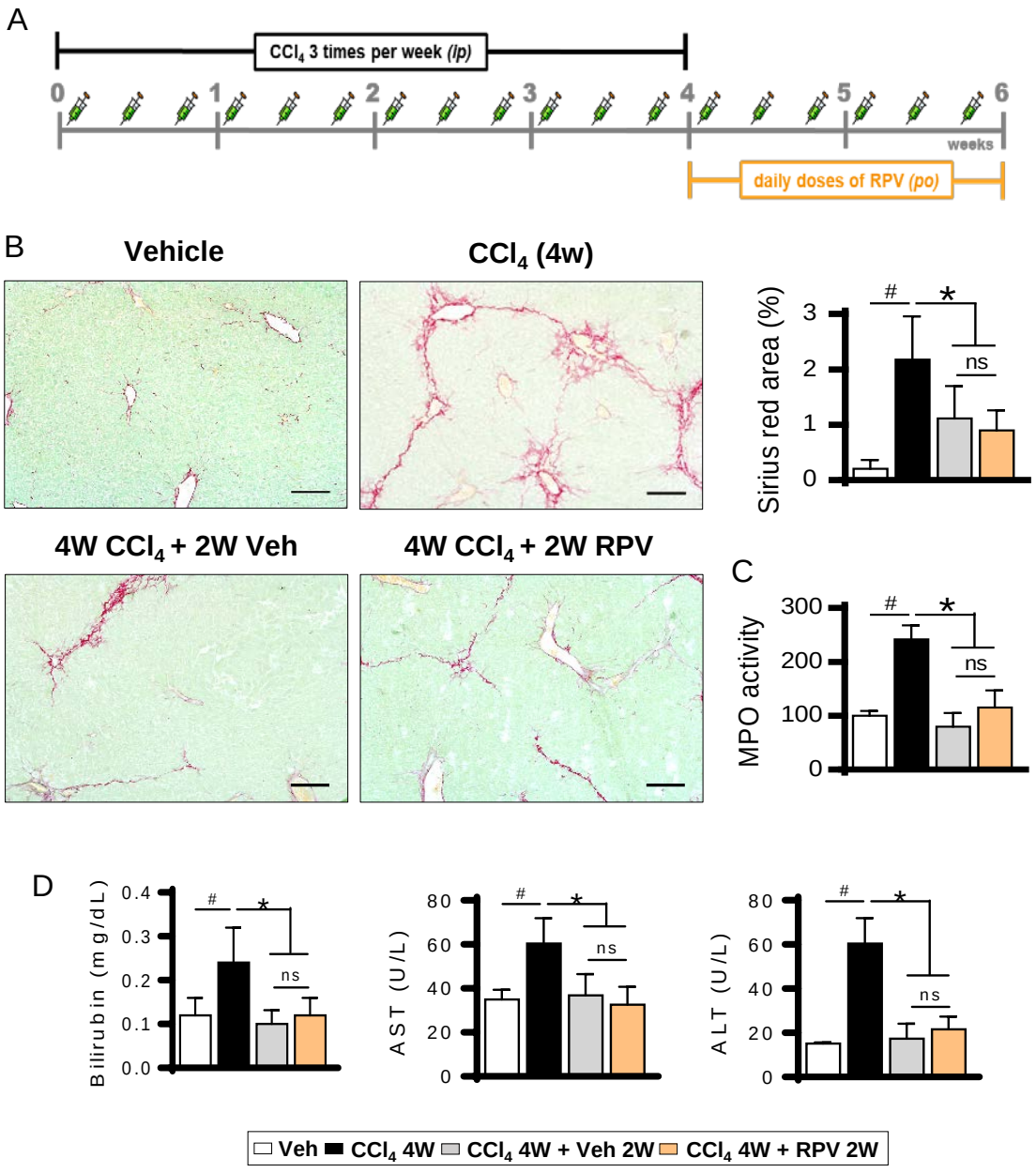

Figure IV.B.17. RPV do not accelerate the spontaneous liver regeneration. Schematic representation of the mouse model employed (A). Representative images and quantifications of Sirius Red staining (n=5) (B). Enzymatic determination of MPO activity (n=5) (C). Determination of plasmatic levels of bilirubin, AST and ALT (n=5) (D). Data are mean ± SD; #p<0.05 vs. Veh group, *p<0.05 vs. CCl_4 group; Student's *t*-test. Scale bar = 0.1 mm.

IV.B.3. *In vitro* study of RPV-induced actions in different liver cell subpopulations

According to the existing literature about STAT regulation and cellular phenotypic responses, we hypothesised that the over-expression of both STAT3 and STAT1 in different cell subtypes could be the main responsible of the hepatoprotective effects of RPV. In order to prove this, we carried out an extensive *in vitro* study where the two cell populations more directly involved in the fibrotic response, hepatocytes and HCS, were studied.

We directly treated both hepatocyte (Hep3B and HepG2) and HSC (LX-2) human cell lines with increasing concentrations of RPV (from 1 to 8 µM) and their viability and proliferation/survival were evaluated through MTT and fluorescence determinations, respectively. HSC were also co-treated with low concentrations of TGFβ in order to increase their pro-fibrogenic activation to myofibroblast-like cells.

As it can be observed in the MTT determinations displayed in Figure IV.B.18, RPV did not alter cell viability of hepatocyte cell lines (only a slightly decrease was observed with the highest dose of this compound in HepG2), but it induced a significant and concentration-dependent cytotoxic effect in LX-2 cells (Figure IV.B.18 A). This effect was confirmed assessing cell proliferation/survival through fluorescence microscopy in these same cell line (Figure IV.B.18 B). Furthermore, observation of LX-2 cells phenotype under light microscopy suggested the activation of cell death processes after 48 h treatment (Figure IV.B.18 C).

We next studied gene expression of several markers of HSC activation and fibrosis progression using these same experimental conditions, namely, treatment with RPV (1-8 µM) for 48 h, in the presence or absence of TGFβ. Interestingly, RPV exerted a discrete effect that was only evident at higher doses in non-stimulated cells, except for *Serpine-1* gene expression, which was clearly reduced. However, the anti-fibrotic effect of RPV was perfectly observed in cells stimulated with TGFβ co-treatment, in which this NNRTI down-regulated fibrogenic genes in a concentration-dependent fashion.

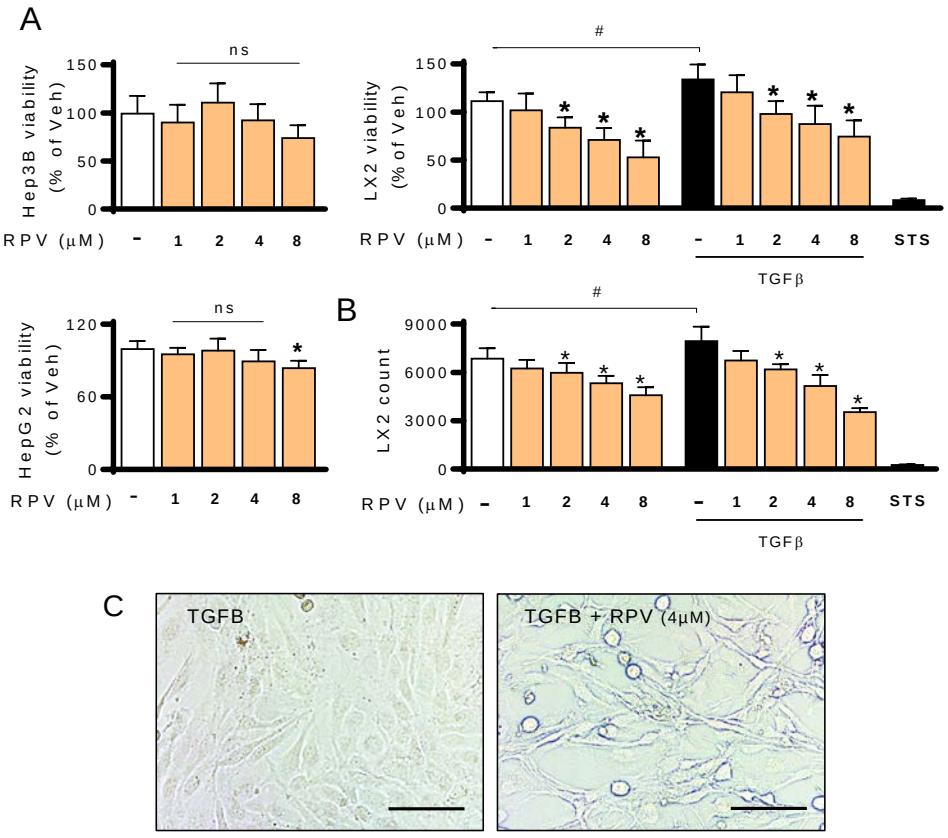

Figure IV.B.18. RPV exerts a cytotoxic effect in HSC but not in hepatocytes. Analysis of cell viability of Hep3B, HepG2 and LX-2 cells after 72 h of treatment with RPV (1-8 μM) by MTT assay (n=6) (A). Cell viability assay in LX-2 cell line by fluorescence microscopy (n=6) (B). Representative images by optical microscopy of LX-2 cells after 48 h of treatment with TGFβ and TGFβ + RPV 4 μM (C). Data are mean ± SD. #p<0.05 'Veh' vs. 'Veh+TGFβ' groups, Student's *t*-test. *p<0.05 'Veh' or 'Veh + TGFβ' vs. 'RPV' or 'RPV + TGFβ', respectively; one-way ANOVA multiple comparison test followed by Bonferroni post-test. Staurosporine (STS) was used as a positive control of cytotoxicity. Scale bar = 0.1 mm.

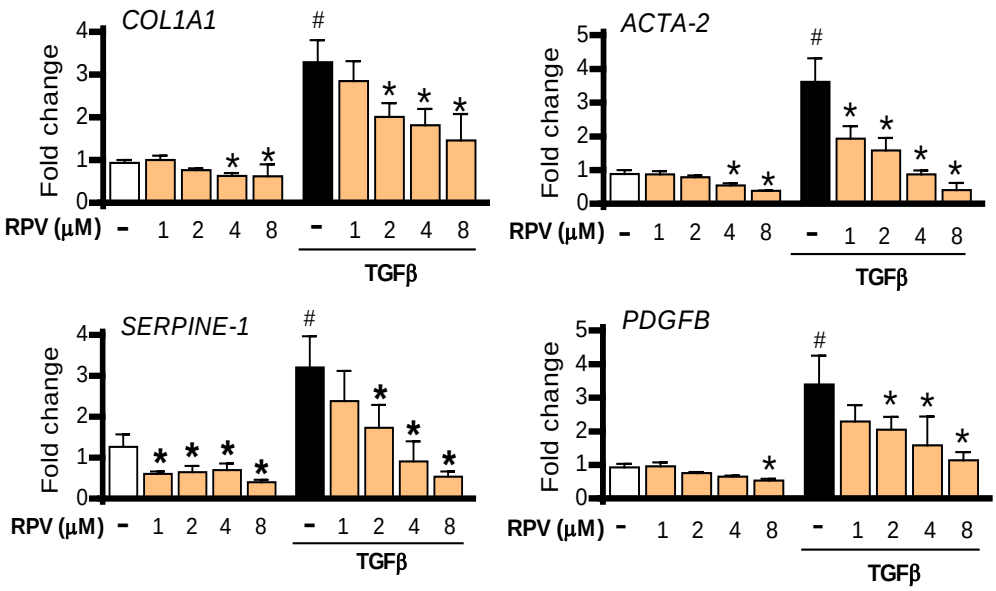

Figure IV.B.19. (Previous page) RPV down-regulates gene expression of fibrogenesis markers in HSC. Gene expression of fibrogenic markers in LX-2 cells after 48 h treatment with RPV (1-8 μM), with or without TGFβ stimulation, assessed by RT-PCR (n=5). Gene expression data were normalized versus the expression of *Actb* gene. Data are mean ± SD. #p<0.05 'Veh' vs. 'Veh+TGFβ' groups, Student's *t*-test. *p<0.05 'Veh' or 'Veh + TGFβ' vs. 'RPV' or 'RPV + TGFβ', respectively; one-way ANOVA multiple comparison test followed by Bonferroni post-test.

In addition, we also studied this RPV-induced inactivation in LX-2 cells at the protein level. WB analyses of Col1A1 expression after 48 h treatment revealed an intense increase in its expression in response to TGFβ if compared with non-stimulated conditions. Surprisingly, RPV treatment did not exert evident changes in non-stimulated conditions, but it induced a significant concentration-dependent decrease in the Col1A1 expression in all the conditions co-treated with TGFβ (Figure IV.B.20 A). Regarding pSTAT3 and pSTAT1 protein expression, we observed an opposite effect induced by RPV: in both non-stimulated and stimulated conditions, but especially in the latter, RPV induced a concentration-dependent decrease in pSTAT3 protein expression, and a great increase in that of pSTAT1 (Figure IV.B.20 A).

To assess whether RPV could trigger also apoptosis in HSC *in vitro*, a bivariate apoptosis assay was performed using flow cytometry. As displayed in Figure IV.B.20 B, we observed that RPV induced a concentration-dependent pro-apoptotic effect in LX-2 cells after 72 h of treatment. Interestingly, the effect observed both in non-stimulated and in stimulated cells was quite similar. Moreover, if compared with the classical positive control Staurosporine (STS), RPV had only a mild pro-apoptotic effect; however, this response was really reproducible among all the experimental replicates. In addition, it is important to note that this pro-apoptotic effect was time-dependent, not being detected when LX-2 cells were treated with RPV for shorter periods of time (24 and 48 h incubations induced no changes).

As previously explained, there are three main molecular mechanisms that drive HSC inactivation: apoptosis, cell cycle arrest and senescence. Although we have only shown the results for apoptosis induction in LX-2 cells in this thesis, the other two options were also explored and revealed negative results (data not shown). We could then confirm that RPV did not induce significant changes in cell cycle progression nor in cellular senescence of HSC in our experimental conditions.

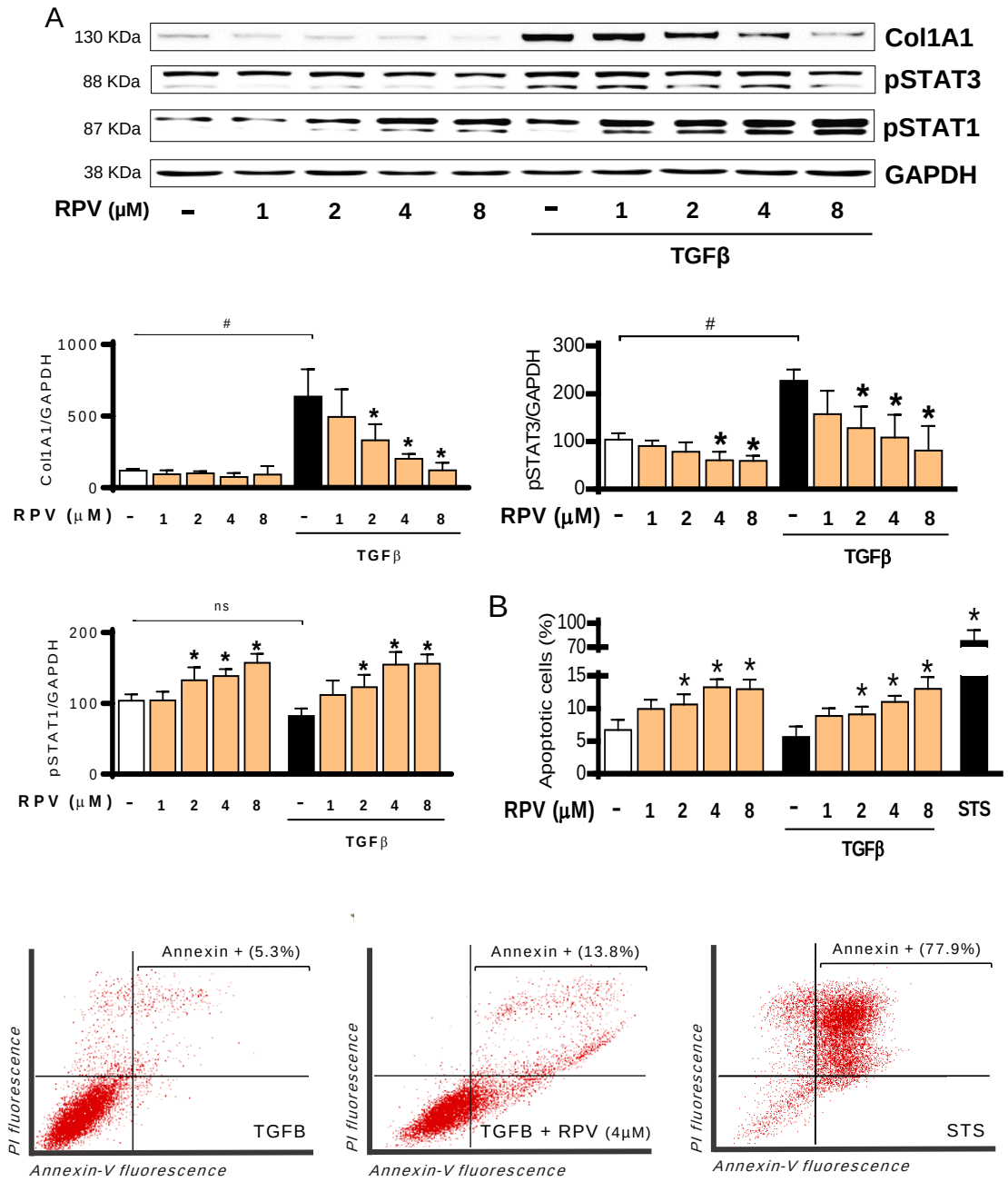

Figure IV.B.20. RPV inactivates and induces apoptosis of HSC. Representative WB images and quantifications of Col1A1, pSTAT3 and pSTAT1 in LX-2 cells, both stimulated and non-stimulated with TGFβ, after treatment with RPV for 48 h at different concentrations (from 1 to 8 μM) (n=5) (A). In all cases, protein expression was normalized versus GAPDH expression. Flow cytometry analysis of apoptosis induction in LX-2 cells after 72 h of treatment with RPV (n=4) (B). In the quantification graph all conditions are displayed, but the cytograms correspond only to 'TGFβ', 'TGFβ + RPV 4 μM' and STS. Data are mean ± SD. #p<0.05 'Veh' vs. 'Veh + TGFβ' groups, Student's *t*-test; *p<0.05 'Veh' or 'Veh + TGFβ' vs. 'RPV' or 'RPV + TGFβ', respectively; one-way ANOVA multiple comparison test followed by Bonferroni post-test.

According to literature, STAT1 activation leads to cell cycle arrest and apoptosis, and these were exactly the effects observed in our LX-2 cell cultures. Thus, we decided to assess the cause-consequence relationship between this molecular pathway and the phenotypic and functional alterations found in this cell line in response to RPV. With this purpose, we first decided to chemically inhibit STAT1 activation in LX-2 cells pre-incubating them with fludarabine, which is an antineoplastic drug used in many *in vitro* studies as a specific inhibitor of STAT1 activation, directly inhibiting its phosphorylation [355–357]. In our experimental approach, LX-2 cells were pre-treated for 2 h with fludarabine at 5 μM before adding TGFβ and RPV treatments.

Figure IV.B.21 demonstrates that pre-treatment with fludarabine clearly inhibited STAT1 phosphorylation, but this inhibition was not specific since STAT3 phosphorylation was also substantially down-regulated (Figure IV.B.21 A). It is also important to note that fludarabine-treated cells could still respond to TGFβ stimulation (Figure IV.B.21 A), although their viability was significantly decreased (Figure IV.B.21 B). Interestingly, RPV-induced decrease in Col1A1 protein expression disappeared, and even increased, when STAT1 was not activated (Figure IV.B.21 A). Moreover, despite the general decrease in viability induced by fludarabine, MTT analysis showed that the cytotoxic effect of RPV in these cells was blocked in presence of this inhibitor (Figure IV.B.21 B).

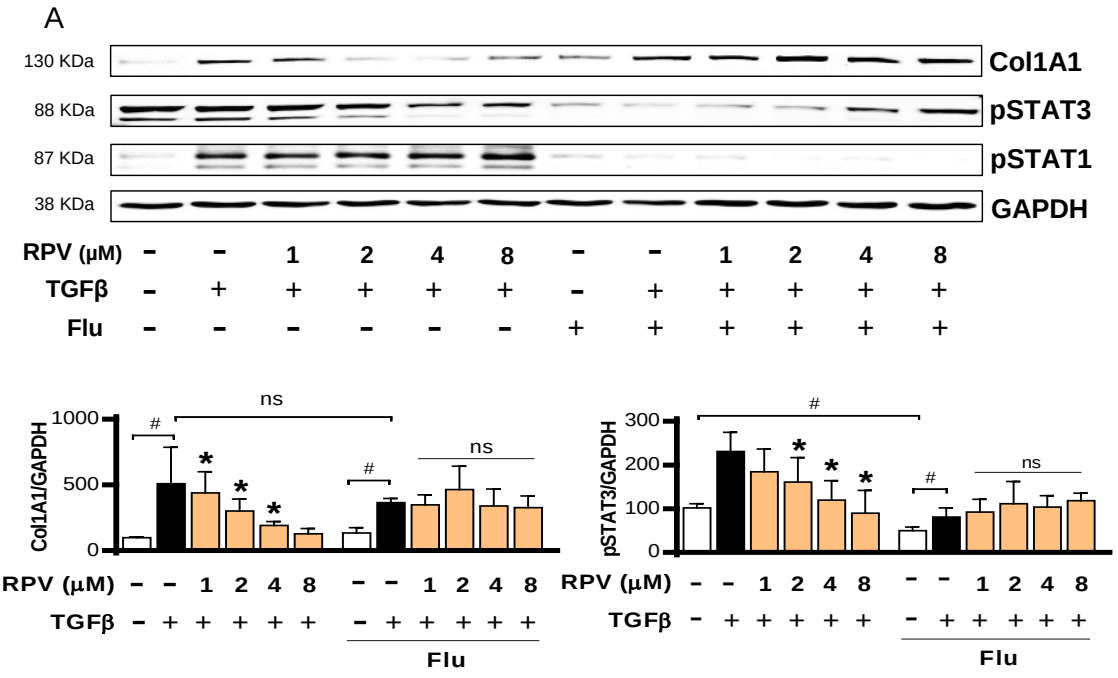

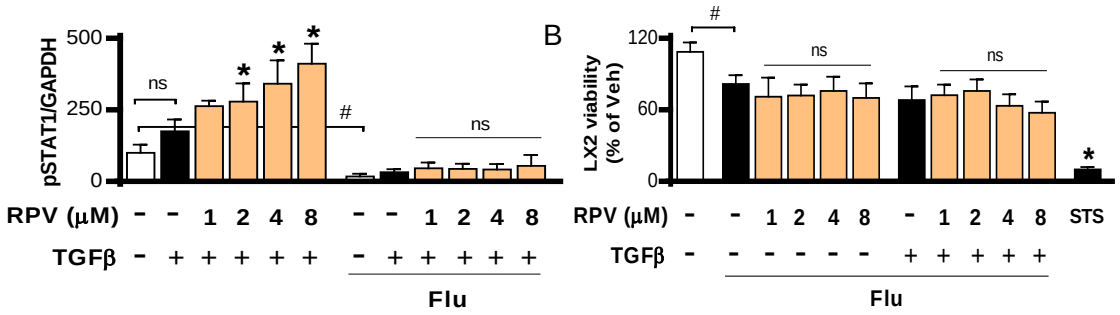

Figure IV.B.21. RPV-induced cytotoxicity in HSC disappear when STAT1 activation is blocked. Representative WB images and quantifications of Col1A1, pSTAT3 and pSTAT1 in LX-2 cells, both stimulated and non-stimulated with TGFβ, following treatment with RPV (from 1 to 8 μM) for 48 h, with and without pre-incubation with fludarabine (n=5) (A). Determination of cell viability of LX-2 cells following 72 h of treatment with the same experimental conditions (n=6) (B). Data are mean ± SD. #p<0.05 'Veh' vs. 'Veh+TGFβ' groups, Student's *t*-test. *p<0.05 'Veh' or 'Veh + TGFβ' vs. 'RPV' or 'RPV + TGFβ', respectively; one-way ANOVA multiple comparison test followed by Bonferroni post-test.

From these data we got the first evidence that pointed to STAT1 as the main responsible for the cytotoxic effect of RPV in HSC. Additionally, we could suggest that this regulation in the STAT1 pathway could be, at least in part, the responsible for the effect observed in mice.

Considering that the use of fludarabine had several evident limitations that could bias this study, we performed lipofectamine-mediated transient gene silencing by using esiRNA targeting STAT1 to confirm the crucial role of this factor in the RPV-induced actions in HSC. Through this methodology we did not block STAT1 activation but we inhibited their gene expression upstream. After silencing, we analysed the same parameters previously described in Figure IV.B.20, but only using intermediate concentrations of RPV (2 and 4 μM). As observed in Figure IV.B.22, STAT1 silencing resulted in an intense inhibition of this factor, maintaining unaltered, in this case, STAT3 activation (Figure IV.B.22 A); furthermore, cell viability was also unchanged by the silencing process. However, a small and non-significant increase in the number of necrotic cells was detected in the cytometric analysis for all the transfected conditions, both from siC and siSTAT1 (Figure IV.B.22 B), and effect characteristic of this type of approach/methodology.

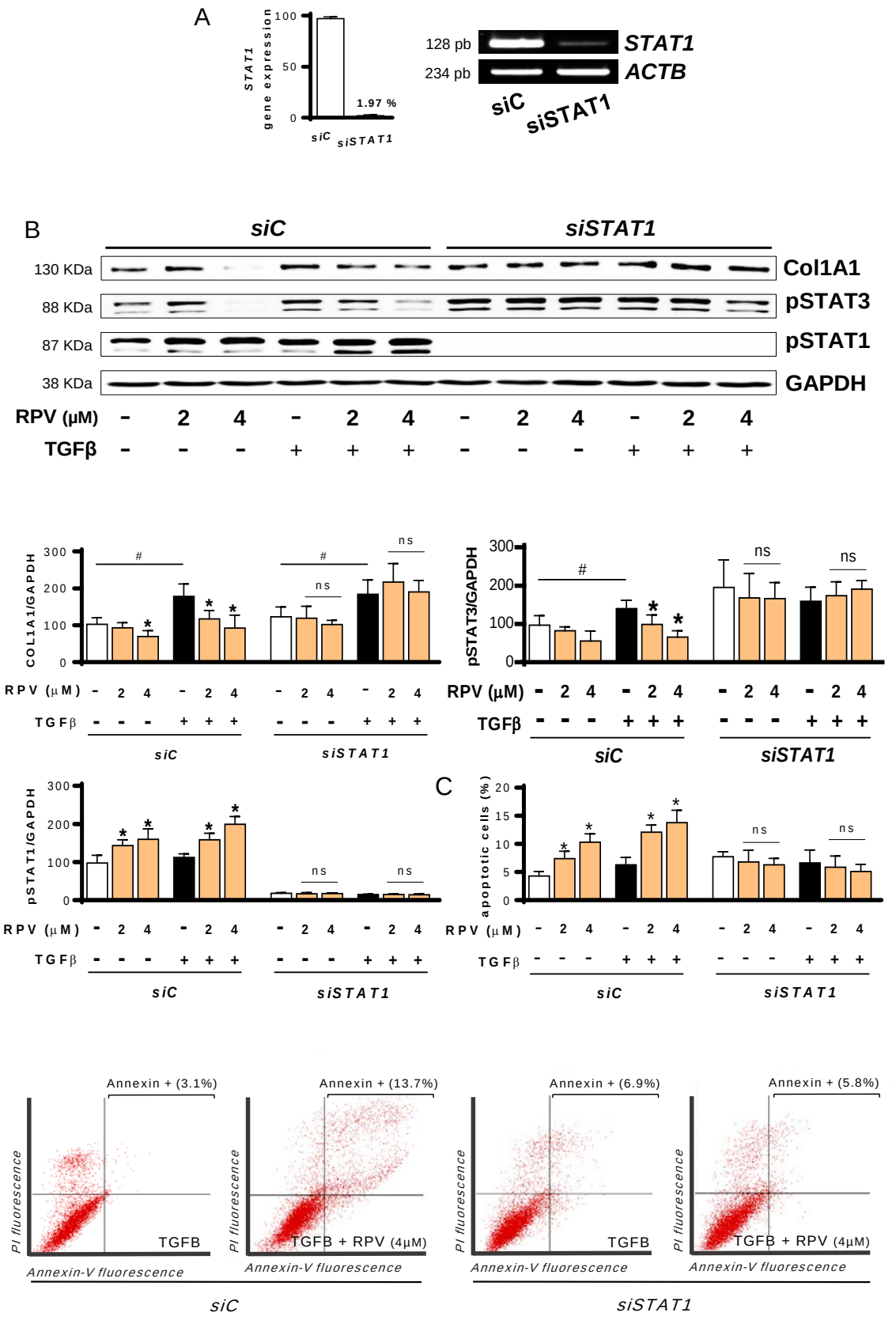
A
STAT1 gene expression
100
50
0
1.97 %
siC
siSTAT1
128 pb
234 pb
STAT1
ACTB
siC
siSTAT1
B
siC
siSTAT1
130 KDa
88 KDa
87 KDa
38 KDa
Col1A1
pSTAT3
pSTAT1
GAPDH
RPV (µM) - 2 4 - 2 4 - 2 4 - 2 4
TGFβ - - - + + + - - - + + +
COL1A1/GAPDH
pSTAT3/GAPDH
pSTAT1/GAPDH
apoptotic cells (%)
ns
C
Annexin + (3.1%)
Annexin + (13.7%)
Annexin + (6.9%)
Annexin + (5.8%)
PI fluorescence
Annexin-V fluorescence
TGFB
TGFB + RPV (4µM)
siC
siSTAT1

Figure IV.B.22. (Previous page) RPV-induced cytotoxicity in HSC disappear when STAT1 is not expressed. Efficacy of STAT1 silencing by qPCR (A). Representative WB and quantifications of Col1A1, pSTAT3 and pSTAT1 in LX-2 transfected cells (siC and siSTAT1), stimulated and non-stimulated with TGFβ, after treatment with RPV for 48 h at 2 and 4 μM (n=4) (B). Cytometric analysis of the apoptosis induction in transfected LX-2 cells after 72 h of treatment with RPV. In the quantification graph all conditions are displayed, but the cytograms correspond only to 'TGFβ', 'TGFβ + RPV 4 μM' (n=4) (C). Data are mean ± SD. #p<0.05 'Veh' vs. 'Veh+TGFβ' groups, Student's *t*-test. *p<0.05 'Veh' or 'Veh + TGFβ' vs. 'RPV' or 'RPV + TGFβ', respectively; one-way ANOVA multiple comparison test + Bonferroni post-test.

In line with the results shown in Figure IV.B.21, RPV-mediated decrease in Col1A1 and pSTAT3 protein expression was not present when STAT1 expression was blocked (Figure IV.B.22 B). Importantly, also the pro-apoptotic effect of RPV disappeared once STAT1 signaling was impaired, as it can be observed in the quantification of flow cytometry experiments and in the corresponding cytograms displayed in Figure IV.B.22 C.

These results demonstrated that RPV had a direct STAT1-dependent pro-apoptotic effect in LX-2 cells, an *in vitro* mechanism that could be the main driver of the hepatoprotective effect observed *in vivo*. However, we were not able to reproduce *in vitro* all the results observed in hepatocytes *in vivo*. In our mice models, hepatocytes could restore their physiological expression of STAT3 in response to RPV in injured mice. Nevertheless, as shown below (Figure IV.B.23), direct treatment with RPV at different concentrations (from 1 to 8 μM) and times (from 6 to 48 h) failed to increase pSTAT3 expression in Hep3B cells. Further experiments were done combining RPV with low doses of IL6, the endogenous activator of STAT3, and once again, RPV did not enhance the expression of this protein. As displayed in Figure IV.B.23, the only changes observed in STAT3 activation were due to IL6 treatment, especially between 12 and 24 h of incubation (Figure IV.B.22).

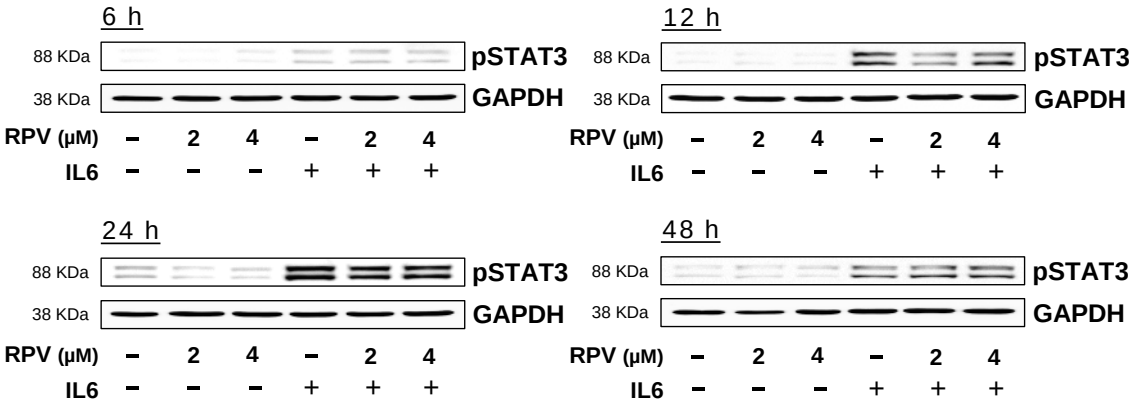

Figure IV.B.23. (Previous page) Treatment with RPV does not activate STAT3 in hepatocytes. Representative WB of pSTAT3 in Hep3B cells after treatment with RPV, alone or in combination with IL6 (5 ng/mL), at different concentrations (2 and 4 µM) and time points (from 6 to 48 h) (n=4).

Given these results, we decided to carry out conditioned medium experiments to explore the possibility of an active interplay between HSC and hepatocytes, driven by alterations in the STAT3/STAT1 balance and induced by RPV. We hypothesised that STAT3 activation in hepatocytes could be triggered in response to the secretome of apoptotic HSC, so we collected the culture medium from HSC previously treated with RPV for 72 h, which were consequently apoptotic, and cultured Hep3B cells directly with this medium for further 16 h (this incubation period was chosen because it was when we found the maximal STAT3 activation in these cells, see Figure IV.B.23).

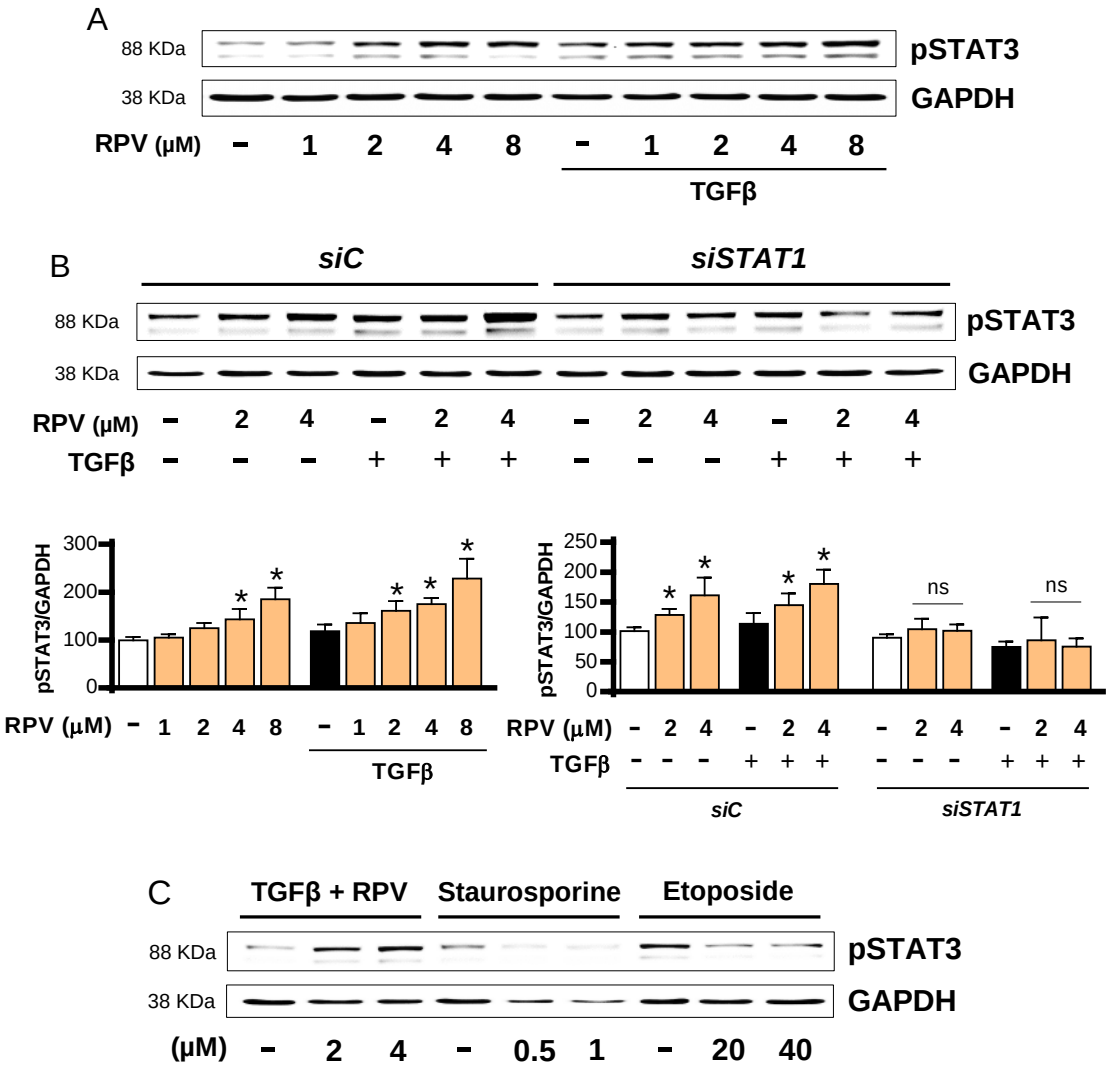

Figure IV.B.24. (Previous page) STAT3 in hepatocytes is activated in response to the secretome of RPV-induced apoptotic HSC. Representative WB and quantifications of pSTAT3 in protein extracts from Hep3B cells treated with conditioned medium for 16 h. This medium came from wild-type LX-2 cells (A) and transfected LX-2 cells (B) previously treated with RPV for 72 h (from 1 to 8 µM) (n=4). Representative WB of pSTAT3 in protein extracts from Hep3B cells treated with conditioned medium from LX-2 for 16 h. These LX-2-conditioned media were obtained by treating LX-2 cells with RPV (at 2 and 4 µM) for 72 h, or with staurosporine (at 0.5 and 1 µM) and etoposide (at 20 and 40 µM) for 24 h (n=3) (C). Data are mean ± SD. #p<0.05 'Veh' vs. 'Veh + TGFβ' groups, Student's *t*-test. *p<0.05 'Veh' or 'Veh + TGFβ' vs. 'RPV' or 'RPV + TGFβ', respectively; one-way ANOVA multiple comparison test + Bonferroni post-test.

As displayed above, treatment of Hep3B cells with conditioned medium coming from RPV-treated LX-2 cells, induced a concentration-dependent STAT3 activation (Figure IV.B.24 A and B). This over-expression of pSTAT3, despite being not very intense, completely correlated with the discrete but constant pro-apoptotic effect of RPV in LX-2 cells (Figures IV.B.20 and IV.B.22). Moreover, we confirmed that this STAT3 activation in hepatocytes was totally dependent on the amount of LX-2 cells that underwent apoptotic in response to RPV. Treatment of Hep3B cells with conditioned medium from LX-2 cells treated for shorter periods of time (24 or 48 h) did not induce any change in STAT3 activation (as described above, shorter incubations with RPV did not induced apoptosis in LX-2; data not shown). It is extremely important to note that, as shown in Figure IV.B.24 B, also STAT1 silencing in LX-2 cells abolished this pSTAT3 overexpression in Hep3B cells in the same experimental conditions, since the STAT1 deletion in LX-2 cells blocked the pro-apoptotic effect of RPV (Figure IV.B.22 B). We also induced apoptosis in LX-2 cells with different concentrations of pro-apoptotic molecules like STS and etoposide, whose cytotoxic mechanisms do not involve JAK-STAT signaling, and treated Hep3B cells with these conditioned media, detecting no enhancement of STAT3 activation in hepatocytes (Figure IV.B.24 C).

Finally, to conclude this *in vitro* study we tested RPV in human primary HSC (hHSC), mainly obtained from discarded tissue after liver transplantation. hHSC were treated with the same conditions as LX-2 cells for 72 h, with intermediate doses of RPV (2 and 4 µM) and the same amount of TGFβ to stimulate their proliferation (2.5 ng/mL). Differently to what we observed in LX-2 cells, relevant phenotypic alterations in response to RPV were not observed in hHSC among the different experimental conditions (Figure IV.B.24 A). However, gene expression of several fibrogenic markers (Figure IV.B.25 B), as well as protein

expression of pSTAT3 and pSTAT1 (Figure IV.B.25 C), completely reproduced the results obtained in LX-2 cells. In addition, a slight increase in pSTAT3 was observed in Hep3B cultures treated with the conditioned medium from primary HSC, although they did not show a clear apoptotic phenotype under the light microscope (Figure IV.B.25 D).

It should be highlighted that we were able to confirm *in vitro* all the observations made *in vivo* and, moreover, that this effect was also reproduced in human primary cells, which could be clinically relevant, as it will be discussed in the following sections of this thesis.

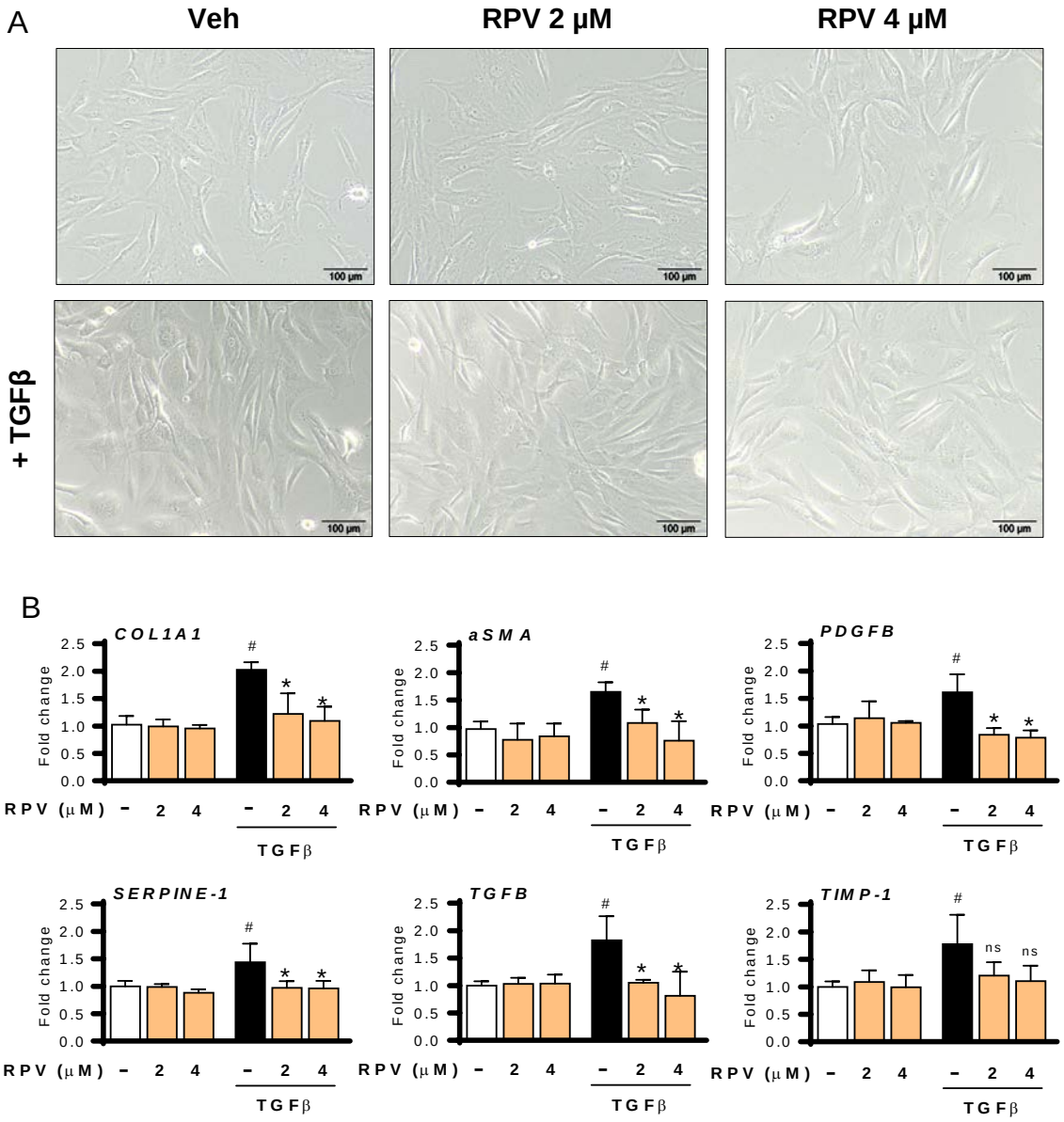

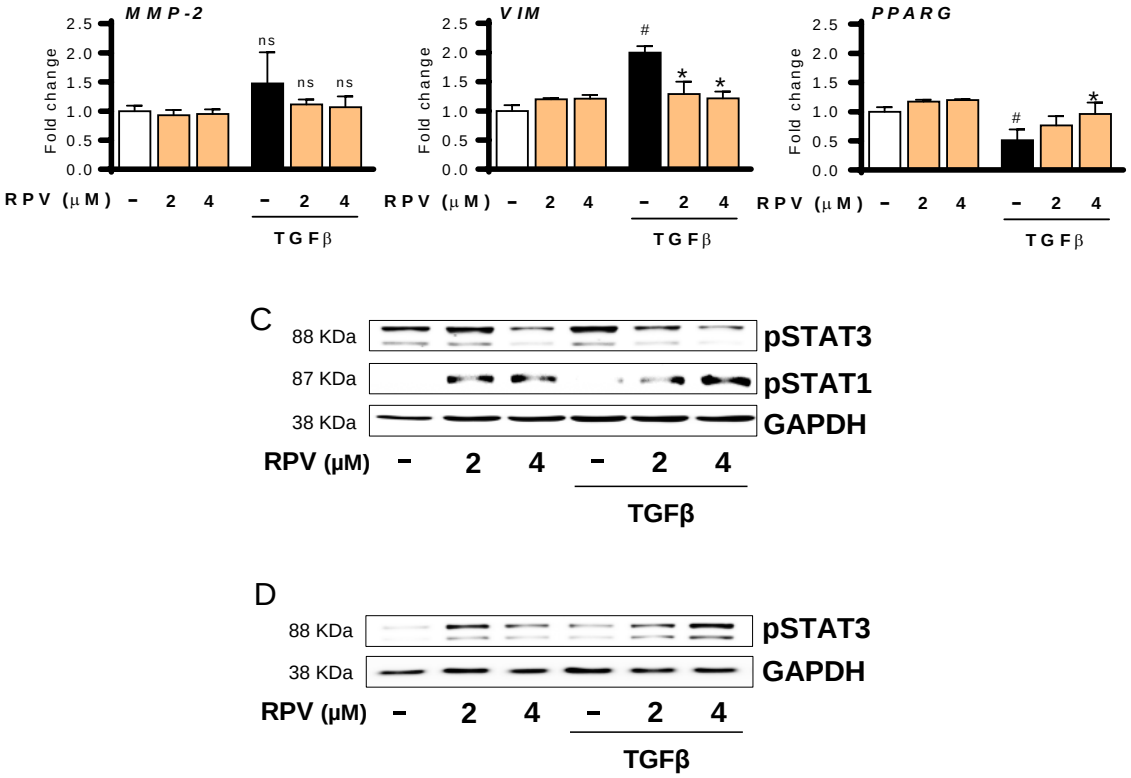

Figure IV.B.25. RPV inactivates hHSC. Representative optical microscopy pictures of primary hHSC after 72 h of treatment with RPV (2 and 4 μM) with or without co-stimulation with TGFβ (2.5 ng/mL) (n=3) (A). Gene expression of fibrogenic markers of HSC activation after 72 h of treatment. Gene expression was normalized versus the expression of *ACTB* gene (n=3) (B). Representative WB and quantifications of pSTAT3 and pSTAT1 in protein extracts from hHSC treated for 72 h (C) and pSTAT3 in protein extracts from Hep3B cells treated with conditioned medium from hHSC for 16 h (previously treated for 72 h) (n=3) (D). Protein expression was normalized versus GAPDH. Data are mean ± SD. #p<0.05 'Veh' vs. 'Veh + TGFβ' groups, Student's *t*-test. *p<0.05 'Veh' or 'Veh + TGFβ' vs. 'RPV' or 'RPV + TGFβ', respectively; one-way ANOVA multiple comparison test + Bonferroni post-test. Scale bar = 0.1 mm.

Chapter V: DISCUSSION

Combined antiretroviral regimens are the main responsible for the global demographic shift that HIV-infected population has experienced in the last twenty years [13,358]. In early 80s, when antiretroviral drugs were not available to face the virus, HIV-infected patients had really short life expectancy and high rates of morbidity [31,34,36]. Quick reaction of both scientific community and industry led to the development of therapeutic agents that were able to reduce the viral replication and the subsequent immunosuppression-related deaths [359,360]. However, many acute and chronic side effects were progressively described and attributed to these drugs and their clinical use was constantly re-evaluated, mainly based on their efficacy and safety [3,18].

Modern era of antiretroviral therapy began in the late 90s with the introduction of cART, whose success substantially decreased HIV-related morbidity and mortality. However, HIV-infected patients develop many age-related comorbidities, like cardiovascular or metabolic disorders, neurodegenerative diseases and even cancer, earlier than general population, mainly due to the virus infection itself, but also due to chronic antiviral treatment [361,362]. Therefore, current selection criteria are basically focused on the long-term safety of the different drugs and, thus, therapeutic management of HIV infection still constitutes a clinical challenge [1,3]. In this context, basic research focused on describing the underlying molecular mechanisms involved in acute and chronic side effects of cART is crucial to improve the clinical management of HIV population, as well as to facilitate the development of newer and safer antiviral drugs.

In this thesis two different studies have been carried out, both of them aiming to elucidate the underlying molecular pathways implicated in the liver-related alterations observed in clinics due to cART and, more specifically, to clarify whether the effects of these compounds could be enhanced by the presence of other risk factors contributing to liver toxicity.

In the first study, focused on the acute hepatotoxicity of NRTI, we demonstrate, for the first time, that clinically relevant concentrations of the purine analogues ABC and ddI [363], but not of other NRTI, inhibit O_2 consumption and interfere with CI and CIII activity in the ETC. These effects are concentration-dependent and unconnected to the classic mitochondrial toxicity described following prolonged treatment with NRTI, which involves pol-γ inhibition and mitochondrial DNA depletion [364]. This inhibitory action is accompanied by an immediate and

significant undermining of mitochondrial function, expressed by augmented production of ROS and reduction of $\Delta\Psi_m$ and intracellular ATP levels, which does not compromise cell survival, as these parameters return to basal values after 24 h treatment. However, the discrepancies observed between the effects of ABC and ddI on various parameters of mitochondrial dysfunction create a complex picture. In particular, the fact that the effects of ddI on ETC complexes appear earlier and are more pronounced than those of ABC suggests differences between each compound in their capacity to interact with mitochondria. It should be noted that, despite such differences, the ultimate consequences for hepatic cells are similar with either NRTI, as shown by the fact that basic parameters of cellular functioning (intracellular ATP levels, viability, etc) were equally affected.

Purine analogues have previously been reported to induce adverse hepatic events, and their use is accompanied by severe increases in liver enzyme concentrations in up to 6% of subjects, which, with the exception of d4T, makes these compounds the most hepatotoxic NRTI [365]. ABC is one of the most widely used NRTI, and it has a record of producing immune-related and non-concentration-dependent hypersensitivity reactions that affect the liver [366,367]. The use of ddI is no longer recommended, mainly because it has been associated with the development of severe hepatotoxicity involving mitochondrial damage (characterized by lactic acidosis and steatosis), portal hypertension and nodular regenerative hyperplasia [368–370]. Several clinical cases of DILI by ABC and ddI in the absence of hypersensitivity and pol-γ interference have also been reported. The causes of this injury are still unknown [371,372], but the NRTI-related damage rate seems to increase when these compounds are used in combination with potentially hepatotoxic drugs [373]. One such example is APAP, one of the most hepatotoxic drugs when administered in overdose. Clinical evidence indicates that plasma concentrations following APAP overdosing usually range between 1 and 2 mM [374,375]. However, *in vitro* studies have generally been conducted in the 5–10 mM range (or at even higher doses), as this is the concentration at which cytotoxicity first becomes evident in hepatoma cell lines, including Hep3B cells [376–380]. In keeping with these data, our experiments revealed mitochondrial dysfunction and cytotoxicity at 5 and 10 mM, whereas 1.25 mM APAP failed to induce significant changes in cellular viability and mitochondrial parameters such as superoxide production and $\Delta\Psi_m$. A reduction in cell number and substantial

alteration of the cell cycle were observed at all the concentrations evaluated, suggesting that the lowest of the four inhibits cellular proliferation, even though it does not compromise cell survival. However, co-incubation of ABC or ddI (10 µM) with 1.25 mM APAP significantly exacerbated the deleterious effects of either treatment on mitochondrial function (reduced $\Delta\Psi_m$ and increased mitochondrial superoxide production), cell number and cellular viability. This finding implies that purine analogues increase the risk of APAP-induced hepatotoxicity at concentrations below the established toxicity threshold. Although not detrimental to cellular survival *per se*, the acute mitochondrial interference produced by purine analogues may increase the vulnerability of hepatic cells to other physiological and/or pharmacological insults, making otherwise innocuous stimuli potentially harmful. However, no changes were observed in mitochondrial function or cell number when ABC or ddI was co-administered with sub-toxic concentrations of other hepatotoxic compounds, such as RIT, NPV and ethanol. This result suggests that only drugs which directly affect mitochondria are liable to have their hepatotoxicity influenced by purine analogues.

APAP-induced damage is related to the production of a toxic metabolite, NAPQI, by the CYP system [381]. Thus, the presence of an active CYP system in Hep3B cells makes them a reliable *in vitro* model for studying drug-induced hepatotoxicity. This finding was confirmed by our experiments with HepaRG cells and human liver tissue, which suggest that primary human hepatocytes are more susceptible to this toxicity [382].

Considering the well-established role of GSH in counteracting APAP-induced liver injury, we hypothesised that NRTI-induced alterations in GSH levels and metabolism were an underlying mechanism of the synergetic effects observed in our experiments. Following 24 h exposure to APAP, alone or in combination with purine analogues, no significant reduction in GSH levels was observed in hepatocytes. However, following 48 h of treatment, there was a significant depletion of GSH in cells with low levels of GSH but not in those with high levels. These results, together with the increased ROS production we observed (probably a consequence of the inhibition of CI and CIII), demonstrate that ABC and ddI alter the redox status of hepatic cells and increase susceptibility to APAP-induced liver injury. The positive correlation observed between GSH depletion and the reduction of cell viability emphasizes the importance of the former in the

deleterious effects produced by these drug combinations. A decrease in GSH has previously been reported in patients taking d4T [383], and it is important to note that the HIV infection itself has been shown to provoke GSH depletion [384]. In this context, it is tempting to speculate that the aforementioned effects of ABC/ddI + APAP are more pronounced in HIV patients.

In conclusion, this study demonstrates that clinical concentrations of ABC and ddI, but not of other NRTI, directly undermine mitochondrial function in hepatocytes, though this inhibition is not intense or prolonged enough to compromise cell survival. However, liver injury is clearly present when either of these purine analogues is administered in combination with sub-toxic concentrations of APAP, but not when combined with other hepatotoxic stimuli in which mitochondrial dysfunction plays a lesser role. Our findings are of relevance given the frequent use of APAP by HIV-infected patients taking NRTI, and they call for caution regarding the use of these antiretrovirals in combination with other potentially hepatotoxic stimuli capable of interfering with the mitochondria.

In our second study, focused on the implication of several NNRTI in the progression of chronic liver disease, we described the potential hepatoprotective effect of two compounds, EFV and RPV, in different mouse models of chronic liver disease. These previously unreported effects were first observed in an animal model of NAFLD, demonstrating that these two compounds exert a clear anti-lipogenic, anti-inflammatory and anti-fibrogenic effect in damaged murine livers.

Despite both EFV and RPV correspond to the same therapeutic family (NNRTI), we observed that they use different hepatoprotective mechanisms. It is well known that during NAFLD progression, an altered interplay between adipose tissue and liver triggers lipotoxicity in hepatocytes and leads to parenchymal inflammation and increased lipid accumulation (200,205). In this line, ongoing studies in our group analysing the effects induced by EFV in our NAFLD model, point to a complex and not completely understood crosstalk between hepatic and adipose tissue where autophagy, adipose tissue browning and metabolic dysregulation could play an important role. On its hand, RPV-induced actions clearly pointed to a direct beneficial mechanism in injured livers. Moreover, RPV showed that it is not only able to decrease severe liver inflammation and fibrosis

progression induced by overnutrition (HFD) and by CCl_4, but also it can decrease hepatic fibrosis and inflammation when administered after generation and consolidation of fibrosis. The mechanistic study of this effect, performed both *in vivo* and *in vitro*, revealed an interesting and selective pro-apoptotic effect induced by RPV in activated HSC through STAT1 activation. Importantly, RPV-induced apoptosis does not affect hepatocytes, in accordance with previous studies [385–387]. Furthermore, we described for the first time an interesting interplay between HSC and hepatocytes *via* JAK-STAT signaling which leads to liver regeneration: RPV treatment also increased the number of proliferative hepatocytes, thereby restoring the parenchymal homeostasis through the activation of STAT3 signaling in these cells. Nevertheless, this activation was secondary and dependent on the RPV-mediated apoptosis induction on HSC through STAT1.

NAFLD is the most common chronic liver disease worldwide and it is considered the hepatic manifestation of the metabolic syndrome. It affects up to 30% of global adult population, and more than 75% of those individuals are obese and diabetic; this prevalence is rapidly increasing in association with unhealthy lifestyle habits and metabolic diseases [192,193]. Nowadays, it is the major cause of liver-related morbidity and mortality and eventually progresses to HCC [194,195]. In the last years, numerous attempts of treating liver diseases have yielded promising results but they were not successful in the clinics due to several reasons, such as the lack of specificity of their formulations or the difficulty of directly targeting pathogenic mechanisms of hepatic fibrosis [388,389].

Both EFV and RPV are drugs available in clinics for many years (since 1995 and 2011, respectively), whose side effects and safety profile in chronic treatments are well known. Over the time, acute treatment with EFV has been correlated with few cases of liver failure [91,390,391]. Additionally, *in vitro* experiments performed by our group and others have shown that acute treatment with EFV provokes deleterious effects in hepatocytes involving mitochondrial dysfunction, cell survival-promoting autophagy, bioenergetic and endoplasmic reticulum stress and intracellular lipid accumulation [96–101]. Liver-related EFV toxicity in clinics appears shortly after treatment instauration and disappears in several days or weeks. However, it is crucial to bear in mind that, despite very infrequent, this toxicity can be really severe and lead to fatal liver failure [103,104,392,393]. Despite

that, EFV has been extensively used in HIV therapy worldwide and its use in long-term therapies is considered safe to the liver, but close clinical monitoring is mandatory to assess the liver functionality over the time [103,105,392]. With regard to RPV, some mild-to-moderate abnormalities have been considered as RPV-related hepatic adverse events, including increased AST, ALT, LDL cholesterol, lipase, bilirubin and triglyceride levels. However, all those minor alterations rapidly went back to normal levels and remained stable over time, being considered not clinically relevant in the vast majority of cases [106].

Overall, clinical evidence supports the use of EFV and RPV in lifelong treatments as they are considered safe drugs for the liver. However, their particular contribution to liver disease progression and their actions on different cell subpopulations under different pathological conditions were uncertain. One of the main reasons that could have masked the protective effect that we describe here is the fact that these compounds are always administered in combined therapies and, thus, their particular contribution to either beneficial or deleterious effects in patients is extremely difficult to identify in clinical practice. This thesis is the first study that has yielded some light in describing the individual potential of these drugs to modulate the natural history of chronic liver disease.

In this context, it is tempting to speculate that our results could be important for the management of patients with liver diseases. Provided they are reproduced in further *in vivo* studies (with animals and humans), our data suggest that the clinical utilization of EFV, and especially RPV, could be recommended for all those HIV-infected patients with special susceptibility to liver disease (e.g., individuals with severe metabolic syndrome or HCV-HIV co-infected patients).

After revising clinical and basic evidence, we decided to focus in RPV as a more promising option for the treatment of chronic liver diseases in base to numerous reasons. First, it has been reported that RPV improves lipid profiles after switching from EFV-containing therapies in dyslipemic HIV patients [112,113,350], which would be in line with its more pronounced actions decreasing lipid levels and liver inflammation in our *in vivo* studies. Second, plasmatic levels of RPV, and its subsequent clinical effectivity, remain unaltered even in those patients whose hepatic function is dramatically altered (for instance, those in which HIV-HCV co-infection and liver cirrhosis coexist), which is a really useful feature to be considered in clinical practice [110]. Third, attending to our previous publications in

this field, we have described that EFV, but not RPV, exert an acute cytotoxic effect in hepatocytes *in vitro* [60]. Taking all these data together, we thought that it made more sense to further study the RPV-related hepatic effects since these results could achieve more clinical relevance.

Although the main core of this study has been focused on the progression of hepatic inflammation and fibrosis, it is also important to highlight the intense anti-adipogenic capacity that RPV displayed in our animal model. Although we did not deeply characterize the molecular mechanisms involved in this effect, we consider these actions extremely interesting in the context of NAFLD pandemic and they will be necessarily studied by ourselves in the future.

JAK-STAT signaling has been largely postulated as a good target for the treatment of liver diseases [394]: selective STAT1 activation in non-parenchymal cells would slow down progression of liver damage driven by activated HSC and by local or recruited immune cells, while specific STAT3 activation in parenchymal cells would lead to liver regeneration. However, molecules able to modulate this balance and ameliorate liver fibrosis have not been developed or identified up to now.

In this study we describe for the first time a hepatoprotective molecule able to induce a differential effect in hepatocytes and HSC *via* JAK-STAT signaling, leading to liver regeneration. RPV-mediated hepatoprotection primarily comes from its ability to directly induce apoptosis in HSC through STAT1 activation. Secondary to this effect, we also observed an intense proliferative response in liver parenchyma, driven by the restoration of STAT3 signaling. Given this combined effect, we firmly state that RPV-mediated effects in the liver constitute a true regenerative response, and not only a mere consequence of the discontinuation of injury progression produced by direct HSC inactivation (which would also be an interesting anyway), and thus, it may have potential as a novel therapeutic target.

RPV-induced actions show certain unexpected and interesting characteristics that make it a unique case and may support its clinical application in liver diseases. Furthermore, RPV differentially regulates JAK-STAT signaling pathways in both parenchymal and non-parenchymal cells, finally triggering an effective regenerative response. Although the extraordinary regeneration capacity of the healthy liver has been widely demonstrated, this ability extremely

decreases when this organ is chronically damaged. Hepatocytes become increasingly senescent and unable to divide, and HSC, liver macrophages and immune cells are activated to a pro-inflammatory and pro-fibrogenic status. Surprisingly, RPV demonstrated that it is able to activate an efficient regeneration even in a damaged liver, which represents a considerable clinical breakthrough. Considering the short list of drugs effective in improving liver function in this pathogenic context, the therapeutic potential of this study becomes evident [395–399].

STAT1 signaling has been proven fundamental in the hepatoprotective actions of RPV, suggesting that it is a novel and interesting target that should be further investigated for therapy development, not only for liver fibrosis, but also for other hyper-proliferative diseases, including different fibrotic disorders (not only in the liver) and even cancer. Specifically, different high-throughput approaches, like *in silico* studies of quantitative structure–activity relationship or *in vitro* studies of cell-based phenotypic screens, should be applied in order to find molecules able to selectively activate this transcription factor in specific cell types. Furthermore, in order to enhance the selectivity of these molecules (STAT1 is a ubiquitous protein present in many different cells), nanotechnology could be employed [388]. Through specific nano-formulations with different organic, inorganic, quantum dot or liposome-based formulations we could selectively target those hyper-proliferating cells mainly involved in the pathology we would like to treat with RPV. In addition, it is well described that alternative splicing of STAT1 produces two different isoforms: α, known as the active form, and β, largely shown to act as a dominant-negative factor. Most studies have attributed STAT1-mediated regulation of cell growth and death to the STAT1-α variant, whose action always involves the downstream transcriptional activation of the tumoral suppressor protein p53 [400–402]. However, recent studies have shown that STAT1-β is not only a mere regulator and, once activated, it is able to induce cell death through a mechanism that is independent of the nuclear function of p53 [403,404]. In our experiments in LX-2 cells, pSTAT1 WB images show a clear concentration-dependent activation in response to RPV treatment. However, comprehensive analysis of these representative pictures reveals that this activation is conducted mainly through the activation of the β subunit (lower band), while the α subunit (upper band) expression does not significantly change in response to the

treatment. In addition, we studied both gene and protein expression of the activated form of p53 and we did not find significant differences in response to RPV (data not shown), which reinforces our hypothesis that RPV-related hepatoprotection is mainly mediated through the specific activation of the STAT1-β transcript variant.

STAT3 is largely over-expressed by tumor liver cells and, consequently, it has been deeply studied as a key target in therapy against HCC [240,249,261,271,272]. In particular, sorafenib, whose capacity to selectively modulate STAT3 signaling in different hepatic cells has been widely described, is currently used as a first-line standard systemic agent for advanced HCC treatment. Its effectivity combating tumor progression has been largely demonstrated in two large-scale phase III clinical trials (ClinicalTrial.gov identifiers: NCT11849 and NCT100554) [405,406]. It primarily acts as a multi-kinase inhibitor that blocks cellular signaling within tumor cells (mainly PDGF, vascular endothelial-growth factor and Raf serine/threonine kinase), leading to anti-proliferative, pro-apoptotic and anti-angiogenic effects [407–409]. Complementary to these anti-tumoral effects, sorafenib has been also reported to decrease liver fibrosis progression and to increase parenchymal regeneration. This dual effect seems to be similar to that described with RVP, but sorafenib-mediated actions are mediated by the direct inactivation of STAT3 signaling in HSC [410–412], as well as by its activation in hepatocytes at the expense of the IL6 released by local KC [413]. Additional mechanisms of hepatoprotection have been attributed to this compound, such as decrease in the epithelial-mesenchymal transition of damaged hepatocytes through the inhibition of TGFβ1 signaling [413], inhibition of the NLRP3 inflammasome activation by directly blocking Caspase 1 expression [414], or direct activation of autophagic cell death and apoptosis in HSC through JNK and Akt signaling pathways [412,415]. However, the utilization of sorafenib as an antifibrotic agent still has several important limitations mainly related with its toxicity. In fact, it is a really toxic compound whose narrow therapeutic window limits its clinical use and efficacy. To overcome this limitation several studies are attempting to obtain nano-formulations of this compound to increase its selectivity and reduce the doses, but they have not been able to translate these strategies to the clinic so far [416].

At this point, it is tempting to compare the profile of protective actions exerted by sorafenib and by RPV. Sorafenib seems to reduce the proliferation of HSC by

decreasing STAT3 signaling [410], whereas RPV directly activates STAT1 in this same cell type, triggering a similar net response. Regarding hepatocytes, it has been described that sorafenib can indirectly increase STAT3 signaling in these cells due to the release of IL6 from Kupffer cells [408], while the RPV-induced over-expression of STAT3 directly depends on the apoptotic death induced in HSC. Apart from this mechanistic complementarity, also an interesting pharmacodynamic aspect could be relevant: given the narrow therapeutic window of sorafenib, its combination with RPV, with a wider therapeutic range, would allow clinicians to reduce its doses while maintaining (or even improving) the final therapeutic results and reducing its inherent toxicity. Given these previous observations, it would be really interesting to carry out *in vitro* and *in vivo* studies aimed to determine the therapeutic effect of these drugs in the liver when administered in combination.

On the other hand, we have not yet performed further experiments to identify the molecule or combination of molecules present in the secretome of RPV-induced apoptotic HSC that are responsible for this specific activation of STAT3 in hepatocytes, but it would be an extremely interesting aim for future studies. However, according to literature, we cannot rule out the involvement of IL6 released by apoptotic HSC in these effects.

An important point that must be clarified before firmly proposing RPV as a therapeutic option for chronic liver diseases is whether RPV-induced over-expression of STAT3 in hepatocytes could induce some kind of pro-carcinogenic transformation in these cells, given that this hyper-expression of STAT3 is a typical feature of most types of cancer cells, included those in HCC [407,408,411,414,415]. The results obtained in our *in vivo* models demonstrate that RPV-induced STAT3 activation is always enhanced if compared with steatotic or fibrotic mice without antiretroviral treatment (all those fed with HFD or injected with CCl_4, respectively). However, STAT3 activation in RPV-treated mice groups does never significantly differ from that found in healthy mice (control groups). For this reason, more than a real over-expression, RPV is actually restoring physiological levels of STAT3. This effect clearly points to an enhanced regenerative response in injured hepatocytes mediated by RPV that would never involve a hyper-proliferative response capable of generating neoplastic disorders in the liver.

Many other cell subsets implicated in the progression of chronic liver disease have been largely studied and targeted with potential drugs for therapy development. Specifically, C-C chemokine receptors type 2 and 5 (CCR2 and CCR5) antagonists play a central role as coordinators of the immune cell subset infiltration during the progression of chronic liver disease [417,418]. Plasmatic levels of these chemokines directly correlate with the severity of liver disease [114,419–421] and, thus, the therapeutic inhibition of this route represents a promising strategy for controlling inflammatory liver diseases, particularly NASH and fibrosis [389,420,422,423]. In this line, the dual CCR2/CCR5 inhibitor cenicriviroc (CVC) has been deeply evaluated in different experimental models of chronic liver disease, from NAFLD and fibrosis [396,397,421] to alcohol-related chronic liver damage [395]. Surprisingly, in all these studies CVC was able to exert protective properties by decreasing the infiltration of monocytes and immune cells into the damaged liver, and by significantly inactivating HSC. Consequently, therapeutic use of CVC against NAFLD and fibrosis is currently being tested in several ongoing clinical trials (ClinicalTrial.gov identifiers NCT03059446, NCT02217475, NCT03517540 and NCT03028740) [424,425]. In addition, Maraviroc (MVC), another CCR5 inhibitor initially approved for HIV therapy, has been studied in mouse models of NAFLD and showed a clear protecting role by ameliorating the plasmatic lipid profile and by decreasing steatosis progression [419].

In light of this evidence, combination of either compounds with RPV may be clinically relevant. Especially, combined administration of MVC and RPV in the treatment of HIV infection could have benefits in all those patients with high risk of liver diseases. Similarly, combination of CVC and RPV constitutes an interesting therapeutic option, as both drugs have the ability to decrease lipid infiltration in animal models of NAFLD. Moreover, RPV also induced a general decrease in the macrophage content in treated animals, as well as a decreased MPO enzymatic activity, which correlates with a decreased neutrophil infiltration, an effect also attributed to CVC. In summary, we firmly propose the convenience of carry out further studies employing combined therapies in liver diseases.

The liver sinusoid, formed by a specialized endothelium composed of LSEC, plays a key role in liver homeostasis. Damage and dysregulation at this level is a common feature in the pathogenesis of both acute and chronic hepatic disorders and, consequently, their therapeutic modulation has been deeply evaluated

during the last years [159–161]. Specifically, extensive studies of the role of statins in the hepatic vascular biology have demonstrated that, independently of their lipid lowering potential, these drugs, and especially simvastatin, improve endothelial function of LSEC [399,426,427], decrease portal pressure [428,429] and limit the fibrotic progression upon liver injury due to an interesting interplay between LSEC and HSC [430–432]. Additionally, it has been recently described how simvastatin effectively ameliorates sinusoidal function even in animal models of acute-on-chronic liver failure [398]. Considering this, therapeutic combination of simvastatin and RPV in different models of acute and chronic liver injury should be the focus of increasing attention. Although their mechanisms largely differ, both are molecules widely used in clinics for different purposes, and so, their pharmacokinetics, toxicity, interactions and long-term security are well known. Therefore, obtained observations could be really beneficial and easily translated into the clinics.

The results presented in this thesis firmly support that RPV could be an interesting therapeutic option to control the progression of fibrotic disorders in the liver and, more importantly, they contribute to identify novel pharmacological targets, using JAK-STAT1 and JAK-STAT3 signaling pathways as a starting point. However, several limitations in both our *in vivo* and *in vitro* studies should be discussed and considered. In the former, we cannot ignore the difficulty of expanding scientific results from animal models to humans. In this line, an ideal animal model of liver disease must be able to reproduce the pathological pattern of liver injury as well as the systemic metabolic and immune responses that humans develop. However, none of the available models have fully reproduced all these vital features up to now. The main reasons are the inherent complexity of the multiple etiologies involved in disease progression, and the long time required for its development [229,230]. In our case, we chose a nutritional model of NALFD that was carried out for 12 weeks. According to the literature, this is time enough to develop hepatic steatosis and inflammation in mice [232,234]. However, this model worked beyond our expectations and we were able to observe even a clear incipient fibrotic response with evident collagen deposition. Regarding our fibrosis models, we decided to carry them out for 4 and 6 weeks because we wanted to induce a clear fibrosis but we were not interested in more severe stages like cirrhosis, which require longer experimental procedures. Evidently, in

both cases, if we had prolonged these protocols we would have obtained more severe manifestations of the disease. However, we consider that the duration of our protocols was enough to obtain clinically relevant results.

In addition, we decided to use only female mice in all our models, which theoretically could constitute a clear bias in the study. However, we considered that, practically, female mice display a less aggressive behavior than males, avoiding hierarchical fights among animals that would increase their stress and complicate our chronic procedures, consequently increasing their variability. In this line, as we cannot yet affirm whether the effect of RPV could be conditioned by gender, we will approach this problem in the future by reproducing these studies in male mice.

Regarding drug dosage and administration, it is important to note that we calculated the daily doses by using an interspecies allometric scaling factor widely accepted and stablished by FDA [297,298]. Although we did not determine the plasmatic levels reached in our mice, considering the high metabolic rate of these rodents, the pharmacokinetics of RPV and the obtained results, we consider that the study was conducted in optimal or sub-optimal concentrations, if compared to humans. Using these doses, animals did not reach significant toxic levels and displayed a surprising and reproducible therapeutic effect. The dosage method we employed also differs from the methods generally employed in similar studies. We decided to perform an individualized oral administration to carefully control the exact amount of drug that each animal took instead of dissolving the drugs in drinking water. Finally, is it important to consider that our drugs were dissolved in pure DMSO prior administration. Chronic treatment with DMSO in animals has been classically associated with gastrointestinal and inflammatory disturbances [235,236,417]. However, studies about its specific toxicity in mice also demonstrated that daily administration of very small volumes, between 10 and 20 µL, could be totally safe [433–435]. In accordance to these studies, our drugs were dissolved in only 10 µL of DMSO and no oral or gastrointestinal lesions were found [433–435].

With regard to *in vitro* RPV concentrations (from 1 to 8 µM), it is important to state that, although the lower concentrations employed (1 to 4 µM) are clinically relevant, the highest concentration (8 µM) is clearly supra-therapeutic considering the doses administered and the plasmatic levels found in humans,. However, it was used as a routine treatment to clearly understand whether RPV-

induced alterations were concentration-dependent. Although 8 μM is a supra-therapeutic condition, this concentration was not toxic in the different hepatocyte cell lines we employed (Hep3B and HepG2), in line with previous studies that also used this range of concentrations [386,387]. Importantly, RPV treatment was restricted to clinical concentrations (just 2 and 4 μM) in key experiments of STAT1 silencing and hHSC primary cells. In addition, it is well described that RPV suffers an intense bioaccumulation in the liver and the intrahepatic concentration that it can reach is greater than those found in plasma [16,106,436,437]. For this reason, we justify the convenience of the doses employed in our *in vitro* study since they better correlate with those intrahepatic concentrations found in patients that are exposed to chronic therapeutic regimes.

Interestingly, there are still questions that must be answered if we want to describe the whole sequence of events leading to the hepatoprotective effects of RPV. In order to confirm that the hepatic effects of RPV are primarily mediated by STAT1 activation in HSC, further proof-of-concept experiments with STAT1-knock-out mice should be necessarily performed. In this sense, it would be fundamental to develop mice strains in which STAT1 silencing is constrained to HSC. In addition, also STAT3-knock-in models in hepatocytes would be helpful to assure whether the indirect parenchymal response to RPV would be strong enough to induce regeneration without producing some ulterior pro-carcinogenic growth in the liver. Moreover, a deeper evaluation of JAK-STAT signaling, taking into account the activity of different intrinsic regulators, like SOCS and PIAS proteins, must be done.

On the other hand, it has been reported that RPV is a Pregnane-X receptor (PXR) agonist [386] and, consequently, we cannot rule out the involvement of this transcription factor in RPV-mediated hepatic effects. In fact, it has been described that PXR activation decreases hepatic lipogenesis and increases fatty acid oxidation [438–440]. Furthermore, its activity is mainly modulated by inflammatory cytokines from monocytes, macrophages and stromal cells within the liver [441], and triggering of PXR inhibits the activation and proliferation of HSC [442]. Additionally, PXR is involved in liver regeneration *via* the activation of different signaling pathways [443] and the secretion of IL6 by different cells [442]. Considering all these data together with our experimental results, we firmly believe that, theoretically, PXR could perfectly suit as the original orchestrator of all effects

induced by RPV in the liver, including all those related with hepatic fat accumulation. Thus, future studies in our group will be certainly aimed to decipher the implication of this receptor in the clinical effect displayed by RPV.

In addition, in order to study the therapeutic potential of RPV in response to different deleterious stimuli and/or different clinical situations, many other animal models, like bile-duct ligation, partial hepatectomy, liver ischemia-reperfusion, alcohol-induced liver disease or acute-on-chronic liver failure (among others) must be performed.

Furthermore, extensive analysis must be done in other different hepatic cell subpopulations directly involved in the progression and regression of liver damage. At this point, we are certainly convinced that the effect of RPV is not limited to HSC and hepatocytes. Thus, further studies should focus in the role of liver macrophages (both KC and recruited macrophages), immune cells, LSEC and dendritic cells, to better understand how RPV mediates its effects. It would also help us to understand how different cell subtypes paracrinely communicate to each other within the liver in pathogenic circumstances, and which kind of interactions they establish with diverse immune cells through the whole organism. Additionally, we firmly believe that RPV could also be interacting with different subsets of liver stem cells to enhance the hepatic regenerative capacity and its defense potential, as well as it could be stimulating bone marrow hematopoietic stem cells to shape effective immune responses aimed to restore homeostasis in the liver.

As a final take-home message, in this study it has been described for the first time an unexpected off-target effect of RPV which points to a protective role in the liver through anti-adipogenic, anti-inflammatory and anti-fibrogenic activity. This effect results of especial relevance since it is partially supported by few clinical studies and it seems to be independent of the etiology of chronic liver injury. In our experiments, RPV effectively decreased the progression of steatosis as well as the inflammatory and fibrogenic responses. Surprisingly, it also decreased the progression of chronic injury and improved liver function once administered as a treatment in a fibrotic liver. In all models, this effect is clearly mediated by a direct activation of STAT1 in non-parenchimal cells and a subsequent apoptosis induction in HSC. These apoptotic cells promoted an

enhanced proliferation of hepatocytes, which seems to be mediated by an increased activation of STAT3 signaling.

Under the paradigm of the translationality, despite the inherent limitations of this study, and considering that the protective role of RPV was reproduced in human primary HSC, we firmly defend the clinical relevance of our data and we consider they are strong enough to further explore whether this new indication of RPV could be definitely expanded to the clinics, from the bench to the bed side.

Chapter VI: CONCLUSIONS

1. Acute treatment of hepatocytes with clinical concentrations of abacavir and didanosine, but not of other nucleoside-analogue reverse transcriptase inhibitors, directly undermine their mitochondrial function, though this effect is not intense or prolonged enough to compromise cell survival.

2. Cytotoxicity in hepatocytes becomes evident when they are treated with either abacavir or didanosine, at clinical doses, in combination with subtoxic concentrations of acetaminophen, but not when combined with other hepatotoxic stimuli in which mitochondrial impairment is not directly involved.

3. Chronic administration of the non-nucleoside-analogue reverse transcriptase inhibitors efavirenz and rilpivirine in mice induces an anti-adipogenic, an-inflammatory and anti-fibrotic response that reduces non-alcoholic fatty liver disease progression. The effect induced by rilpivirine is significantly more intense than that showed by efavirenz.

4. Chronic administration of rilpivirine reduces the progression of liver fibrosis in mice. Additionally, it is also able to revert liver damage once fibrosis is consolidated even when the toxic insult is still present. However, rilpivirine does not accelerate physiologic hepatic recovery once the insult disappears.

5. The anti-inflammatory effect of rilpivirine is essentially mediated by NF-κB and NLRP3 inflammasome inactivation.

6. Regardless the aetiology of liver damage, JAK-STAT1 and JAK-STAT3 signaling pathways are involved in the hepatoprotection induced by rilpivirine.

7. Rilpivirine selectively induces apoptosis in hepatic stellate cells by STAT1 activation. At the same time, it increases hepatocyte proliferation, and subsequent liver regeneration, by selective STAT3 activation in these parenchymal cells.

8. This differential response induced by rilpivirine in both cell populations originally depends on the STAT1 activation in hepatic stellate cells.

BIBLIOGRAPHY

1 Barré-Sinoussi F, Ross AL, Delfraissy JF. Past, present and future: 30 years of HIV research. *Nat Rev Microbiol* 2013; **11**: 877–883.

2 Deeks SG, Overbaugh J, Phillips A, Buchbinder S. HIV infection. *Nat Rev Dis Prim* 2015; **1**: 15035.

3 Maartens G, Celum C, Lewin SR. HIV infection: Epidemiology, pathogenesis, treatment, and prevention. *Lancet* 2014; **384**: 258–271.

4 Naghavi M, Wang H, Lozano R, Davis A, Liang X, Zhou M *et al.* Global, regional, and national age-sex specific all-cause and cause-specific mortality for 240 causes of death, 1990-2013: A systematic analysis for the Global Burden of Disease Study 2013. *Lancet* 2015; **385**: 117–171.

5 Yoshimura K. Current status of HIV/AIDS in the ART era. *J Infect Chemother* 2017; **23**: 12–16.

6 Liu Y, Liu H, Kim BO, Gattone VH, Li J, Nath A *et al.* CD4-Independent Infection of Astrocytes by Human Immunodeficiency Virus Type 1 : Requirement for the Human Mannose Receptor. *J Virol* 2004; **78**: 4120–4133.

7 Chen P, Chen BK, Mosoian A, Hays T, Ross MJ, Klotman PE *et al.* Virological Synapses Allow HIV-1 Uptake and Gene Expression in Renal Tubular Epithelial Cells. *J Am Soc Nephrol* 2011; **22**: 496–507.

8 Laskey SB, Siliciano RF. A mechanistic theory to explain the efficacy of antiretroviral therapy. *Nat Rev Microbiol* 2014; **12**: 772–780.

9 Freed EO. HIV-1 assembly, release and maturation. *Nat Rev Microbiol* 2015; **13**: 484–496.

10 Moir S, Chun T-W, Fauci AS. Pathogenic Mechanisms of HIV Disease. *Annu Rev Pathol Mech Dis* 2011; **6**: 223–248.

11 Stevenson M. HIV-1 pathogenesis. *Nat Med* 2003; **9**: 853–860.

12 Gurunathan S, Habib R El, Baglyos L, Meric C, Plotkin S, Dodet B *et al.* Use of predictive markers of HIV disease progression in vaccine trials. *Vaccine* 2009; **27**: 1997–2015.

13 Deeks SG, Overbaugh J, Phillips A, Buchbinder S. HIV infection. *Nat Rev Dis Prim* 2015; **1**: 15035.

14 Broder S. Twenty-five years of translational medicine in antiretroviral therapy: Promises to keep. *Sci Transl Med* 2010; **2**(39): 39ps33.

15 Larder B a, Darby G, Richman DD. Reduced Sensitivity. *Science* 1989; **243**: 1731–1734.

16 Thompson MA. Antiretroviral Treatment of Adult HIV Infection. *Jama* 2012; **308**:

387–402.

17 Wei X, Ghosh SK, Taylor ME, Johnson VA, Emini EA, Deutsch P *et al.* Viral dynamics in human immunodeficiency virus type 1 infection. *Nature* 1995; **373**: 117–122.

18 Arts EJ, Hazuda DJ. HIV-1 antiretroviral drug therapy. *Cold Spring Harb Perspect Med* 2012; **2**: a007161.

19 Young FE. The role of the FDA in the effort against AIDS. *Public Health Rep*; **103**: 242–245.

20 Hart GJ, Orr DC, Penn CR, Figueiredo HT, Gray NM, Boehme RE *et al.* Effects of 2'-deoxy-3'-thiacytidine 5'-triphosphate on human immunodeficiency virus reverse transcriptase and mammalian DNA polymerases alpha, beta, and gamma. *Antimicrob Agents Chemother* 1992; **36**: 1688–1694.

21 De Clercq E. The Nucleoside Reverse Transcriptase Inhibitors, Nonnucleoside Reverse Transcriptase Inhibitors, and Protease Inhibitors in the Treatment of HIV Infections. *AIDS* 2013; **67**: 317–358.

22 Nurutdinova D, Overton ET. A review of nucleoside reverse transcriptase inhibitor use to prevent perinatal transmission of HIV. *Expert Opin Drug Saf* 2009; **8**: 683–694.

23 Apostolova N, Blas-García A, Esplugues JV. Mitochondrial interference by anti-HIV drugs: mechanisms beyond Pol-γ inhibition. *Trends Pharmacol Sci* 2011; **32**: 715–725.

24 Apostolova N, Blas-García A, Esplugues JV. Mitochondrial toxicity in HAART: an overview of in vitro evidence. *Curr Pharm Des* 2011; **17**: 2130–2144.

25 Usach I, Melis V, Peris J-E. Non-nucleoside reverse transcriptase inhibitors: a review on pharmacokinetics, pharmacodynamics, safety and tolerability. *J Int AIDS Soc* 2013; **16**: 18567.

26 Blas-Garcia A, Esplugues JV, Apostolova N. Twenty years of HIV-1 non-nucleoside reverse transcriptase inhibitors: time to reevaluate their toxicity. *Curr Med Chem* 2011; **18**: 2186–2195.

27 Usach I, Melis V, Peris J-E. Non-nucleoside reverse transcriptase inhibitors: a review on pharmacokinetics, pharmacodynamics, safety and tolerability. *J Int AIDS Soc* 2013; **16**: 1–14.

28 Commissioner of the HIV/AIDS Treatment: Antiretroviral drugs used in the treatment of HIV infection.
https://www.fda.gov/ForPatients/Illness/HIVAIDS/Treatment/ucm118915.htm
(accessed 14 Aug 2018).

29 Kanters S, Vitoria M, Doherty M, Socias ME, Ford N, Forrest JI *et al.* Comparative efficacy and safety of first-line antiretroviral therapy for the treatment of HIV infection: a systematic review and network meta-analysis. *Lancet HIV* 2016; **3**: e510–e520.

30 Badowski ME, Pérez SE, Biagi M, Littler JA. New Antiretroviral Treatment for HIV. *Infect Dis Ther* 2016; **5**: 329–352.

31 De Clercq E. Antiretroviral drugs. *Curr Opin Pharmacol* 2010; **10**: 507–515.

32 Kanters S, Vitoria M, Doherty M, Socias ME, Ford N, Forrest JI *et al.* Comparative efficacy and safety of first-line antiretroviral therapy for the treatment of HIV infection: a systematic review and network meta-analysis. *Lancet HIV* 2016; **3**: e510–e520.

33 De Clercq E. Anti-HIV drugs: 25 compounds approved within 25 years after the discovery of HIV. *Int J Antimicrob Agents* 2009; **33**: 307–320.

34 Yoshimura K. Current status of HIV/AIDS in the ART era. *J Infect Chemother* 2017; **23**: 12–16.

35 Badowski ME, Pérez SE, Biagi M, Littler JA. New Antiretroviral Treatment for HIV. *Infect Dis Ther* 2016; **5**: 329–352.

36 Slim J, Saling CF. A Review of Management of Inflammation in the HIV Population. *Biomed Res Int* 2016; **2016**: 3420638.

37 Domingo P, Lozano F. Manejo de la toxicidad por fármacos antirretrovirales. *Enferm Infecc Microbiol Clin* 2011; **29**: 535–544.

38 Margolis AM, Heverling H, Pham PA, Stolbach A. A Review of the Toxicity of HIV Medications. *J Med Toxicol* 2014; **10**: 26–39.

39 Kalapila AG, Marrazzo J. Antiretroviral Therapy for Prevention of Human Immunodeficiency Virus Infection. *Med Clin North Am* 2016; **100**: 927–950.

40 Blas-García A, Apostolova N, Ballesteros D, Monleón D, Morales JM, Rocha M *et al.* Inhibition of mitochondrial function by efavirenz increases lipid content in hepatic cells. *Hepatology* 2010; **52**: 115–125.

41 Fernandez-Montero JV, Eugenia E, Barreiro P, Labarga P, Soriano V. Antiretroviral drug-related toxicities – clinical spectrum, prevention, and management. *Expert Opin Drug Saf* 2013; **12**: 697–707.

42 Domingo P, Lozano F. Manejo de la toxicidad por fármacos antirretrovirales. *Enferm Infecc Microbiol Clin* 2011; **29**: 535–544.

43 Rodríguez-Nóvoa S, Barreiro P, Jiménez-Nácher I, Soriano V. Overview of the pharmacogenetics of HIV therapy. *Pharmacogenomics J* 2006; **6**: 234–245.

44 What to Start. Adult and Adolescent ARV. AIDSinfo. https://aidsinfo.nih.gov/guidelines/html/1/adult-and-adolescent-arv/11/what-to-start--initial-combination-regimens-for-the-antiretroviral-naive-patient (accessed 16 Aug 2018).

45 Deeks SG, Overbaugh J, Phillips A, Buchbinder S. HIV infection. *Nat Rev Dis Prim* 2015; **1**: 15035.

46 Cihlar T, Fordyce M. Current status and prospects of HIV treatment. *Curr Opin Virol* 2016; **18**: 50–56.

47 Neukam K, Espinosa N, Collado A, Delgado-Fernández M, Jiménez-Aguilar P, Rivero-Juárez A *et al.* Hepatic safety of rilpivirine/emtricitabine/tenofovir disoproxil fumarate fixed-dose single-tablet regimen in HIV-infected patients with active hepatitis C virus infection: The hepatic study. *PLoS One* 2016; **11**: 3–4.

48 Puoti M, Moioli M, Travi G, Rossotti R. The Burden of Liver Disease in Human Immunodeficiency Virus-Infected Patients. *Semin Liver Dis* 2012; **32**: 103–113.

49 Calmy A, Hirschel B, Cooper DA, Carr A. A new era of antiretroviral drug toxicity. *Antivir Ther* 2009; **14**: 165–179.

50 Núñez M. Clinical syndromes and consequences of antiretroviral-related hepatotoxicity. *Hepatology* 2010; **52**: 1143–1155.

51 Jones M, Núñez M. Liver toxicity of antiretroviral drugs. *Semin Liver Dis* 2012; **32**: 167–176.

52 Medina-Caliz I, Robles-Diaz M, Garcia-Muñoz B, Stephens C, Ortega-Alonso A, Garcia-Cortes M *et al.* Definition and risk factors for chronicity following acute idiosyncratic drug-induced liver injury. *J Hepatol* 2016; **65**: 532–542.

53 Neukam K, Mira JA, Collado A, Rivero-Juárez A, Monje-Agudo P, Ruiz-Morales J *et al.* Liver Toxicity of Current Antiretroviral Regimens in HIV-Infected Patients with Chronic Viral Hepatitis in a Real-Life Setting: The HEPAVIR SEG-HEP Cohort. *PLoS One* 2016; **11**: e0148104.

54 Hernandez L V, Gilson I, Jacobson J, Affi A, Puetz TR, Dindzans VJ. Antiretroviral hepatotoxicity in human immunodeficiency virus-infected patients. *Aliment Pharmacol Ther* 2001; **15**: 1627–1632.

55 Sulkowski MS, Thomas DL, Mehta SH, Chaisson RE, Moore RD. Hepatotoxicity associated with nevirapine or efavirenz-containing antiretroviral therapy: role of hepatitis C and B infections. *Hepatology* 2002; **35**: 182–189.

56 Spengler U, Lichterfeld M, Rockstroh JK. Antiretroviral drug toxicity -- a challenge for the hepatologist? *J Hepatol* 2002; **36**: 283–294.

57 Abrescia N, D'Abbraccio M, Figoni M, Busto A, Maddaloni A, De Marco M.

Hepatotoxicity of antiretroviral drugs. *Curr Pharm Des* 2005; **11**: 3697–3710.

58 Domingo P, Lozano F. Management of antiretroviral drug toxicity. *Enferm Infecc Microbiol Clin* 2011; **29**: 535–544.

59 Kovari H, Weber R. Influence of antiretroviral therapy on liver disease. *Curr Opin HIV AIDS* 2011; **6**: 272–277.

60 Blas-García A, Polo M, Alegre F, Funes HA, Martínez E, Apostolova N *et al.* Lack of mitochondrial toxicity of darunavir, raltegravir and rilpivirine in neurons and hepatocytes: a comparison with efavirenz. *J Antimicrob Chemother* 2014; **69**: 2995–3000.

61 Neukam K, Mira JA, Ruiz-Morales J, Rivero A, Collado A, Torres-Cornejo A *et al.* Liver toxicity associated with antiretroviral therapy including efavirenz or ritonavir-boosted protease inhibitors in a cohort of HIV/hepatitis C virus co-infected patients. *J Antimicrob Chemother* 2011; **66**: 2605–2614.

62 Athersuch TJ, Antoine DJ, Boobis AR, Coen M, Daly AK, Possamai L *et al.* Paracetamol metabolism, hepatotoxicity, biomarkers and therapeutic interventions: a perspective. *Toxicol Res (Camb)* 2018; **7**: 347–357.

63 Yan M, Huo Y, Yin S, Hu H. Mechanisms of acetaminophen-induced liver injury and its implications for therapeutic interventions. *Redox Biol* 2018; **17**: 274–283.

64 Bunchorntavakul C, Reddy KR. Acetaminophen (APAP or N-Acetyl-p-Aminophenol) and Acute Liver Failure. *Clin Liver Dis* 2018; **22**: 325–346.

65 Bunchorntavakul C, Reddy KR. Acetaminophen-related Hepatotoxicity. *Clin Liver Dis* 2013; **17**: 587–607.

66 Lancaster EM, Hiatt JR, Zarrinpar A. Acetaminophen hepatotoxicity: an updated review. *Arch Toxicol* 2015; **89**: 193–199.

67 Blas-García A, Martí-Rodrigo A, Víctor VM, Polo M, Alegre F, Funes HA *et al.* The purine analogues abacavir and didanosine increase acetaminophen-induced hepatotoxicity by enhancing mitochondrial dysfunction. *J Antimicrob Chemother* 2016; **71**: 916–926.

68 Barbarino JM, Kroetz DL, Altman RB, Klein TE. PharmGKB summary: abacavir pathway. *Pharmacogenet Genomics* 2014; **24**: 276–282.

69 Wang X, Chai H, Lin PH, Yao Q, Chen C. Roles and mechanisms of human immunodeficiency virus protease inhibitor ritonavir and other anti-human immunodeficiency virus drugs in endothelial dysfunction of porcine pulmonary arteries and human pulmonary artery endothelial cells. *Am J Pathol* 2009; **174**: 771–781.

70 Baum PD, Sullam PM, Stoddart CA, McCune JM. Abacavir increases platelet

reactivity via competitive inhibition of soluble guanylyl cyclase. *AIDS* 2011; **25**: 2243–2248.

71 Sabin CA, Reiss P, Ryom L, Phillips AN, Weber R, Law M *et al.* Is there continued evidence for an association between abacavir usage and myocardial infarction risk in individuals with HIV? A cohort collaboration. *BMC Med* 2016; **14**: 61.

72 Strategies for Management of Anti-Retroviral Therapy/INSIGHT, DAD Study Groups. Use of nucleoside reverse transcriptase inhibitors and risk of myocardial infarction in HIV-infected patients. *AIDS* 2008; **22**: F17-24.

73 Yuen GJ, Weller S, Pakes GE. A Review of the Pharmacokinetics of Abacavir. *Clin Pharmacokinet* 2008; **47**: 351–371.

74 Wyles DL, Gerber JG. Antiretroviral Drug Pharmacokinetics in Hepatitis with Hepatic Dysfunction. *Clin Infect Dis* 2005; **40**: 174–181.

75 Ficha Técnica. https://cima.aemps.es/cima/pdfs/es/ft/63302/FT_63302.html. (accessed 27 Aug 2018).

76 Videx 25mg Chewable or Dispersible Tablet. Summary of Product Characteristics. https://www.medicines.org.uk/emc/product/6743/smpc/print (accessed 27 Aug 2018).

77 Postmarket Drug Safety Information for Patients and Providers. Didanosine https://www.fda.gov/Drugs/DrugSafety/PostmarketDrugSafetyInformationforPatientsandProviders/ucm201885.htm (accessed 27 Aug 2018).

78 European Medicines Agency. Scientific conclusions and overall summary of the scientific evaluation of didanosine. http://www.ema.europa.eu/docs/en_GB/document_library/Referrals_document/Didanosine_29/WC500157752.htm (accessed 27 Aug 2018).

79 Postmarket Drug Safety Information for Patients and Providers. Didanosine https://www.fda.gov/Drugs/DrugSafety/PostmarketDrugSafetyInformationforPatientsandProviders/ucm201885.htm (accessed 27 Aug 2018).

80 Waters L, John L, Nelson M. Non-nucleoside reverse transcriptase inhibitors: a review. *Int J Clin Pract* 2007; **61**: 105–118.

81 Kanters S, Vitoria M, Doherty M, Socias ME, Ford N, Forrest JI *et al.* Comparative efficacy and safety of first-line antiretroviral therapy for the treatment of HIV infection: a systematic review and network meta-analysis. *Lancet HIV* 2016; **3**: e510–e520.

82 Neukam K, Mira JA, Collado A, Rivero-Juárez A, Monje-Agudo P, Ruiz-Morales J *et al.* Liver Toxicity of Current Antiretroviral Regimens in HIV-Infected Patients with Chronic Viral Hepatitis in a Real-Life Setting: The HEPAVIR SEG-HEP Cohort.

PLoS One 2016; **11**: e0148104.

83 Young SD, Britcher SF, Tran LO, Payne LS, Lumma WC, Lyle TA *et al.* L-743, 726 (DMP-266): a novel, highly potent nonnucleoside inhibitor of the human immunodeficiency virus type 1 reverse transcriptase. *Antimicrob Agents Chemother* 1995; **39**: 2602–2605.

84 Stöhr W, Back D, Dunn D, Sabin C, Winston A, Gilson R *et al.* Factors influencing efavirenz and nevirapine plasma concentration: Effect of ethnicity, weight and co-medication. *Antivir Ther* 2008; **13**: 675–685.

85 Burger D, Van Der Heiden I, La Porte C, Van Der Ende M, Groeneveld P, Richter C *et al.* Interpatient variability in the pharmacokinetics of the HIV non-nucleoside reverse transcriptase inhibitor efavirenz: The effect of gender, race, and CYP2B6 polymorphism. *Br J Clin Pharmacol* 2006; **61**: 148–154.

86 Kryst J, Kawalec P, Pilc A. Efavirenz-based regimens in antiretroviral-naive HIV-infected patients: A systematic review and meta-analysis of randomized controlled trials. *PLoS One* 2015; **10**: 1–23.

87 Mathiesen S, Justesen US, Lüttichau H Von. Genotyping of CYP2B6 and therapeutic drug monitoring in an HIV-infected patient with high efavirenz plasma concentrations and severe CNS. *Scand J Infect Dis* 2009; **38**: 733–735.

88 Loko MA, Bani-Sadr F, Winnock M, Lacombe K, Carrieri P, Neau D *et al.* Impact of HAART exposure and associated lipodystrophy on advanced liver fibrosis in HIV/HCV-coinfected patients. *J Viral Hepat* 2011; **18**(7): e307-314.

89 Echenique IA, Rich JD. EFV / FTC / TDF-Associated Hepatotoxicity : A case report and review. *AIDS Patient Care STDS* 2013; **27**: 493–497.

90 Mugusi S, Ngaimisi E, Janabi M, Minzi O, Bakari M, Riedel D *et al.* Liver Enzyme Abnormalities and Associated Risk Factors in HIV Patients on Efavirenz-Based HAART with or without Tuberculosis Co-Infection in Tanzania. 2012; **7**: 1–9.

91 Sonderup MW, Wainwright H, Hall P, Hairwadzi H, Spearman CWN. A Clinicopathological Cohort Study of Liver Pathology. 2015; : 1721–1729.

92 Macías J, Neukam K, Mallolas J, López-Cortés LF, Cartón J a., Domingo P *et al.* Liver Toxicity of Initial Antiretroviral Drug Regimens Including Two Nucleoside Analogs Plus One Non-Nucleoside Analog or One Ritonavir-Boosted Protease Inhibitor in HIV/HCV-Coinfected Patients. *HIV Clin Trials* 2012; **13**: 61–69.

93 Elsharkawy AM, Schwab U, McCarron B, Burt AD, Daly AK, Hudson M *et al.* Efavirenz induced acute liver failure requiring liver transplantation in a slow drug metaboliser. *J Clin Virol* 2013; **58**: 331–333.

94 Walker U a, Setzer B, Venhoff N. Increased long-term mitochondrial toxicity in

combinations of nucleoside analogue reverse-transcriptase inhibitors. *Aids* 2002; **16**: 2165–2173.

95 Feng JY, Johnson AA, Johnson KA, Anderson KS. Insights into the Molecular Mechanism of Mitochondrial Toxicity by AIDS Drugs. *J Biol Chem* 2001; **276**: 23832–23837.

96 Apostolova N, Gomez-Sucerquia LJ, Gortat A, Blas-Garcia A, Esplugues JV. Autophagy as a rescue mechanism in Efavirenz-induced mitochondrial dysfunction: A lesson from hepatic cells. *Autophagy* 2011; **7**: 1402–1404.

97 Gomez-Sucerquia LJ, Blas-Garcia A, Marti-Cabrera M, Esplugues JV., Apostolova N. Profile of stress and toxicity gene expression in human hepatic cells treated with Efavirenz. *Antiviral Res* 2012; **94**: 232–241.

98 Apostolova N, Gomez-Sucerquia LJ, Moran A, Alvarez A, Blas-Garcia A, Esplugues JV. Enhanced oxidative stress and increased mitochondrial mass during Efavirenz-induced apoptosis in human hepatic cells. *Br J Pharmacol* 2010; **160**: 2069–2084.

99 Apostolova N, Gomez-Sucerquia LJ, Gortat A, Blas-Garcia A, Esplugues JV. Compromising mitochondrial function with the antiretroviral drug efavirenz induces cell survival-promoting autophagy. *Hepatology* 2011; **54**: 1009–1019.

100 Polo M, Alegre F, Funes HA, Blas-Garcia A, Victor VM, Esplugues JV. *et al.* Mitochondrial (dys)function - A factor underlying the variability of efavirenz-induced hepatotoxicity? *Br J Pharmacol* 2015; **172**: 1713–1727.

101 Apostolova N, Gomez-Sucerquia LJ, Alegre F, Funes HA, Victor VM, Barrachina MD *et al.* ER stress in human hepatic cells treated with Efavirenz: Mitochondria again. *J Hepatol* 2013; **59**: 780–789.

102 Hu J, Han H, Lau MY, Lee H, Macveigh-Aloni M, Ji C. Effects of Combined Alcohol and Anti-HIV Drugs on Cellular Stress Responses in Primary Hepatocytes and Hepatic Stellate and Kupffer Cells. *Alcohol Clin Exp Res* 2015; **39**: 11–20.

103 Maggiolo F. Efavirenz: a decade of clinical experience in the treatment of HIV. *J Antimicrob Chemother* 2009; **64**: 910–928.

104 Manfredi R, Calza L, Chiodo F. Efavirenz versus nevirapine in current clinical practice: a prospective, open-label observational study. *J Acquir Immune Defic Syndr* 2004; **35**: 492–502.

105 Welzen B, Mudrikova T, Arends J, Hoepelman A. No increased risk of hepatotoxicity in long-term use of nonnucleoside reverse transcriptase inhibitors in HIV-infected patients. *HIV Med* 2012; **13**: 448–452.

106 Rilpivirine. Dosage and Side Effects. AIDSinfo.

https://aidsinfo.nih.gov/drugs/426/rilpivirine/0/patient (accessed 29 Aug 2018).

107 Annex I. Summary of Product Characteristics of RPV. http://www.ema.europa.eu/docs/en_GB/document_library/EPAR_-_Product_Information/human/002264/WC500118874.htm (accessed 28 Aug 2018).

108 CHMP. Anexo I. Ficha técnica y resumen de las características del producto. https://cima.aemps.es/cima/pdfs/es/ft/11737001/FT_11737001.htm (accessed 28 Aug 2018).

109 Boxwell D, Leader T, Cao K. Postmarketing, Pharmacovigilance and Safety Review. Endurant, Complera and Odefsey. 2017. https://www.fda.gov/downloads/AdvisoryCommittees/CommitteesMeetingMaterials/PediatricAdvisoryCommittee/UCM591609.pdf (accessed 28 Aug 2018).

110 Merli M, Galli L, Marinaro L, Ariaudo A, Messina E, Uberti-Foppa C *et al.* Pharmacokinetics of dolutegravir and rilpivirine in combination with simeprevir and sofosbuvir in HIV/hepatitis C virus-coinfected patients with liver cirrhosis. *J Antimicrob Chemother* 2017; **72**: 812–815.

111 Rilpivirine. Dosage and Side Effects. AIDSinfo. https://aidsinfo.nih.gov/drugs/426/rilpivirine/patient (accessed 28 Aug 2018).

112 Thamrongwonglert P, Chetchotisakd P, Anunnatsiri S, Mootsikapun P. Improvement of lipid profiles when switching from efavirenz to rilpivirine in HIV-infected patients with dyslipidemia. *HIV Clin Trials* 2016; **17**: 12–16.

113 Tebas P, Sension M, Arribas J, Duiculescu D, Florence E, Hung CC *et al.* Lipid levels and changes in body fat distribution in treatment-naive, HIV-1-infected adults treated with rilpivirine or efavirenz for 96 weeks in the ECHO and THRIVE trials. *Clin Infect Dis* 2014; **59**: 425–434.

114 Ramachandran P, Henderson NC. Antifibrotics in chronic liver disease: tractable targets and translational challenges. *Lancet Gastroenterol Hepatol* 2016; **1**: 328–340.

115 Bird TG, Forbes SJ. Two Fresh Streams to Fill the Liver's Hepatocyte Pool. *Cell Stem Cell* 2015; **17**: 377–378.

116 Heymann F, Tacke F. Immunology in the liver-from homeostasis to disease. *Nat Rev Gastroenterol Hepatol* 2016; **13**: 88–110.

117 Forbes SJ, Newsome PN. Liver regeneration-mechanisms and models to clinical application. *Nat Rev Gastroenterol Hepatol* 2016; **13**: 473–485.

118 Friedman SL. Evolving challenges in hepatic fibrosis. *Nat Rev Gastroenterol Hepatol* 2010; **7**: 425–436.

119 Gordillo M, Evans T, Gouon-Evans V. Orchestrating liver development. *Development* 2015; **142**: 2094–2108.

120 Miyajima A, Tanaka M, Itoh T. Stem/Progenitor Cells in Liver Development, Homeostasis, Regeneration, and Reprogramming. *Cell Stem Cell* 2014; **14**: 561–574.

121 Wree A, Mehal WZ, Feldstein AE. Targeting Cell Death and Sterile Inflammation Loop for the Treatment of Nonalcoholic Steatohepatitis. *Semin Liver Dis* 2016; **36**: 27–36.

122 Luedde T, Kaplowitz N, Schwabe RF. Cell death and cell death responses in liver disease: mechanisms and clinical relevance. *Gastroenterology* 2014; **147**: 765–783.

123 Tu T, Calabro SR, Lee A, Maczurek AE, Budzinska MA, Warner FJ *et al.* Hepatocytes in liver injury: Victim, bystander, or accomplice in progressive fibrosis? *J Gastroenterol Hepatol* 2015; **30**: 1696–1704.

124 Zhou Z, Xu M-J, Gao B. Hepatocytes: a key cell type for innate immunity. *Cell Mol Immunol* 2016; **13**: 301–315.

125 Crispe IN. Hepatocytes as Immunological Agents. *J Immunol* 2016; **196**: 17–21.

126 Schuster S, Cabrera D, Arrese M, Feldstein AE. Triggering and resolution of inflammation in NASH. *Nat Rev Gastroenterol Hepatol* 2018; **15**: 349–364.

127 Krysko D V., Agostinis P, Krysko O, Garg AD, Bachert C, Lambrecht BN *et al.* Emerging role of damage-associated molecular patterns derived from mitochondria in inflammation. *Trends Immunol* 2011; **32**: 157–164.

128 Galluzzi L, Kepp O, Kroemer G. Mitochondria: master regulators of danger signalling. *Nat Rev Mol Cell Biol* 2012; **13**: 780–788.

129 Gray MW, Burger G, Lang BF. Mitochondrial evolution. *Science* 1999; **283**: 1476–1481.

130 Jaeschke H. Reactive oxygen and mechanisms of inflammatory liver injury: Present concepts. *J Gastroenterol Hepatol* 2011; **26 Suppl 1**: 173–179.

131 Galluzzi L, Kepp O, Kroemer G. Mitochondria: master regulators of danger signalling. *Nat Rev Mol Cell Biol* 2012; **13**: 780–788.

132 Kroemer G, Galluzzi L, Brenner C. Mitochondrial Membrane Permeabilization in Cell Death. *Physiol Rev* 2007; **87**: 99–163.

133 Puche JE, Saiman Y, Friedman SL. Hepatic stellate cells and liver fibrosis. *Compr Physiol* 2013; **3**: 1473–1492.

134 Friedman SL. Mechanisms of hepatic fibrogenesis. *Gastroenterology* 2008; **134**:

1655–1669.

135 Hernandez-Gea V, Friedman SL. Pathogenesis of liver fibrosis. *Annu Rev Pathol* 2011; **6**: 425–456.

136 Wallace MC, Friedman SL, Mann DA. Emerging and disease-specific mechanisms of hepatic stellate cell activation. *Semin Liver Dis* 2015; **35**: 107–118.

137 Iredale JP, Thompson A, Henderson NC. Extracellular matrix degradation in liver fibrosis: Biochemistry and regulation. *Biochim Biophys Acta - Mol Basis Dis* 2013; **1832**: 876–883.

138 Pellicoro A, Ramachandran P, Iredale JP, Fallowfield JA. Liver fibrosis and repair: Immune regulation of wound healing in a solid organ. *Nat Rev Immunol* 2014; **14**: 181–194.

139 Hemmann S, Graf J, Roderfeld M, Roeb E. Expression of MMPs and TIMPs in liver fibrosis - a systematic review with special emphasis on anti-fibrotic strategies. *J Hepatol* 2007; **46**: 955–975.

140 Tsuchida T, Friedman SL. Mechanisms of hepatic stellate cell activation. *Nat Rev Gastroenterol Hepatol* 2017; **14**: 397–411.

141 Brenner C, Galluzzi L, Kepp O, Kroemer G. Decoding cell death signals in liver inflammation. *J Hepatol* 2013; **59**: 583–594.

142 Vaughn BP, Robson SC, Longhi MS. Purinergic signaling in liver disease. *Dig Dis* 2014; **32**: 516–524.

143 Cohen-Naftaly M, Friedman SL. Current status of novel antifibrotic therapies in patients with chronic liver disease. *Therap Adv Gastroenterol* 2011; **4**: 391–417.

144 Weiskirchen R, Tacke F. Cellular and molecular functions of hepatic stellate cells in inflammatory responses and liver immunology. *Hepatobiliary Surg Nutr* 2014; **3**: 344–363.

145 Seki E, Schwabe RF. Hepatic inflammation and fibrosis: functional links and key pathways. *Hepatology* 2015; **61**: 1066–1079.

146 Viñas O, Bataller R, Sancho-Bru P, Ginès P, Berenguer C, Enrich C *et al.* Human hepatic stellate cells show features of antigen-presenting cells and stimulate lymphocyte proliferation. *Hepatology* 2003; **38**: 919–929.

147 Ju C, Tacke F. Hepatic macrophages in homeostasis and liver diseases: from pathogenesis to novel therapeutic strategies. *Cell Mol Immunol* 2016; **13**: 316–327.

148 Possamai LA, Thursz MR, Wendon JA, Antoniades CG. Modulation of monocyte/macrophage function: a therapeutic strategy in the treatment of acute liver failure. *J Hepatol* 2014; **61**: 439–445.

149 Krenkel O, Tacke F. Liver macrophages in tissue homeostasis and disease. *Nat Rev Immunol* 2017; **17**: 306–321.

150 Sica A, Mantovani A. Macrophage plasticity and polarization: in vivo veritas. *J Clin Invest* 2012; **122**: 787–795.

151 Murray PJ, Wynn TA. Protective and pathogenic functions of macrophage subsets. *Nat Rev Immunol* 2011; **11**: 723–737.

152 Martinez FO, Helming L, Gordon S. Alternative Activation of Macrophages: An Immunologic Functional Perspective. *Annu Rev Immunol* 2009; **27**: 451–483.

153 Zimmermann HW, Trautwein C, Tacke F. Functional Role of Monocytes and Macrophages for the Inflammatory Response in Acute Liver Injury. *Front Physiol* 2012; **3**: 56.

154 Rőszer T. Understanding the Mysterious M2 Macrophage through Activation Markers and Effector Mechanisms. *Mediators Inflamm* 2015; **2015**: 816460.

155 Tacke F, Zimmermann HW. Macrophage heterogeneity in liver injury and fibrosis. *J Hepatol* 2014; **60**: 1090–1096.

156 Böttcher JP, Knolle PA, Stabenow D. Mechanisms Balancing Tolerance and Immunity in the Liver. *Dig Dis* 2011; **29**: 384–390.

157 Böttcher JP, Knolle PA, Stabenow D. Mechanisms balancing tolerance and immunity in the liver. *Dig Dis* 2011; **29**: 384–390.

158 Lee YA, Wallace MC, Friedman SL. Pathobiology of liver fibrosis: a translational success story. *Gut* 2015; **64**: 830–841.

159 Miyao M, Kotani H, Ishida T, Kawai C, Manabe S, Abiru H *et al.* Pivotal role of liver sinusoidal endothelial cells in NAFLD/NASH progression. *Lab Investig* 2015; **95**: 1130–1144.

160 Marrone G, Shah VH, Gracia-Sancho J. Sinusoidal communication in liver fibrosis and regeneration. *J Hepatol* 2016; **65**: 608–617.

161 Shetty S, Lalor PF, Adams DH. Liver sinusoidal endothelial cells — gatekeepers of hepatic immunity. *Nat Rev Gastroenterol Hepatol* 2018; **15**(9): 555-567.

162 Tian Z, Chen Y, Gao B. Natural killer cells in liver disease. *Hepatology* 2013; **57**: 1654–1662.

163 Gao B, Radaeva S, Park O. Liver natural killer and natural killer T cells: immunobiology and emerging roles in liver diseases. *J Leukoc Biol* 2009; **86**: 1–16.

164 Novobrantseva TI, Majeau GR, Amatucci A, Kogan S, Brenner I, Casola S *et al.* Attenuated liver fibrosis in the absece of B cells. *J Clin Invest* 2005; **115**: 3072–

3082.

165 Szabo G, Petrasek J, Bala S. Innate immunity and alcoholic liver disease. *Dig Dis* 2012; **30 Suppl 1**: 55–60.

166 Lee YA, Wallace MC, Friedman SL. Pathobiology of liver fibrosis: a translational success story. *Gut* 2015; **64**: 830–841.

167 Guo H, Callaway JB, Ting JP. Inflammasomes: mechanism of action, role in disease, and therapeutics. *Nat Med* 2015; **21**: 677–687.

168 Tilg H, Moschen AR, Szabo G. Interleukin-1 and inflammasomes in ALD/AAH and NAFLD/NASH. *Hepatology* 2016; **64**(3): 955-965.

169 Szabo G, Petrasek J. Inflammasome activation and function in liver disease. *Nat Rev Gastroenterol Hepatol* 2015; **12**: 387–400.

170 Wree A, Eguchi A, McGeough MD, Pena CA, Johnson CD, Canbay A *et al.* NLRP3 inflammasome activation results in hepatocyte pyroptosis, liver inflammation, and fibrosis in mice. *Hepatology* 2014; **59**: 898–910.

171 Strowig T, Henao-Mejia J, Elinav E, Flavell R. Inflammasomes in health and disease. *Nature* 2012; **481**: 278–286.

172 Sutterwala FS, Haasken S, Cassel SL. Mechanism of NLRP3 inflammasome activation. *Ann N Y Acad Sci* 2014; **1319**: 82–95.

173 Elliott EI, Sutterwala FS. Initiation and perpetuation of NLRP3 inflammasome activation and assembly. *Immunol Rev* 2015; **265**: 35–52.

174 Latz E. The inflammasomes: mechanisms of activation and function. *Curr Opin Immunol* 2010; **22**: 28–33.

175 Latz E, Xiao TS, Stutz A. Activation and regulation of the inflammasomes. *Nat Rev Immunol* 2013; **13**: 397–411.

176 Creagh EM. Caspase crosstalk: integration of apoptotic and innate immune signalling pathways. *Trends Immunol* 2014; **35**: 631–640.

177 Elliott EI, Sutterwala FS. Initiation and perpetuation of NLRP3 inflammasome activation and assembly. *Immunol Rev* 2015; **265**: 35–52.

178 Patel MN, Carroll RG, Galván-Peña S, Mills EL, Olden R, Triantafilou M *et al.* Inflammasome Priming in Sterile Inflammatory Disease. *Trends Mol Med* 2017; **23**: 165–180.

179 Arrese M, Cabrera D, Kalergis AM, Feldstein AE. Innate Immunity and Inflammation in NAFLD/NASH. *Dig Dis Sci* 2016; **61**: 1294–1303.

180 Liu X, Zhang Z, Ruan J, Pan Y, Magupalli VG, Wu H *et al.* Inflammasome-activated gasdermin D causes pyroptosis by forming membrane pores. *Nature* 2016; **535**:

153–158.

181 Arend WP, Palmer G, Gabay C. IL-1, IL-18, and IL-33 families of cytokines. *Immunol Rev* 2008; **223**: 20–38.

182 Heymann F, Tacke F. Immunology in the liver - from homeostasis to disease. *Nat Rev Gastroenterol Hepatol* 2016; **13**: 88–110.

183 Friedman SL. Liver fibrosis in 2012: Convergent pathways that cause hepatic fibrosis in NASH. *Nat Rev Gastroenterol Hepatol* 2013; **10**: 71–72.

184 Yaping Z, Ying W, Luqin D, Ning T, Xuemei A, Xixian Y. Mechanism of interleukin-1beta-induced proliferation in rat hepatic stellate cells from different levels of signal transduction. *Apmis* 2014; **122**: 392–398.

185 Reiter FP, Wimmer R, Wottke L, Artmann R, Nagel JM, Carranza MO *et al.* Role of interleukin-1 and its antagonism of hepatic stellate cell proliferation and liver fibrosis in the Abcb4(-/-) mouse model. *World J Hepatol* 2016; **8**: 401–410.

186 Szabo G, Csak T. Inflammasomes in liver diseases. *J Hepatol* 2012; **57**: 642–654.

187 Negash AA, Ramos HJ, Crochet N, Lau DT, Doehle B, Papic N *et al.* IL-1beta production through the NLRP3 inflammasome by hepatic macrophages links hepatitis C virus infection with liver inflammation and disease. *PLoS Pathog* 2013; **9**: e1003330.

188 Wree A, McGeough MD, Pena CA, Schlattjan M, Li H, Inzaugarat ME *et al.* NLRP3 inflammasome activation is required for fibrosis development in NAFLD. *J Mol Med* 2014; **92**: 1069–1082.

189 Trautwein C, Friedman SL, Schuppan D, Pinzani M. Hepatic fibrosis: Concept to treatment. *J Hepatol* 2015; **62**: S15–S24.

190 Cordero-Espinoza L, Huch M. The balancing act of the liver: tissue regeneration versus fibrosis. *J Clin Invest* 2018; **128**: 85–96.

191 Ramachandran P, Henderson NC. Antifibrotics in chronic liver disease: tractable targets and translational challenges. *Lancet Gastroenterol Hepatol* 2016; **1**: 328–340.

192 Wong RJ, Aguilar M, Cheung R, Perumpail RB, Harrison SA, Younossi ZM *et al.* Nonalcoholic Steatohepatitis Is the Second Leading Etiology of Liver Disease Among Adults Awaiting Liver Transplantation in the United States. *Gastroenterology* 2015; **148**: 547–555.

193 Bellentani S. The epidemiology of non-alcoholic fatty liver disease. *Liver Int* 2017; **37**: 81–84.

194 Ong JP, Pitts A, Younossi ZM. Increased overall mortality and liver-related mortality in non-alcoholic fatty liver disease. *J Hepatol* 2008; **49**: 608–612.

195 Marquardt JU, Andersen JB, Thorgeirsson SS. Functional and genetic deconstruction of the cellular origin in liver cancer. *Nat Rev Cancer* 2015; **15**: 653–667.

196 Tsochatzis EA, Bosch J, Burroughs AK. Liver cirrhosis. *Lancet* 2014; **383**: 1749–1761.

197 Byrne CD, Targher G. NAFLD: A multisystem disease. *J Hepatol* 2015; **62**: S47–S64.

198 Stickel F, Hellerbrand C. Non-alcoholic fatty liver disease as a risk factor for hepatocellular carcinoma: mechanisms and implications. *Gut* 2010; **59**: 1303–1307.

199 Starley BQ, Calcagno CJ, Harrison SA. Nonalcoholic fatty liver disease and hepatocellular carcinoma: A weighty connection. *Hepatology* 2010; **51**: 1820–1832.

200 Pimpin L, Cortez-Pinto H, Negro F, Corbould E, Lazarus J V., Webber L *et al.* Burden of liver disease in Europe: Epidemiology and analysis of risk factors to identify prevention policies. *J Hepatol* 2018; **69**: 718–735.

201 Buzzetti E, Pinzani M, Tsochatzis EA. The multiple-hit pathogenesis of non-alcoholic fatty liver disease (NAFLD). *Metabolism* 2016; **65**: 1038–1048.

202 Peverill W, Powell L, Skoien R, Peverill W, Powell LW, Skoien R. Evolving Concepts in the Pathogenesis of NASH: Beyond Steatosis and Inflammation. *Int J Mol Sci* 2014; **15**: 8591–8638.

203 Cusi K. Role of Insulin Resistance and Lipotoxicity in Non-Alcoholic Steatohepatitis. *Clin Liver Dis* 2009; **13**: 545–563.

204 Kirpich IA, Marsano LS, McClain CJ. Gut–liver axis, nutrition, and non-alcoholic fatty liver disease. *Clin Biochem* 2015; **48**: 923–930.

205 Lade A, Noon LA, Friedman SL. Contributions of metabolic dysregulation and inflammation to nonalcoholic steatohepatitis, hepatic fibrosis, and cancer. *Curr Opin Oncol* 2014; **26**: 100–107.

206 Schaffner F, Poper H. Capillarization of hepatic sinusoids in man. *Gastroenterology* 1963; **44**: 239–242.

207 Shetty S, Lalor PF, Adams DH. Liver sinusoidal endothelial cells — gatekeepers of hepatic immunity. *Nat Rev Gastroenterol Hepatol* 2018; **15**: 555–567.

208 Singh S, Allen AM, Wang Z, Prokop LJ, Murad MH, Loomba R. Fibrosis Progression in Nonalcoholic Fatty Liver vs Nonalcoholic Steatohepatitis: A Systematic Review and Meta-analysis of Paired-Biopsy Studies. *Clin Gastroenterol Hepatol* 2015; **13**: 643–654.e9.

209 Bataller R, Gao B. Liver Fibrosis in Alcoholic Liver Disease. *Semin Liver Dis* 2015;

35: 146–156.

210 Bataller R, Brenner DA. Liver fibrosis. *J Clin Invest* 2005; **115**: 209–218.

211 Hammel P, Couvelard A, O'Toole D, Ratouis A, Sauvanet A, Fléjou JF *et al.* Regression of liver fibrosis after biliary drainage in patients with chronic pancreatitis and stenosis of the common bile duct. *N Engl J Med* 2001; **344**: 418–423.

212 Michalopoulos GK. Hepatostat: Liver regeneration and normal liver tissue maintenance. *Hepatology* 2017; **65**: 1384–1392.

213 Forbes SJ, Rosenthal N. Preparing the ground for tissue regeneration: from mechanism to therapy. *Nat Med* 2014; **20**: 857–869.

214 D'Ambrosio R, Aghemo A, Rumi MG, Ronchi G, Donato MF, Paradis V *et al.* A morphometric and immunohistochemical study to assess the benefit of a sustained virological response in hepatitis C virus patients with cirrhosis. *Hepatology* 2012; **56**: 532–543.

215 Mallet V, Gilgenkrantz H, Serpaggi J, Verkarre V, Vallet-Pichard A, Fontaine H *et al.* Brief communication: the relationship of regression of cirrhosis to outcome in chronic hepatitis C. *Ann Intern Med* 2008; **149**: 399–403.

216 Issa R, Williams E, Trim N, Kendall T, Arthur MJ, Reichen J *et al.* Apoptosis of hepatic stellate cells: involvement in resolution of biliary fibrosis and regulation by soluble growth factors. *Gut* 2001; **48**: 548–557.

217 Iredale JP. Hepatic stellate cell behavior during resolution of liver injury. *Semin Liver Dis* 2001; **21**: 427–436.

218 Murphy FR, Issa R, Zhou X, Ratnarajah S, Nagase H, Arthur MJP *et al.* Inhibition of apoptosis of activated hepatic stellate cells by tissue inhibitor of metalloproteinase-1 is mediated via effects on matrix metalloproteinase inhibition: implications for reversibility of liver fibrosis. *J Biol Chem* 2002; **277**: 11069–11076.

219 Elsharkawy AM, Oakley F, Mann DA. The role and regulation of hepatic stellate cell apoptosis in reversal of liver fibrosis. *Apoptosis* 2005; **10**: 927–939.

220 CHMP. Anexo I. Ficha técnica y resumen de las características del producto. https://cima.aemps.es/cima/pdfs/es/ft/11737001/FT_11737001.htm (accessed 10 Sep 2018).

221 Radaeva S, Sun R, Jaruga B, Nguyen VT, Tian Z, Gao B. Natural killer cells ameliorate liver fibrosis by killing activated stellate cells in NKG2D-dependent and tumor necrosis factor-related apoptosis-inducing ligand-dependent manners. *Gastroenterology* 2006; **130**: 435–452.

222 Oakley F, Trim N, Constandinou CM, Ye W, Gray AM, Frantz G *et al.* Hepatocytes express nerve growth factor during liver injury: evidence for paracrine regulation of

hepatic stellate cell apoptosis. *Am J Pathol* 2003; **163**: 1849–1858.

223 Chua CEL, Chan SN, Tang BL. Non-Cell Autonomous or Secretory Tumor Suppression. *J Cell Physiol* 2014; **229**: 1346–1352.

224 Lujambio A, Akkari L, Simon J, Grace D, Tschaharganeh DF, Bolden JE *et al.* Non-Cell-Autonomous Tumor Suppression by p53. *Cell* 2013; **153**: 449–460.

225 Kisseleva T, Cong M, Paik Y, Scholten D, Jiang C, Benner C *et al.* Myofibroblasts revert to an inactive phenotype during regression of liver fibrosis. *Proc Natl Acad Sci* 2012; **109**: 9448–9453.

226 Troeger JS, Mederacke I, Gwak G-Y, Dapito DH, Mu X, Hsu CC *et al.* Deactivation of hepatic stellate cells during liver fibrosis resolution in mice. *Gastroenterology* 2012; **143**: 1073–1083.

227 Song G, Pacher M, Balakrishnan A, Yuan Q, Tsay H-C, Yang D *et al.* Direct Reprogramming of Hepatic Myofibroblasts into Hepatocytes In Vivo Attenuates Liver Fibrosis. *Cell Stem Cell* 2016; **18**: 797–808.

228 Rezvani M, Español-Suñer R, Malato Y, Dumont L, Grimm AA, Kienle E *et al.* In Vivo Hepatic Reprogramming of Myofibroblasts with AAV Vectors as a Therapeutic Strategy for Liver Fibrosis. *Cell Stem Cell* 2016; **18**: 809–816.

229 Nakamura A, Terauchi Y. Lessons from mouse models of high-fat diet-induced NAFLD. *Int J Mol Sci* 2013; **14**: 21240–21257.

230 Larter CZ, Yeh MM. Animal models of NASH: Getting both pathology and metabolic context right. *J Gastroenterol Hepatol* 2008; **23**: 1635–1648.

231 Shao W, Espenshade PJ. Expanding roles for SREBP in metabolism. *Cell Metab* 2012; **16**: 414–419.

232 Fan J-G, Qiao L. Commonly used animal models of non-alcoholic steatohepatitis. *Hepatobiliary Pancreat Dis Int* 2009; **8**: 233–240.

233 Kanuri G, Bergheim I. In vitro and in vivo models of non-alcoholic fatty liver disease (NAFLD). *Int J Mol Sci* 2013; **14**: 11963–11980.

234 Van Herck MA, Vonghia L, Francque SM. Animal models of nonalcoholic fatty liver disease—a starter's guide. *Nutrients* 2017; **9**: 1–13.

235 Kim YO, Popov Y, Schuppan D. Optimized Mouse Models for Liver Fibrosis. *Methods Mol Biol* 2017; **1559**: 279-296.

236 Kohli R, Feldstein AE. NASH animal models: Are we there yet? *J Hepatol* 2011; **55**: 941–943.

237 Collins S, Martin TL, Surwit RS, Robidoux J. Genetic vulnerability to diet-induced obesity in the C57BL/6J mouse: Physiological and molecular characteristics.

Physiol Behav 2004; **81**: 243–248.

238 Kirsch R, Clarkson V, Shephard EG, Marais DA, Jaffer MA, Woodburne VE *et al.* Rodent nutritional model of non-alcoholic steatohepatitis: Species, strain and sex difference studies. *J Gastroenterol Hepatol* 2003; **18**: 1272–1282.

239 Rawlings JS, Rosler KM, Harrison DA. The JAK/STAT signaling pathway. *J Cell Sci* 2004; **117**: 1281–1283.

240 O'Shea JJ, Schwartz DM, Villarino A V., Gadina M, McInnes IB, Laurence A. The JAK-STAT Pathway: Impact on Human Disease and Therapeutic Intervention. *Annu Rev Med* 2015; **66**: 311–328.

241 Darnell JE, Kerr IM, Stark GR. Jak-STAT pathways and transcriptional activation in response to IFNs and other extracellular signaling proteins. *Science* 1994; **264**: 1415–1421.

242 Levy DE, Darnell JE. Stats: transcriptional control and biological impact. *Nat Rev Mol Cell Biol* 2002; **3**: 651–662.

243 Darnell JE. STATs and gene regulation. *Science* 1997; **277**: 1630–1635.

244 Malakhova OA, Yan M, Malakhov MP, Yuan Y, Ritchie KJ, Kim K Il *et al.* Protein ISGylation modulates the JAK-STAT signaling pathway. *Genes Dev* 2003; **17**: 455–460.

245 Fu XY, Zhang JJ. Transcription factor p91 interacts with the epidermal growth factor receptor and mediates activation of the c-fos gene promoter. *Cell* 1993; **74**: 1135–1145.

246 Shuai K, Horvath CM, Huang LH, Qureshi SA, Cowburn D, Darnell JE. Interferon activation of the transcription factor Stat1 involves dimerization through SH2-phosphotyrosyl peptide interactions. *Cell* 1994; **76**: 821–828.

247 Xu X, Sun YL, Hoey T. Cooperative DNA binding and sequence-selective recognition conferred by the STAT amino-terminal domain. *Science* 1996; **273**: 794–797.

248 Shuai K, Liao J, Song MM. Enhancement of antiproliferative activity of gamma interferon by the specific inhibition of tyrosine dephosphorylation of Stat1. *Mol Cell Biol* 1996; **16**: 4932–4941.

249 Shuai K, Liu B. Regulation of JAK–STAT signalling in the immune system. *Nat Rev Immunol* 2003; **3**: 900–911.

250 Greenhalgh CJ, Hilton DJ. Negative regulation of cytokine signaling. *J Leukoc Biol* 2001; **70**: 348–356.

251 Yoshimura A. The CIS family: negative regulators of JAK-STAT signaling. *Cytokine Growth Factor Rev*; **9**: 197–204.

252 Sasaki A, Yasukawa H, Shouda T, Kitamura T, Dikic I, Yoshimura A. CIS3/SOCS-3 suppresses erythropoietin (EPO) signaling by binding the EPO receptor and JAK2. *J Biol Chem* 2000; **275**: 29338–29347.

253 Dodington DW, Desai HR, Woo M. JAK/STAT - Emerging Players in Metabolism. *Trends Endocrinol Metab* 2018; **29**: 55–65.

254 Penas-Steinhardt A, Tellechea ML, Gomez-Rosso L, Brites F, Frechtel GD, Poskus E. Association of common variants in JAK2 gene with reduced risk of metabolic syndrome and related disorders. *BMC Med Genet* 2011; **12**: 166.

255 Mishra J, Verma RK, Alpini G, Meng F, Kumar N. Role of Janus Kinase 3 in Predisposition to Obesity-associated Metabolic Syndrome. *J Biol Chem* 2015; **290**: 29301–29312.

256 Inoue H, Ogawa W, Asakawa A, Okamoto Y, Nishizawa A, Matsumoto M *et al.* Role of hepatic STAT3 in brain-insulin action on hepatic glucose production. *Cell Metab* 2006; **3**: 267–275.

257 Stanya KJ, Jacobi D, Liu S, Bhargava P, Dai L, Gangl MR *et al.* Direct control of hepatic glucose production by interleukin-13 in mice. *J Clin Invest* 2013; **123**: 261–271.

258 Kineman RD, Majumdar N, Subbaiah P V., Cordoba-Chacon J. Hepatic PPARγ Is Not Essential for the Rapid Development of Steatosis After Loss of Hepatic GH Signaling, in Adult Male Mice. *Endocrinology* 2016; **157**: 1728–1735.

259 Cordoba-Chacon J, Majumdar N, List EO, Diaz-Ruiz A, Frank SJ, Manzano A *et al.* Growth Hormone Inhibits Hepatic De Novo Lipogenesis in Adult Mice. *Diabetes* 2015; **64**: 3093–3103.

260 Ricardo-Gonzalez RR, Red Eagle A, Odegaard JI, Jouihan H, Morel CR, Heredia JE *et al.* IL-4/STAT6 immune axis regulates peripheral nutrient metabolism and insulin sensitivity. *Proc Natl Acad Sci USA* 2010; **107**: 22617–22622.

261 Gao B, Wang H, Lafdil F, Feng D. STAT proteins - key regulators of anti-viral responses, inflammation, and tumorigenesis in the liver. *J Hepatol* 2012; **57**: 430–441.

262 Subleski JJ, Hall VL, Back TC, Ortaldo JR, Wiltrout RH. Enhanced antitumor response by divergent modulation of natural killer and natural killer T cells in the liver. *Cancer Res* 2006; **66**: 11005–11012.

263 Kaplan MH. STAT4: a critical regulator of inflammation in vivo. *Immunol Res* 2005; **31**: 231–242.

264 Hosui A, Kimura A, Yamaji D, Zhu B, Na R, Hennighausen L. Loss of STAT5 causes liver fibrosis and cancer development through increased TGFβ and STAT3

activation. *J Exp Med* 2009; **206**: 819–831.

265 Ferbeyre G, Moriggl R. The role of Stat5 transcription factors as tumor suppressors or oncogenes. *Biochim Biophys Acta - Rev Cancer* 2011; **1815**: 104–114.

266 Mueller KM, Kornfeld J-W, Friedbichler K, Blaas L, Egger G, Esterbauer H *et al.* Impairment of hepatic growth hormone and glucocorticoid receptor signaling causes steatosis and hepatocellular carcinoma in mice. *Hepatology* 2011; **54**: 1398–13409.

267 Friedbichler K, Themanns M, Mueller KM, Schlederer M, Kornfeld J-W, Terracciano LM *et al.* Growth-hormone-induced signal transducer and activator of transcription 5 signaling causes gigantism, inflammation, and premature death but protects mice from aggressive liver cancer. *Hepatology* 2012; **55**: 941–952.

268 Rehermann B. Hepatitis C virus versus innate and adaptive immune responses: a tale of coevolution and coexistence. *J Clin Invest* 2009; **119**: 1745–1754.

269 Kato A, Okaya T, Lentsch AB. Endogenous IL-13 protects hepatocytes and vascular endothelial cells during ischemia/reperfusion injury. *Hepatology* 2003; **37**: 304–312.

270 Cao Z, Yuan Y, Jeyabalan G, Du Q, Tsung A, Geller DA *et al.* Preactivation of NKT cells with alpha-GalCer protects against hepatic ischemia-reperfusion injury in mouse by a mechanism involving IL-13 and adenosine A2A receptor. *Am J Physiol Gastrointest Liver Physiol* 2009; **297**: 249-258.

271 Wang H, Lafdil F, Kong X, Gao B. Signal transducer and activator of transcription 3 in liver diseases: a novel therapeutic target. *Int J Biol Sci* 2011; **7**: 536–550.

272 Mair M, Blaas L, Österreicher CH, Casanova E, Eferl R. JAK-STAT signaling in hepatic fibrosis. *Front Biosci* 2011; **16**: 2794–2811.

273 Park O, Wang H, Weng H, Feigenbaum L, Li H, Yin S *et al.* In vivo consequences of liver-specific interleukin-22 expression in mice: Implications for human liver disease progression. *Hepatology* 2011; **54**: 252–261.

274 Wang H, Park O, Lafdil F, Shen K, Horiguchi N, Yin S *et al.* Interplay of hepatic and myeloid signal transducer and activator of transcription 3 in facilitating liver regeneration via tempering innate immunity. *Hepatology* 2010; **51**: 1354–1362.

275 Fujiyoshi M, Ozaki M. Molecular mechanisms of liver regeneration and protection for treatment of liver dysfunction and diseases. *J Hepatobiliary Pancreat Sci* 2011; **18**: 13–22.

276 Gu Y-J, Sun W-Y, Zhang S, Li X-R, Wei W. Targeted blockade of JAK/STAT3 signaling inhibits proliferation, migration and collagen production as well as inducing the apoptosis of hepatic stellate cells. *Int J Mol Med* 2016; **38**: 903–911.

277 Lu C, Xu W, Shao J, Zhang F, Chen A, Zheng S. Nrf2 induces lipocyte phenotype via a SOCS3-dependent negative feedback loop on JAK2/STAT3 signaling in hepatic stellate cells. *Int Immunopharmacol* 2017; **49**: 203–211.

278 Cummins C, Wang X, Nunez Lopez O, Graham G, Tie H-Y, Zhou J *et al.* Luteolin-Mediated Inhibition of Hepatic Stellate Cell Activation via Suppression of the STAT3 Pathway. *Int J Mol Sci* 2018; **19**: 1567.

279 Xiang D-M, Sun W, Ning B-F, Zhou T-F, Li X-F, Zhong W *et al.* The HLF/IL-6/STAT3 feedforward circuit drives hepatic stellate cell activation to promote liver fibrosis. *Gut* 2018; **67**: 1704–1715.

280 Gao B, Radaeva S, Jeong W-I. Activation of natural killer cells inhibits liver fibrosis: a novel strategy to treat liver fibrosis. *Expert Rev Gastroenterol Hepatol* 2007; **1**: 173–180.

281 Zhang H, Chen F, Fan X, Lin C, Hao Y, Wei H *et al.* Quantitative Proteomic analysis on Activated Hepatic Stellate Cells reversion Reveal STAT1 as a key regulator between Liver Fibrosis and recovery. *Sci Rep* 2017; **7**: 44910.

282 Wu X-X, Wu L-M, Fan J-J, Qin Y, Chen G, Wu X-F *et al.* Cortex Dictamni extract induces apoptosis of activated hepatic stellate cells via STAT1 and attenuates liver fibrosis in mice. *J Ethnopharmacol* 2011; **135**: 173–178.

283 Mair M, Zollner G, Schneller D, Musteanu M, Fickert P, Gumhold J *et al.* Signal transducer and activator of transcription 3 protects from liver injury and fibrosis in a mouse model of sclerosing cholangitis. *Gastroenterology* 2010; **138**: 2499–2508.

284 Lafdil F, Wang H, Park O, Zhang W, Moritoki Y, Yin S *et al.* Myeloid STAT3 inhibits T cell-mediated hepatitis by regulating T helper 1 cytokine and interleukin-17 production. *Gastroenterology* 2009; **137**: 2125-2135.

285 Ogata H, Kobayashi T, Chinen T, Takaki H, Sanada T, Minoda Y *et al.* Deletion of the SOCS3 gene in liver parenchymal cells promotes hepatitis-induced hepatocarcinogenesis. *Gastroenterology* 2006; **131**: 179–93.

286 Jeong W, Park O, Gao B. Abrogation of the Antifibrotic Effects of Natural Killer Cells/Interferon-γ Contributes to Alcohol Acceleration of Liver Fibrosis. *Gastroenterology* 2008; **134**: 248–258.

287 Fausto N, Campbell JS, Riehle KJ. Liver regeneration. *Hepatology* 2006; **43**: S45-53.

288 Michalopoulos GK. Liver regeneration after partial hepatectomy: critical analysis of mechanistic dilemmas. *Am J Pathol* 2010; **176**: 2–13.

289 Gao B, Wang H, Lafdil F, Feng D. STAT proteins - Key regulators of anti-viral responses, inflammation, and tumorigenesis in the liver. *J Hepatol* 2012; **57**: 430–

441.

290 Suwandi JS, Toes REM, Nikolic T, Roep BO. Inducing tissue specific tolerance in autoimmune disease with tolerogenic dendritic cells. *Clin Exp Rheumatol* 2015; **33**: 97–103.

291 Lin J, Schyschka L, Mühl-Benninghaus R, Neumann J, Hao L, Nussler N *et al.* Comparative analysis of phase i and II enzyme activities in 5 hepatic cell lines identifies Huh-7 and HCC-T cells with the highest potential to study drug metabolism. *Arch Toxicol* 2012; **86**: 87–95.

292 Gripon P, Rumin S, Urban S, Le Seyec J, Glaise D, Cannie I *et al.* Infection of a human hepatoma cell line by hepatitis B virus. *Proc Natl Acad Sci USA* 2002; **99**: 15655–15660.

293 Chesne C, Li R, Camus S, Lahoz A, Picazo L, Turpeinen M *et al.* in Differentiated HepaRG Cells. *Pharmacology* 2010; **38**: 516–525.

294 Ortega-Ribera M, Fernández-Iglesias A, Illa X, Moya A, Molina V, Maeso-Díaz R *et al.* Resemblance of the human liver sinusoid in a fluidic device with biomedical and pharmaceutical applications. *Biotechnol Bioeng* 2018; **115**(10): 2585-2594.

295 Vilaseca M, García-Calderó H, Lafoz E, García-Irigoyen O, Avila MA, Reverter JC *et al.* The anticoagulant rivaroxaban lowers portal hypertension in cirrhotic rats mainly by deactivating hepatic stellate cells. *Hepatology* 2017; **65**: 2031–2044.

296 Vilaseca M, García-Calderó H, Lafoz E, Ruart M, López-Sanjurjo CI, Murphy MP *et al.* Mitochondria-targeted antioxidant mitoquinone deactivates human and rat hepatic stellate cells and reduces portal hypertension in cirrhotic rats. *Liver Int* 2017; **37**: 1002–1012.

297 Volunteers AH. Guidance for Industry and Reviewers Estimating the Safe Starting Dose in Guidance for Industry and Reviewers Estimating the Safe Starting Dose in. *Fed Regist* 2002.

298 Reagan-Shaw S, Nihal M, Ahmad N. Dose translation from animal to human studies revisited. *FASEB J* 2007; **22**: 659–661.

299 Kittler R, Surendranath V, Heninger AK, Slabicki M, Theis M, Putz G *et al.* Genome-wide resources of endoribonuclease-prepared short interfering RNAs for specific loss-of-function studies. *Nat Methods* 2007; **4**: 337–344.

300 Theis M, Buchholz F. MISSION esiRNA for RNAi Screening in Mammalian Cells. *J Vis Exp* 2010; **39**: 3–5.

301 Mosmann T. Rapid Colorimetric Assay for Cellular Growth and Survival : Application to Proliferation and Cytotoxicity Assays. *J Immunol Methods* 1983; **65**: 55–63.

302 Clark LC. J, Wolf R, Granger D, Taylor Z. Continuous Recording of Blood Oxygen Tensions by Polarography. *J Appl Physiol* 1953; **6**: 189–193.

303 Loken MR. Simultaneous quantitation of hoechst 33342 and immunofluorescence on viable cells using a fluorescence activated cell sorter. *Cytometry* 1980; **1**: 136–142.

304 Sazanov LA. A giant molecular proton pump: Structure and mechanism of respiratory complex I. *Nat Rev Mol Cell Biol* 2015; **16**: 375–388.

305 Vinothkumar KR, Zhu J, Hirst J. Architecture of mammalian respiratory complex I. *Nature* 2014; **515**: 80–84.

306 Compton SJ, Jones CG. Mechanism of dye response and interference in the Bradford protein assay. *Anal Biochem* 1985; **151**: 369–374.

307 Bradford MM. A rapid and sensitive method for the quantitation of microgram quantities of protein utilizing the principle of protein-dye binding. *Anal Biochem* 1976; **72**: 248–254.

308 Wojtovich AP, Wei AY, Sherman TA, Foster TH, Nehrke K. Chromophore-Assisted Light Inactivation of Mitochondrial Electron Transport Chain Complex II in Caenorhabditis elegans. *Sci Rep* 2016; **6**: 1–13.

309 Wojtovich AP, Smith CO, Haynes CM, Nehrke KW, Brookes PS. Physiological consequences of complex II inhibition for aging, disease, and the mKATP channel. *Biochim Biophys Acta - Bioenerg* 2013; **1827**: 598–611.

310 Fedor JG, Hirst J. Mitochondrial Supercomplexes Do Not Enhance Catalysis by Quinone Channeling. *Cell Metab* 2018; **28**(3):525-531.

311 Luo C, Long J, Liu J. An improved spectrophotometric method for a more specific and accurate assay of mitochondrial complex III activity. *Clin Chim Acta* 2008; **395**: 38–41.

312 Balsa E, Marco R, Perales-Clemente E, Szklarczyk R, Calvo E, Landázuri MO *et al.* NDUFA4 is a subunit of complex IV of the mammalian electron transport chain. *Cell Metab* 2012; **16**: 378–386.

313 Letts JA, Sazanov LA. Clarifying the supercomplex: The higher-order organization of the mitochondrial electron transport chain. *Nat Struct Mol Biol* 2017; **24**: 800–808.

314 Bernhard F, Tozawa Y. Cell-free expression—making a mark. *Curr Opin Struct Biol* 2013; **23**: 374–380.

315 Cossarizza A, Ferraresi R, Troiano L, Roat E, Gibellini L, Bertoncelli L *et al.* Simultaneous analysis of reactive oxygen species and reduced glutathione content in living cells by polychromatic flow cytometry. *Nat Protoc* 2009; **4**: 1790–1797.

316 Nagata S, Suzuki J, Segawa K, Fujii T. Exposure of phosphatidylserine on the cell surface. *Cell Death Differ* 2016; **23**: 952–961.

317 Birge RB, Boeltz S, Kumar S, Carlson J, Wanderley J, Calianese D *et al.* Phosphatidylserine is a global immunosuppressive signal in efferocytosis, infectious disease, and cancer. *Cell Death Differ* 2016; **23**: 962–978.

318 Suzuki J, Denning DP, Imanishi E, Horvitz HR, Nagata S. Xk-related protein 8 and CED-8 promote phosphatidylserine exposure in apoptotic cells. *Science* 2013; **341**: 403–406.

319 Smith PK, Krohn RI, Hermanson GT, Mallia AK, Gartner FH, Provenzano MD *et al.* Measurement of protein using bicinchoninic acid. *Anal Biochem* 1985; **150**: 76–85.

320 Whitehead TP, Kricka LJ, Carter TJ, Thorpe GH. Analytical luminescence: its potential in the clinical laboratory. *Clin Chem* 1979; **25**.

321 Bolstad BM, Speed TP, Irizarry RA, Astrand M. A comparison of normalization methods for high density oligonucleotide array data based on variance and bias. *Bioinformatics* 2003; **19**: 185–193.

322 Smyth GK. Linear Models and Empirical Bayes Methods for Assessing Differential Expression in Microarray Experiments. *Stat Appl Genet Mol Biol* 2004; **3**: 1–25.

323 Conesa A, Nueda MJ, Ferrer A, Talón M. maSigPro: A method to identify significantly differential expression profiles in time-course microarray experiments. *Bioinformatics* 2006; **22**: 1096–1102.

324 Benjamini Y, Hochberg Y. Controlling the False Discovery Rate: A Practical and Powerful Approach to Multiple Testing. *Source J R Stat Soc Ser B J R Stat Soc Ser B J R Stat Soc B* 1995; **57**: 289–300.

325 Sartor MA, Leikauf GD, Medvedovic M. LRpath: A logistic regression approach for identifying enriched biological groups in gene expression data. *Bioinformatics* 2009; **25**: 211–217.

326 Montaner D, Dopazo J. Multidimensional gene set analysis of genomic data. *PLoS One* 2010; **5**(4):e10348.

327 Ge Y, Sealfon SC, Speed TP. Some step-down procedures controlling the false discovery rate under dependence. *Stat Sin* 2008; **18**: 881–904.

328 García-Alcalde F, García-López F, Dopazo J, Conesa A. Paintomics: A web based tool for the joint visualization of transcriptomics and metabolomics data. *Bioinformatics* 2011; **27**: 137–139.

329 Young LM, Kheifets JB, Ballaron SJ, Young JM. Edema and cell infiltration in the phorbol ester-treated mouse ear are temporally separate and can be differentially modulated by pharmacologic agents. *Agents Actions* 1989; **26**: 335–341.

330 Pulli B, Ali M, Forghani R, Schob S, Hsieh KLC, Wojtkiewicz G *et al.* Measuring Myeloperoxidase Activity in Biological Samples. *PLoS One* 2013; **8**(7): e67976.

331 Souza DG, Cassali GD, Poole S, Teixeira MM. Effects of inhibition of PDE4 and TNF-α on local and remote injuries following ischaemia and reperfusion injury. *Br J Pharmacol* 2001; **134**: 985–994.

332 Matos IM, Souza DG, Seabra DG, Freire-maia L. Effects of tachykinin NK 1 or PAF receptor blockade on the lung injury induced by scorpion venom in rats. *Eur J Pharmacol* 1999; **376**: 293–300.

333 Montes GS, Junqueira LC. The use of the Picrosirius-polarization method for the study of the biopathology of collagen. *Mem. Inst. Oswaldo Cruz* 1991; **86 Suppl 3**: 1–11.

334 Junqueira LCU, Bignolas G, Brentani RR. Picrosirius staining plus polarization microscopy, a specific method for collagen detection in tissue sections. *Histochem J* 1979; **11**: 447–455.

335 Coen M, Menegatti E, Salvi F, Mascoli F, Zamboni P, Gabbiani G *et al.* Altered collagen expression in jugular veins in multiple sclerosis. *Cardiovasc Pathol* 2013; **22**: 33–38.

336 Lattouf R, Younes R, Lutomski D, Naaman N, Godeau G, Senni K *et al.* Picrosirius Red Staining: A Useful Tool to Appraise Collagen Networks in Normal and Pathological Tissues. *J Histochem Cytochem* 2014; **62**: 751–758.

337 Brouwer JR, Mientjes EJ, Bakker CE, Nieuwenhuizen IM, Severijnen LA, Van der Linde HC *et al.* Immunohistochemistry Application Guide. *Exp Cell Res* 2007; **313**: 244–253.

338 Hsu S-M, Raine L. Protein A , Avidin , Immunohistochemistry Biotin in prepared. *J Histochem Cytochem* 1981; **29**: 1349–1353.

339 Cardiff RD, Miller CH, Munn RJ. Manual immunohistochemistry staining of mouse tissues using the avidin–biotin complex (ABC) technique. *Cold Spring Harb Protoc* 2014; **2014**(6): 659–662.

340 Shmuel A. Identification of Programmed Cell Death In Situ. *Cell* 1992; **119**: 493–501.

341 Negoescu A, Lorimier P, Labat-Moleur F, Robert C, Guillermet C, Brambilla C. Improvement and Evaluation of the Method for In Situ Apoptotic Cell Identification. *Cardiovasc Res* 1997; **2**: 12–17.

342 Kyrylkova K, Kyryachenko S, Leid M, Kioussi C. *Methods Mol Biol* 2012; **887**: 41-47.

343 Fayzullina S, Martin LJ. Detection and Analysis of DNA Damage in Mouse Skeletal

Muscle in situ using the TUNEL Method. *J Vis Exp* 2014; **94**: 1–9.

344 Roche. In Situ Cell Death Detection Kit, POD. 2012.

345 Ma Z, Deng C, Hu W, Zhou J, Fan C, Di S *et al.* Liver X Receptors and their Agonists: Targeting for Cholesterol Homeostasis and Cardiovascular Diseases. *Curr Issues Mol Biol* 2017; **22**: 41–64.

346 Wang B, Tontonoz P. Liver X receptors in lipid signalling and membrane homeostasis. *Nat Rev Endocrinol* 2018; **14**: 452–463.

347 Maqdasy S, Trousson A, Tauveron I, Volle DH, Baron S, Lobaccaro J-MA. Once and for all, LXRα and LXRβ are gatekeepers of the endocrine system. *Mol Aspects Med* 2016; **49**: 31–46.

348 Oeckinghaus A, Hayden MS, Ghosh S. Crosstalk in NF-κB signaling pathways. *Nat Immunol* 2011; **12**: 695–708.

349 Baker RG, Hayden MS, Ghosh S. NF-κB, Inflammation, and Metabolic Disease. *Cell Metab* 2011; **13**: 11–22.

350 Palacios R, Mayorga M, Pérez-Hernández IA, Rivero A, Arco A Del, Lozano F *et al.* Lipid Changes in Virologically Suppressed HIV-Infected Patients Switching from any Antiretroviral Therapy to the Emtricitabine/Rilpivirine/Tenofovir Single Tablet. *J Int Assoc Provid AIDS Care* 2013; **15**: 189–193.

351 Yang C, Zhang J, Ding M, Xu K, Li L, Mao L *et al.* Ki67 targeted strategies for cancer therapy. *Clin Transl Oncol* 2018; **20**: 570–575.

352 Takagi M, Natsume T, Kanemaki MT, Imamoto N. Perichromosomal protein Ki67 supports mitotic chromosome architecture. *Genes to Cells* 2016; **21**: 1113–1124.

353 Larter CZ, Yeh MM. Animal models of NASH: Getting both pathology and metabolic context right. *J Gastroenterol Hepatol* 2008; **23**: 1635–1648.

354 Kohli R, Feldstein AE. NASH animal models: are we there yet? *J Hepatol* 2011; **55**: 941–943.

355 Mir SA, Chatterjee A, Mitra A, Pathak K, Mahata SK, Sarkar S. Inhibition of signal transducer and activator of transcription 3 (STAT3) attenuates interleukin-6 (IL-6)-induced collagen synthesis and resultant hypertrophy in rat heart. *J Biol Chem* 2012; **287**: 2666–2677.

356 Renga B, Francisci D, Schiaroli E, Carino A, Cipriani S, D'Amore C *et al.* The HIV Matrix Protein p17 Promotes the Activation of Human Hepatic Stellate Cells through Interactions with CXCR2 and Syndecan-2. *PLoS One* 2014; **9**: e94798.

357 Odendall C, Dixit E, Stavru F, Bierne H, Franz KM, Durbin AF *et al.* Diverse intracellular pathogens activate type III interferon expression from peroxisomes. *Nat Immunol* 2014; **15**: 717–726.

358 Deeks SG, Lewin SR, Havlir D V. The end of AIDS: HIV infection as a chronic disease. *Lancet* 2013; **382**: 1525–1533.

359 De Clercq E. Anti-HIV drugs: 25 compounds approved within 25 years after the discovery of HIV. *Int J Antimicrob Agents* 2009; **33**: 307–320.

360 Flexner C. HIV drug development: the next 25 years. *Nat Rev Drug Discov* 2007; **6**: 959–966.

361 Caron-Debarle M, Lagathu C, Boccara F, Vigouroux C, Capeau J. HIV-associated lipodystrophy: from fat injury to premature aging. *Trends Mol Med* 2010; **16**: 218–229.

362 Lagathu C, Cossarizza A, Béréziat V, Nasi M, Capeau J, Pinti M. Basic science and pathogenesis of ageing with HIV. *AIDS* 2017; **31**: S105–S119.

363 Wang X, Chai H, Lin PH, Yao Q, Chen C. Roles and mechanisms of human immunodeficiency virus protease inhibitor ritonavir and other anti-human immunodeficiency virus drugs in endothelial dysfunction of porcine pulmonary arteries and human pulmonary artery endothelial cells. *Am J Pathol* 2009; **174**: 771–781.

364 Koczor CA, Lewis W. Nucleoside reverse transcriptase inhibitor toxicity and mitochondrial DNA. *Expert Opin Drug Metab Toxicol* 2010; **6**: 1493–1504.

365 Núñez M. Clinical syndromes and consequences of antiretroviral-related hepatotoxicity. *Hepatology* 2010; **52**: 1143–1155.

366 Mallal S, Phillips E, Carosi G, Molina J-M, Workman C, Tomazic J *et al.* HLA-B*5701 screening for hypersensitivity to abacavir. *N Engl J Med* 2008; **358**: 568–579.

367 Bannister WP, Friis-Møller N, Mocroft A, Viard J-P, van Lunzen J, Kirk O *et al.* Incidence of abacavir hypersensitivity reactions in euroSIDA. *Antivir Ther* 2008; **13**: 687–696.

368 Lactic Acidosis International Study Group. Risk factors for lactic acidosis and severe hyperlactataemia in HIV-1-infected adults exposed to antiretroviral therapy. *AIDS* 2007; **21**: 2455–2464.

369 Kovari H, Ledergerber B, Peter U, Flepp M, Jost J, Schmid P *et al.* Association of noncirrhotic portal hypertension in HIV-infected persons and antiretroviral therapy with didanosine: a nested case-control study. *Clin Infect Dis* 2009; **49**: 626–635.

370 McGovern BH, Ditelberg JS, Taylor LE, Gandhi RT, Christopoulos KA, Chapman S *et al.* Hepatic steatosis is associated with fibrosis, nucleoside analogue use, and hepatitis C virus genotype 3 infection in HIV-seropositive patients. *Clin Infect Dis* 2006; **43**: 365–372.

371 Soni S, Churchill DR, Gilleece Y. Abacavir-induced hepatotoxicity: a report of two cases. *AIDS* 2008; **22**: 2557–2558.

372 Di Filippo E, Ripamonti D, Rizzi M. Abacavir-induced liver toxicity in an HIV-infected patient. *AIDS* 2014; **28**: 613.

373 Lederman JC, Nawaz H. Toxic interaction of didanosine and acetaminophen leading to severe hepatitis and pancreatitis: a case report and review of the literature. *Am J Gastroenterol* 2001; **96**: 3474–3475.

374 Prescott LF. Paracetamol: past, present, and future. *Am J Ther* 2000; **7**: 143–147.

375 Pierce RH, Franklin CC, Campbell JS, Tonge RP, Chen W, Fausto N *et al.* Cell culture model for acetaminophen-induced hepatocyte death in vivo. *Biochem Pharmacol* 2002; **64**: 413–424.

376 Neuman MG. Synergetic signaling for apoptosis in vitro by ethanol and acetaminophen. *Alcohol* 2002; **27**: 89–98.

377 Manov I, Hirsh M, Iancu TC. Acetaminophen hepatotoxicity and mechanisms of its protection by N-acetylcysteine: a study of Hep3B cells. *Exp Toxicol Pathol* 2002; **53**: 489–500.

378 Manov I, Bashenko Y, Hirsh M, Iancu TC. Involvement of the multidrug resistance P-glycoprotein in acetaminophen-induced toxicity in hepatoma-derived HepG2 and Hep3B cells. *Basic Clin Pharmacol Toxicol* 2006; **99**: 213–224.

379 McGill MR, Yan H-M, Ramachandran A, Murray GJ, Rollins DE, Jaeschke H. HepaRG cells: a human model to study mechanisms of acetaminophen hepatotoxicity. *Hepatology* 2011; **53**: 974–982.

380 Jiang J, Briedé JJ, Jennen DGJ, Van Summeren A, Saritas-Brauers K, Schaart G *et al.* Increased mitochondrial ROS formation by acetaminophen in human hepatic cells is associated with gene expression changes suggesting disruption of the mitochondrial electron transport chain. *Toxicol Lett* 2015; **234**: 139–150.

381 Moling O, Cairon E, Rimenti G, Rizza F, Pristerá R, Mian P. Severe hepatotoxicity after therapeutic doses of acetaminophen. *Clin Ther* 2006; **28**: 755–760.

382 Hardie DG. AMP-activated/SNF1 protein kinases: conserved guardians of cellular energy. *Nat Rev Mol Cell Biol* 2007; **8**: 774–785.

383 Gerschenson M, Kim C, Berzins B, Taiwo B, Libutti DE, Choi J *et al.* Mitochondrial function, morphology and metabolic parameters improve after switching from stavudine to a tenofovir-containing regimen. *J Antimicrob Chemother* 2009; **63**: 1244–1250.

384 Fraternale A, Paoletti MF, Casabianca A, Nencioni L, Garaci E, Palamara AT *et al.* GSH and analogs in antiviral therapy. *Mol Aspects Med* 2009; **30**: 99–110.

385 Blas-García A, Polo M, Alegre F, Funes HA, Martínez E, Apostolova N *et al.* Lack of mitochondrial toxicity of darunavir, raltegravir and rilpivirine in neurons and hepatocytes: a comparison with efavirenz. *J Antimicrob Chemother* 2014; **69**: 2995–3000.

386 Sharma D, Lau AJ, Sherman MA, Chang TKH. Agonism of human pregnane X receptor by rilpivirine and etravirine: Comparison with first generation non-nucleoside reverse transcriptase inhibitors. *Biochem Pharmacol* 2013; **85**: 1700–1711.

387 Sharma D, Lau AJ, Sherman MA, Chang TKH. Differential activation of human constitutive androstane receptor and its SV23 and SV24 splice variants by rilpivirine and etravirine. *Br J Pharmacol* 2015; **172**: 1263–1276.

388 Moog KE, Barz M, Bartneck M, Beceren-Braun F, Mohr N, Wu Z *et al.* Polymeric Selectin Ligands Mimicking Complex Carbohydrates: From Selectin Binders to Modifiers of Macrophage Migration. *Angew Chem Int Ed Engl* 2017; **56**: 1416–1421.

389 Tacke F, Weiskirchen R. An update on the recent advances in antifibrotic therapy. *Expert Rev Gastroenterol Hepatol* 2018; **27**:1-10.

390 Martín-Carbonero L, Núñez M, González-Lahoz J, Soriano V. Incidence of Liver Injury After Beginning Antiretroviral Therapy with Efavirenz or Nevirapine. *HIV Clin Trials* 2003; **4**: 115–120.

391 Freshney R. Protocol 22.2.8 HepaRG Human Hepatocytes. In: *Culture of Animal Cells: A Manual of Basic Technique and Specialized Applications, Sixth Edition*. 2011, 383–432.

392 Palmon R, Koo BCA, Shoultz DA, Dieterich DT. Lack of hepatotoxicity associated with nonnucleoside reverse transcriptase inhibitors. *J Acquir Immune Defic Syndr* 2002; **29**: 340–345.

393 Luz M-C, Marina N, Juan G-L, Vincent S. Incidence of Liver Injury After Beginning Antiretroviral Therapy with Efavirenz or Nevirapine. *HIV Clin Trials* 2003; **4**: 115–120.

394 Zhang H, Chen F, Fan X, Lin C, Hao Y, Wei H *et al.* Quantitative Proteomic analysis on Activated Hepatic Stellate Cells reversion Reveal STAT1 as a key regulator between Liver Fibrosis and recovery. *Sci Rep* 2017; **7**: 44910.

395 Ambade A, Lowe P, Kodys K, Catalano D, Gyongyosi B, Cho Y *et al.* Pharmacological inhibition of CCR2/5 signaling prevents and reverses alcohol-induced liver damage, steatosis and inflammation in mice. *Hepatology* 2018. doi:10.1002/hep.30249.

396 Krenkel O, Puengel T, Govaere O, Abdallah AT, Mossanen JC, Kohlhepp M *et al.*

Therapeutic inhibition of inflammatory monocyte recruitment reduces steatohepatitis and liver fibrosis. *Hepatology* 2018; **67**: 1270–1283.

397 Lefebvre E, Moyle G, Reshef R, Richman LP, Thompson M, Hong F *et al.* Antifibrotic Effects of the Dual CCR2/CCR5 Antagonist Cenicriviroc in Animal Models of Liver and Kidney Fibrosis. *PLoS One* 2016; **11**: e0158156.

398 Tripathi DM, Vilaseca M, Lafoz E, Garcia-Caldero H, Haute GV, Fernández-Iglesias A *et al.* Simvastatin Prevents Progression of Acute on Chronic Liver Failure in Rats With Cirrhosis and Portal Hypertension. *Gastroenterology* 2018. doi:10.1053/j.gastro.2018.07.022.

399 Gracia-Sancho J, García-Calderó H, Hide D, Marrone G, Guixé-Muntet S, Peralta C *et al.* Simvastatin maintains function and viability of steatotic rat livers procured for transplantation. *J Hepatol* 2013; **58**: 1140–1146.

400 Bhardwaj N, Rosas LE, Lafuse WP, Satoskar AR. Leishmania inhibits STAT1-mediated IFN-gamma signaling in macrophages: increased tyrosine phosphorylation of dominant negative STAT1beta by Leishmania mexicana. *Int J Parasitol* 2005; **35**: 75–82.

401 Alvarez GR, Zwilling BS, Lafuse WP. Mycobacterium avium inhibition of IFN-gamma signaling in mouse macrophages: Toll-like receptor 2 stimulation increases expression of dominant-negative STAT1 beta by mRNA stabilization. *J Immunol* 2003; **171**: 6766–6773.

402 Baran-Marszak F, Feuillard J, Najjar I, Le Clorennec C, Béchet J-M, Dusanter-Fourt I *et al.* Differential roles of STAT1alpha and STAT1beta in fludarabine-induced cell cycle arrest and apoptosis in human B cells. *Blood* 2004; **104**: 2475–2483.

403 Semper C, Leitner NR, Lassnig C, Parrini M, Mahlakoiv T, Rammerstorfer M *et al.* STAT1 Is Not Dominant Negative and Is Capable of Contributing to Gamma Interferon-Dependent Innate Immunity. *Mol Cell Biol* 2014; **34**: 2235–2248.

404 Najjar I, Schischmanoff PO, Baran-Marszak F, Deglesne P-A, Youlyouz-Marfak I, Pampin M *et al.* Novel function of STAT1beta in B cells: induction of cell death by a mechanism different from that of STAT1alpha. *J Leukoc Biol* 2008; **84**: 1604–1612.

405 Cheng A-L, Guan Z, Chen Z, Tsao C-J, Qin S, Kim JS *et al.* Efficacy and safety of sorafenib in patients with advanced hepatocellular carcinoma according to baseline status: Subset analyses of the phase III Sorafenib Asia–Pacific trial. *Eur J Cancer* 2012; **48**: 1452–1465.

406 Cheng A-L, Kang Y-K, Chen Z, Tsao C-J, Qin S, Kim JS *et al.* Efficacy and safety of sorafenib in patients in the Asia-Pacific region with advanced hepatocellular carcinoma: a phase III randomised, double-blind, placebo-controlled trial. *Lancet*

Oncol 2009; **10**: 25–34.

407 Llovet JM, Ricci S, Mazzaferro V, Hilgard P, Gane E, Blanc J-F *et al.* Sorafenib in Advanced Hepatocellular Carcinoma. *N Engl J Med* 2008; **359**: 378–390.

408 Deng Y-R, Ma H-D, Tsuneyama K, Yang W, Wang Y-H, Lu F-T *et al.* STAT3-mediated attenuation of CCl4-induced mouse liver fibrosis by the protein kinase inhibitor sorafenib. *J Autoimmun* 2013; **46**: 25–34.

409 Saeki I, Yamasaki T, Maeda M, Hisanaga T, Iwamoto T, Fujisawa K *et al.* Treatment strategies for advanced hepatocellular carcinoma: Sorafenib *vs* hepatic arterial infusion chemotherapy. *World J Hepatol* 2018; **10**: 571–584.

410 Su T-H, Shiau C-W, Jao P, Liu C-H, Liu C-J, Tai W-T *et al.* Sorafenib and its derivative SC-1 exhibit antifibrotic effects through signal transducer and activator of transcription 3 inhibition. *Proc Natl Acad Sci USA* 2015; **112**: 7243–7248.

411 Villanueva A, Llovet JM. Targeted Therapies for Hepatocellular Carcinoma. *Gastroenterology* 2011; **140**: 1410–1426.

412 Higashi T, Friedman SL, Hoshida Y. Hepatic stellate cells as key target in liver fibrosis. *Adv Drug Deliv Rev* 2017; **121**: 27–42.

413 Deng Y-R, Ma H-D, Tsuneyama K, Yang W, Wang Y-H, Lu F-T *et al.* STAT3-mediated attenuation of CCl4-induced mouse liver fibrosis by the protein kinase inhibitor sorafenib. *J Autoimmun* 2013; **46**: 25–34.

414 Li J, Zhou Y, Liu Y, Dai B, Zhang Y-H, Zhang P-F *et al.* Sorafenib inhibits caspase-1 expression through suppressing TLR4/stat3/SUMO1 pathway in hepatocellular carcinoma. *Cancer Biol Ther* 2018; **2**: 1–8.

415 Hao H, Zhang D, Shi J, Wang Y, Chen L, Guo Y *et al.* Sorafenib induces autophagic cell death and apoptosis in hepatic stellate cell through the JNK and Akt signaling pathways. *Anticancer Drugs* 2016; **27**: 192–203.

416 Lin T-T, Gao D-Y, Liu Y-C, Sung Y-C, Wan D, Liu J-Y *et al.* Development and characterization of sorafenib-loaded PLGA nanoparticles for the systemic treatment of liver fibrosis. *J Control Release* 2016; **221**: 62–70.

417 Kirsch R, Clarson V, Shepard EG, Marais DA, Jaffer MA, Woodburne VE *et al.* Rodent nutritional model of non-alcoholic steatohepatitis: Species, strain and sex difference studies. *J Gastroenterol Hepatol* 2003; **18**: 1272–1282.

418 Musso G, Cassader M, Gambino R. Non-alcoholic steatohepatitis: emerging molecular targets and therapeutic strategies. *Nat Rev Drug Discov* 2016; **15**: 249–274.

419 Perez-Martinez L, Perez-Matute P, Aguilera-Lizarraga J, Rubio-Mediavilla S, Narro J, Recio E *et al.* Maraviroc, a CCR5 antagonist, ameliorates the development of

hepatic steatosis in a mouse model of non-alcoholic fatty liver disease (NAFLD). *J Antimicrob Chemother* 2014; **69**: 1903–1910.

420 Marra F, Tacke F. Roles for chemokines in liver disease. *Gastroenterology* 2014; **147**: 577–594.

421 Seki E, de Minicis S, Inokuchi S, Taura K, Miyai K, van Rooijen N *et al.* CCR2 promotes hepatic fibrosis in mice. *Hepatology* 2009; **50**: 185–197.

422 Tacke F. Cenicriviroc for the treatment of non-alcoholic steatohepatitis and liver fibrosis. *Expert Opin Investig Drugs* 2018; **27**: 301–311.

423 Wong VW-S. Current Prevention and Treatment Options for NAFLD. *Adv Exp Med Biol* 2018; **1061**: 149-157.

425 Friedman S, Sanyal A, Goodman Z, Lefebvre E, Gottwald M, Fischer L *et al.* Efficacy and safety study of cenicriviroc for the treatment of non-alcoholic steatohepatitis in adult subjects with liver fibrosis: CENTAUR Phase 2b study design. *Contemp Clin Trials* 2016; **47**: 356–365.

426 Abraldes JG, Rodríguez-Vilarrupla A, Graupera M, Zafra C, García-Calderó H, García-Pagán JC *et al.* Simvastatin treatment improves liver sinusoidal endothelial dysfunction in CCl4 cirrhotic rats. *J Hepatol* 2007; **46**: 1040–1046.

427 La Mura V, Pasarín M, Meireles CZ, Miquel R, Rodríguez-Vilarrupla A, Hide D *et al.* Effects of simvastatin administration on rodents with lipopolysaccharide-induced liver microvascular dysfunction. *Hepatology* 2013; **57**: 1172–1181.

428 Trebicka J, Hennenberg M, Laleman W, Shelest N, Biecker E, Schepke M *et al.* Atorvastatin lowers portal pressure in cirrhotic rats by inhibition of RhoA/Rho-kinase and activation of endothelial nitric oxide synthase. *Hepatology* 2007; **46**: 242–253.

429 Abraldes JG, Albillos A, Bañares R, Turnes J, González R, García–Pagán JC *et al.* Simvastatin Lowers Portal Pressure in Patients With Cirrhosis and Portal Hypertension: A Randomized Controlled Trial. *Gastroenterology* 2009; **136**: 1651–1658.

430 Marrone G, Maeso-Díaz R, García-Cardena G, Abraldes JG, García-Pagán JC, Bosch J *et al.* KLF2 exerts antifibrotic and vasoprotective effects in cirrhotic rat livers: behind the molecular mechanisms of statins. *Gut* 2015; **64**: 1434–1443.

431 Hide D, Ortega-Ribera M, Garcia-Pagan J-C, Peralta C, Bosch J, Gracia-Sancho J. Effects of warm ischemia and reperfusion on the liver microcirculatory phenotype of rats: underlying mechanisms and pharmacological therapy. *Sci Rep* 2016; **6**: 22107.

432 Guixé-Muntet S, de Mesquita FC, Vila S, Hernández-Gea V, Peralta C, García-

Pagán JC *et al.* Cross-talk between autophagy and KLF2 determines endothelial cell phenotype and microvascular function in acute liver injury. *J Hepatol* 2017; **66**: 86–94.

433 Jacob SW, Herschler R. Pharmacology of DMSO. *Cryobiology* 1986; **23**: 14–27.

434 Jacob SW, Herschler RJ, Rosenbaum EE. Dimethyl sulfoxide (DMSO): laboratory and clinical evaluation. *J Am Vet Med Assoc* 1965; **147**: 1350–1359.

435 O'Donnell JR, Burnett AK, Sheehan T, Tansey P, McDonald GA. Safety of dimethylsulphoxide. *Lancet* 1981; **1**: 498.

436 Annex I Summary of Product Characteristics of RPV. http://www.ema.europa.eu/docs/en_GB/document_library/EPAR_-_Product_Information/human/002264/WC500118874.htm (accessed 24 Sep 2018).

437 Casado JL. Liver toxicity in HIV-infected patients receiving novel second-generation nonnucleoside reverse transcriptase inhibitors etravirine and rilpivirine. *AIDS Rev*; **15**: 139–145.

438 Nakamura K, Moore R, Negishi M, Sueyoshi T. Nuclear pregnane X receptor cross-talk with FoxA2 to mediate drug-induced regulation of lipid metabolism in fasting mouse liver. *J Biol Chem* 2007; **282**: 9768–9776.

439 Zhou J, Febbraio M, Wada T, Zhai Y, Kuruba R, He J *et al.* Hepatic fatty acid transporter Cd36 is a common target of LXR, PXR, and PPARgamma in promoting steatosis. *Gastroenterology* 2008; **134**: 556–567.

440 He J, Gao J, Xu M, Ren S, Stefanovic-Racic M, O'Doherty RM *et al.* PXR ablation alleviates diet-induced and genetic obesity and insulin resistance in mice. *Diabetes* 2013; **62**: 1876–1887.

441 Jamwal R, de la Monte SM, Ogasawara K, Adusumalli S, Barlock BB, Akhlaghi F. Nonalcoholic Fatty Liver Disease and Diabetes Are Associated with Decreased CYP3A4 Protein Expression and Activity in Human Liver. *Mol Pharm* 2018; **15**: 2621–2632.

442 Haughton EL, Tucker SJ, Marek CJ, Durward E, Leel V, Bascal Z *et al.* Pregnane X receptor activators inhibit human hepatic stellate cell transdifferentiation in vitro. *Gastroenterology* 2006; **131**: 194–209.

443 Jiang Y, Feng D, Ma X, Fan S, Gao Y, Fu K *et al.* Pregnane X Receptor Regulates Liver Size and Liver Cell Fate via Yes-associated Protein Activation. *Hepatology* 2018. doi:10.1002/hep.30131.

ANNEXES

30 anys D'IDENTITAT

GENERALITAT VALENCIANA

CONSELLERIA DE PRESIDENCIA Y AGRICULTURA, PESCA, ALIMENTACION Y AGUA

Unión Europea

AUTORIZACION PROCEDIMIENTO 2014/VSC/PEA/00188

Vista la solicitud realizada en fecha **31/10/14** con nº reg. entrada **20463** por D/Dª. **Pilar Campins Falcó**, Vicerrectora Investigación y Política Científica, centro usuario **ES462500001003**, para realizar el procedimiento:

"Estudio del efecto de la terapia antirretroviral sobre un modelo vivo de esteatohepatitis inducida con dieta rica en grasa "

Teniendo en cuenta la documentación aportada, según se indica en el artículo 33, punto 5 y 6, y puesto que dicho procedimiento se halla sujeto a autorización en virtud de lo dispuesto en el artículo 31 del Real Decreto 53/2013, de 1 de febrero,

Vista la propuesta del jefe del servicio de Sanidad y Bienestar Animal.

AUTORIZO:

la realización de dicho procedimiento al que se le asigna el código: **2014/VSC/PEA/00188** tipo **2,** de acuerdo con las características descritas en la propia documentación para el número de animales, especie y periodo de tiempo solicitado. Todo ello sin menoscabo de las autorizaciones pertinentes, por otras Administraciones y entidades, y llevándose a cabo en las siguientes condiciones:

Usuario: **Universitat de València**

Responsable del proyecto: **Ana Blas García**

Establecimiento: **Animalario Unidad Central de Investigación**

Necesidad de evaluación restrospectiva:

Condiciones específicas:

Observaciones:

Valencia a, 26 de noviembre de 2014

El director general de Producción Agraria y Ganadería

José Miguel Ferrer Arranz

GENERALITAT VALENCIANA
CONSELLERIA DE PRESIDENCIA Y AGRICULTURA, PESCA, ALIMENTACIÓN Y AGUA

Unión Europea

DIRECCIÓN GENERAL DE PRODUCCIÓN AGRARIA Y GANADERÍA
Ciutat Administrativa 9 d'Octubre
Castán Tobeñas, 77. Edif. B3 P2 46018 VALENCIA

AUTORIZACION PROCEDIMIENTO 2015/VSC/PEA/00016

Vista la solicitud realizada en fecha **07/01/15** con nº reg. entrada **177** por D/Dª. **Pilar Campins Falcó**, Vicerrectora Investigació i Política Científica, centro usuario **ES462500001003**, para realizar el procedimiento:

"Estudio de los efectos de los inhibidores de la transcriptasa inversa análogos de nucleósido sobre el daño hepático inducido por paracetamol "

Teniendo en cuenta la documentación aportada, según se indica en el artículo 33, punto 5 y 6, y puesto que dicho procedimiento se halla sujeto a autorización en virtud de lo dispuesto en el artículo 31 del Real Decreto 53/2013, de 1 de febrero,

Vista la propuesta del jefe del servicio de Sanidad y Bienestar Animal.

AUTORIZO:

la realización de dicho procedimiento al que se le asigna el código: **2015/VSC/PEA/00016** tipo **2,** de acuerdo con las características descritas en la propia documentación para el número de animales, especie y periodo de tiempo solicitado. Todo ello sin menoscabo de las autorizaciones pertinentes, por otras Administraciones y entidades, y llevándose a cabo en las siguientes condiciones:

Usuario: **Universidad de Valencia-Estudio General**

Responsable del proyecto: **Ana Blas García**

Establecimiento: **Animalario Unidad Central de Investigación (Fac. Medicina y Odontología) Valencia**

Necesidad de evaluación restrospectiva:

Condiciones específicas:

Observaciones:

Valencia a, 29 de enero de 2015

El director general de Producción Agraria y Ganadería

José Miguel Ferrer Arranz

David del Álamo I EMBO I Meyerhofstr. 1 I 69117 Heidelberg I Germany

Mr. Alberto Martí-Rodrigo
Pharmacology Department
Faculty of Medicine
Blasco Ibañez, 15-17
Lab 0E2
46010 Valencia
Spain

FELLOWSHIP PROGRAMME

Dr. David del Álamo
Programme Manager

phone +49-6221-8891-122
fax +49-6221-8891-215

fellowships@embo.org

15 November 2017

Certificate for EMBO Short-Term Fellowship Number 7033

To whom it may concern,

This is to certify that Mr. Alberto Martí-Rodrigo is the recipient of an EMBO Short-Term Fellowship (number 7033) to carry out research in the lab of Dr. Matthias Bartneck (Department of Gastroenterology and Metabolic Disorders (Internal Medicine III), University Hospital (Uniklinikum), North Rhine-Westphalia Technical University (RWTH), Pauwelsstraße 30, 52074 Aachen, Germany). The topic of the research project is "Modulation of immune cell migration using selectin-directed nanocarriers".

The fellowship started on 1 May 2017, and EMBO funding had been granted for a total period of 90 days.

Please contact me if you require any further confirmation or information.

Yours sincerely,

David del Álamo

UNIKLINIK
RWTH AACHEN

**Medizinische Klinik III, Gastroenterologie,
Stoffwechselkrankheiten,
Internistische Intensivmedizin,
Sektion: Endokrinologie, Diabetologie**

Uniklinik RWTH Aachen · Medizinische Klinik III
Pauwelsstraße 30 · 52074 Aachen

Klinikdirektor
Univ.-Prof. Dr. med.
Christian Trautwein

Universitätsklinikum Aachen
Anstalt öffentlichen Rechts (AöR)
Pauwelsstraße 30
52074 Aachen

www.ukaachen.de

Kontakt
Tel.: 0241 80-80866
ctrautwein@ukaachen.de

Sekretariat des Klinikdirektors
Elisabeth Steffens
Brigitte van Treeck
Tel.: 0241 80-80866
Fax: 0241 80-82455

To whom it may concern

March 7, 2018

Dear Sir or Madam:

This is to certify that Alberto Marti Rodrigo performed his research stay in the laboratories of the medical clinic III (from 1st May to 31th of July, 2017) under my supervision. The title of his work is "Modulation of immune cell migration using selectin-directed nanocarriers".

With kind regards

Prof. Dr. Frank Tacke, PhD